GEOLOGICAL AND GEOCHEMICAL STUDIES OF GROUNDWATER IN KOHIMA TOWN, NAGALAND

AKHRULU VERO
DEPARTMENT OF GEOLOGY
NAGALAND UNIVERSITY
KOHIMA, NAGALAND, INDIA
2023

GEOLOGICAL AND GEOCHEMICAL STUDIES OF GROUNDWATER IN KOHIMA TOWN, NAGALAND

By

AKHRULU VERO

Thesis submitted to Nagaland University in partial fulfilment of the requirement for the degree of Doctor of Philosophy in Geology

Dedicated

to my Redeemer, my Lord

NAGALAND UNIVERSITY

Kohima, August 2023

DECLARATION

I, **Ms. Akhrulu Vero**, hereby declare that the work embodied in this thesis is the record of the investigations done by me under the supervision of Dr. B.V. Rao Professor, Department of Geology, Nagaland University, Kohima Campus, Meriema. The work contained in this thesis is original and in part or in full, has not been submitted by me for any research degree to any other university/Institute.

This thesis is being submitted to Nagaland University for the award of the degree of Doctor of Philosophy degree in Geology

(Ms. Akhrulu Vero)
Candidate

(Prof. S.K. Singh)
Head

(Prof. B.V. Rao)
Research Supervisor

NAGALAND UNIVERSITY

(A Central University Estd by the Act of Parliament No.35 of 1989)
Headquarters: Lumami: Kohima Campus: Meriema-797004
DEPARTMENT OF GEOLOGY

Prof. B. V. Rao
M.Sc., P.G.G., PhD., FGS (Ind)
Nagaland University
Department of Geology
Kohima Campus, Meriema

Mobile: 08837489243
E- mail: bvrao97@yahoo.com

CERTIFICATE

This is to certify that the thesis entitled "**Geological and geochemical studies of groundwater in Kohima town, Nagaland**" submitted by **Ms. Akhrulu Vero** bearing Registration No: Ph.D/GEL/00087 of 29/08/2017 for the degree of Doctorate of Philosophy in Geology, Nagaland University is based on the work carried out by her under my supervision and guidance.

I certify that the work contained in this thesis has not been previously submitted for any degree /diploma or any academic award to any University/Institute and that the sources from which ideas are borrowed have been duly referred to. The candidate has fulfilled all conditions laid down by the university.

(Prof. B. V. Rao)
Research Supervisor

NAGALAND UNIVERSITY

Prof. B. V. Rao
Department of Geology

Mobile: 09436001911
E-mail: bvrao97@yahoo.com

PLAGIARISM-FREE UNDERTAKING

Name of the Research Scholar	Akhrulu Vero
Ph.D. Registration Number	Ph.D/GEL/00087
Title of the Ph.D thesis	Geological and geochemical studies of groundwater in Kohima town, Nagaland
Name & Institutional address of the Supervisor	Prof. B.V. Rao, Department of Geology, Nagaland University, Kohima campus, Meriema
Name of the Department & School	Department of Geology/ School of Sciences
Date of submission	
Date of plagiarism check	16-08-2023
Percentage of similarity detected by the URKUND software	6%

I hereby declare/ certify that the Ph.D. thesis submitted by me is complete in all respects, as per the guidelines of Nagaland University for the purpose. I also certify that the thesis (soft copy) has been checked for plagiarism using URKUND similarity-check software. It is also certified that the contents of the electronic version of the thesis are the same as the final hard copy of the thesis. A copy of the report generated by the URKUND software is also enclosed.

Date: (Name & Signature of the Scholar)

Place: Kohima

Name & Signature of the Supervisor with seal:

ACKNOWLEDGEMENT

I would like to express my heartfelt gratitude to my supervisor Professor B.V. Rao for helping me throughout my research over the past six years for his relentless guidance, support and unyielding patience. His encouragement and explicit knowledge have taught me so many invaluable lessons and made me more refined, helping me to successfully complete my thesis work on time. I record my profound sense of gratitude to him.

I would like to express my sincere appreciation to the Head, Department of Geology, Nagaland University and Dr. Temsulemba Walling for providing me with the instruments and laboratory needed for my research. I sincerely thank all the faculty and staff in this Department for their valuable suggestions and support.

I would like to acknowledge UGC for funding me with CSIR-UGC NET JRF/ SRF fellowship without which I could not have completed my research work.

I express my sincere thanks to the Chemical Section Lab. staff of DGM, Govt. of Nagaland, Dimapur; Water Testing and Referral Lab. staff, NASTEC, Govt. of Nagaland and CSIR-NEIST, Jorhat for granting me permission to use their laboratories and extending all the facilities and help.

I extend my sincere gratitude to Madam Meripeni Ezung and Dr. Paolenmang Haokip for graciously extending their help and sharing their valuable knowledge during the course of my research work.

I was surrounded by the best of friends and colleagues. I thank my research partner Miss Vilavonuo Keditsu for being with me throughout my research work. I would not have been able to complete my work without her constant support, motivation and prayers. I extend my deepest sense of gratitude to Dr. Mademshila Jamir, Miss Diezeneino Meyase, Mrs. Hievinu Olivia Vadeo, Mr. Keneisazo Nagi and Mr. Mehilo Apon. They have been with me all throughout my research work and I could not have asked for better friends to work alongside with. I also extend my special thanks to Dr. Sheyamong Pechongri, Mr. Notoka Zhimomi, Mr. Arenlong Aier and Mr. Vetho Lohe for helping me during the fieldwork.

I am grateful to Dr. Rudowhelie Peseyie and Dr. Chonchibeni for their invaluable suggestions during the progress of the research work. I also extend my sincere gratitude to Mrs. B.V. Rao for warmly welcoming me into their home during my research work and I remain grateful for her hospitality and kindness.

I extend my special thanks to Mr. Thsope Medo to whom I remain forever grateful. He has been a pillar of constant support, prayers, and guidance. His knowledge and

expertise have greatly enlightened me and I could not have completed my research work without his help.

I extend my gratefulness to Mr. Khruvo Vadeo and my maternal aunt Azu Neile for warmly extending their help and providing me with a place to stay during my laboratory analysis in Dimapur.

I am very grateful to my well-wishers and family, especially my parents Apoi Züvehü and Azai Zewete-ü, my brother Akulo, my sisters Adulu, Atale, Angolu, Asolu and Neiwele, my niece Vera and my nephews Umane and Lutho. I thank them for their constant moral, financial and prayer support. My family members put up with me through everything and enabled me to accomplish this arduous task.

And in all these, I can do all things through Christ who gives me the strength. God is my rock and I write this as a witness to the faithfulness of God. With man it is impossible but with God, all things are possible. I owe everything to my gracious Heavenly Father who has sustained me thus far.

(Akhrulu Vero)

PREFACE

Water is vital for life and the right to clean drinking water is recognized as a fundamental human right. Water pollution and scarcity have become essential issues worldwide and will continue to be so in the future. In order to use and sustainably conserve groundwater resources, it is essential to implement efficient groundwater management strategies.

Water quality monitoring has become an important exercise that helps in evaluating the nature and extent of pollution. In water quality analysis, the hydro-chemical study reveals whether the quality of water is suitable for drinking or agriculture purposes. It is also possible to understand the change in quality due to rock-water interaction or any type of anthropogenic influence.

The study area Kohima town, is the capital of Nagaland state, situated in the northeastern region of India and is located between Latitudes 25˚37′30″ N to 25˚42′32″ N and Longitudes 94˚04′40″ E to 94˚07′34″ E. It has a total area of 915.43 hectares and lies at an elevation of 1444 meters above mean sea level. The geology of the study area comprises the Disang, Disang-Barail Transitional Sequence and Barail Group of rocks made up mostly of shale, sandstone and siltstone. The rocks in the area are highly fractured, splintery, sheared and weathered through which groundwater moves.

The rise in population and urbanization have resulted in a significant increase in water demands and water quality degradation becomes an important issue. As a result, it becomes essential to analyze and monitor groundwater quality on a regular basis. The present study aims to assess the quality of groundwater in Kohima town by using geological, geochemical and geophysical methods. GIS-based maps have been used to better understand the hydrological conditions of the study area.

The results of the study are presented in seven chapters addressing various parts of the research. The **first** chapter presents the general information on the study area, literature review and the aim & scope of the research work.

The **second** chapter includes the regional geology, geology of Nagaland and geology, hydrogeology of the study area along with the hydrological data.

The **third** chapter describes the methodology including various field and laboratory techniques that is done in the study.

The **fourth** chapter studies the subsurface geology in the study area to find the potential layer for groundwater using the geoelectrical VES resistivity method.

The **fifth** chapter discusses the hydro-geochemistry of groundwater in the study area. The major type of water, major ion chemistry and factors affecting the hydrochemistry and quality of groundwater are discussed in this chapter. Statistical techniques are used to determine the important physico-chemical parameters of groundwater in this study area.

The assessment of groundwater quality for drinking and irrigation purposes is presented in the **sixth** chapter.

The **seventh** chapter gives the summary and conclusions of the whole work done in the study area.

The results of this study are likely to provide much-needed information about the groundwater quality, especially for drinking and irrigation purposes and the effects of anthropogenic activity on the groundwater of Kohima town. They will serve to provide a broader knowledge of the town's groundwater resource management which will be helpful for related future research.

***

PARTICULARS OF THE CANDIDATE

Name of the Candidate	: Ms. Akhrulu Vero
Degree	: Ph.D
Deparment	: Geology
Title of the Thesis	: **Geological and geochemical studies of groundwater in Kohima town, Nagaland**
Date of Admission	: 29th August 2017
Approval of Research proposal	: 16th August 2018
Registration number & date	: Ph.D/GEL/00087 (w.e.f. 29.08.2017)

(Research Supervisor) (Head of the Department)

CONTENTS

LIST OF TABLES

Page no.

LIST OF FIGURES

Page no.

CHAPTER 1
INTRODUCTION

1.1 INTRODUCTION

Water is the most vital component of any area's growth, and human habitation is highly dependent on the availability of water resources. 96.5% of the earth's surface is covered by seas and oceans, 1.7% by glaciers and ice caps, 1.7% by groundwater, 0.001% by vapour and clouds in the atmosphere, and a minor proportion in other major bodies of water. Only 2.5% of this water is freshwater, with 98.8% being in ice and groundwater. Less than 0.3% of total freshwater is in lakes, rivers, and the atmosphere, and an even smaller quantity (0.003%) is in living organisms and manufactured items.

The water on the earth is constantly moving in the water cycle and changing its chemical composition and components. The water below the earth's surface is divided into two components: the vadose water, which occurs above the saturation zone where the void spaces are filled with water and air. The second component is the groundwater, which occurs in the saturation zone and fills all the interconnecting spaces in the rocks with water. Water levels can change due to variances in groundwater supply and withdrawal.

Groundwater is one of the primary sources of water supply worldwide and is used mainly in domestic, irrigation and industries (Todd, 2013). Groundwater occurs in weathered areas, mainly along the joints and fractures of rocks. As a source of water supply, groundwater offers several significant benefits over surface water. Groundwater is typically of greater quality, more resistant to pollution and illness, less susceptible to seasonal and perennial changes, and more consistently dispersed across broad regions than surface water. In regions where there is no surface water, groundwater is usually accessible.

Groundwater development has a long history. Understanding the origin, occurrence, and transport of groundwater came much later. By the late seventeenth century, a good knowledge of the hydrologic cycle had been gained. Fundamentals in geology were developed during the eighteenth century providing a foundation for understanding the occurrence and flow of groundwater. Many artesian wells were drilled in France during the first part of the nineteenth century, sparking interest in groundwater. Darcy's rule (1856) governs groundwater flow in most alluvial and sedimentary

formations and was formulated by the French hydraulic engineer Henry Darcy after studying the movement of groundwater through the sand.

The assessment of India's water resources dates back to 1901 when the First Irrigation Commission estimated the surface water resources to be 144 million hectare metres (M.ham) (NABARD, 2006). Since then, several committees formed by the government of India have made attempts from time to time to assess the country's groundwater resources based on existing data and in accordance with developmental requirements.

India is the world's greatest consumer of groundwater. It consumes an estimated 230 cubic kilometres of groundwater each year, accounting for more than a fourth of the world's total. Groundwater has increasingly evolved as the core of India's agricultural and drinking water supply. Groundwater contributes almost 85% of rural water supply, 62% of irrigation, and 50% of urban water supply. Due to unpredictable and insufficient municipal water supply, urban people increasingly rely on groundwater. Groundwater quality is deteriorating due to geogenic and anthropogenic activity, causing major concern.

According to the CGWB, the total annual groundwater recharge in the nation (as of 2020) is 436.15 billion cubic metres (bcm). Taking into account natural discharge, the annual extractable groundwater resource has been estimated to be 397.62 bcm. The annual groundwater extraction is 244.92 bcm, and the average stage of groundwater extraction in the nation is around 61.6%. India is the world's greatest consumer of groundwater. It consumes an estimated 230 cubic kilometres of groundwater each year, accounting for more than a fourth of the world's total.

Due to erratic and insufficient municipal water supply, urban people are increasingly dependent on groundwater. Water quality is a major concern for humanity since it is directly related to human well-being. Water quality issues are mostly caused either by humans or industrial operations. Several centuries ago, there were minimal quality concerns when populations were low and widely spread, and significant industrial discharges were nonexistent. Nonetheless, with development, populations increased in cities, and significant quantities of waste were disposed of into streams without safe and hygienic disposal methods. These circumstances frequently resulted in catastrophic epidemics of cholera, typhoid, fever, and other water-borne diseases. As a result of rising urbanization, these issues were increasingly serious in the nineteenth century.

There is significant worry about groundwater quality decline caused by geogenic and anthropogenic practices. Anthropogenic pollution/contamination occurs when the primary source and cause of groundwater quality degradation are due to human activities such as municipal, industrial, and agricultural operations. The phrase geogenic pollution/contamination, on the other hand, refers to naturally occurring increased concentrations of specific elements in groundwater that have a detrimental health impact. Geogenic contamination of groundwater may result from geochemical properties of the aquifer material, high concentrations of elements in rock matrix dissolved during rock-water interaction, or from environmental conditions such as a variety of climatic conditions, redox conditions in the aquifer, and groundwater flow congestion, which allow the contaminant to enter the aqueous phase. The flow of groundwater is from the upstream to the downstream, which is a natural phenomenon, and in this process, water-rock interactions can occur, thus naturally increasing the concentration of ions in groundwater (Todd, 1980; Hem, 1991). Additionally, ionic concentrations can also be increased by anthropogenic activities (Subba Rao, 2002; Subba Rao et al., 2012; Li et al., 2016).

Groundwater quality is as important as quantity when evaluating groundwater resources. Groundwater is a renewable resource with inherent benefits over surface water. Because of population development, there has been a significant increase in the need for fresh water. The quality of groundwater varies according to the depth of the water table. As a result, assessing water quality is as crucial as determining its quantity. The quality of groundwater provides vital clues to the geological record of rocks as well as signs of groundwater recharge, discharge, transport, and storage. The solutes and gases dissolved in water, along with materials suspended in and flowing in the water, influence water quality. As a result, monitoring water quality is a vital activity that aids in determining the kind and degree of pollution control that is needed.

1.2 GROUNDWATER IMPORTANCE

Groundwater is an excellent source of water for a variety of reasons, including:

- Groundwater is often of good quality, and it requires far less treatment than river water which can be used for drinking purposes.
- Groundwater performs a variety of functions in both our environment and society, especially during the dry months when there is minimal direct input from rainfall.

- The movement of groundwater into rivers through seepage through the river bed, known as baseflow, is important for the survival of aquatic species and plants.
- It is frequently found in areas that have a limited supply of surface water.
- The quality does not vary greatly throughout the year, which can be important for industrial use.
- Groundwater does not need the construction of costly reservoirs to store water before it is used.
- Because groundwater responds slowly to fluctuations in rainfall, it remains available during the summer and drought seasons when rivers and streams have run dry.
- Groundwater, unlike other natural resources, is available all over the earth and can be obtained throughout the year if appropriate replenishment is done and the source is safeguarded from contamination.

1.3 LOCATION AND ACCESSIBILITY

The study area, Kohima town is located in India's North Eastern Region. It is situated in the Kohima district, the capital of Nagaland state, which is the sixteenth state to be established in the Indian Union. Nagaland is bordered by Myanmar to the East and the neighbouring states of Arunachal Pradesh to the North, Assam to the West and Manipur to the South. Kohima is located in the Japfü region of the Barail Range, south of the district. It lies between Latitudes 25˚37′30″ N to 25˚42′32″ N and Longitudes 94˚04′40″ E to 94˚07′34″ E and falls in the survey of India Toposheet No. 83 K/2.

Kohima is well connected to the rest of the country and other parts of the state by road networks like National Highway 2 and National Highway 29, while the nearest train station and airport are located 74 kilometres away in Dimapur city. The Dimapur-Kohima Highway is a tolled four-lane dual road in Nagaland that connects Kohima with the state's major city, Dimapur. The study area boundary has been demarcated based on the availability of wells and a buffer distance of 50 metres around the wells was drawn to mark the boundary. The research area has a total area of 915.43 hectares. The landscape in the study area is undulated and rugged, having a hilly environment mostly with elevations ranging from 800 to 1500 metres above mean sea level, and the highest elevation within the town is 1528 metres above mean sea level. The highest elevations in the vicinity of the town include Puliebadze at 2296 metres above mean sea level and Japfü

peak at 3048 metres above mean sea level, with general elevation increasing to the south. The location map of the study area is shown in Fig. 1.1 and Fig. 1.2.

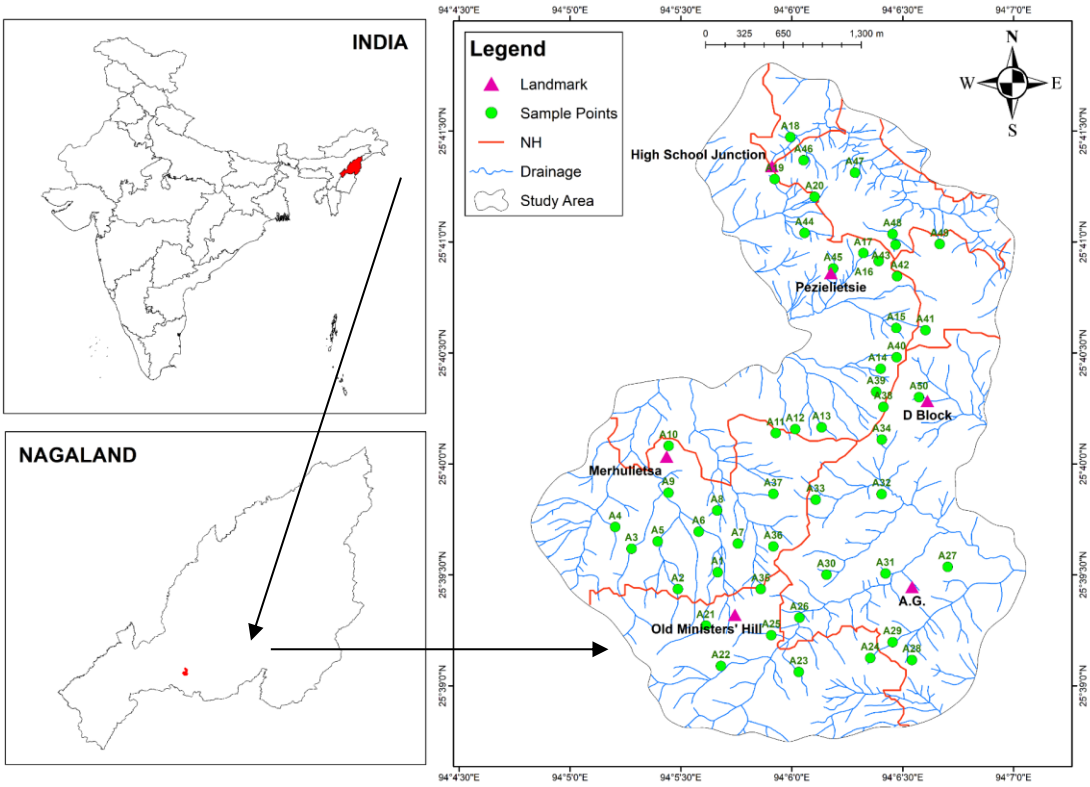

Fig. 1.1: Location map of the study area

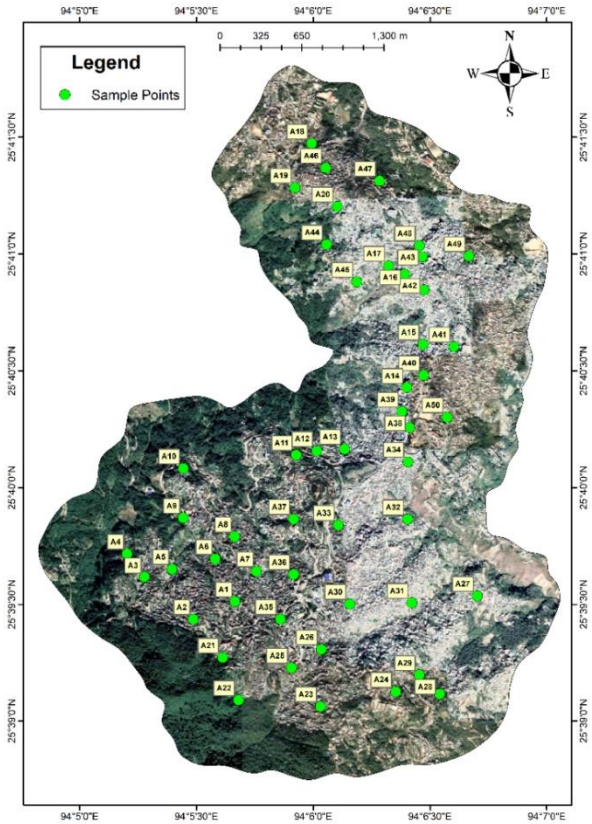

Fig. 1.2: Google Earth Pro imagery of the study area

1.4 HABITATION

Kohima was originally a big village called Kewhira, which is now a part of the Kohima Urban Area. The major indigenous inhabitants of Kohima town are the Angami Nagas. Kohima being the capital of the state, is inhabited by all tribes of Nagaland as well as some communities from mainland India. Kohima is one of the smart cities under the Smart Cities Mission under the Government of India and is a rapidly developing city. According to Census India 2011, the Kohima Municipal Committee has a population of 99,039 people with 22,312 households. Kohima is a hilly region and most of the houses are constructed on steep slopes.

1.5 CLIMATE AND RAINFALL

The study region lies in the humid tropical climatic zone and the average rainfall is around 2000 mm. There are around nine rainy months where the majority of rain falls between June to August, with sporadic rain from September through October. Winter is bitterly cold, with minimum temperatures as low as 2°C. The coldest months of the year are December and January. Summer is mildly warm, with an annual high temperature of 28°C. Cloudbursts are a typical occurrence in parts of the state, particularly Kohima and storms are common in seasonal periods. The area experiences south-east monsoon and rainfall in the study region has a high spatial and temporal variability. The influence of climate change has resulted in major changes in the mean rainfall pattern.

1.6 LAND USE LAND COVER (LULC)

The most effective method for generating LULC in any area is by using satellite Imageries through the aid of visual interpretation method. The same method has been employed in generating LULC in the present study. The aid of Google Earth image forms the base layer for the classification. The methodology of the National Remote Sensing Centre (NRSC) scheme classification was used.

As per observation from the LULC classification, the agricultural activities covering an area of 2.55 Ha includes Jhum paddy, maize, cabbage, potato, tomato, etc. which are a source of livelihood. Some of the areas also include livestock rearing, poultry farming etc. Builtup-Urban covers a maximum area of 909.96 Ha. The area includes infrastructure buildings, residential areas, community, institutions, government buildings, recreational parks etc. The forest area (0.95 Ha) comprises mostly of open to moderately dense as per the canopy coverage. Sokhriezie Pond which consists of an area of 0.2 Ha is located at the centre of the study area and acts as an attraction spot for local people.

Scrubland comprises mostly of culturable wasteland which is left fallow after jhum activities and is predominantly secondary forest regeneration, shrubs and bushes. The area statistics and LULC map is shown in Table 1.1 and Fig. 1.3, respectively.

Table 1.1: LULC Classification of Kohima town

LULC Categories	Area (Hectare)	Area (%)
Agricultural land	2.55	0.278558
Builtup-Urban	909.96	99.40247
Forest	0.95	0.103776
Pond	0.2	0.021848
Scrubland	1.77	0.193352
Total	915.43	100

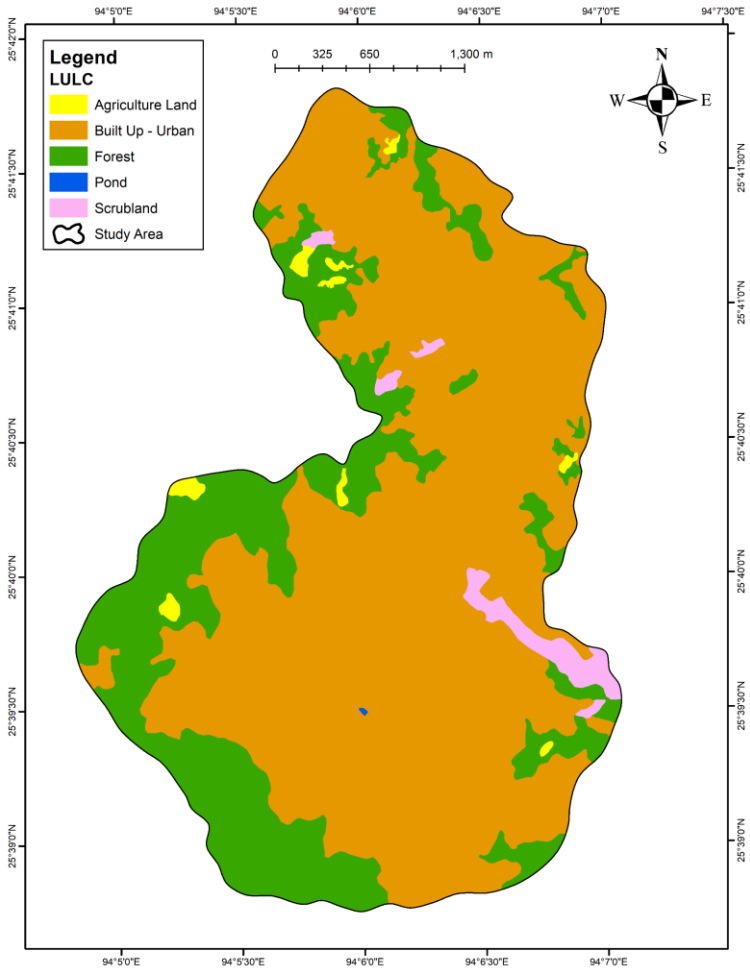

Fig. 1.3: LULC map of the study area

1.7 SOIL

The soil is an essential component of Nagaland's terrain and geography, and the soils are formed from tertiary rocks of the Barail and Disang formations. They are grouped into alluvial and residual soils, which are as follows:

1) Alluvial soils: Alluvial soils are more fertile and usually found in low-lying regions in the west and along river banks.
    i. Recent alluvium (Entisol)- Recent alluvium, also known as Entisol, is found mostly in the western and southwestern parts of the state.
    ii. Old alluvium (Oxizols and Ultisol)- The old alluvium is found primarily in the north-western part of Nagaland, bordering the state of Assam along Sibsagar District.
    iii. Mountain valley soil (Entisol)- They have pH in the range of 4.4 - 4.6, and span approximately 224.8 sq. km, which are found mostly in the valleys of the state's central and eastern regions.
2) Residual soils: The residual soils are porous and have light textures and they predominate across much of Nagaland.
    i. Laterite soils (Oxizols and Ultisol)- The most prevalent soil type in the state is laterite soil, which is found in the mid-southern and eastern regions. It has a pH range of 4.2 to 4.5 and makes up 4,495.8 sq. km of Nagaland's total land area.
    ii. Brown forest soils (Mollisols and Inceptisols)- The brown forest soils cover 4,952.7 sq. km of Nagaland’s total land area and have a pH content of 5.3-5.8, which are found in the intermediate high hill ranges. The incepticols have fine soil textures of loamy clay, fine clay and fine loamy clay.
    iii. Podzolic soils (Spodosols)- Podzolic soil covers about 4,835.0 sq. km. of Nagaland's central, southern, and eastern regions. They are found at high altitude in humid and temperate climates and has a pH range of 5.4 to 6.0.

The soil type found in the study area is composed of Entisols, Inceptisols and Ultisols.

1.8 GEOMORPHOLOGY

The topography of Nagaland is mostly characterised by regular intervals of hills and valleys trending NE to SW. The structural trend associated with the history of

orogenic tectonics governs the general topography. The hills have rugged terrain with long continuous parallel ridges separated by deep and narrow river valleys where active erosion and weathering processes are still taking place. Kohima district is classified geomorphologically into Low to Moderate Hills, Moderate Structural Hills, Denudo-Structural Hills and High Structural Hills.

- Low to Moderate Hills - In the western section of the district, low-lying dissected, sub-parallel hills orientated in NE-SW with little valley development are found. Sandstone, siltstone, shale, and mudstone are the rock types found in these hills.
- Moderate Structural Hills - The district's north-central region is dominated by moderately high linear structural hills with narrow valleys. Hills are made up of semi-consolidated sandstone, siltstone, shale, and claystone and are prone to erosion.
- Denudo-Structural Hills - Linear, curvilinear, and irregularly shaped denuded hills linked with smaller valleys are found in the district's south-central region. These are mostly semi-consolidated sandstone and shale with a reduced degree of erosion.
- High Structural Hills - Long parallel to sub-parallel linear hills which are rigid, occupy the district's central and south-western areas. These consist primarily of hard and compact sandstone, shale, and siltstone with little erosional activity.

The study area Kohima town is established along the linear ridge, which trends NNW-SSE and it has moderate slopes on each side of the ridge with a slight depression at places. The terrain in the study area consists mostly of moderately and highly dissected hills and valleys. This area has a relatively rugged landscape with sub-rounded hills, narrow valleys, deep gorges, and such. The southern hill ranges, which are covered with evergreen forests, are quite rugged and cultivation is done on the lower slopes of the hills. Hilltops and ridges have the least potential for groundwater accumulation since there is little rainwater infiltration into the subsurface, whereas narrow river valleys have the most potential.

1.9 DRAINAGE

The drainage pattern in Kohima is asymmetrical, deep, and narrow because a majority of them are controlled by faults, joints, fractures and lineaments where groundwater is discharged as runoff through these structures. The evergreen forest-

covered southern hill ranges have extremely rugged and uneven terrain. Terrace and jhum cultivation have rendered the lower hills and lowlands barren.

The drainage map of the study area shown in Fig. 1.4 has been prepared from Toposheet 83K/2 (1:10,000), and Strahler's classification system was used for creating the stream/drainage network with stream order (Strahler, 1964). The Sanuo Ru and Phe Ru are the principal perennial streams draining north of the study area. Major stream Dzucha Ru originates from Puliebadze and flows north-easterly, bending towards the confluence of Tekhobazou Ru. Sitsie Ru, Dzuvu Ru, and Karozou Ru are the minor streams. Several first and second order streams, most of which are ephemeral in nature, cut through the area. The third and fourth order streams of high order are perennial and they typically cut through the road sections as well. In the winter, some of these streams dry up. The highest stream order identified is the 5th order (Dzuyu Ru). The Vurie, Sanuo, Dzuvu, Kharu, Sitsie, Dzuyu and Dzulikha streams flow through the town of Kohima.

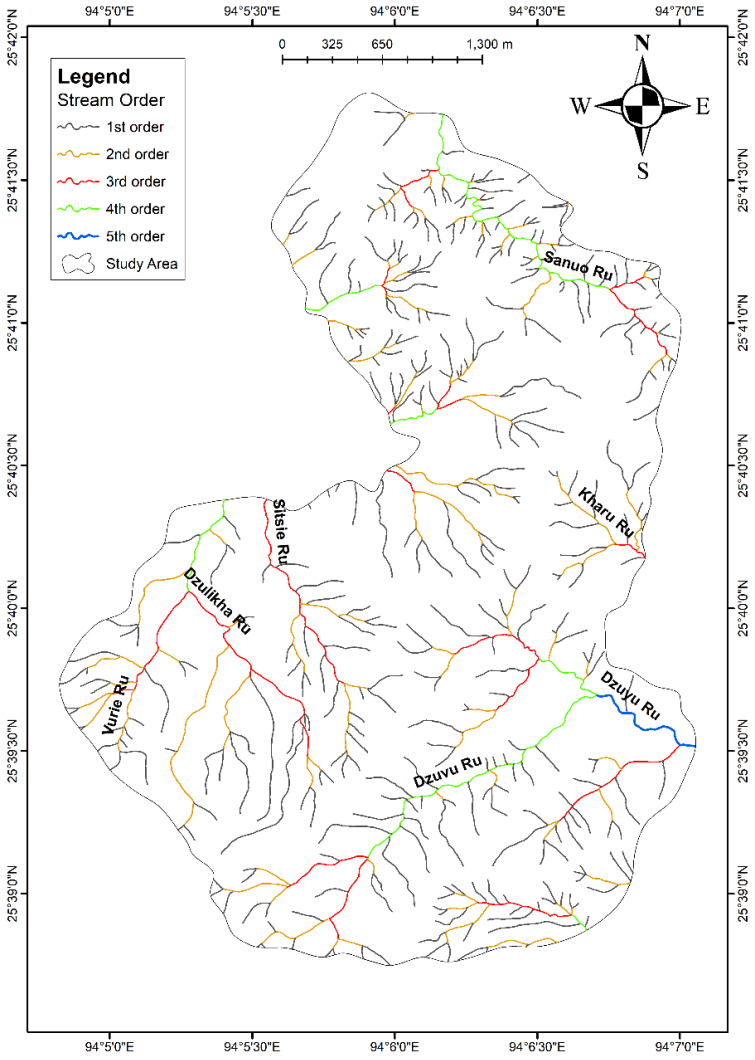

Fig. 1.4: Drainage map of the study area

1.10 VEGETATION

The part of the study region which is not inhabited is covered in dense evergreen or semi-evergreen virgin forests. Large sections of lowland terrain are occasionally cleared for agricultural purposes. The majority of the plants in this area are shrubs and trees like alder, wild apple, wild cherry, walnut, etc. are also present.

1.11 AGRICULTURE AND IRRIGATION

There are no medium or large irrigation projects underway in the state at the moment. In comparison to a net sown area of 312770 Ha, irrigation potential is assessed at 165000 Ha. Kohima, Dimapur, Phek, Wokha, and Tuensang are the districts with extensive irrigation systems. However, irrigation is primarily surface water that is completely dependent on monsoon rain, with the exception of a few pockets in the foothills. As a result, all irrigated regions are classified as rainfed. The majority of irrigation is carried out by utilising solely surface water, with little to no groundwater input.

People in the Kohima district mostly engage in agriculture. The majority of farming in the area is done using archaic, traditional agriculture techniques and hand tools. The potential for using groundwater resources for irrigation is constrained by the rugged geography. Jhum/shifting cultivation (slash and burn) is used since the terrain is hilly. In areas with a moderate slope, terrace cultivation is nevertheless also used, but to a lower extent.

1.12 GROUNDWATER RESOURCES

The groundwater resource of India (as of 2020) has been investigated by the CGWB and State Ground Water Departments under the direction of State level Committees. The total annual groundwater recharge for the entire nation has been estimated at 436.15 billion cubic metres (bcm), and the total natural discharge equals 38.51 bcm. Thus, the nation's total annual extractable groundwater resource is 397.62 bcm. Due to a lack of block-level data, the groundwater resources for Nagaland state was evaluated district-wise. The state's annual extractable groundwater resource is estimated to be 1.95 bcm and the total annual groundwater recharge to be 2.17 bcm. Groundwater extraction on an annual basis is 0.021 bcm, and the stage of groundwater extraction is 1.04%. Every district has been designated as “Safe”.

1.13 LITERATURE REVIEW

For the purpose of conducting the research, study materials from a variety of sources, including research journals, government publications and papers, books, websites, etc., have been studied.

Pioneers Mallet (1876) and Hayden (1910) conducted geological studies in Nagaland, including some parts of the Kohima district. Evans (1932), Mathur and Evans (1964), Brunnschweiler (1966) and Acharyya (1986) attempted to understand the geology, stratigraphy, structural, and tectonic framework in some parts of the Kohima division.

Piper (1944) by applying a graphical technique, made a contribution to the chemical interpretation of groundwater analysis. Wilcox (1955) categorised groundwater for irrigational use. The chemical properties of natural water were studied and interpreted by Hem (1985), while Handa (1975) provided a brief overview of groundwater pollution in India.

Bambry and Sharda (1997) prepared a geotechnical map of Kohima Township, demarcating regions that were more suitable for development based on assessments of slope stability and overburden thickness. Chakradhar, Naik, and Jayaraman (1986, 1987) carried out systematic geological mapping of the Kohima district. The Kohima urban area's geo-environmental assessment was done by RC Shukla in 1987.

Mondal et al. (2010) studied the interaction between groundwater and saline water on the southeast coast of India, located about 70 km south of Chennai city and 10 km SSW of Mahabalipuram by determining the groundwater major ions chemistry. 18 groundwater samples were collected during pre-monsoon and post-monsoon seasons from bore wells. The data revealed that about 99.9% of the EC variability was caused by the combined effect of Cl^-, Na^+, SO_4^{2-}, HCO_3^-, NO_3^- and $Ca^{2+} + Mg^{2+}$ in both seasons, where 54.0% was due to Cl^- alone in the pre-monsoon and 43.1% in the post-monsoon. The factor analysis revealed the influence of mixing zones between saline water and groundwater. The exchange processes between groundwater and seawater chemistry in coastal aquifers were proved by using multivariate statistical analysis and ionic changes of main hydrochemical ions. The study thus served as a foundation for future hydrochemical research in groundwater management planning, protection, and decision-making.

Selvam and Sivasubramanian (2012) investigated subsurface geology and groundwater potential zones in Medak District of Andhra Pradesh, India by carrying out

a geoelectrical resistivity survey using Vertical Electrical Soundings (VES). 26 VES soundings were recorded with the Schlumberger electrode configuration with current electrode spacing (AB/2) from 1 to 150 m. The curve matching and electrical imaging computer programme IPI2WIN were used to interpret the field data. The thickness and water-bearing capacity of the subsurface strata were then revealed through interpretations. The second layer, with fractured/weathered rock formations, was found to be the best layer serving as a reliable aquifer in the Medak areas.

In order to identify freshwater pockets in sedimentary aquifers in the Vanur block of Villupuram District, Tamilnadu, Thiruneelakandan et al. (2014) have conducted geoelectrical resistivity surveys at 9 different sites. IPI2WIN software was used to analyze the data and the AB/2 spacing was up to 100m. Three VES locations had favourable resistivity values of 50 to 150 Ωm. Thus, these three locations were determined from the interpretation analysis to develop shallow freshwater potential pockets.

S. Karuppannan (2015) worked on the Kadayampatty Panchayat Union in Tamil Nadu's Salem district. In this work, geophysical techniques were done to demarcate the groundwater potential zone with 10 Vertical Electrical Sounding (VES) using Schlumberger electrode arrangement. The electrodes were stretched out in stages of five metres up to 50 metres and ten metres up to 150 metres. With respect to topographic features, VES stations were chosen accordingly. The geoelectrical results revealed a maximum of five geoelectrical formations, including topsoil, weathered zone, fissure and fractured zone, fracture basement, and fresh basement. Based on the interpretation of the results, a number of large diametres, circular dug wells and shallow depth bore wells could be dug in the discharge area for increased groundwater production. The villages of Kadayampatty, Chinnathirupathi, Semmandapatty, and Pannapatty were then designated as groundwater potential zones in the mountainous, forested terrain of the Kadayampatty Panchayat Union.

Kshetrimayum and Hegeu (2016) used cross plots, Pearson correlation, principal component analysis, and flow net methods to analyze 32 water samples for the toxicity and origin of elevated iron and manganese concentrations in surface water and groundwater in the Naga thrust of the Assam-Arakan basin of northeastern India. The EPA standards for Fe and Mn were found to be exceeded in every sample, respectively, by 28 and 136 times. They concluded that baseflow discharge into low-lying areas, the discharge of water from the Dhansiri and Chathe rivers into the surrounding water table,

and the dissociation of Fe and Mn oxides by organic metabolism in a reduced environment were the main causes of the high Fe and Mn concentrations.

Heavy metal contamination was found by Rao et al. (2016) in and around Peddacheruvu, which is located near Hyderabad city, India. They used inductively coupled plasma mass spectrometer and X-ray fluorescence to examine samples of groundwater, surface water, soil and sediment for the presence of heavy metals. When compared to sediment and groundwater, surface water was shown to be less contaminated with heavy metals, namely Fe, Mn, Ni, and Al. They came to the conclusion that the activity of heavy metal precipitation in the water body is what causes these heavy metals to be deposited in the sediment.

The quality of the groundwater in and around Tuticorin town, on India's southeast coast, was examined by Singh et al. (2017). In their investigation, the techniques of Brown et al. (1983) and APHA (1985) were used to analyze 29 groundwater samples. Correlation matrix analysis, Piper, Wilcox, and Gibbs diagrams were created. Total dissolved solids (TDS), sodium (Na^+), magnesium (Mg^{2+}), chloride (Cl^-), and sulphate (SO_4^{2-}) analysis of major ions revealed anomalous values, which led to a decline in the quality of groundwater. Major cations and anions were found in the following order: $Na^+ > Mg^{2+} > Ca^{2+} > K^+$ and $Cl^- > SO_4^{2-} > HCO_3^- > NO_3^- > F^-$ respectively. A cross plot of the molar ratios of HCO_3^-/Cl^- against TDS revealed that 72% of the examined samples were brackish and saline in origin. According to the interpretation of the US Salinity Diagram, the majority of the samples had very high sodium and salinity hazards, which indicated evaporation dominance.

Peseyie and Rao (2017) used parameters such as Turbidity, pH, TH, TDS, Ca^{2+}, Mg^{2+}, Na^+, K^+, Cl^-, Fe, SO_4^{2-}, and F^- to investigate the groundwater quality in Dimapur town for drinking purposes in accordance to BIS (1998) standards. pH measurements showed values ranging from acidic to neutral. In 11.33% of the groundwater samples, the turbidity levels were higher than the permissible limit. For Na^+ concentrations, 74.58% of the water samples were within permissible limit. In terms of total K^+ contents, 51% of the samples were within the acceptable limit for human consumption as per the BIS (1998) criteria. The range of Fe concentrations was 0.18 to 2.5 mg/L, and the majority of the samples were above the permissible limit and required further treatment. According to their research, the study area needed a proper monitoring system and treatment of water should be adopted for drinking.

Datta et al. (2018) used the hydrochemical data to generate the Water Quality Index using the weighted arithmetic method to assess the quality of groundwater in and around Guwahati, Assam, India. 66 water samples were collected for a thorough physicochemical analysis and WQI was estimated from 12 parameters, including pH, turbidity, total hardness, calcium, magnesium, bicarbonate, chloride, nitrate, sulphate, total dissolved solids, iron, and fluorides. The high values of WQI were shown to be from the locations with higher levels of iron, nitrate, total dissolved solids, hardness, fluorides, and bicarbonate. According to their research, WQI proved to be a very useful instrument for evaluating water quality and helpful for the general public or any intended application, as well as in pollution mitigation plans and water quality management.

N. Subba Rao (2018) studied the quality of groundwater in 30 different areas around the Prakasam region of Andhra Pradesh, India. He worked on the evaluation of groundwater quality on pH, TDS, Ca^{2+}, Mg^{2+}, Na^{+}, HCO_3^{-}, Cl^{-}, SO_4^{2-}, NO_3^{-} and F^{-} and found the water was unfit for consumption as per WHO (2011) and BIS (2012) drinking water standard. In order to determine the suitability of groundwater samples for irrigation, the sodium adsorption ratio, percent sodium, permeability index, residual sodium carbonate, magnesium ratio, and Kelly's ratio were computed. The USSL, Wilcox, and Doneen's diagrams were also utilized for evaluation of groundwater quality for irrigation and most groundwater samples were unfit. pH, TDS, HCO_3^{-}, Cl^{-} and SO_4^{2-} were assessed for industrial purpose with respect to incrustation and corrosion activities on metal surfaces and was found to be unfit.

Sunitha and Sudharshan (2019) evaluated the hydrogeochemistry of groundwater in and around Lakkireddipalli and Ramapuram, Y.S.R District of Andhra Pradesh in India. 30 groundwater samples were taken to assess the groundwater for drinking and irrigation practices. The majority of groundwater samples were safe as per W.H.O. drinking water levels. Fluoride and nitrate were found to come mostly from geogenic and human sources, respectively. The main hydrogeochemical component affecting water chemistry was rock domination. The Piper's figure revealed a mixed Ca Mg Cl type. The majority of groundwater samples were in the unsuitable category for irrigation. Hence, they suggested growing more saline-tolerant plants to combat soil salinization and applying lime or gypsum to reduce soil permeability.

Rao et al. (2021) worked on the assessment of groundwater quality in Kohima Village, Nagaland for drinking purposes. 21 samples were analyzed on the parameters of pH, turbidity, TH, Fe, Cl, TA, F, Ca, Mg, and nitrate which were compared with the

standards of BIS (2012). Except for turbidity and nitrate, which exceeded the permissible limit, the overall groundwater study showed a suitable drinking water quality. A good water quality monitoring system was thus advised to be done at some intervals of time for the assessment of water.

Zhang et al. (2021) evaluated the groundwater quality in the Nanchong area of southwest China, and identified any potential health risks associated with nitrate-enriched groundwater. Using 70 groundwater samples, they examined the hydrochemistry using several computerized approaches such as geomodelling, EWQI, GIS mapping, and USEPA mathematical model. According to a Box and Whisker plot, the cations concentrations were in the following order: Ca^{2+} > Na^{+}>Mg^{2+}> K^{+}, while anion concentrations were HCO_3^{-}> SO_4^{2-}> Cl^{-}> NO_3^{-}> F^{-}. Ca-HCO_3 was suggested as the hydrochemical type using the Piper triangle diagram. Ion exchange and calcite dissolution were the two main hydrochemical processes. Domestic sewage and agricultural activities were responsible for NO_3^{-} contaminations. According to the health risk assessment, infants in the research area were more vulnerable to health risks from ingesting NO_3^{-} contamination than children, adult females and males.

Ezung et al. (2022) investigated the subsurface conditions at a landslide in Perizie colony, Kohima, Nagaland using the vertical electrical sounding (VES) technique and the Schlumberger depth sounding method. With regard to slope instability, the VES curves revealed varying lithology and also suggested that a weak zone, which was not visible from the surface, was present at a depth of roughly 10 meters. The analysis also showed that the VES approach could be used to determine the depths of water tables and viable aquifers. So, the 1-D resistivity survey offered insightful data regarding the subsurface circumstances that might have contributed to the occurrence of landslides in the study area.

Keditsu et al. (2022) assessed the quality of groundwater for drinking in Chiephobozou town, Kohima district, Nagaland. 30 samples were taken during pre-monsoon and post-monsoon periods in 2021 and they studied the hydrogeochemical properties by evaluating the physico-chemical parameters where 66.67% of pre-monsoon water samples and 53.33% of post-monsoon water samples were within the permissible limit for drinking as per BIS (2012) and WHO (2004). Water Quality Index revealed that the groundwater was mostly unsuitable for drinking because of the high iron concentration in the samples. Na and HCO_3 were the dominant cation and anion in both seasons. Piper's trilinear diagram revealed that the majority of the water was of mixed

type, with 66.7% in pre-monsoon and 40% in post-monsoon. The Gibbs diagram gave the rock water interaction dominance for the groundwater in Chiephobozou town.

Kumar (2022) created a GIS-based mapping of water-level fluctuations and their effects on groundwater in India's Thanjavur district, Tamil Nadu. He used topographic survey data to determine the groundwater level and elevation before and after the monsoon season. The maps of spatial variation helped visualize the seasonal water level and fluctuations in Thanjavur.

1.14 PREVIOUS WORK IN THE STUDY AREA

The Central Groundwater Board, Ministry of Water Resources, Government of India started conducting groundwater exploration in Nagaland in the early 1970s with a few exploratory drillings in the Dimapur, Changki, and Tizit valleys. Their research focused on the geological, geomorphological, and hydrogeological aspects of hill valley exploration, as well as the potential of groundwater resources. In the latter part of 1980, the Nagaland government's Directorate of Geology and Mining (DGM) began groundwater drilling which was restricted to the Dimapur valley only.

E. Kikon and Katiwaba Ao (2006) worked on groundwater development in the hilly terrain of Nagaland, in and around Kohima town. An increase in the development activities was considered a major factor in water scarcity during lean periods in most of the hilly areas. They worked on four exploratory drilling shallow tube wells within 120 m depth which were drilled by the state DGM around Kohima town. The static water level varied from 5m to 39 mbgl (metres below ground level) with discharge from 6000 to 9000 L/hr. for drawdown within 7m. The construction of dug/ring wells was found to be feasible at specific geo-structural set-ups. They found the presence of potential secondary porosity within 50 to 200 mbgl in hilly areas.

The CGWB dynamic groundwater resource (2020) indicated that the Total Annual extractable Groundwater resource of Kohima district is 15542.08-hectare meters. The current annual gross groundwater extraction for Industrial use is 0.6-hectare meters. The annual allocation of groundwater for domestic water supply as on 2025 is 249.54-hectare meters. Net annual groundwater availability for 'Future Use' is 15291.95-hectare meters. Net annual groundwater availability for 'Future Use' per unit area is 124.45 millimetres. Separate data for Kohima town has not been prepared.

B.V. Rao et al. (2021) have worked on assessing groundwater quality for drinking purposes in Kohima village.

No thorough published work has been done in Kohima town regarding the prospective groundwater zones, as well as the quality and management of the groundwater.

1.15 AIM AND SCOPE OF WORK

Water is extremely essential for survival of all living organisms and changes in its quality can have serious consequences. The present study aims to mainly assess the geochemical spatial distribution and determine groundwater quality as it provides helpful information for managing regional groundwater resources in Kohima Town. This investigation will help establish proper management of the groundwater. There is a need to carefully monitor groundwater and check its quality, especially for drinking purposes. The present study has therefore been undertaken with the following objectives:

- To delineate the geological units and prepare geological and hydrological maps of the study area.
- To depict the hydrological condition based on the subsurface geology.
- Physico- chemical characters of groundwater from the study area.
- Assessment of the groundwater quality for drinking and irrigation purposes.

CHAPTER 2

GEOLOGICAL SETTING AND HYDROGEOLOGY

2.1 REGIONAL GEOLOGY

To the eastern boundary of Northeast India bordering Myanmar occur spectacular NE-SW trending domain of Himalaya's cousin named Naga Hills. The Naga Hills tectonic evolution of northeastern India is associated with the movement of the Indian plate and its collision with the Burmese plate in the east during the Late Cretaceous- Eocene period. It is an ideal representation of how a passive margin setting (Kumar and Naik, 2006) can change into an active margin setting over time in response to plate movement.

The Naga Hills is a unique Cretaceous-Tertiary mobile belt that ends in the north at the Brahmaputra Valley. The south of the Naga Hills is bounded by the Chin Hills and towards the south-eastern part of the Naga Hills lies the Arakan Yoma fold thrust belt and the Chindwin basin. The Naga Hills is bordered on the west by the Pre-Cambrian Mikir Massif and Tertiary Shelf Sediments of Assam, and towards the east, they are bounded by the Myanmar tectonic sediments. The Naga Hills, which run NE-SW, are divided into two sections: the central Naga Hills Paleogene flysch sediments and the Naga-Chin Hills ophiolite belt (Acharyya, 1986).

2.2 MAJOR STRUCTURES OF NAGALAND

In Nagaland, igneous and crystalline rocks of Mesozoic-Cenozoic age comprise around 10 percent of the area, while around 90 percent of the surface area is covered by Cenozoic sedimentary rocks. The study area is part of the Tertiary fold belt which is made up of structurally or lithologically controlled hill ranges. The study area is located in the middle of the Naga Hills and is composed of Paleogene flysch sediments.

Nagaland is subdivided into three major tectonic units based on their morphotectonic features: Naga Ophiolites in the east, Schuppen Belt in the west, and Inner Fold Belt occupied by Kohima and Patkai synclinoria in the middle (Mathur and Evans, 1964). They are briefly discussed below:

Schuppen Belt

The northern edge of the Naga hills is marked by the NE-SW trending narrow Belt of Schuppen. The Schuppen belt is made up of eight to nine tectonic slices/overthrusts along which the Naga hills have shifted northwesterly relative to the foreland spur (Evans,

1964). The eastern and western boundaries of the Schuppen Belt are marked by the Halflong-Disang Thrust and the Naga Thrust respectively in Nagaland. It's a complicated network of crisscrossing faults (Rao, 1983) with en-echelon deposition. According to Aier et al. (2011), the Schuppen Belt is a distinct tectono-geomorphic unit that is around 400 km long and 25 km wide and is terminated at the northeast by the Mishmi Thrust and at the southwest by the Dauki Fault. The Schuppen Belt is distinguished by Eocene-Oligocene and Plio-Pleistocene sediments, with no Disang deposits. The various lithostratigraphic units found in the Belt of Schuppen are the Barial, Surma, Tipam, Namsang, and Dupitilla Groups of rocks.

Inner Fold Belt

The Inner Fold Belt is located in the interior region of the Naga Hills and is characterised by its extensive Disang rock formations and limited Barail coverings. The Inner Fold Belt is bounded on its west by the Halflong-Disang thrust and the Ophiolite-Disang thrust to the east. Geographically, the Inner Fold Belt made up of the argillaceous unit of Disang Shales covers up the majority of the Nagaland state. The Palaeogene strata exposed between the Barail and Disang formations in the Inner Fold Belt have been termed the Disang-Barail Transition due to their heterogeneous lithology (Pandey and Srivastava, 1998). The rocks have undergone a series of folding forming anticlines and synclines. There are two main synclinorium in the Inner Fold Belt- the Patkai Synclinorium in the north and the Kohima Synclinorium in the south. In Kohima Synclinorium, the younger Surma rocks are developed in its core (DGM, 1978).

Naga Ophiolite Belt

The Naga Ophiolite (NOB) is a remnant of the Tethyan oceanic crust and Upper mantle developed at a spreading centre in a narrow, short-lived basin formed by rifting and spreading during the Late Cretaceous period. The opening and closing of this basin are associated with the fragmentation of Gondwanaland. The NOB extending over 90 km in length and a width varying from 2 to 15 km, covers an area of roughly 1000 sq. km. Between the Disang Formation on the west and the Nimi Formation on the east, the ophiolites are exposed as an arcuate linear belt. The ophiolite complexes are made up mainly of the mafic volcanics, mafic (gabbros) and ultramafic cumulates (peridotite, pyroxenite, serpentinites) and plagiogranites. They are mixed together with some oceanic sediments such as limestone, chert and greywacke along with some intrusives (Ranjit et al., 2013). The ophiolite complex is thrusted over by the Naga metamorphics in the east.

2.3 STRATIGRAPHIC SUCCESSION OF NAGALAND

The Cenozoic stratigraphic framework of Nagaland is made up of the following litho-units and presented in Table 2.1: Naga Metamorphics, Nimi Formation, Zepuhu Formation, Disang Group, Disang-Barail Transitional Sequences, Barail Group, Jopi Formation, Surma Group, Tipam Group, Namsang Bed and the Dihing Group (after Mathur and Evans, 1964; Agarwal and Ghose, 1986; and Srivastava et al., 2004). They have been briefly described below.

Naga Metamorphics

The Naga Metamorphics mostly consists of Proterozoic rocks like quartzite, marble, mica schist and gneisses. The base of this formation is not exposed but it is tectonically juxtaposed against or even overlay the Ophiolites as well as the Phokphur Formation. It occurs in the eastern part of the Ophiolite belt and is found exposed in Saramati Hill and adjoining areas.

Nimi Formation

The Nimi Formation lies on the eastern margin of the Naga Hills Ophiolite belt along the Indo-Myanmar border. It stretches over 216 kilometres and is assumed to be of Pre-Mesozoic age. This formation consists of phyllite, quartzite, marble, and quartz-sericite schist.

Zipu Formation

The Zipu Formation represents the Ophiolite complex of Nagaland and lies between the Nimi Formation on the east and the Disang Group on the west. It has a linear NE-SW trend. The rocks of this formation include peridotite, serpentinite, basalts, gabbro and dunite mixed with oceanic sediments such as chert, greywacke, limestone, etc.

Table 2.1: Stratigraphic succession of Naga Hills (Mathur and Evans, 1964)

Age	Group	Formations		
		Outer and Intermediate Hills		**Eastern Hills**
Recent-Pleistocene		Alluvium and high level terraces		
	Dihing	Boulder beds		
----Unconformity----				
Mio-Pliocene	Dupitila	Namsang beds		
----Unconformity----				
Miocene	Tipam	Girujan clay Tipam sandstone		
	Surma	Upper Bhuban Middle Bhuban Lower Bhuban		
----Unconformity----				
Oligocene	Barail	Renji	Tikak Parbat	<u>Jopi/Phokpur Formation</u> Tuffaceous shale, sandstone, greywacke,grit, conglomerate,minor limestone and carbonaceous matter
		Jenam	Baragolai	
		Laisong	Naogoan	
Eocene-Cretaceous	Disang	Upper		Shale/slate/phyllites with calcareous lenses in basal section and invertebrate and plant fossils in upper section with brine springs
		Lower		
Base not seen				-----Thrust/Fault-----
Cretaceous-Upper Jurassic	Ophiolite complex			<u>Zipu Formation</u> Marine sediments (shale, phyllite, greywacke, iron-rich sediments, chert and limestone with radiolaria and coccoliths), volcanics (basalt, spilite, volcaniclastics),metabasics greenschist, glaucophane schist/ glaucophane- bearing metachert, eclogite), layered cumulate sequence (peridotite, pyroxenite, gabbroids, plagiogranite, anorthosite), and peridotite tectonite and serpentinite associated with deposits of podiform chromite and nickleferous magnetite, minor Cu-Mo sulphides associated with late felsic intrusions and some dolerite dykes
Base not seen				-----Thrust/Fault-----
Pre-Mesozoic (?)	Naga Metamorphic complex			<u>Nimi Formation</u> Weakly metamorphosed limestone, phyllite, quartzite and quartz sericite schist <u>Naga Metamorphics</u> Mica schist, granitoid gneiss and feldspathic metagreywacke with tectonic slices of ophiolite in variable dimensions

Disang Group

More than half of Nagaland's surface is covered by the Disang Group of rocks. The Disang are represented by thick beds of splintery shale with intercalations of sandstone and siltstones of greywacke composition. This flysch facies, which range in age from the Upper Cretaceous to the Eocene, is further subdivided into two distinct formations, a basal argillaceous and an upper arenaceous horizon designated as Lower and Upper Disang formations respectively (Sinha et al., 1982). The Disang shales are prone to spheroidal weathering and the development of concretions. The formation is shaly towards the basal part, while coarse-grained layers are more abundant higher up. Shale pellets are seen parallel to the bedding (Devdas and Gandhi, 1986; Sarma, 1985). The Disang shale is carbonaceous to very carbonaceous (Thong and Rao, 1999). An unconformity between the Lower and Upper Disang is indicated by the conglomerate bed between them. The unconformity reveals that the Disang sediments underwent folding and low-grade metamorphism as a result of orogenic activity.

Disang-Barail Transitional Sequences

The Disang-Barail Transitional Sequences (DBTS) is made up of a thick heterogeneous succession of 80-100 metres thick sand-mud lithology. The succession's sand-silt unit contains multiple alternations of thin, flaggy, fine-grained sandstone and silty/sandy shale. The thickest sandstone beds are almost 1m thick.

Barail Group

In the Assam shelf and Schuppen Belt, the Barail Group is composed of the oldest Laisong Formation, the middle Jenam Formation, and the youngest Renji Formation, while it is undifferentiated in the Inner Fold Belt. The upper part is composed of medium-grained sandstones with shale intercalations and thin coal bands. According to Nandy (2017), the Barail rocks' extensive coal seams indicate that there was a great supply of sediments with shallow water deposition. The uplifted island arc due to the Indo-Myanmar Orogen produced the tuff and volcanogenic debris found in the Barail sediments. They are observed along the western margin of the state, in the eastern regions of Nagaland and in the south of Kohima.

Jopi Formation

The Jopi Formation is thought to be the equivalent of the Barail Group. The Jopi Formation occurs unconformably on top of the Naga Ophiolite suite of rocks, occupying

various topographic levels. It is composed of a thick pile of polymictic conglomerate-grit-pebbly and cobble-like sandstone, greywacke, and shale in an alternating and repeated sequence. The thickness of the individual cycles ranges from less than a metre to more than ten metres, with the overall thickness of the formation exceeding 600 metres. The succession grades upward into grit, lithic greywacke, siltstone and shale. The sandstone gradually become arkosic towards the top.

Surma Group

The Surma Group of rocks are exposed in the Belt of Schuppen as a series of long, narrow strips. These Surma rocks are also found in the core of the Kohima Synclinorium (DGM, 1978). Surma rocks in Nagaland are of Lower Miocene age. It is composed of alternating succession of grey laminated shale, sand, and conglomerate. The overall thickness ranges from 300 to 1250 m. The Surma is subdivided into the Bhuban and Bokabil Formations. Of these two, the former is characterised by the presence of some conglomerates.

Tipam Group

The Tipam Group of rocks unconformably overlie the Surma rocks. The unconformity is, however, not clear in Nagaland. The Tipam rocks are made up of a sequence of massive sandstones that are highly friable and contain subordinate clay and shale. The rocks are characterised by multi-storied, channelled false-bedded sandstones and are generally coarse-grained, occasionally gritty and ferruginous. The Tipam Group is composed of two Formations: older Tipam Sandstones and the younger Girujan Clays. Tipam Sandstones are exposed in the Belt of Schuppen.

Namsang Formation

The Namsang Beds of the Dupitila Group lie unconformably over Girujun Clays and are found in the northern area of the Schuppen Belt. These Mio-Pliocene strata are composed of sandstone, conglomerate, grit, mottled clay, lignite pebbles and lenticular lignite seams. The thickness ranges from 400 to 1080 m.

Dihing Formation

The Dihing Formation consists mostly of unconsolidated mass 0f boulders and pebble beds with clays and sands lying unconformably over the Tipam Group and

Namsang beds. The Dihing Formation rocks are well-developed in Nagaland along the western margin of the Schuppen Belt.

Alluvium and high level terraces

The alluvium and high-level terraces occur in the western part of Nagaland. The high-level terraces are dominantly made up of boulder beds with gravels and coarse sands and unsorted clays. The clays are of different types namely gravely clay, sandy clay, carbonaceous clay, and silty clay. The older alluvium covers the north-eastern tract of Naga-Patkai ranges while the newer alluvium covers the western border of Nagaland.

2.4 GEOLOGY OF THE STUDY AREA

Tectonism has caused large-scale folding and faulting in the study area that has resulted in severe fracturing and crumbling of the rocks. Folding has also led to the formation of anticlines and synclines at places in the rocks which have been further altered by geomorphic processes. Neotectonic activity has given rise to slope instability in the area. Tectonic activity plays an important role in forming drainage patterns and regulating river behaviour (Vaidyanadhan, 1971; Sinha-Roy, 2001). The lineaments in the study area were delineated by using a satellite image (LISS III) and several lineaments were found to have NW-SE trend which is oblique to the regional NE-SW trend in the Belt of Schuppen to the north and the ophiolite complex to the south of Kohima. This orientation indicates that the delineated lineaments in the area are structurally controlled. The geological map of the study area is shown in Fig. 2.1.

The study area may be divided into two broad topographic units. These include the highly mountainous terrain fringing the south of Kohima town and the comparatively low denuded hills of the rest of the town. The southern fringe of high mountains is the area covered by the Barail sediments which are dominantly made up of sandstones and have dense forest areas. The northern and central part of the study area is made up of the lower hills which are covered by the Disang sediments and are more or less devoid of vegetation. The area is primarily being used for human habitation.

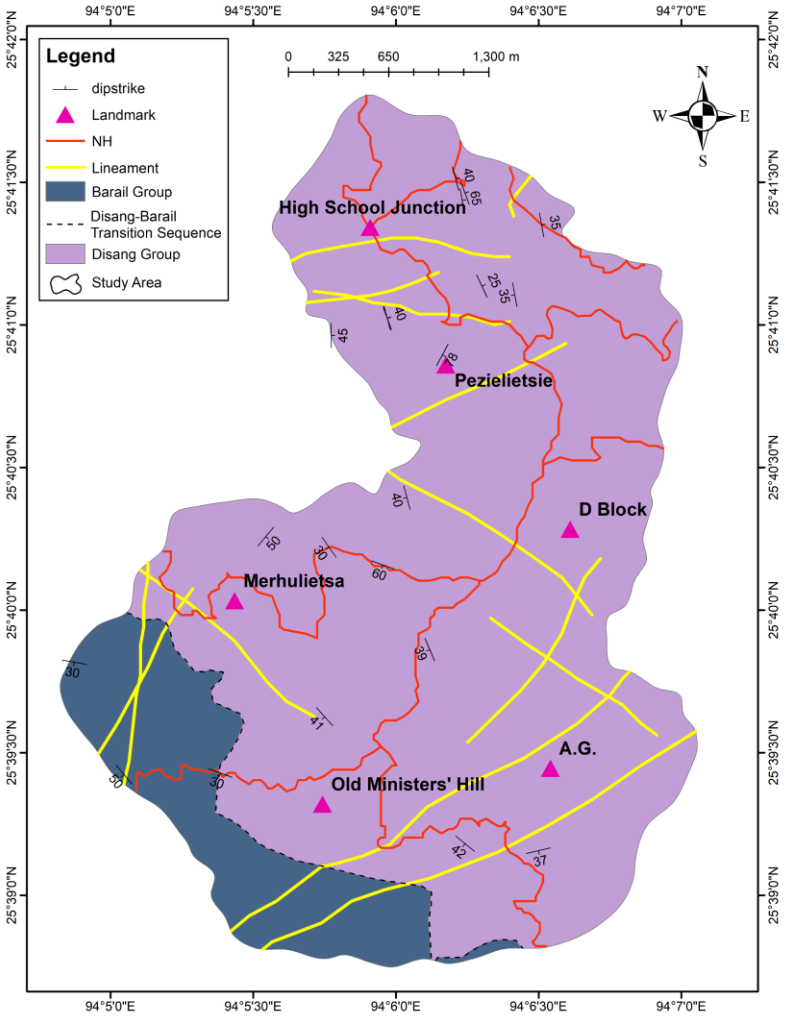

Fig. 2.1: Geological map of the study area (Modified after GSI, 2015)

Kohima town lies within the Kohima Synclinorium of the Inner Fold belt. The Tertiary sedimentary rocks in this synclinorium range in age from Upper Cretaceous to Recent and trend along the linear NNW-SSE ridge to form an important water divide zone that is related to the town's radial drainage pattern (DGM Report, 1978). The stratigraphic succession is characterized by the oldest Disang Group followed by the Disang- Barail Transitional Sequences and the younger Barail Group of rocks. The stratigraphic succession of the study area is shown in Table 2.2.

Table 2.2: Stratigraphic succession of Kohima town (after Mathur and Evans, 1964; Rajkumar et al., 2019)

Group	Formations	Age	Lithology
Barail Group	Renji/ Tikak Parbat (Upper Barail)	Late Oligocene to Late Eocene	Primarily hard, massive sandstones.
	Jenam/ Baragoloi (Middle Barail)		Mainly shales with some bedded sandstones and carbonaceous shale horizons.
	Renji/ Naogaon (Lower Barail)		Intercalation of bedded sandstone with relatively thin siltstone and shale beds. Horizon is characterized by trace fossils and invertebrates, plant/ leaf impressions.
Upper Disang/ Lower Barail Transition Sequences which is gradational as well as (local) tectonic contact			
Disang Group	Upper Disang	Late Eocene to Late Cretaceous	Dark grey splintery shales with intercalations of thin siltstone and sandstone beds
	Lower Disang		Dark grey to black shale. Shales slightly metamorphosed to phyllites and slates.

Disang Group

The Disang Group of rocks is the most common rock in the Inner Fold Belt of Nagaland. The Disang Group range in age from Upper Cretaceous to Middle Eocene and is mostly argillaceous (Krishnan, 1982). This group comprises flysch sediments which are classified as geosynclinal facies. It is predominantly represented by thick monotonous sequences of splintery shale, that is grey, khaki grey, or black in colour, with intercalations of siltstones and fine-grained sandstones (Mallet, 1876; Mathur and Evans, 1964). Due to the weathering of shales and their compression, crumpling, and shearing, surface instability also happens. The sandstones are only a few centimetres thick at the base, but they gradually pass upward and become prominent at the top and laterally into the Barail. The Disang shales are finely laminated and commonly exhibit curved or concentric surfaces. Carbonaceous shales intercalated with massive shales and occasionally fine-

grained sandstones also occur in certain areas, especially at the junction of faults within the Diasng. The Disang beds are commonly crumpled and squeezed.

Ferruginous concretionary structures and nodules are common, especially in areas of red ferruginous soil. Pyrites and brine springs are also common. Rao (1983) proposed some parts of the Disang Group to be of brackish water and tidal flat environment of deposition. Its sedimentary record indicates the continuity of a shelf environment, where quick subsidence prompted the accumulation of a large mass of Palaeogene rocks.

The northern part of the research area is covered by highly weathered, splintery, grey, and carbonaceous shale. The shale is finely laminated, and their splintery nature make it susceptible to weathering. Within the Disang shale, compositional variations of black/carbonaceous shale and grey shale (sometimes with iron concretions) are present. Around Naga Bazaar, Daklane and the down slope of High school areas, carbonaceous shales can be found. While the grey shale is mainly found exposed towards the eastern and south eastern parts of Kohima town around Kitsubozou, Chandmari, A.G. colony, and Police new reserve (GSI, 2015). Some field photographs taken in the Disang beds are shown in Fig. 2.2.

Fig. 2.2: a, b) Jointed Disang shale exposure and shale lens at PWD colony, Kohima

c) Inclined Disang rock exposure at Cathedral, New Ministers' Hill colony, Kohima

d) Bed reading taken along the Disang sandstone bed at Upper Bayavu colony, Kohima

Disang-Barail Transition sequence (DBTS)

There is a transitional sequence between the older Disang and the younger Barail group called the Disang-Barail Transitional sequence (DBTS) belonging to the Upper Eocene age (Pandey and Srivastava, 1998). The rocks of the DBTS consist of mixed lithology of silt, shale, and very fine to fine-medium sand fractions.

The Disang-Barail Transition Sequences in Nagaland is represented by the 80-100 m thick succession of heterogeneous sand-mud lithology that lies over the repetitive argillaceous Disang sediments and continues upward into the predominantly arenaceous Barail Group of rocks. The succession's sand-silt units are characterized by frequent alternations of fine and occasionally medium-grained sandstones, thin, flaggy, well-cemented siltstones, and sandy or silty shales. The first appearance of multistoried sandstones, which define the base of the Barail Group, is used to distinguish the Disang Group from the Barail Group. Although this method is useful for lithostratigraphic subdivision, there are some practical limitations (Devdas and Gandhi, 1986). The similarities between the lower units of the Laisong shales and the underlying Disang shales have also been identified by Evans (1932). The precise delineation of the contact is not possible due to the rapid alternation of 3–4 metres of sandstones and shales near the base of the Laisong Formation.

Barail Group

The younger Barail Group of rocks is dominantly arenaceous and of Oligocene age (Krishnan, 1982). The Barail Group of rocks is located to the south of Kohima Town. The Disang Group and DBTS are conformably overlain by this arenaceous suite of rocks, which consists of sandstones intercalated with thin beds of siltstone and shale, representing flysch facies. A series of faults, thrusts, fractures, and joint sets affect the rocks in and around the township.

The Barail Group of rocks dips with a moderate dip amount towards the southwesterly direction and trends in the NW-SE direction. Fresh bedrock exposure is

quite rare in Kohima because of the urban built-up. Due to the splintery nature of the shale and phyllites which is prone to weathering, reddish brown and black-coloured soil is formed above the bedrock. The highly weathered shales with intercalations of sandstone/siltstone make the local streams vigorously erode the base and toes of their channels and groundwater flow in such areas. According to Gaur and Chakradhar (1985), the Barail Group has compact and well-bedded sandstones that display a variety of colours and herringbone cross beddings that indicate periodic fluctuation in the flow direction of the transportation medium.

The Barail may be divided into three formations in the south and south-west of Nagaland including Laisong, Jenam and Renji. In the intermediate hills of Nagaland, they are recognized as the Tikak Parbat, Baragolai, and Naogaon Formations. The Laisong Formation consists of hard, grey and thin-bedded sandstones alternating with hard, silty, and sandy shales with occasional intercalations of carbonaceous shale, calcareous and ferruginous shales. The Jenam Formation has gradational contacts with the Laisong and Renji Formations. It is predominantly composed of grey and carbonaceous shales with silts and thin to massive bedded sandstones. The youngest member of the Barail is the Renji Formation which extends towards the southwest of Nagaland and beyond into Assam and south into Manipur. They are hard, massive, ferruginous bedded and are intercalated with minor shales. Just south of Kohima town, they form a thick forested range with high peaks such as Japfü (3048 m) which is the second-highest mountain in Nagaland.

2.5 TECTONIC SETTING OF THE STUDY AREA

The oblique subduction and subsequent collision of the Indian and Central-Eastern Myanmar continental blocks during the Late Cretaceous-Eocene period are related to the geological history of the Naga Hills. Disang sediments were deposited in a deep, linear arcuate basin that formed next to the leading edge of the subducting Indian plate. The Disang Group of rocks is made up of an accretionary prism and related sediment that was deposited at the east end of the subduction zone. The source material appears to have come from the Ophiolite belt and the Myanmar Volcanics (Pandey, 2005).

Tectonic impulses brought about by changing plate interaction caused swallowing of the basin which then caused the deposition of heterogeneous transitional lithology, the Disang Barail Transitional Sequences (DBTS). Indo-Burman Ranges (IBR) were raised as a result of the suturing of the Myanmar and Indian plates. To the west of the uplifted

IBR, molasses basins developed throughout the Oligocene-Miocene and formed sites for the deposition of Barail sediments. Most of the Barail rocks are marine, while a few are fluvio-marine.

2.6 HYDROGEOLOGY

Hydrogeologically, Nagaland can be differentiated into three formations which are briefly discussed below:

Consolidated formations

Consolidated formations are found in the high hill ridges towards the south-eastern region of Nagaland, along the Myanmar border. The rocks are highly fractured and have many faults, joints, fissures, fractures and shear zones where they serve as potential zones for the development of groundwater. However, due to the inaccessibility of the terrain, as well as the difficulty of organising heavy duty water well drilling rigs, the area's groundwater resources development remains unexplored.

Semi-consolidated formations

Semi-consolidated formations are particularly common on moderate to high hill ridges. They are found in the rocks of the Disang Group, Barail Group, Surma Group, Tipam Group and Dihing Group. The Disang and Surma Groups are mostly composed of argillaceous rocks, whereas the Barail and Tipam Groups are of arenaceous rock layers. The Disang formation, which is highly fractured, splintery and sheared, has been found to have the greatest potential for groundwater production in the hilly areas.

Unconsolidated formations

The unconsolidated formations are found in low-lying plain areas of Nagaland with narrow, intermontane valleys that occur along the foothills bordering the upper reaches of the Brahmaputra flood plains of Assam. The valleys are generally structurally controlled, and the rock types are mostly of unconsolidated nature comprising of the assemblages of boulder, cobble, pebble, gravel, sand, silt and clay indicating potential aquifer zones. The unconsolidated formations serve as potential valley areas for groundwater development in Nagaland.

2.7 HYDROLOGICAL DATA

2.7.1 Precipitation

The rainfall data was collected from the Soil and Water Conservation Department, Government of Nagaland for a period of 14 years from 2008 to 2021. There has been a decrease in the trend of annual rainfall from 2017 to 2021. The annual rainfall during the year 2021 is found to be the least during the past 14 years with 1105.10 mm. The rainfall data is presented in Table 2.3.

Table 2.3: Rainfall data of Kohima (Source: Soil and Water Conservation Department, Government of Nagaland, 2022)

Year	Jan	Feb	March	April	May	June	July	Aug	Sep	Oct	Nov	Dec	Annual Rainfall in mm
2008	43.8	5	54.1	35	170.7	398.4	453.1	393.5	320	12.57	0	0	1886.2
2009	0	10.6	24.6	32.1	138.4	205.7	277.2	388.2	216.8	129.4	0	0	1423.00
2010	1.4	8.2	56.9	60.8	119.5	347.1	53.76	464.3	226.5	162	2.1	21.2	1523.8
2011	9.8	5.2	56.8	34.9	265.6	308.2	437.7	239.9	336.3	31.7	9.7	0	1735.80
2012	33	15.2	49.2	81.5	130.8	218.8	295.7	258.7	123.6	124.3	40.2	0	1371.00
2013	0	0	45.2	115	332.5	298.2	350.9	268.5	226.3	112.1	0	0	1749.10
2014	0	16.8	31.8	77.6	145.5	139	332.4	350.6	231.4	58.2	0	0	1383.30
2015	25.8	18.4	18.4	201	50.3	224.1	316.4	374.1	212.2	74	2.1	5.6	1522.10
2016	4.3	5.7	36.2	97.8	243.8	317.2	255.2	256.4	242.7	204.2	72.8	1.4	1737.70
2017	2.2	0.8	93	164	234.6	326.9	482.1	250.4	340.6	204.2	5.4	31.9	2135.80
2018	13.2	3.6	45	128	279.2	338.1	568.4	359.4	139.6	85.2	1.2	65.4	2025.90
2019	80.6	15.4	58.2	83	175	208.1	286.4	355.9	266.6	212.6	37.2	0	1779.00
2020	35.8	9.4	21	130	181.6	319.6	328	215.6	154	237.6	62.2	0	1695.00
2021	0.3	0	25.2	42.4	78.2	171.6	187.4	233.2	241.8	111.4	0	13.6	1105.10
Average	17.87	8.16	43.97	91.62	181.84	272.93	330.33	314.91	234.17	125.68	16.64	9.94	1648.05

2.7.2 Depth to water level measurement (DTWL)

The depth to water level (DTWL) measurements which is the depth of water level in wells from the local ground surface have been carried out at 50 locations spread over the study area. The depth to water level data was recorded during pre-monsoon and post-monsoon periods (2019 and 2021) and plotted according to the well locations. All groundwater samples were collected from shallow aquifers (<50 m). The DTWL table is shown below in Table 2.4.

Table 2.4: Depth to water level data of groundwater samples (mbgl)

Sample no.	2019 Pre-monsoon (mbgl)	2019 Post-monsoon (mbgl)	2021 Pre-monsoon (mbgl)	2021 Post-monsoon (mbgl)
A1	4.26	3.05	3.17	2.11
A2	2.25	1.55	1.86	1.23
A3	2.13	2.77	6.10	4.34
A4	3.19	1.56	4.57	2.45
A5	1.88	1.25	3.05	2.76
A6	3.40	2.65	3.90	2.64
A7	5.47	1.37	3.69	1.98
A8	3.04	2.01	3.05	2.87
A9	2.98	2.23	2.74	2.67
A10	22.80	19.02	23.01	20.73
A11	10.31	3.60	10.94	4.53
A12	1.82	1.92	1.98	1.89
A13	2.43	2.74	3.66	2.37
A14	10.94	6.86	11.19	8.43
A15	1.88	1.01	3.66	2.54
A16	9.70	6.89	9.75	7.91
A17	9.73	8.72	10.06	9.21
A18	6.08	5.00	6.10	5.92
A19	6.51	4.60	6.10	5.86
A20	5.47	2.16	2.68	2.19
A21	0.61	0.43	0.73	0.56
A22	6.51	3.05	6.19	4.53
A23	3.34	1.01	4.88	3.46
A24	6.87	6.13	8.53	7.93
A25	8.76	4.42	7.76	5.67
A26	5.17	4.27	4.30	4.08
A27	10.79	4.30	9.66	7.34
A28	6.08	2.41	7.16	4.37
A29	3.34	2.35	4.08	3.85

A30	3.34	2.07	2.62	2.19
A31	12.77	12.53	13.11	12.87
A32	8.00	7.01	7.50	6.54
A33	4.74	4.88	4.97	4.83
A34	5.32	5.67	5.79	5.66
A35	3.28	1.22	3.35	2.13
A36	11.28	6.10	7.13	6.12
A37	6.08	6.46	7.50	7.02
A38	9.88	9.48	10.06	9.76
A39	6.69	5.18	6.10	5.89
A40	7.90	6.25	9.45	8.25
A41	2.89	2.96	3.05	2.65
A42	1.79	1.25	2.44	1.67
A43	1.76	2.65	5.46	4.24
A44	5.29	3.23	6.95	4.86
A45	10.88	9.08	11.06	10.72
A46	4.80	3.08	3.05	2.87
A47	5.78	2.96	4.08	3.56
A48	6.99	6.28	7.07	6.89
A49	5.08	3.60	7.65	4.65
A50	3.04	3.66	3.75	3.23

The DTWL measurements taken in pre-monsoon (2019) is geospatially plotted in Fig. 2.3 which shows the occurrence of groundwater at shallow aquifers (<50 m). The very shallow groundwater occurs in the south-western, north-eastern and small pockets around the central parts at depths between 0-5 mbgl (meters below ground level). The major part of the shallow groundwater with depths ranging between 5.01-10 mbgl is found all over the study area. The water at a depth between 10.01-15 mbgl occurs in small pockets over the western, south-eastern and very small pockets in the northern area. Groundwater depths below 15 mbgl occurs in the western part.

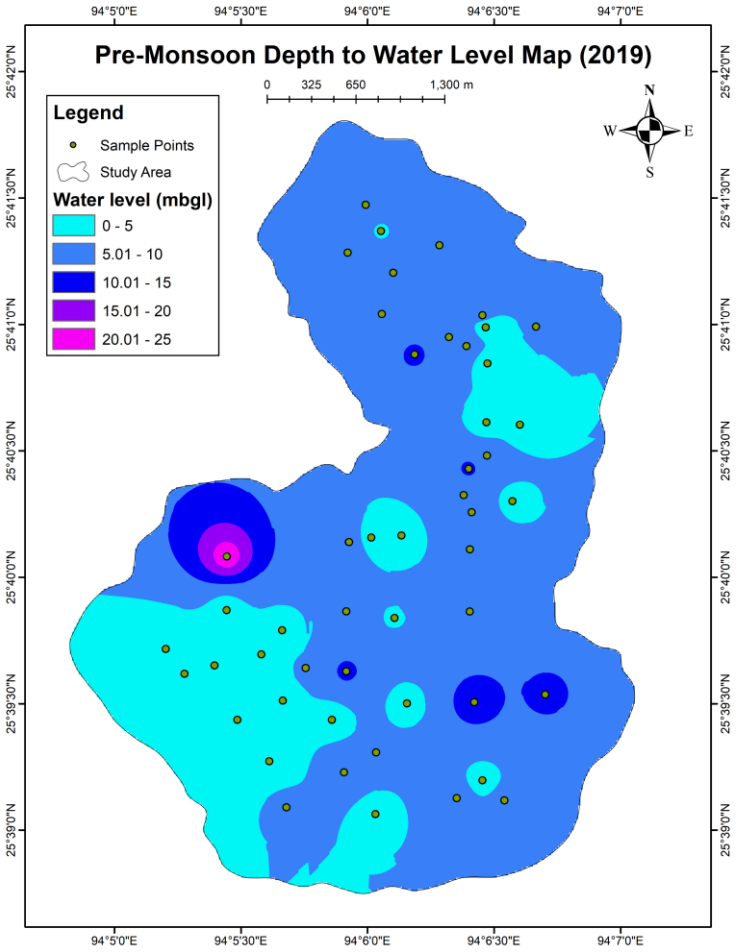

Fig. 2.3: Depth to water level map of pre-monsoon 2019

The DTWL measurements taken in pre-monsoon (2021) shown in geospatial Fig. 2.4 shows the occurrence of groundwater at shallow aquifers (<50 m). The very shallow groundwater occurring at depths of 0-5 mbgl is found in the south-western and small pockets scattered around the northern, central and southern parts. The majority of the shallow groundwater (5.01-10 mbgl) is found all throughout the study area. The groundwater occurrence at a depth between 10.01-15 mbgl is found scattered in small pockets in the western, south-eastern and central parts. Groundwater depth below 15 mbgl occurs in the western part only.

The deepest groundwater level in pre-monsoon of 2019 is at a depth of 22.8 mbgl and the deepest pre-monsoon DTWL in 2021 is 23.01 mbgl. The pre-monsoon groundwater level with respect to the ground surface increased in the year 2021. There is not much significant difference in DTWL measured in 2019 and 2021 except that the groundwater level in the northern area occurs at a shallower depth in 2021 pre-monsoon than in 2019.

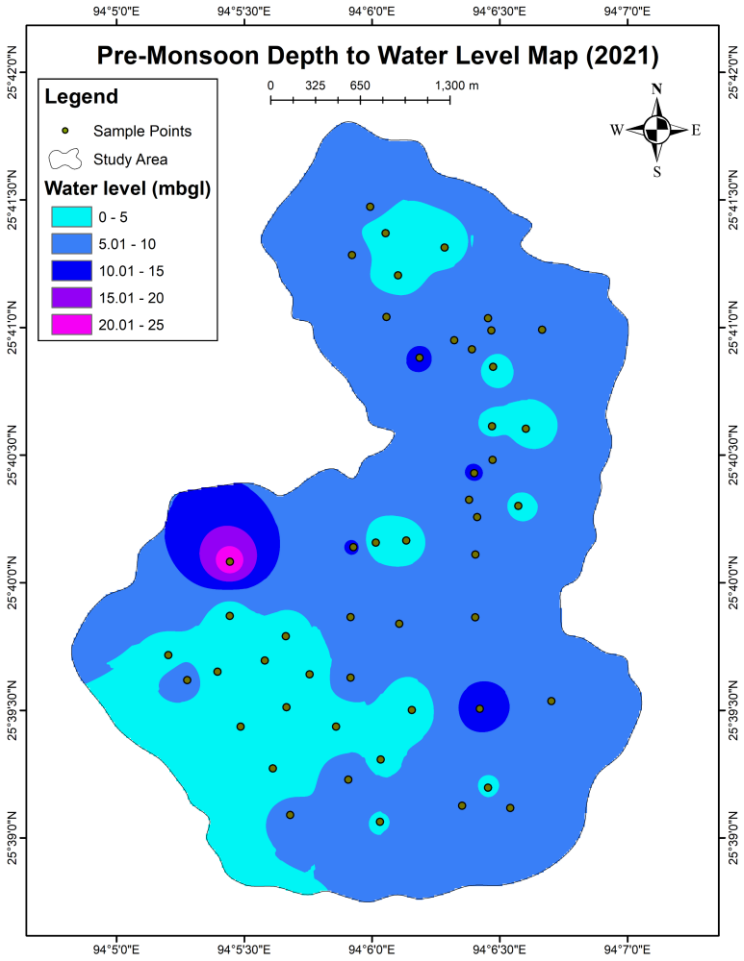

Fig. 2.4: Depth to water level map of pre-monsoon 2021

The DTWL measurements taken in post-monsoon (2019) show the occurrence of groundwater at shallow aquifers (<50 m) which has been geospatially plotted in Fig. 2.5. The majority of the groundwater in the post-monsoon of 2019 falls under very shallow groundwater with depths lower than 5 mbgl. The water at a depth between 5.01-10.01 mbgl occurs mostly in the western and eastern parts. The water at a depth between 10.01-15 mbgl occurs in very small pockets in the western and south-eastern areas. DTWL below 15 mbgl occurs in the western part.

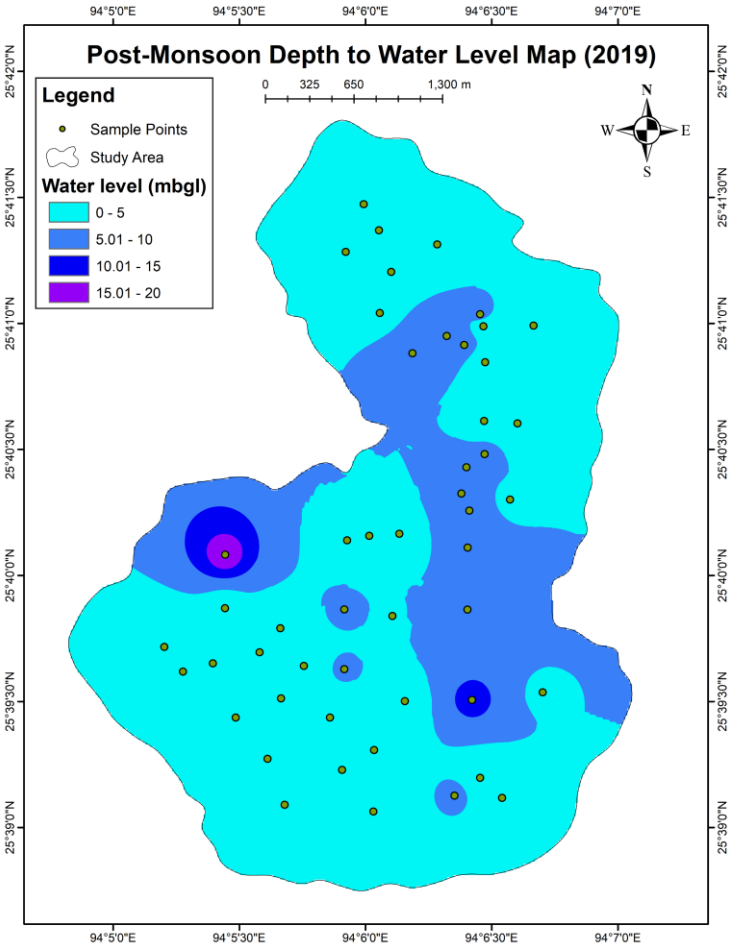

Fig. 2.5: Depth to water level map of post-monsoon 2019

The DTWL measurements taken in post-monsoon (2021) show the occurrence of groundwater at shallow aquifers (<50 m) which has been geospatially plotted in Fig. 2.6. The very shallow groundwater occurring at depths of 0-5 mbgl is mostly found in the south-western area and also scattered around in the northern part. The post-monsoon groundwater of 2021 witnessed reduced size of very shallow groundwater occurrence in the northern and southern parts with a significant occurrence of groundwater at depths between 5.01-10 mbgl which is found scattered all throughout the study area. The groundwater occurrence at a depth between 10.01-15 mbgl is found scattered in very small pockets in the western and south-eastern parts. DTWL of groundwater below 15 mbgl occurs in the western part only.

The deepest groundwater level in 2019 post-monsoon is found at a depth of 19.02 mbgl and the deepest post-monsoon DTWL in 2021 is at 20.73 mbgl. There is not much significant difference in DTWL between 2019 and 2021 post-monsoon measurements.

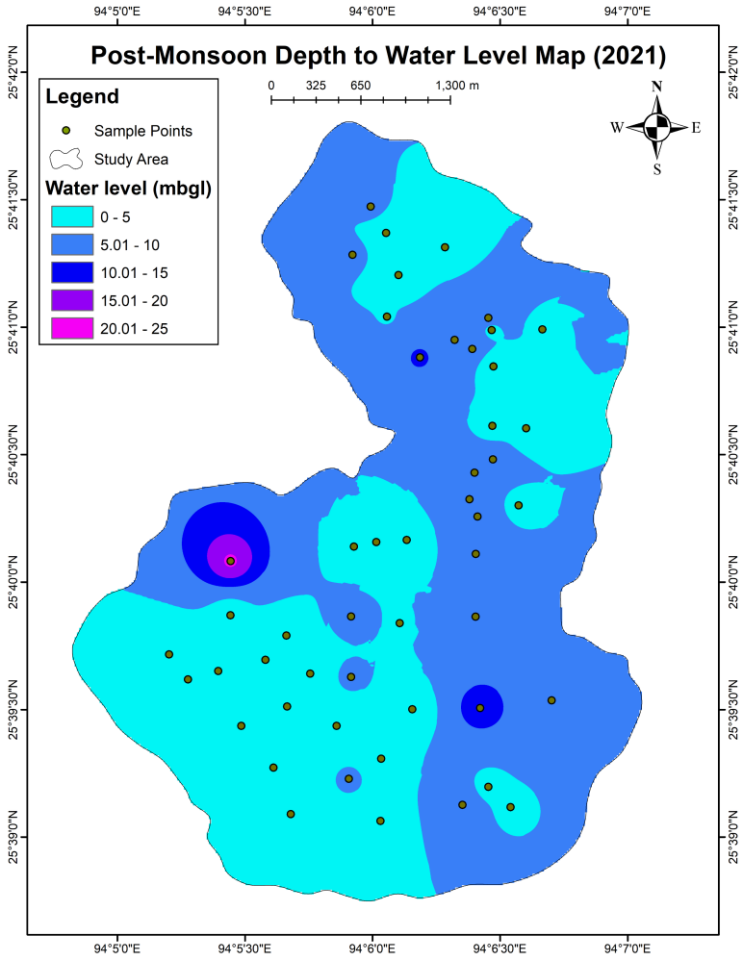

Fig. 2.6: Depth to water level map of post-monsoon 2021

From both the pre-monsoon and post-monsoon DTWL maps, the deepest groundwater level is found in the western part and the very shallow groundwater level (0-5 mbgl) is found in the southwestern area in both seasons.

2.7.3 Annual groundwater level fluctuations

The groundwater level fluctuation is recorded between pre-monsoon and post-monsoon seasons during the 2019 and 2021 assessments and shown in Figs. 2.7 and 2.8 respectively. The changes in the water level from the fluctuation maps indicate that the groundwater level is either rising or going down. The fluctuation map of pre-monsoon and post-monsoon 2019 with a fluctuation range from -0.86 to 6.7 m is shown in Fig. 2.7. Majority of the area is showing less water level fluctuation in the range of 0.01-4.81 m. The positive value in water level fluctuation indicates that there is a rise in groundwater level in post-monsoon compared to pre-monsoon. There is a negative value in water level fluctuation in some very small pockets scattered mostly around the central part of the study area. The fall of groundwater level in these areas found during the post-monsoon

of 2019 could be attributed to over-exploitation of water where discharge has become greater than recharge of groundwater.

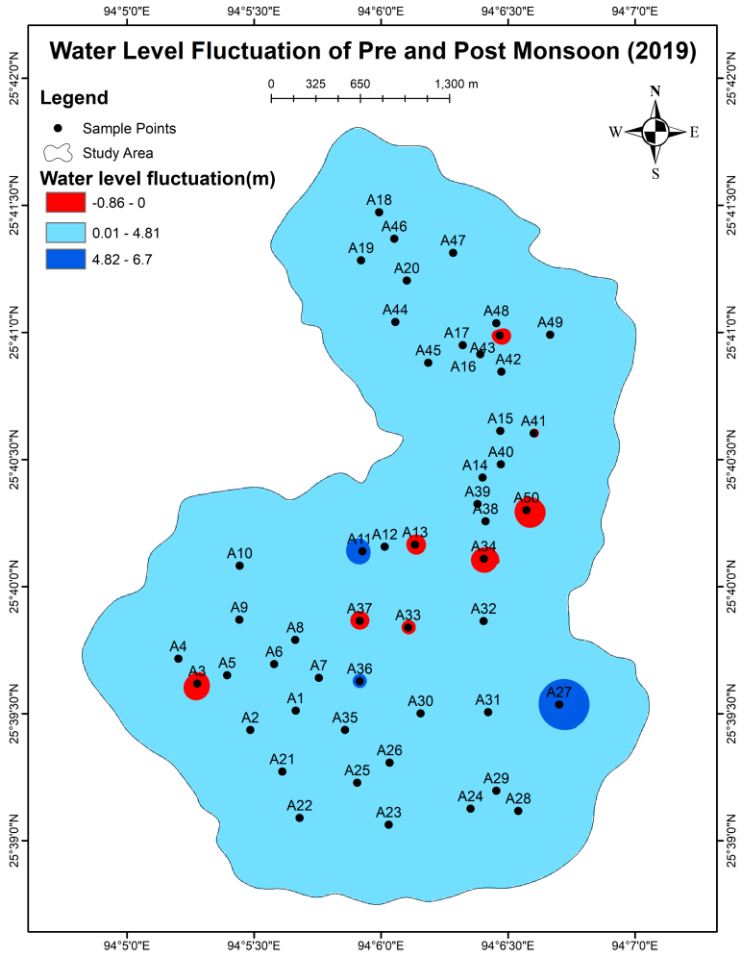

Fig. 2.7: Groundwater level fluctuation map of 2019

The fluctuation map of pre-monsoon and post-monsoon in the year 2021 is given in Fig. 2.8 which shows a fluctuation range from 0.07 to 6.4 m. The majority of the study area is showing less water level fluctuation in the range of 0.07- 1.65 m. The whole study area shows a positive value in water level fluctuation which indicates that there is a rise in groundwater level in post-monsoon as compared to pre-monsoon in the year 2021.

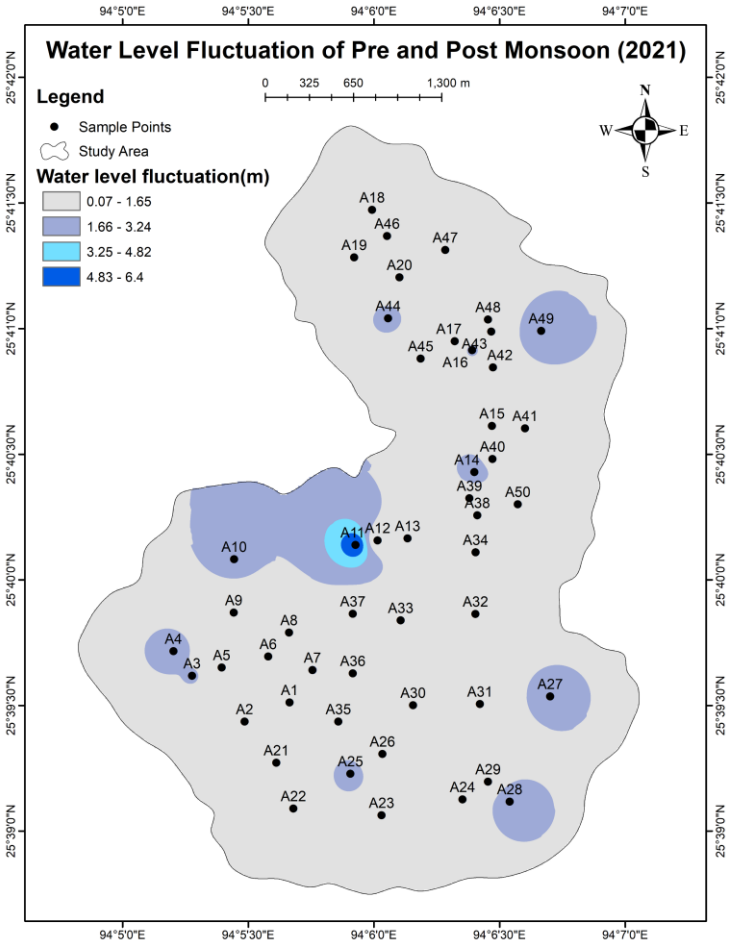

Fig. 2.8: Groundwater level fluctuation map of 2021

2.7.4 Seasonal groundwater level fluctuations

The seasonal groundwater level fluctuation maps were also prepared for both the pre-monsoon periods of 2019 & 2021 and for the post-monsoon periods of 2019 & 2021. The water level in the pre-monsoon seasons indicates a fluctuation range from -3.97 to 4.15 m which is shown in Fig. 2.9. The pre-monsoon groundwater level fluctuation map indicates an increase of water level in the pre-monsoon year of 2021 in the north, south and more towards east along the south-eastern part of the study area with fluctuation in the range of 0.01- 4.15m. The major part of the study area in the east, west and south-east more towards the south is showing a fall in groundwater level in the year 2021 in pre-monsoon with fluctuation in the range of -3.97 to 0 m.

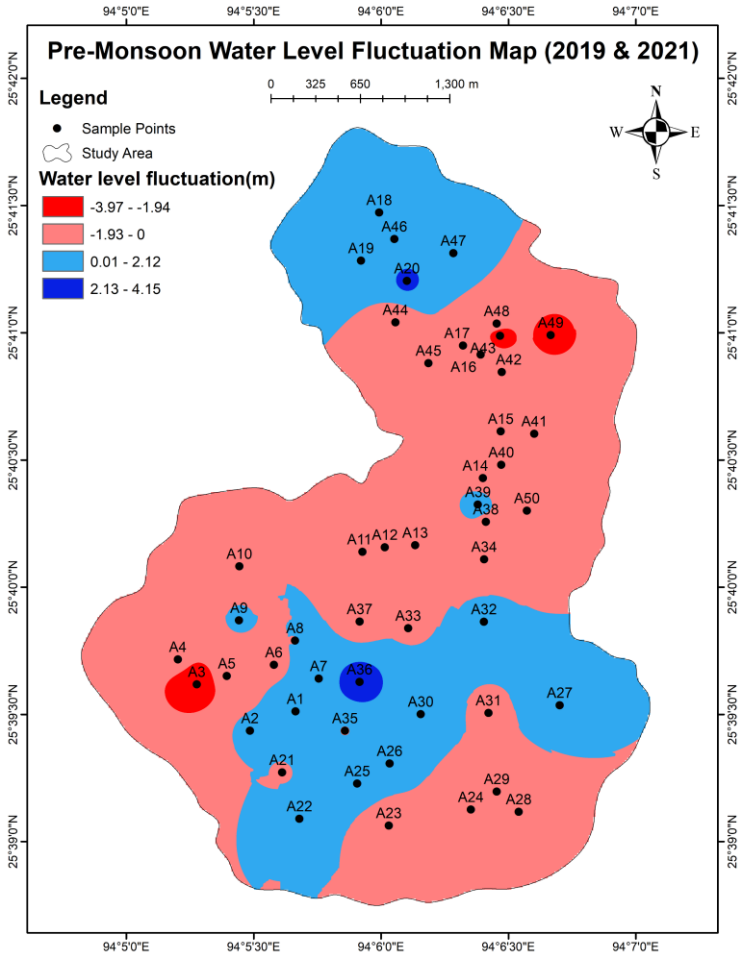

Fig. 2.9: Pre-monsoon groundwater level fluctuation map

The post-monsoon seasonal groundwater level fluctuation map of 2019 & 2021 years is given in Fig.2.10. The water level in the post-monsoon seasons indicates a fluctuation range from -3.04 to 0.94 m. The fluctuation map of the study area in post-monsoon water level indicates that the increase of water level in the year 2021 post-monsoon is lesser compared to the year 2019 with fluctuation in the range of 0.01-0.94 m. The major part of the study area is showing negative fluctuation values with fluctuation ranging from -3.04 to 0 m. This implies that the recharge of groundwater in post-monsoon 2021 is lesser in comparison to that of post-monsoon 2019. The amount of rainfall in the year 2021 (Table 3.3) is very less and this could be the main reason for the decrease of groundwater level in the year 2021.

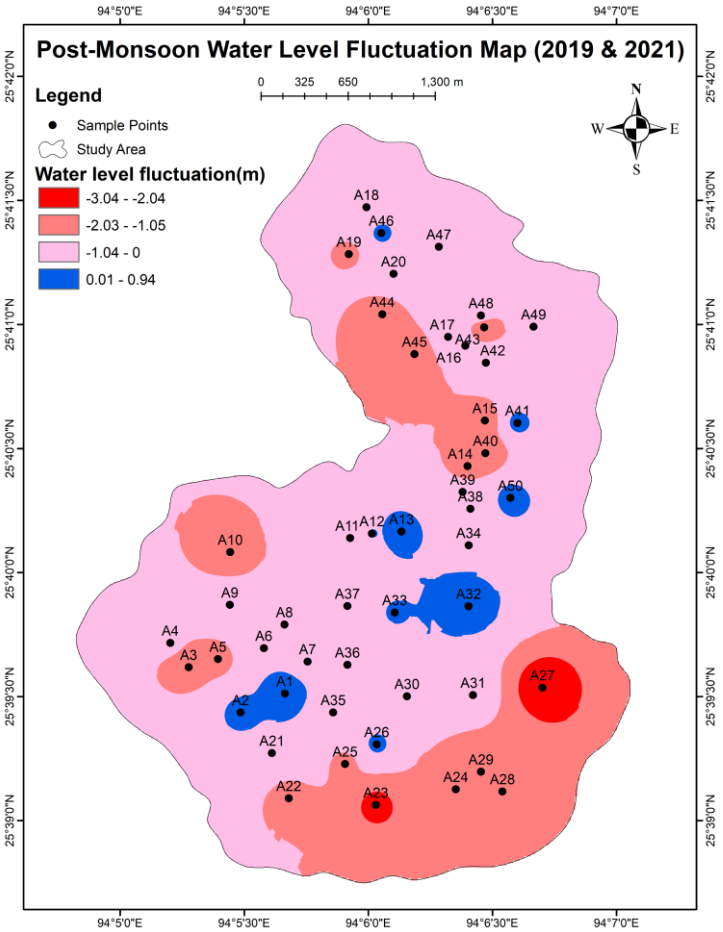

Fig. 2.10: Post-monsoon groundwater level fluctuation map

2.7.5 Interrelationship between topographic contours and groundwater table contours

Topographic contours and water table contours were generated by using IDW (Inverse Distance Weight) method in a GIS environment. The elevation points for both maps were collected from the field for four seasons as plotted in the maps (Fig. 2.11). The topography influence on the groundwater table was created by superimposing the groundwater table elevation over the topographic elevation. The contours have been plotted at an interval of 20 m. The water table and topographic elevation maps superimposed on one another showing how closely related and parallel most of the data sets are to one another revealing that the groundwater level followed the topographic elevation of the study area. The maps indicate the importance of topographic elevation which plays an important role in the groundwater flow.

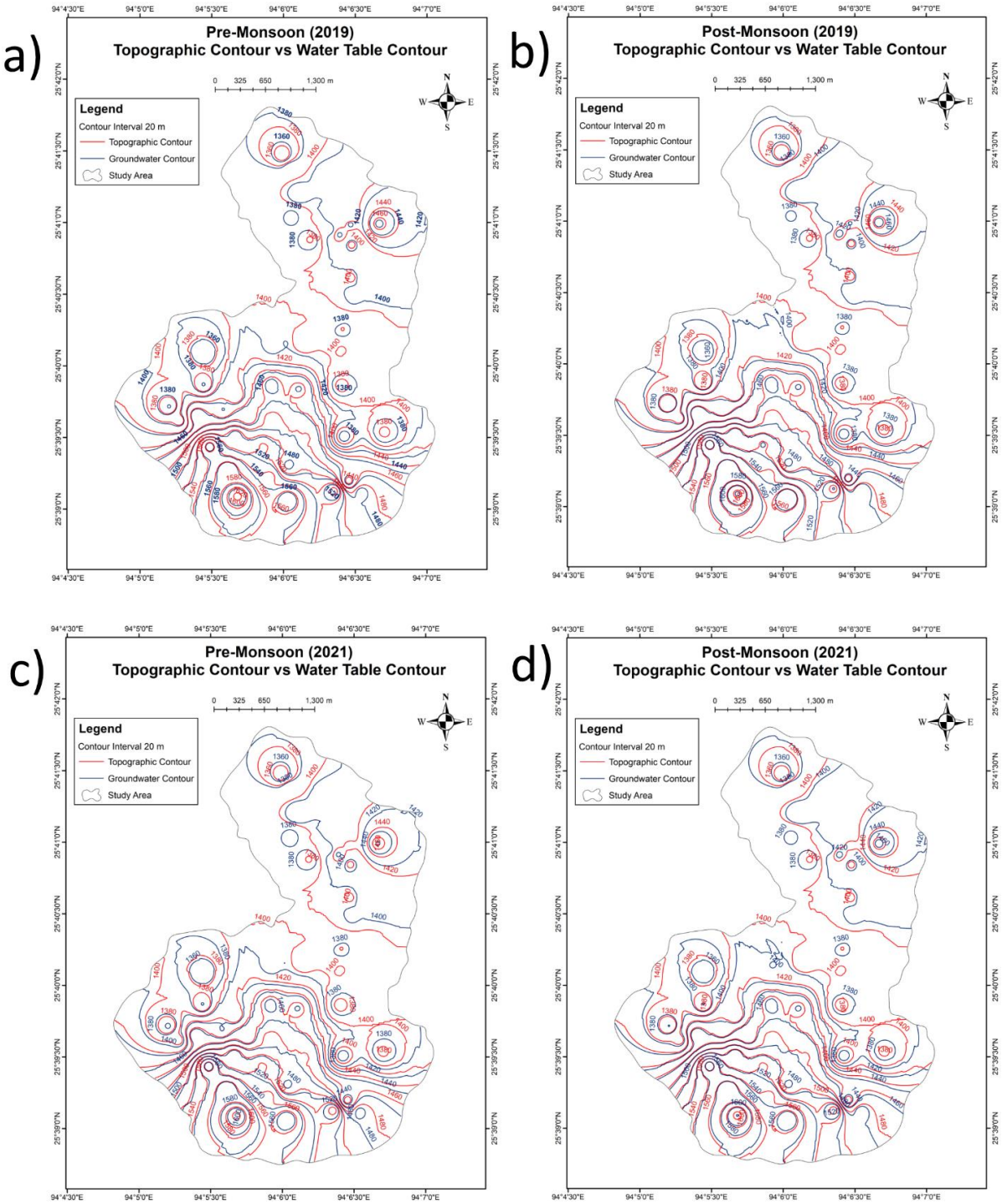

Fig. 2.11: Topographic contour versus Groundwater table contour maps of (a) Pre-monsoon 2019 (b) Post-monsoon 2019 (c) Pre-monsoon 2021 and (d) Post-monsoon 2021

CHAPTER 3
METHODOLOGY

3.1 INTRODUCTION

The methodology involves field investigations and laboratory work to study the geological and geochemical properties of groundwater. The methodology employed in the current research is given below

3.2 FIELD STUDIES

3.2.1 Hydrological fieldwork

The field studies include the study of geology and hydrogeology of Kohima town. A preliminary investigation of the study area was done before the samples were collected. The groundwater samples were collected from 50 locations (A1-A50) scattered in and around the main Kohima town for two seasons, i.e., pre-monsoon and post-monsoon seasons during the years 2019 and 2021 in accordance with (APHA 1998) guidelines. The samples could not be collected in the year 2020 because of COVID-19 pandemic.

Groundwater samples were collected in one-litre polyethylene water bottles. Before groundwater samples were collected, the bottles were carefully washed with distilled water. At the site, the bottles were cleansed with the sampling water before filling the bottles with groundwater. Each sample bottle was carefully marked with a marker and information about each sample was recorded. In the field journal, observations made at the site were recorded, including the groundwater table's depth from the surface and its location, elevation, and name. The samples were then transported to the lab for analysis while being protected from sunlight. (Chaurasia *et al.* 2018). Some of the field photographs were taken during water sampling and are shown in Fig. 3.1.

Fig. 3.1: a) A person fetching water for use at community well number A35 at PR Hill colony

b) Displaced well rings in well number A7 in a landslide-affected area at Lower Jail colony

c) Collecting water sample in polyethylene bottle from well number A10 at Lower Merhulietsa colony

d) Water sample collection from well number A22 at Old Ministers' Hill colony

3.2.2 Subsurface studies

The subsurface geological studies were done by using the Vertical Electrical Resistivity method and Schlumberger configuration. An efficient and often-used technique for locating groundwater potential zones and determining the quality of groundwater is geophysical prospecting. Additionally, it offers details on geological features like faults, joints, fissures, and fractures. The physical properties and composition of the subsurface geological units, level of weathering, thickness, and depth of the underlying bedrock are other factors that geophysical investigation can greatly influence. Five Vertical Electrical Sounding (VES) stations were taken in the study area. The coordinate locations are shown in Table 3.1. When performing VES in Schlumberger

configurations, the potential electrodes were set in place while the current electrodes were moved symmetrically on the outer edges. After the resistivity measurements, the current electrodes were then symmetrically placed further away from the centre point. The technique yields the resistivity depths.

Table 3.1 Location table of the VES stations

VES Stations	Location (Colony)	Coordinates
VES 1	Lower Forest	N 25° 39.697', E 94° 05.191'
VES 2	New Ministers' Hill (Cathedral)	N 25° 39.178', E 94° 06.248'
VES 3	D Block	N 25° 40.214', E 94° 06.451'
VES 4	Kenuozou	N 25° 41.033', E 94° 06.647'
VES 5	High School	N 25° 41.418', E 94° 05.926'

Fig. 3.2: a) Taking VES 1 data at Forest colony

b) Measuring the length of spacing for current electrodes from VES 2 at Cathedral

c) Noting the resistivity data from VES 4 data at Kenuozou colony

d) Measuring the resistivity data from VES 5 at High School colony

e) SSR-MP-ATS Resistivity meter instrument

3.3 LABORATORY STUDIES

Groundwater samples were collected during pre-monsoon and post-monsoon seasons from fifty locations in and around Kohima town (Table 3.2). According to standard procedures, the samples were analyzed in the laboratory for drinking water quality parameters (Bureau of Indian Standards, 2012).

Table 3.2: Location table of the groundwater samples

SAMPLE NO.	LOCATION (NAME OF COLONY)	TYPE OF WELL	COORDIN-ATES	ELEVA-TION (m)	WELL DEPT-H (m)	WELL DIAM-ETER(m)
A1	Agri Farm	Ring Well (Private)	N 25˚39.512′ E 94˚05.665′	1512	8.53	0.91
A2	Upper Agri	Ring Well (Private)	N 25˚39.436′ E 94˚05.486′	1571	12.80	0.91
A3	Upper Forest	Ring Well (Private)	N 25˚39.618′ E 94˚05.277′	1394	8.08	0.91
A4	Lower Forest	Ring Well (Private)	N 25˚39.716′ E 94˚05.203′	1362	7.04	0.91
A5	Forest	Ring Well (Private)	N 25˚39.651′ E 94˚05.395′	1455	3.54	0.91
A6	Lower Agri	Ring Well (Private)	N 25˚39.695′ E 94˚05.580′	1423	4.88	0.91
A7	Lower Jail	Ring Well (Private)	N 25˚39.641′ E 94˚05.756′	1446	6.34	0.91
A8	Upper Merhulietsa	Ring Well (Private)	N 25˚39.769′ E 94˚05.667′	1405	9.45	0.79

A9	Lower Merhulietsa	Ring Well (Private)	N 25˚39.870′ E 94˚05.443′	1362	8.38	0.91
A10	Lower Merhulietsa	Ring Well (Private)	N 25˚40.082′ E 94˚05.444′	1365	26.25	0.91
A11	Hospital	Ring Well (Community)	N 25˚40.139′ E 94˚05.927′	1404	10.94	0.91
A12	New Market	Spring (Private)	N 25˚40.157′ E 94˚06.015′	1402	1.98	0.91
A13	Daklane	Ring Well (Private)	N 25˚40.165′ E 94˚06.134′	1391	3.66	0.91
A14	Daklane	Ring Well (Private)	N 25˚40.429′ E 94˚06.400′	1400	11.58	0.91
A15	Naga Bazar	Ring Well (Private)	N 25˚40.613′ E 94˚06.470′	1398	3.66	0.82
A16	Pezielietsie	Ring Well (Private)	N 25˚40.914′ E 94˚06.391′	1432	9.75	0.91
A17	Pezielietsie	Ring Well (Private)	N 25˚40.950′ E 94˚06.322′	1404	10.06	0.82
A18	High School	Ring Well (Private)	N 25˚41.473′ E 94˚05.993′	1347	6.40	0.91
A19	High School	Ring Well (Private)	N 25˚41.284′ E 94˚05.922′	1400	12.19	0.91
A20	Peraciezie	Ring Well (Private)	N 25˚41.204′ E 94˚06.102′	1418	5.79	0.91
A21	Old Ministers' Hill	Pond (Community)	N 25˚39.285′ E 94˚05.589′	1577	0.91	0.91
A22	Old Ministers' Hill	Ring Well (Private)	N 25˚39.090′ E 94˚05.680′	1625	9.45	0.79

A23	New Ministers' Hill	Ring Well (Private)	N 25˚39.063′ E 94˚06.031′	1579	4.88	0.76
A24	New Ministers' Hill	Ring Well (Private)	N 25˚39.126′ E 94˚06.353′	1547	8.53	0.91
A25	Old Ministers' Hill	Ring Well (Private)	N 25˚39.228′ E 94˚05.907′	1543	9.36	0.91
A26	Lerie	Ring Well (Private)	N 25˚39.307′ E 94˚06.034′	1480	6.10	0.91
A27	AG	Ring Well (Private)	N 25˚39.536′ E 94˚06.702′	1377	12.92	0.91
A28	Lerie	Ring Well (Community)	N 25˚39.117′ E 94˚06.541′	1490	7.16	0.91
A29	Lerie	Ring Well (Private)	N 25˚39.197′ E 94˚06.570′	1434	4.88	0.91
A30	Upper Chandmari	Ring Well (Private)	N 25˚39.501′ E 94˚06.156′	1481	6.40	0.91
A31	Lower Chandmari	Ring Well (Private)	N 25˚39.506′ E 94˚06.422′	1386	13.11	0.91
A32	Lower PWD	Ring Well (Private)	N 25˚39.864′ E 94˚06.404′	1375	10.12	0.91
A33	Lower Midland	Ring Well (Private)	N 25˚39.839′ E 94˚06.107′	1466	4.97	0.91
A34	Upper Midland	Ring Well (Private)	N 25˚40.110′ E 94˚06.405′	1401	6.71	0.91
A35	PR Hill	Ring Well (Community)	N 25˚39.436′ E 94˚05.859′	1522	3.35	0.91

A36	Lower PR Hill	Ring Well (Private)	N 25˚39.628′ E 94˚05.916′	1485	12.19	0.91
A37	Officer's Hill	Ring Well (Private)	N 25˚39.865′ E 94˚05.916′	1472	7.07	0.91
A38	Daklane	Ring Well (Private)	N 25˚40.257′ E 94˚06.412′	1379	10.06	0.91
A39	Daklane	Ring Well (Private)	N 25˚40.839′ E 94˚06.465′	1397	7.32	0.91
A40	Upper Naga Bazar	Ring Well (Private)	N 25˚40.481′ E 94˚06.472′	1416	9.45	0.91
A41	Kezieke	Ring Well (Private)	N 25˚40.603′ E 94˚06.602′	1416	3.05	0.64
A42	Pezielietsie	Ring Well (Private)	N 25˚40.846′ E 94˚06.474′	1397	4.05	0.82
A43	Pezielietsie	Ring Well (Private)	N 25˚40.988′ E 94˚06.467′	1424	6.40	0.91
A44	Themezie	Ring Well (Private)	N 25˚41.041′ E 94˚06.057′	1380	7.92	0.82
A45	Sepfuzou	Ring Well (Private)	N 25˚40.881′ E 94˚06.186′	1378	11.58	0.91
A46	Lower Bayavu	Ring Well (Private)	N 25˚41.369′ E 94˚06.053′	1397	5.49	0.91
A47	Upper Bayavu	Ring Well (Private)	N 25˚41.313′ E 94˚06.284′	1414	6.10	0.82
A48	Pezielietsie	Ring Well (Community)	N 25˚41.036′ E 94˚06.454′	1411	7.07	0.91
A49	Kenuozou	Ring Well (Private)	N 25˚40.991′ E 94˚06.666′	1469	12.98	0.91
A50	D Block	Ring Well (Private)	N 25˚40.301′ E 94˚06.573′	1396	4.42	0.91

Quantitative estimation of various physico-chemical parameters like pH, TDS, EC, Turbidity, TH, TA, major cations (Ca^{2+}, Mg^{2+}, K^{+}, Na^{+}), major anions (HCO_3^{-}, SO_4^{2-}, NO_3^{-}, Cl^{-}, F^{-}) and heavy metals like Fe, Cu, Cd and As were done. BIS (2012) and WHO (2004) guidelines for drinking water standards were used for the physico-chemical parameters.

The following types of instruments were used to measure the physico-chemical properties of groundwater (Table 3.3 and Fig. 3.3).

Table 3.3: Instruments used to measure the groundwater samples

Sl. No.	**Measured Parameters**	**Instruments/Methods**	**Laboratory**
1.	pH, TDS and EC	Portable pH, TDS and EC meter	Dept. of Geology, Nagaland University, Kohima
2.	TA, Turbidity and Cl^{-}	Colorimetric technique using Orlab Water Testing kit	Dept. of Geology, Nagaland University, Kohima
3.	F^{-}, NO_3^{-} and Fe	Spectrophotometer	Dept. of Geology, Nagaland University, Kohima
	SO_4^{2-}		CSIR, NE Institute of Science and Technology, Jorhat, Assam
4.	Na^{+} and K^{+}	Flame Photometer	DGM, Govt. of Nagaland
5.	TH, HCO_3^{-}, Ca^{2+} and Mg^{2+}	Volumetric methods	DGM, Govt. of Nagaland
6.	Cu, Cd and As	Atomic Absorption Spectroscopy	NASTEC, Dept. of Science and Technology, Govt. of Nagaland

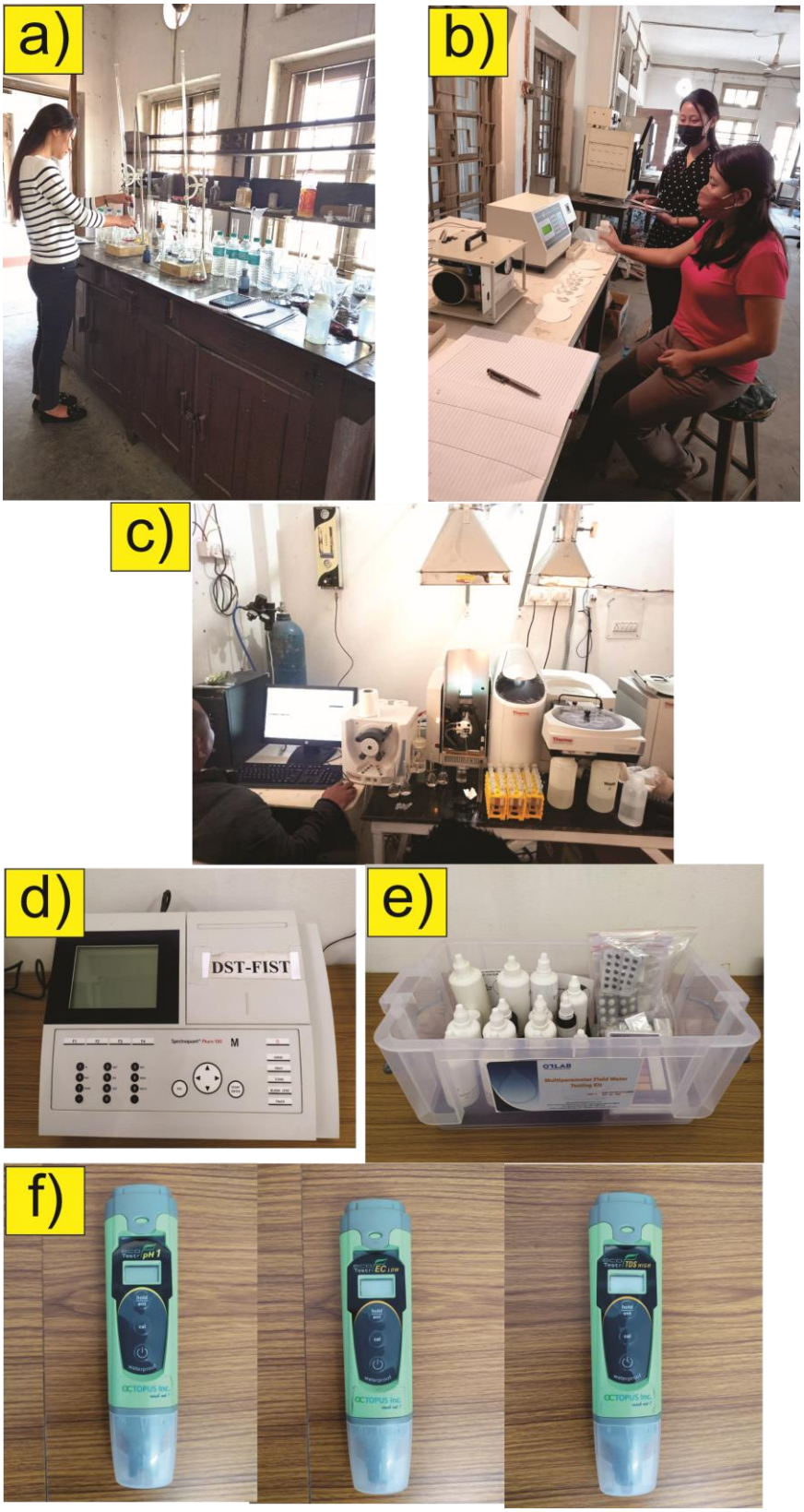

Fig. 3.3: Types of instruments used for testing groundwater samples

a) Titration using volumetric method

b) Flame photometer

c) Atomic Absorption Spectroscopy

d) Spectrophotometer
e) Orlab water testing kit
f) pH, EC and TDS meter

3.3.1 Determination of pH

pH was measured in the field right after groundwater sampling and determined by using Octopus Inc. pH meter Model no Ecotestr pH 1. The groundwater sample was kept in a glass beaker and the pH meter was inserted into the water sample. The readings that are displayed are noted.

3.3.2 Determination of Total Dissolved Solids (TDS)

TDS was measured in the field right after groundwater sampling and determined by using Octopus Inc. TDS meter Model no Ecotestr TDS High. The groundwater sample was kept in a glass beaker and the TDS meter was inserted into the water sample. The readings that are displayed are noted. TDS is measured in mg/L

3.3.3 Determination of Electrical Conductivity (EC)

EC was measured in the field right after groundwater sampling and determined by using Octopus Inc. EC meter Model no Ecotestr EC Low. The groundwater sample was kept in a glass beaker and the EC meter was inserted into the water sample. The readings that are displayed are noted. EC is measured in the unit of μS/cm (microsiemens/centimeter)

3.3.4 Determination of Turbidity

Turbidity was measured using the Turbidity Sacchi Disc Icon. It is measured by the degree to which water loses its transparency due to the presence of suspended solids. The unit of turbidity is Nephelometric Turbidity Unit (NTU) which signifies the intensity of light scattered at 90 degrees as a beam of light passes through the water sample.

3.3.5 Determination of Total Alkalinity (TA)

A 10 ml measure of water sample was taken in a clean conical flask. One alkalinity indicator tablet was added to it and then dissolved by mixing. The colour changed to blue green. Alkalinity reagent was added drop by drop to the conical flask until the solution colour changed from blue-green to pink. The total alkalinity in water was measured by multiplying the number of drops that were added by 25 factor and expressed in mg/L.

3.3.6 Determination of Total Hardness (TH), Calcium and Magnesium

Using the Eriochrome black-T indicator, TH of groundwater sample is calculated by titrating against a standard solution of known strength EDTA

(ethylenediaminetetraethanoic acid). Calcium and Magnesium ions reacts with Eriochrome black-T to produce a wine-red colour under alkaline conditions because EDTA reacts with calcium and magnesium to produce a soluble chelated complex. Calcium and magnesium ions get complexed upon the addition of EDTA as a titrant, resulting in a quick change in colour from wine red to blue, signifying the endpoint of a titration. By computing the difference between TH and calcium, the magnesium concentration in the groundwater was determined. TH, calcium and magnesium are measured in mg/L.

3.3.7 Determination of Sodium and Potassium

Sodium and potassium ions were both calculated using flame photometer. The intensity of the light being emitted is measured using a flame photometer. The wavelength of the flame's colour changes when a metal is introduced, and this wavelength indicates how much of each element is contained in the sample. Sodium and potassium are expressed in mg/L.

3.3.8 Determination of Bicarbonate

Bicarbonate is determined by titration of the water sample utilizing phenolphthalein and methyl orange as indicators against a standard sulphuric acid. First, indicator phenolphthalein is added to the sample. The standard acid is then added drop-wise and the pink colour vanishes when all of the carbonate in the sample water is converted to bicarbonates. Methyl orange indicator is then added to the sample and titrated against the standard sulphuric acid. When the end-point is achieved, the colour turns from yellow to orange. Bicarbonate is expressed in mg/L.

3.3.9 Determination of Chloride

10 ml of water sample is measured in a clean conical flask. One chloride indicator tablet was added into it and dissolved by mixing. The colour then changed to yellow. Chloride reagent was added drop by drop to the solution until the colour changed from yellow to red brown. The chloride content in water was obtained by multiplying the number of drops that were added by 17.73 factor. The concentration of chloride is expressed in mg/L.

3.3.10 Determination of Sulphate, Nitrate, Fluoride and Iron

Sulphate, nitrate, fluoride and iron are determined by Spectrophotometer model number Spectroquant Pharo 100. The method of spectrophotometry measures the intensity of light when a light beam passes through a sample solution to determine how

much light is reflected by a chemical substance. The basic principle is that each molecule has a specific wavelength spectrum where light is either absorbed or emitted.

3.3.11 Trace elements

Copper, Cadmium and Arsenic were measured from Atomic Absorption Spectroscopy. AAS is an analytical method for measuring out how much of a particular element is in a sample. It is based on the principle that atoms and ions may absorb light with a certain, distinct wavelength. The atom absorbs the energy or light when it is present at this particular wavelength. The electrons transition from their ground state to their excited state. The concentration of the element is calculated in the sample by measuring the amount of light that is absorbed.

3.4 DATA PROCESSING

3.4.1 Ionic balance error

For each sample, the accuracy of the concentration of total cations and total anions is expressed in milli equivalent per liter (meq/L) and the ionic-balance-error has been used to check the accuracy of chemical analysis of the groundwater samples. The IBE percentage is given by

$$\%\text{IBE}=\frac{\Sigma\, Cations-\Sigma\, Anions}{\Sigma\, Cations+\Sigma\, Anions}\times 100$$

Where, Cations= (Ca^{2+}+ Mg^{2+}+ K^{+}+ Na^{+})

Anions= (HCO_3^{-}+ SO_4^{2-}+ NO_3^{-}+ Cl^{-}+ F^{-})

The groundwater samples in the present study were detected to have ionic balance error percentages that were ±5% of the acceptable limit (Domenico and Schwartz, 1990).

3.4.2 Statistical analysis

Statistical techniques were employed to describe how much the data set varied and to compare it to other data sets. It is given in four different ways:

1. Central tendency (arithmetic mean) $x = \frac{\Sigma x_i}{n}$
2. Dispersion (standard deviation) $(\sigma) = \sqrt{\frac{\sum (x_i-\bar{x})^2}{df}}$
3. Relative standard deviation (coefficient of variance) $CV = \frac{\sigma}{\bar{x}} \times 100$
4. Degree of association among chemical variables (correlation coefficient)

   $r = \sum \frac{(x_i-\bar{x})-(y_i-\bar{y})}{n.\sigma_x .\sigma_y}$

where, x_i is a random variable,

n is the total number of observations,

df is the degree of freedom,

y_i is another random variable,

σ_x is the standard deviation of x_i and

σ_y is the standard deviation of y_i

3.4.3 Electrical resistivity

The most popular technique for determining subsurface geology and groundwater studies is Electrical Resistivity. Vertical Electrical Sounding (VES) technique was first introduced by Schlumberger in 1934. The VES approach utilizing the Schlumberger setup was chosen for this investigation because it allows for quicker and more cost-effective fieldwork and easy access to software for data interpretation (Todd, 1980; Selvam et al., 2010). The field resistivity data were collected using an SSR-MP-ATS resistivity metre. The IPI2WIN software was used to evaluate the field data.

VES methodology

i. Five electrodes are being used and measurements are made for different values of the expanding current electrode while keeping the centre of the electrode fixed.

ii. The two outer electrodes, which represent the source of the current, are the current electrodes, whereas the two inner electrodes, which represent the receiver, are the potential electrodes.

iii. The potential difference (ρV) is measured with the aid of the potential electrodes pair such as M and N produced by the introduction of the current (I) between the current electrodes pair such as A and B. The illustration is presented in Fig. 3.4.

iv. The current electrode spacing is kept greater than the potential electrode spacing, with all four electrodes stretched out in a straight line. The potential electrode spacing (MN) is five times lesser than the current electrode spacing (AB).

$$\frac{AB}{2} \geq 5\frac{MN}{2}$$

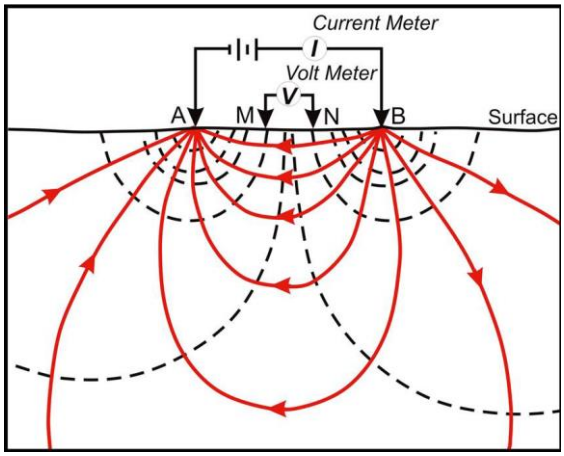

Fig. 3.4: Diagram of Electrical Resistivity principle (Clark and Page, 2011)

v. The resistivity metre calculates and displays the subsurface resistivity for each sounding. The apparent resistivity 'ρ_a' of a geologic formation for a heterogeneous medium, which is equivalent to the true resistivity for a specific electrode configuration, is given by

$$\rho_a = K\frac{\delta V}{I}$$

$$K = \frac{\pi}{2l}(L^2 - l^2),$$

where K is the geometric component that varies depending on the geometry of each electrode spacing configuration (AB = 2L; MN = 2L).

vi. Four basic kinds of sounding curve types with resistivity values of ρ1, ρ2, and ρ3 are offered depending on the resistivity values with depth, with ρ1 being the first resistivity value followed by ρ2 and ρ3:

a) ρ1 > ρ2 > ρ3: Q-type.
b) ρ1 < ρ2 < ρ3: A-type.
c) ρ1 > ρ2 < ρ3: H-type.
d) ρ1 < ρ2 > ρ3: K-type.

3.4.4 Water Quality Index (WQI)

In order for a layman to understand the status of the water source, WQI is used to convert a complex combination of water quality data into comprehensible and exploitable information (Balan et al., 2012). In the current investigation, the "Weighted Arithmetic Water Quality Index" methodology, was employed (Brown et al., 1972 and Cude, 2001).

1. The unit weight (W_n) factors for each parameter is calculated by the formula $W_n = \frac{K}{S_n}$

where, $K = \frac{1}{1/S_1+1/S_2+1/S_3+\cdots\ldots+1/S_n}$

$$K = \frac{1}{\sum\frac{1}{S_n}}$$

S_n= Desirable standard value of the nth parameter

The total of all selected parameters, unit weight factor W_n= 1 (unity)

2. The sub-index value (Q_n) is calculated by the formula $Q_n = \frac{[(V_n - V_o)]}{[(S_n - V_o)]} \times 100$

where, V_n= Mean concentrations of the nth parameter

S_n= Desirable standard value of the nth parameter

V_o= The actual value of parameters in pure water (V_o=0, for majority of the parameters except for pH)

$$Q_P H = \frac{[(V_p H - 7)]}{[(8.5-7)]} \times 100$$

3. From steps 1 and 2, WQI is calculated as follows

$$\text{Overall WQI} = \frac{\sum W_n Q_n}{\sum W_n}$$

3.4.5 Wilcox diagram

Wilcox (1955) defined a Na-percentage in terms of meq/l of the major cations. The relative proportion of K^+ and Na^+ compared to other cations in water is usually given as the percentage of Na among the major cations stated by the relation

$$\% \text{ Na} = \frac{(Na+K)\times 100}{(Ca+Mg+Na+K)}$$

To determine if water is suitable for irrigation, Wilcox presented a diagram in which sodium percentage is plotted against electrical conductivity or total salt content.

3.4.6 U.S. Salinity diagram

A categorization chart for irrigation waters with descriptions of 16 classes was issued by the United States Regional Laboratory (US Salinity Laboratory Staff, 1954). This categorization determines the salinity hazard of irrigation water by measuring TDS in terms of EC. The index for sodium hazard has been determined based on the sodium adsorption ratio (SAR) proposed by Richards (1954). It is described by

$$\text{SAR} = \frac{Na}{\sqrt{Ca+Mg/2}}$$

where meq/L is the unit of measurement for the constituent concentrations

3.4.7 Permeability Index

The ability of water to flow through a rock or soil is referred to as permeability. Permeability data is commonly used in groundwater research, particularly when investigating aquifer contamination. A high concentration of alkaline earth metals in soil reduces soil infiltration and permeability, resulting in decreased production of crops. The Permeability Index (PI) proposed by Doneen (1954) is calculated by

$$\text{PI} = \frac{Na + \sqrt{HCO_3}}{Ca + Mg + Na} \times 100$$

where meq/L is the unit of measurement for the constituent concentrations

3.4.8 Piper's trilinear diagram

Piper (1944) introduced the Piper's trilinear diagram to classify groundwater based on the geochemical characteristics of the constituent ionic concentration. A diamond-shaped field lies between two triangular fields, one at the lower left and the other at the lower right, in the Piper diagram. The ten divisions of the diamond-shaped field are shown in Fig. 3.5 and described below:

1= Calcium bicarbonate type

2= Sodium chloride type

3= Mixed type of calcium sodium bicarbonate type

4= Mixed type of Calcium magnesium chloride type

5= Calcium chloride type

6= Sodium bicarbonate type

7 (1+4+5) = Alkaline earths (Ca & Mg) exceed alkalies (Na & K).

8 (2+3+6) = Alkalies (Na & K) exceed alkaline earths (Ca & Mg).

9 (1+3+6) = Weak acids (CO_3& HCO_3) exceed strong acids (SO_4& Cl).

10 (2+4+5) = Strong acids (SO_4& Cl) exceed weak acids (CO_3& HCO_3).

The divisions of the cationic and anionic triangle are given as follows:

A= Calcium type

B & H= No dominant type

C= Magnesium type

D= Sodium and Potassium type

E= Bicarbonate type

F= Sulphate type

G= Chloride type

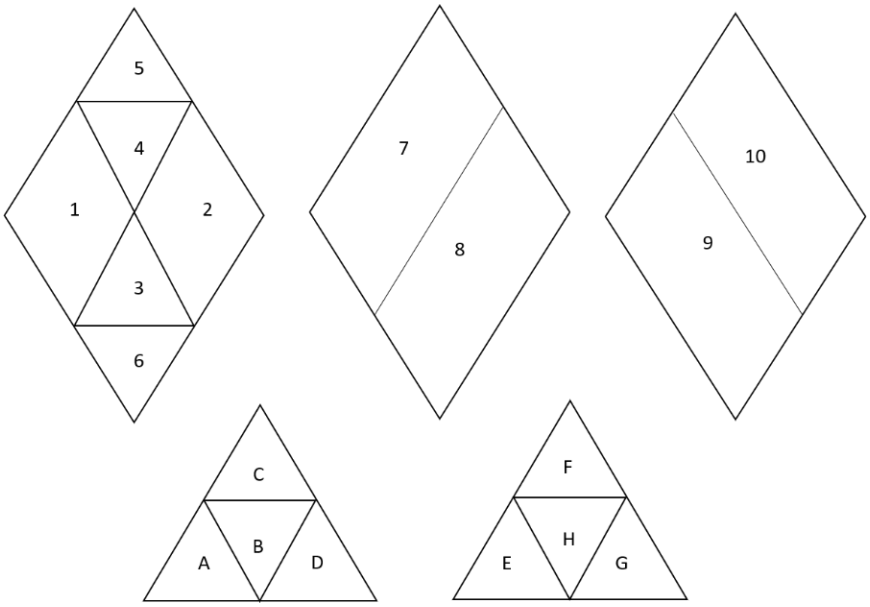

Fig. 3.5: Piper's Trilinear Diagram sub-division

3.4.9 Geospatial techniques

GIS is an important tool for making geospatial maps which has been widely used to compute numerous groundwater applications. (Shirazi et al., 2012; Sadat-Noori et al., 2013; Das et al., 2017; Shimpi et al., 2019; Adimalla et al., 2022). In the current research, the inverse distance weighted (IDW) interpolation technique using the ArcGIS 10.8 software was used to create geospatial distribution maps for all the physico-chemical parameters, hydrological maps for depth to water level maps, groundwater level fluctuation maps, and the WQI geospatial map.

CHAPTER 4
GEOELECTRICAL STUDIES

4.1 INTRODUCTION

Geophysical techniques have been widely utilized in the search for groundwater, minerals and ores, oil, and petroleum. For groundwater and subsurface studies, a number of geophysical exploration techniques are extensively applicable. Gravity, seismic, magnetic, and electrical techniques are a few of the essential geophysical techniques. Seismic prospecting includes logging the intensity and time of elastic wave energy (seismic waves) reflected from a specific depth of the earth (Dobrin and Savit, 1988). On the other hand, the earth's natural force field is measured using gravity and magnetic methods. The electromagnetic and electrical methods use reflection and refraction principles. The source can be either natural or artificial. Geoelectrical surveys of geophysical prospecting is often used for locating groundwater potential zones and determining the quality of groundwater. It offers details on geological features like faults, joints, fissures, and fractures. The physical properties and composition of the subsurface geological units, level of weathering, thickness, and depth of the underlying bedrock are additional factors that geophysical investigation can greatly influence. Based on the geophysical properties of the earth, several methodologies are used to identify groundwater potential zones, delineate aquifers, and locate other natural resources such as minerals, oil, and coal (Harinarayana and Naganjaneyulu, 2003).

Electrical resistivity survey plays an important role in the study of hydrogeology to determine the depth to water-bearing zones by measuring the electrical conductivity of groundwater and the resistivity of rock materials (Shenoy and Lokesh, 2000). The interpretation of the resistivity data can be used to describe the subsurface features. According to Zohdy et al. (1974), if there is a good electrical resistivity contrast between the water-bearing formations and the underlying rocks, resistivity methods can be successfully used for groundwater research. The matrix minerals in rocks are typically insulators. Interstitial fluids in fluid-containing rocks conduct current electrolytically, and porosity, water content, and the quantity of dissolved salts all affect resistivity. However, clay minerals have the ability to store electrical charges, and both electronic and electrolytic current conduction can occur (Zohdy et al., 1974). Compared to fresh rocks, the water-bearing weathered and fractured rocks have lower electrical resistivity values.

4.2 VERTICAL ELECTRICAL SOUNDING (VES)

In the 1920s the principle of vertical electrical sounding was introduced (O.H. Gish and Rooney, 1925). In order to look for groundwater in porous and fissured mediums, resistivity studies can be utilized in the form of vertical electrical soundings (VES) or horizontal profiling (R. Barker, 1980; Van Overmeeren, 1989). A specific field method for identifying the various electrical properties with depth is vertical electrical sounding (VES). This approach involves measuring apparent resistivity values at the same reference point, known as the sounding point, that correlate to progressively increasing electrode spacing. Resistivity distribution in the vertical direction is determined using the VES method. The subsurface is thought to form from lateral homogenous, isotropic layers that are horizontally stratified (Zohdy, 1989).

The use of VES techniques was restricted to shallow investigations until recently, because electronic measuring devices with adequate sensitivity were not readily available and partially because deeper penetration would have required a greater number of resistivity layers than could be included in any set of standard resistivity curves. The only method of interpretation was the standard curves using the curve matching procedures. With the aid of portable equipment and the introduction of powerful computers, recent advancements in electronics have made it possible to conduct investigations in deep depths and interpret the results. The rapid advancements in microprocessors and related numerical modeling methods have significantly boosted the application of geophysics over the past ten years for both the mapping of groundwater resources and the assessment of water quality. Due to the method's ease of use, vertical electrical sounding (VES) has proven to be especially useful with groundwater research. Test hole drilling and log analysis are traditional methods for determining the layer's thickness and lateral extension which have the drawbacks of being time-consuming and expensive (Kalinski et al., 1993)

The electrical resistivity method can be used to find the contamination of groundwater. With the increase in contamination, the electrical resistivity of water decreases as the ion concentration in the water increases (Frohlich and Urish, 2002). However, if ground inhomogeneities and anisotropy are present, limitations with resistivity methods can be anticipated (Matias, 2002). The lithology and fluid content of a rock affects its electrical resistivity. When sandstone which is coarse-grained and well-consolidated is saturated with fresh water, it has a higher resistivity than that of an unconsolidated silt with the same porosity and water. Additionally, identical porous rock samples have different resistivities depending on the salinity of the saturating water. The

rock's resistivity decreases as the water's salinity increases. Thus, when sandstone is saturated with salt water and shale is saturated with fresh water, it is very feasible for two different types of rock, such as shale and sandstone, to be of practically the same resistivity. Because of this, the number and thickness of the geoelectric units discovered using VES measurements at a location could differ from the ones discovered through geological means.

The primary objective of a VES at a particular location is to obtain a real resistivity log without actually drilling the well, similar to the induction log of a well. The resolution of the VES approaches is lower than that of the induction log because of some inherent limitations. The VES however continues to be the most inexpensive technique for subsurface investigations. They are better than the more expensive seismic approach. Whether a sandstone body's pores are filled with fresh or brackish water, the seismic signal associated with it would be the same. On the other hand, if there are minute variations in water salinity, its resistance varies. The low cost and this characteristic make the VES methods ideal for groundwater investigation.

4.3 SCHLUMBERGER CONFIGURATION

In 1934, Schlumberger introduced the VES methods. Since then, a wide range of VES arrays have been created (Keller and Frischknecht, 1966) but the Schlumberger array has remained the finest for depth sounding and depth profiling

The Wenner and Schlumberger arrangements are the most widely used among the conventional electrode spacing configurations that have been adopted. Schlumberger setup was employed in the current investigation because these surveys take less time and money to complete the task than collecting sediment cores and well data. The Schlumberger VES method gives good depth sensitivity, high signal-to-noise ratios, and strong horizontal layer resolution (Ward, 1990). Additionally, borehole data only offers information on the aquifer in close vicinity to the well, whereas geophysical surveys offer non-invasive spatial images of the aquifer.

When performing VES in Schlumberger configuration, the potential electrodes are set in place and left there for a while the current electrodes are moved symmetrically on the outer edges. After the resistivity measurements are recorded, the current electrodes are symmetrically shifted further away from the center point. The resistivity of depths can be found in this manner. The composition of the earth is heterogeneous. Therefore, each

substance and rock in the subsurface must have a unique resistivity. The resistivity of different geological mediums is shown in Fig. 4.1 (Palacky, 1987).

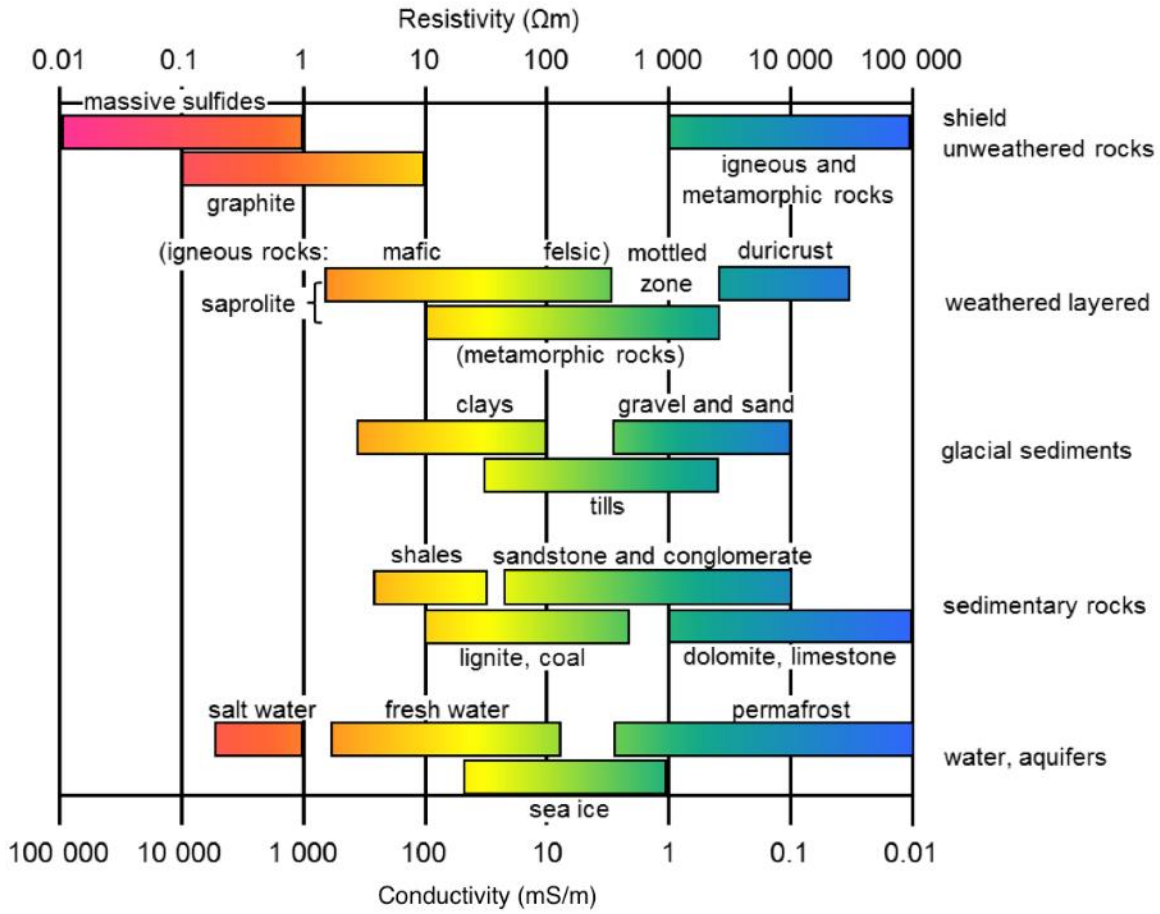

Fig. 4.1: Resistivity values for different geological mediums

4.4 RESULTS OF VES DATA

The properties of subsurface layers have been analyzed qualitatively and quantitatively at five locations in the study region to characterize aquifer characteristics. The location map of the VES stations is given in Fig. 4.2. The interpretation of the results is greatly influenced by the resistivity of layers in shallow depths. There are numerous well-established techniques for interpreting VES data, including curve matching techniques like those described by Orellana and Mooney in 1966 and the automatic interpretation computer program developed by Zohdy in 1974. The parameters 'ρ' and 'h' of a geoelectric model were calculated based on these interpretations. There are standard curves like the A-type, H-type, K-type, and Q-type, and also for multiple layers of structure. These common curves and sets of curves offer a fundamental understanding of the curve-matching technique.

In the present investigation, the resistivity data were collected using an SSR-MP-ATS resistivity metre, and the data were interpreted using the IPI2Win version 3.0.1.a software which was developed by the Moscow State University. IPI2Win has created a numerical computer-automated fit of resistivity data, allowing for quicker and more precise data interpretation. Modern computer software is easily accessible and enables efficient interactive and automatic study of sounding curves. Using a Schlumberger array to carry out VES, resistivity data were collected from the ground, and apparent resistivity data were modelled based on the type of field survey employed. The resistivity model is updated based on a comparison of calculated and observed data. The process of continuously comparing field-collected data with calculated data produces the result.

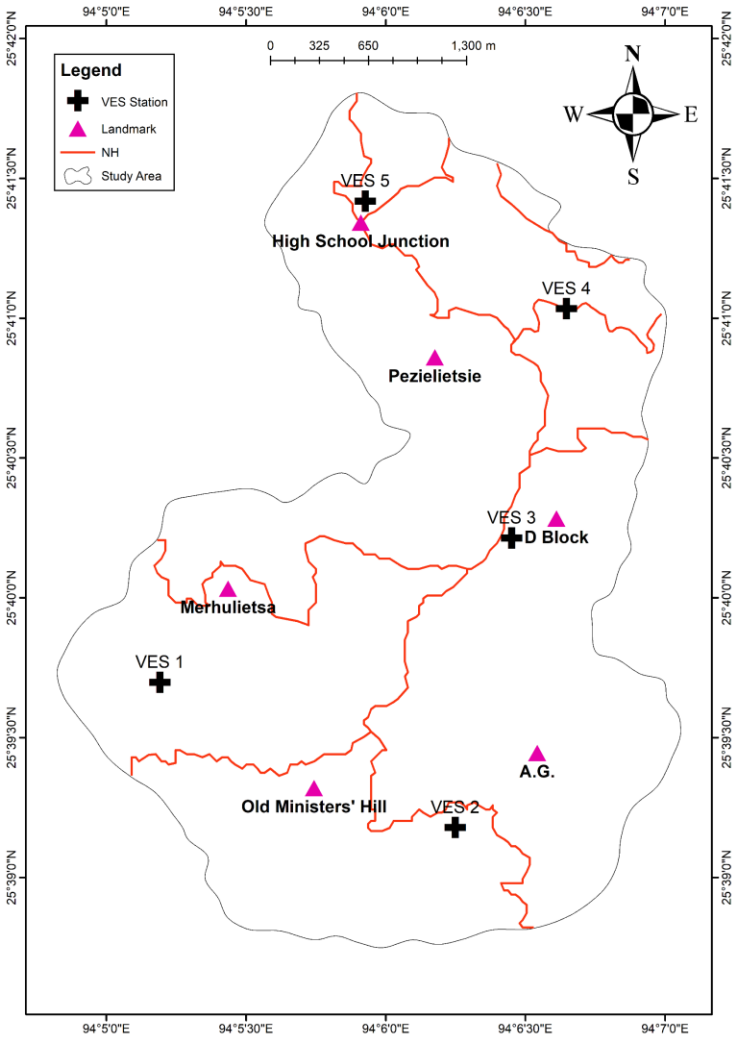

Fig. 4.2: Location map of the VES stations

4.4.1 VES data analysis using quantitative and qualitative method

The VES data is interpreted quantitatively and qualitatively. The direct method, a quantitative interpretation method gives the details of the thickness, depth, true resistivity of the layers and number of layers. The statistics are shown in Table 4.1.

Table 4.1: Quantitative analysis of resistivity and thickness of layers from VES data

VES station	Resistivity ρ (Ω m)	Thickness h (m)	Depth d (m)	Number of layers
VES 1	ρ1= 297	h1= 3.18	d1= 3.18	4
	ρ2= 82.4	h2= 9.48	d2= 12.7	
	ρ3= 8.67	h3= 11.6	d3= 24.2	
	ρ4= 10681	-	-	
VES 2	ρ1= 283	h1 = 1.42	d1= 1.42	4
	ρ2= 1809	h2= 2.02	d2= 3.44	
	ρ3= 114	h3=26.3	d3= 29.7	
	ρ4 = 0.371	-	-	
VES 3	ρ1= 36.8	h1= 0.625	d1= 0.625	4
	ρ2= 243	h2= 6.87	d2= 7.49	
	ρ3= 57.9	h3= 8.29	d3= 15.8	
	ρ4= 27630	-	-	
VES 4	ρ1= 95.8	h1= 0.959	d1= 0.959	4
	ρ2= 5.71	h2= 1.09	d2= 2.05	
	ρ3= 2134	h3= 2.03	d3= 4.08	
	ρ4= 82.4	-	-	
VES 5	ρ1= 637	h1= 1.98	d1= 1.98	3
	ρ2= 183	h2= 15.6	d2= 17.5	
	ρ3= 12.2	-	-	

The qualitative interpretation on the other hand is done using the curve matching method which gives the type of curve and information about the layers (Barseem et al., 2015). These curve types are used to interpret the lithology. For each of the 5 VES locations, the curve types are generated (Table 4.2). The curves have been interpreted using the resistivity values rather than the resulting graphs.

Table 4.2: Qualitative analysis of curve types from VES data

VES	Curve type	Curve Characteristics	No. of Geo-electric layer
VES 1	QH	ρ1> ρ2> ρ3< ρ4	4
VES 2	KQ	ρ1< ρ2> ρ3> ρ4	4
VES 3	KH	ρ1< ρ2> ρ3< ρ4	4
VES 4	HK	ρ1> ρ2< ρ3> ρ4	4
VES 5	Q	ρ1> ρ2> ρ3	3

The sounding curves in the study area are of the type QH, KQ, KH, HK and Q Curve. The interpretation of VES curves gave 4 and 3 geoelectric subsurface layers, namely topsoil, fractured shale, weathered shale and sandstone layers (Loke et al., 1996 and Ezung et al., 2021). Overall, the resistivity varied from 0.371 to 27630 Ω m with the minimum resistivity found in VES station 2 and the maximum resistivity at VES station 3. The VES curve types are briefly discussed below.

4.4.1.1 QH type curve

QH type at VES 1 (Fig. 4.3) shows resistivity of the type ρ1> ρ2> ρ3< ρ4. The first layer is the top soil with a resistivity of 297 Ωm and a thickness of 3.18 m. The second layer is composed of a fractured layer of shale with a resistivity of 82.4 Ωm and a thickness of 9.48 m. The third layer has a resistivity of 8.67 Ωm and is made of weathered shale which constitutes a shallow aquifer of good quality (freshwater) groundwater (Fig. 4.1) found at a depth of 24.2 m. The basement layer is composed of a hard and compact sandstone block with a resistivity of 10681 Ωm.

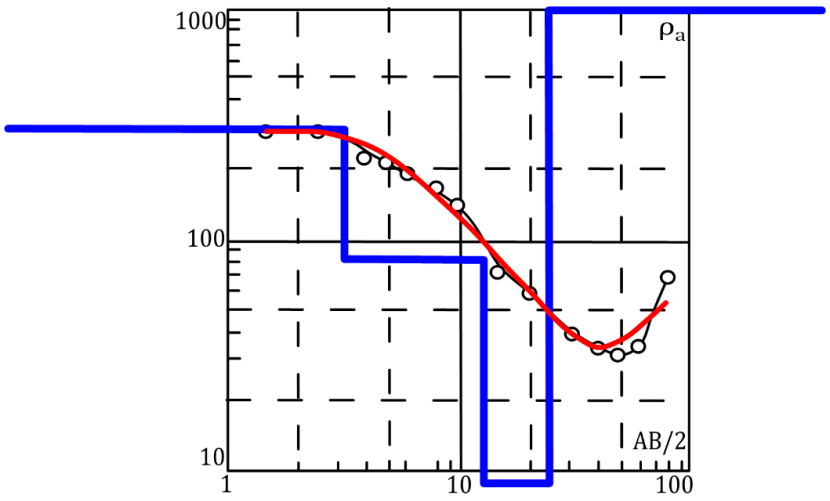

Fig. 4.3: Vertical electrical sounding curve at VES 1 (ρ_a – apparent resistivity (Ωm); AB/2 – distance (m))

4.4.1.2 KQ type curve

KQ type at VES 2 (Fig. 4.4) gives a four-layer model of ρ1< ρ2> ρ3> ρ4. The first layer is the top soil with a resistivity of 283 Ωm and a thickness of 1.42 m. The second layer is composed of a hard and compact layer of sandstone with a resistivity of 1809 Ωm and a thickness of 2.02 m. The third layer has a resistivity of 114 Ωm and is made of a weathered shale layer with a thickness of 26.3 m. The fourth layer is composed of a saline water bearing zone with a resistivity of 0.371 Ωm (Fig. 4.1). There is a large difference in resistivity values of freshwater (Around 10 to 100 Ωm) and saltwater (<1 Ωm) in Fig 4.1 so the presence of saltwater can be easily detected in the aquifer.

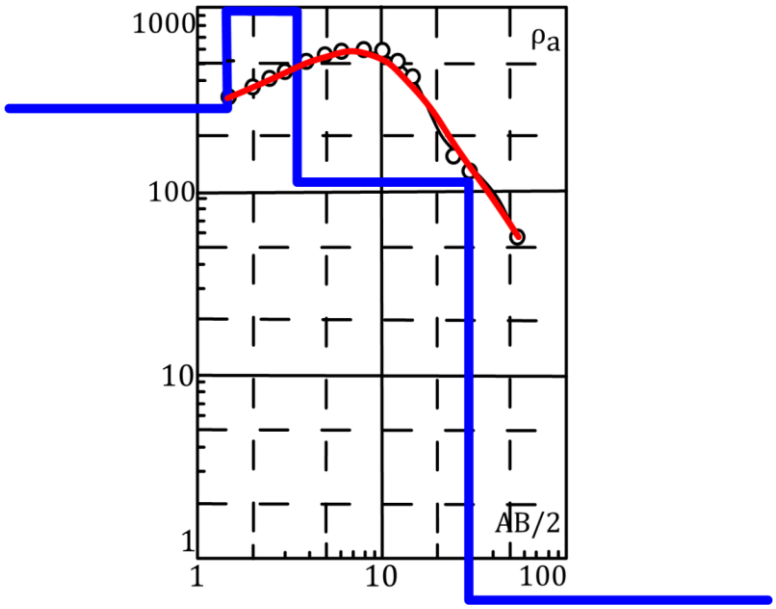

Fig. 4.4: Vertical electrical sounding curve at VES 2 (ρ_a – apparent resistivity (Ωm); AB/2 – distance (m))

4.4.1.3 KH type curve

KH type is found at VES 3 (Fig. 4.5) with a four-layer model of ρ1< ρ2> ρ3< ρ4. The first layer is the top soil with a resistivity of 36.8 Ωm and a thickness of 0.625 m. The second layer has a resistivity of 243 Ωm and a thickness of 6.87 m which is composed of a fractured layer of shale. The third layer has a resistivity of 57.9 Ωm and is made of a weathered shale layer with a thickness of 8.29 m which may be considered a suitable zone for groundwater. The fourth layer composed of the bedrock is of hard and compact sandstone with a high resistivity of 27630 Ωm.

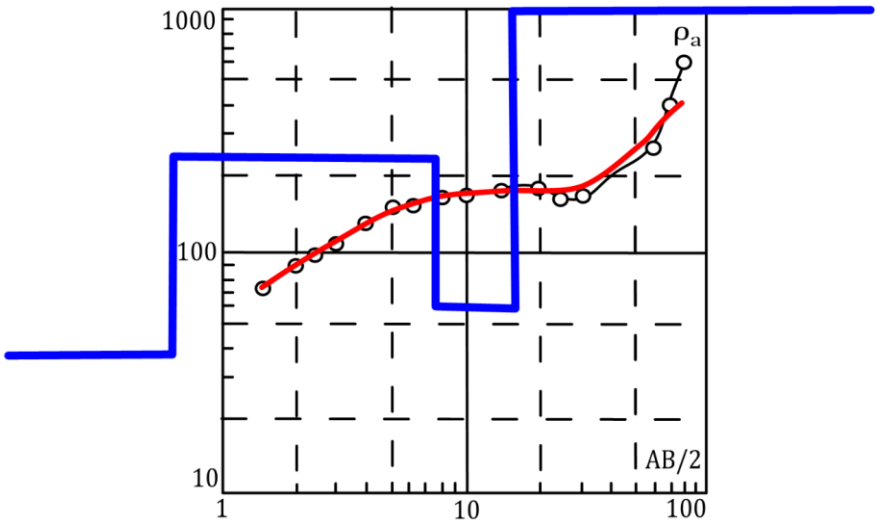

Fig. 4.5: Vertical electrical sounding curve at VES 3 (ρ_a – apparent resistivity (Ωm); AB/2 – distance (m))

4.4.1.4 HK type curve

HK type at VES 4 (Fig. 4.6) gives a four-layer model of ρ1> ρ2< ρ3> ρ4. The first layer is the top soil with a resistivity of 95.8 Ωm and a thickness of 0.959 m. The second layer has a resistivity of 5.71 Ωm with a thickness of 1.09 m which reveals the presence of water. The third layer is made up of a sandstone layer showing a resistivity of 2134 Ωm and a thickness of 2.03 m. The fourth layer is composed of fractured shale with a resistivity of 82.4 Ωm.

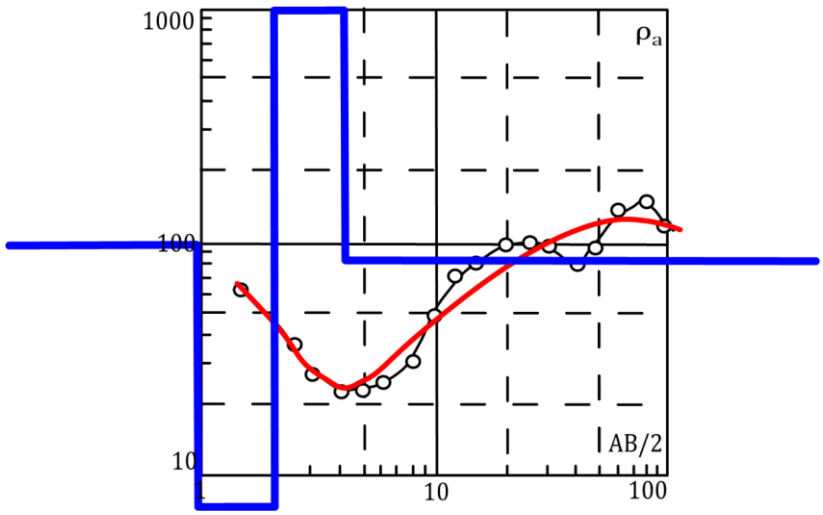

Fig. 4.6: Vertical electrical sounding curve at VES 4 (ρ_a – apparent resistivity (Ωm); AB/2 – distance (m))

4.4.1.5 Q type curve

Q type curve is found at VES 5 (Fig. 4.7) and gives a three-layer model of ρ1> ρ2> ρ3. The first layer is the top soil with a resistivity of 637 Ωm and a thickness of 1.98 m. The second layer is composed of a fractured layer of shale with a resistivity of 183 Ωm and a thickness of 15.6 m. The third layer is the groundwater zone with a resistivity of 12.2 Ωm.

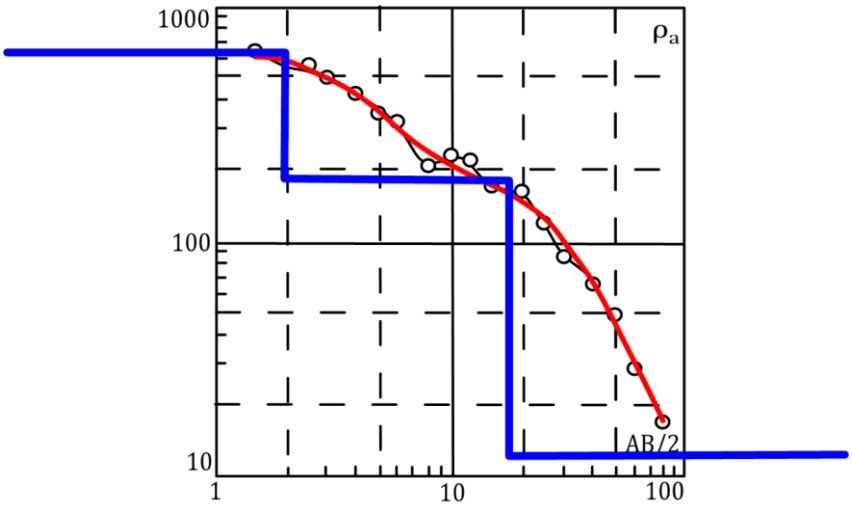

Fig. 4.7: Vertical electrical sounding curve at VES 5 (ρ_a – apparent resistivity (Ωm); AB/2 – distance (m))

CHAPTER 5

PHYSICO-CHEMICAL CHARACTERS OF GROUNDWATER

5.1 INTRODUCTION

Groundwater quality depends on a number of factors like soils, precipitation, weathering, ion exchange, the nature of bedrock and various biological processes (Todd and Mays, 2013). The geochemical processes in an aquifer are strongly related to its geological formations, groundwater flow, residence time, etc. Anthropogenic pollution sources also affect groundwater quality to a great extent. In India, untreated sewage discharge is the main source of pollution in both surface and groundwater. Investigation, treatment and evaluation of groundwater quality are thus needed to improve health conditions.

In the study area, water supply for drinking purposes is mainly from rivers and streams. However, with the increase in population, there has been a scarcity of water, especially during dry seasons and urbanization has led to the production of large amounts of waste and contamination. There is a prerequisite to carefully monitor groundwater and check the quality for drinking purposes in Kohima town. Monitoring drinking water quality has become a vital part of water management and data analysis is fundamental for the characterization and identification of groundwater quality issues.

Several researchers worldwide have used major ion chemistry to evaluate the geochemical processes and groundwater contamination in the aquifer. Hydrogeochemistry and statistical analysis are widely used in groundwater contamination assessment. According to Thilagavathi et al. (2012), understanding hydrogeochemistry is essential to determine the origin of the chemical composition of subsurface water. Hence, the important groundwater parameters like pH, TDS, EC, Turbidity, TH, TA, major cations (Ca^{2+}, Mg^{2+}, K^{+}, Na^{+}), anions (HCO_3^{-}, SO_4^{2-}, NO_3^{-}, Cl^{-}, F^{-}), Fe and trace elements like Cd, Cu and As were analyzed to examine the physico-chemical characters of groundwater in Kohima town.

5.2 HYDROGEOCHEMISTRY

Fifty groundwater samples were evaluated in Kohima town for physico-chemical parameters where the data is given in the tabular form. They have been compared with the guidelines of BIS (2012) and WHO (2004) for drinking purposes which are given in Table 5.1. The trace element As was found to be absent in the groundwater samples in both the pre- monsoon and post-monsoon seasons of 2019 and 2021. The minimum, maximum, mean, standard deviation and coefficient of variance of the groundwater samples during the pre-monsoon and post-monsoon periods of 2019 and 2021 are displayed in Tables 5.2, 5.3, 5.4 and 5.5. The hydrochemical facies are determined by arranging the ion percentages (Khan et al., 1972) in descending order of abundance. The ionic dominance pattern is thus found to be $Na^+ > Ca^{2+} > K^+ > Mg^{2+}$ for cations and $HCO_3^- > Cl^- > SO_4^{2-} > NO_3^- > F^-$ for anions.

Table 5.1: Guidelines for drinking water *BIS (2012) and **WHO (2004)

Parameters	Acceptable limit	Permissible limit
pH	6.5-8.5*	No relaxation*
TDS	500*	2000*
EC	750**	-
Turbidity	1*	5*
TH	200*	600*
TA	200*	600*
Mg^{2+}	30*	100*
Ca^{2+}	75*	200*
K^+	12**	-
Na^+	50**	200**
HCO_3^-	300**	-
SO_4^{2-}	200*	400*
NO_3^-	45*	No relaxation*
Cl^-	250*	1000*
F^-	1*	1.5*
Fe	0.3*	No relaxation*
Cd	0.003*	No relaxation*
Cu	0.05*	1.5*
As	0.01*	0.05*

Table 5.2: Analytical data of the groundwater samples of the study area (Pre-monsoon 2019)

SAMPLE NO.	pH	TDS (mg/L)	EC (µS/cm)	Turbidity (NTU)	TH (mg/L)	TA (mg/L)	Mg (mg/L)	Ca (mg/L)	K (mg/L)	Na (mg/L)	HCO3 (mg/L)	SO4 (mg/L)	NO3 (mg/L)	Cl (mg/L)	F (mg/L)	Fe (mg/L)	Cd (mg/L)	Cu (mg/L)
A1	6	229.6	410	0	126.72	75	15.29	25	31.71	60.08	80.18	25.2	25	100	0	0	BDL	BDL
A2	6.5	231.8	380	0	121.30	75	8.05	35	25.49	60.3	126.27	45.65	0	75	0	0.3	BDL	BDL
A3	7	187.2	260	0	113.72	25	12.20	25	25.95	55.59	70.15	44.33	20	75	0	0.4	BDL	BDL
A4	7.5	131.1	230	0	100.16	75	6.59	29	20.2	55.85	134.18	52.61	10	25	0	0	BDL	BDL
A5	7	540	750	0	234.22	250	2.20	90	53.55	82.98	336.72	55.87	0	75	0	0.3	BDL	BDL
A6	6	388.6	670	0	171.62	50	21.22	33	27.13	65.54	76.12	44.12	45	100	0	0.08	BDL	BDL
A7	8	442.5	750	0	121.10	225	10.98	30	43.75	111.47	392.84	29.68	10	50	0.5	0.21	BDL	BDL
A8	7	466.2	740	0	236.58	150	27.76	48	26	66.13	196.42	54.46	20	75	0	0.23	BDL	BDL
A9	7	352.8	490	0	151.22	75	12.20	40	31.35	60.7	140.3	36.67	10	75	0	0.16	BDL	BDL
A10	6.5	268.4	440	0	189.70	150	21.95	39	16.33	52.56	196.42	38.12	0	50	0	0.16	BDL	BDL
A11	6.5	182	260	0	128.67	50	18.73	20	13.49	53.88	89.18	48.35	10	75	0	0.13	BDL	BDL
A12	8	375.2	670	0	308.95	200	29.51	74	16.55	58.85	364.78	49.06	0	25	0	0	BDL	BDL
A13	9	383.4	540	0	222.66	225	6.59	78	39	201	364.78	167.43	45	75	0.5	0.11	BDL	BDL
A14	9	825.5	1270	0	231.02	350	9.17	77	51.83	92.75	477.02	131.89	10	50	0.5	0.13	BDL	BDL
A15	7	684.4	1180	0	344.72	275	42.20	67	52.79	71.94	505.08	79.65	10	75	0.5	0	BDL	BDL
A16	5	363	550	0	206.78	50	27.80	36	5.32	55.44	112.24	63.97	10	75	0	1.22	BDL	BDL
A17	6.5	441	700	0	280.05	200	40.49	44	5.48	59.29	308.66	78.9	0	75	0.5	0.29	BDL	BDL
A18	7	331.2	480	0	151.83	75	18.29	30	21.35	58	104.18	52.48	10	75	0	0.12	BDL	BDL
A19	6	1207	1700	0	352.96	575	34.63	83	19.7	94.09	302.84	118.97	0	100	0	1	BDL	BDL
A20	7	298.2	420	0	177.34	75	21.39	35	25.98	62.92	128.21	94.54	10	75	0	0.05	BDL	BDL
A21	7.5	276.9	390	0	123.79	150	22.93	11	18.37	53.98	154.33	56.87	0	25	0.5	0.06	BDL	BDL
A22	7	144.95	261	0	82.12	50	11.22	14	9.83	24.74	70.15	29.51	0	25	0.5	0.34	BDL	BDL
A23	7	197.2	290	0	124.89	75	14.85	25	20.31	53.2	104.18	59.45	10	50	0.5	0.21	BDL	BDL
A24	6	365.8	590	0	189.53	25	27.27	30	20.92	53.91	86.12	59.35	45	75	0.5	0.04	BDL	BDL
A25	8.5	390	600	0	130.56	150	15.61	26	50.81	84.41	224.48	14.87	10	75	0.5	0.56	BDL	BDL
A26	7	284	400	0	138.55	50	20.49	21	28	69.28	104.18	75.12	10	75	0	0	BDL	BDL
A27	8	348	600	0	186.99	75	24.88	33	27.17	71.36	168.36	54.16	10	75	0	0.16	BDL	BDL
A28	8.5	200.6	340	0	168.67	50	21.71	31	15.11	55.16	134.18	71.27	10	50	0	0.14	BDL	BDL
A29	6	292.4	430	0	159.82	50	23.17	25	18.33	64.99	112.24	57.71	10	75	0.5	0	BDL	BDL
A30	6	359.6	580	0	161.29	50	22.93	26	25.44	66.8	104.18	75.14	10	75	0.5	0.53	BDL	BDL
A31	6	336	600	0	134.38	100	8.78	39	35.89	67.68	168.36	29.15	20	75	0.5	0.45	BDL	BDL
A32	8.5	993.6	1380	0	245.48	475	19.76	65	56.06	86.9	345.38	23.34	20	100	3	0	BDL	BDL
A33	8.5	547.5	750	0	197.32	150	23.17	40	50.72	72.74	224.48	19.67	10	125	0.5	0.04	BDL	BDL
A34	7.5	285	500	0	163.63	50	16.34	38	33.74	71.54	114.18	58.18	45	75	0.5	0	BDL	BDL
A35	7.5	568	800	0	223.01	50	25.12	47	46.25	77.67	196.42	48.15	20	100	0	0	BDL	BDL
A36	8	524.4	760	0	193.15	150	11.46	58	25.12	56.49	242.54	26.76	10	100	0.5	0	BDL	BDL
A37	6	315	500	2	217.72	75	32.20	33	31.07	81.59	150.3	47.37	10	125	0.5	0.39	BDL	BDL
A38	7.5	336.4	580	2	188.46	50	24.63	34	31.46	82.32	122.24	53.14	10	125	0	1.49	BDL	BDL
A39	6.5	784	754	0	345.59	300	35.85	78	50.52	82.03	392.84	45.19	0	100	0.5	0	BDL	BDL
A40	7.5	649	1100	0	254.89	100	33.90	45	41.95	87.02	168.36	94.18	10	125	0.5	0.19	BDL	BDL
A41	6.5	710	1000	0	444.29	300	62.93	72	51.93	74.85	477.02	54.16	0	100	0.5	0.56	BDL	BDL
A42	6	433.1	610	0	157.73	125	17.32	34	55.57	83.8	112.24	48.19	10	150	0.5	0.2	BDL	BDL
A43	6.5	482.8	680	0	219.46	100	29.63	38	25.2	75.81	170.3	88.15	10	75	0.5	0.08	BDL	BDL
A44	7.5	403.2	720	0	205.30	225	28.05	35	50.33	93.12	280.6	75.12	10	75	0.5	0	BDL	BDL
A45	8.5	522	900	0	244.89	275	33.90	41	50.19	104.15	364.78	85.73	0	75	0.5	2.05	BDL	BDL
A46	6	472.5	750	0	199.40	50	29.02	31	47.07	76.22	116.12	47.12	10	150	0	0.21	BDL	BDL
A47	6.5	389.4	590	8	339.68	175	36.83	74	3.31	55.42	278.66	33.56	0	125	0	2.37	BDL	BDL
A48	7.5	482.4	720	0	310.71	175	37.07	62	32.91	71.01	252.54	81.1	0	100	0.5	3.33	BDL	BDL
A49	6.5	212.4	360	0	112.24	50	12.44	24	30.09	62.01	96.12	42.28	10	75	0.5	0.13	BDL	BDL
A50	6	220.1	310	0	76.22	25	12.20	10	31.47	65.21	76.12	37.37	10	75	0.5	3.53	BDL	BDL
Max	**9**	**1207**	**1700**	**8**	**444.29**	**575**	**62.93**	**90**	**56.06**	**201**	**505.08**	**167.43**	**45**	**150**	**3**	**3.53**	**-**	**-**
Min	**5**	**131.1**	**230**	**0**	**76.22**	**25**	**2.20**	**10**	**3.31**	**24.74**	**70.15**	**14.87**	**0**	**25**	**0**	**0**	**-**	**-**
Mean	**7.04**	**417.11**	**634.7**	**0.24**	**198.22**	**139**	**22.46**	**41.56**	**31.36**	**72.10**	**202.37**	**58.07**	**11.5**	**81**	**0.33**	**0.44**	**-**	**-**
SD	**0.93**	**213.42**	**299.49**	**1.19**	**78.62**	**116.51**	**11.32**	**20.08**	**14.63**	**24.21**	**120.30**	**28.78**	**11.79**	**28.82**	**0.46**	**0.79**	**-**	**-**
CV	**13.22**	**51.17**	**47.19**	**494.87**	**39.66**	**83.82**	**50.40**	**48.33**	**46.64**	**33.58**	**59.45**	**49.56**	**102.53**	**35.58**	**138.97**	**180.31**	**-**	**-**

Max= Maximum, Min= Minimum, SD= Standard Deviation, CV= Coefficient of Variance, BDL= Below detection limit

Table 5.3: Analytical data of the groundwater samples of the study area (Post-monsoon 2019)

SAMPLE NO.	pH	TDS (mg/L)	EC (µS/cm)	Turbidity (NTU)	TH (mg/L)	TA (mg/L)	Mg (mg/L)	Ca (mg/L)	K (mg/L)	Na (mg/L)	HCO3 (mg/L)	SO4 (mg/L)	NO3 (mg/L)	Cl (mg/L)	F (mg/L)	Fe (mg/L)	Cd (mg/L)	Cu (mg/L)
A1	6.7	441.61	695	0	115.83	75	9.80	30	17.12	106.24	95.4	64.1	0	125	0	0.1	BDL	BDL
A2	6.8	510.71	687	5	98.33	125	2.00	36	14.46	132.34	194.2	57.8	0	80	0	4.28	BDL	BDL
A3	7.1	330.09	485	0	73.33	50	8.60	15	13.06	83.74	98.8	52.32	0	65	0.5	0.35	BDL	BDL
A4	7.3	373.61	655	0	100.00	100	2.40	36	12.16	86.26	127.6	50.77	0	65	0.5	0.03	BDL	BDL
A5	7.4	1081.73	1455	0	357.50	450	19.80	110	65.1	168.38	536.8	87.08	0	100	0.5	0.14	BDL	BDL
A6	6.1	818.71	1175	0	127.50	50	13.80	28	40.63	211.92	218.8	150.32	25	135	0.5	0.05	BDL	BDL
A7	6.9	586.09	890	3	111.67	125	10.00	28	27.3	147.07	185.2	97.98	10	85	0.5	0.13	BDL	BDL
A8	7.3	805.81	1095	0	169.17	200	11.80	48	26.36	191.52	290.6	72.09	65	105	0.5	0.13	BDL	BDL
A9	7.1	681.78	969	0	201.67	50	31.60	28	18.34	155.54	198.6	124.1	25	105	0.5	0.09	BDL	BDL
A10	6.5	311.66	557	0	160.00	75	19.20	32	3.6	37.68	137.6	49.09	0	35	0.5	0.05	BDL	BDL
A11	7.1	511.89	779	0	110.00	50	20.40	10	15.02	140.96	101	125.54	0	105	0	0.04	BDL	BDL
A12	7.3	600.31	829	0	305.83	250	25.40	80	6	77.64	276.2	74.62	0	65	0.5	0	BDL	BDL
A13	7.7	1169.21	1595	0	330.00	250	32.40	78	25.5	273.5	347.2	190.12	10	215	0.5	0	BDL	BDL
A14	7.4	1270.61	1728	0	363.33	300	36.80	84	34.8	292.1	351.6	176.8	65	235	0.5	0.13	BDL	BDL
A15	7.2	981.18	1388	0	274.17	300	38.80	45	31.3	211.4	385.2	151.92	25	100	0.5	0.03	BDL	BDL
A16	6	588.46	957	5	170.00	75	24.00	28	7.9	136.5	147.6	46.98	65	135	0.5	0.45	BDL	BDL
A17	7.1	651.76	891	0	245.83	150	35.00	40	14	129.6	215.2	111.48	0	110	0.5	0.16	BDL	BDL
A18	7.4	648.81	938	0	204.17	75	31.00	30	19.2	139.3	207.6	114.75	10	100	0	0.09	BDL	BDL
A19	6.7	1402.89	1885	0	278.33	375	20.00	78	82.4	335.6	439.2	195.2	25	235	0.5	1.52	BDL	BDL
A20	7.4	329.91	598	0	100.00	50	10.20	23	14.4	76	68.8	45.09	10	85	0.5	0	BDL	BDL
A21	6.6	265.45	453	0	68.33	50	11.00	9	5.3	64.69	78.8	32.21	10	60	0	0.04	BDL	BDL
A22	7.4	160.31	287	0	60.00	50	7.20	12	4.62	19.15	71	27.88	0	25	0.5	0.01	BDL	BDL
A23	7.5	339.41	601	0	120.00	50	16.80	20	19.9	66.9	83.2	40.1	10	85	0.5	0.15	BDL	BDL
A24	6.1	345.41	567	0	128.33	50	20.00	18	13.7	65.7	93.2	60.32	10	70	0.5	0.09	BDL	BDL
A25	8.2	499.09	725	0	130.83	125	15.80	26	18.7	112.1	193	39.99	10	85	0.5	0.1	BDL	BDL
A26	6.5	408.96	735	0	91.67	50	11.80	17	15.7	103.8	89.2	95.42	10	70	0	0	BDL	BDL
A27	6.8	622.33	993	0	146.67	75	19.00	27	21.4	153.7	157.6	111.65	25	110	0	0.04	BDL	BDL
A28	6.9	589.05	936	0	137.50	150	21.60	19	43.8	119	217.4	41.76	45	85	0.5	0.05	BDL	BDL
A29	6.2	405.64	728	0	81.67	75	7.60	20	12.1	102.4	123.2	76.32	10	60	0	0.05	BDL	BDL
A30	6.1	523.59	825	0	82.50	50	7.80	20	23.1	145.8	121	75.99	25	110	0	0.2	BDL	BDL
A31	6.5	537.97	925	0	141.67	100	21.40	21	17.2	125.9	154.2	82.75	10	110	0.5	0.26	BDL	BDL
A32	7.5	960.67	1385	0	260.00	425	24.00	64	13.3	179.1	500.2	33.53	0	150	1.5	0	BDL	BDL
A33	8.2	747.78	1124	0	112.50	100	15.00	20	25.6	209.5	245.2	91.1	10	135	0.5	0	BDL	BDL
A34	7.7	452.65	849	0	91.67	50	11.20	18	15.1	116.5	101	70.3	25	100	0.5	0	BDL	BDL
A35	6.7	444.59	801	0	136.67	75	17.20	26	24.9	88.5	156.4	39.99	10	85	0.5	0	BDL	BDL
A36	8.1	639.76	1117	0	186.67	175	11.20	56	5.31	147.8	257.4	52.75	10	105	0.5	0	BDL	BDL
A37	6.6	373.48	608	2	188.33	100	27.80	29	11.3	55	119.8	39.98	10	85	0.5	3.03	BDL	BDL
A38	7.3	546.58	941	0	100.00	50	11.40	21	19.2	150.8	139.2	90.41	0	120	0.5	0.24	BDL	BDL
A39	6.9	877.54	1244	0	252.50	275	33.00	46	16.6	201.6	292.8	154.74	10	125	0.5	0.03	BDL	BDL
A40	6.7	798.11	1258	0	139.17	75	15.40	30	25	222.2	199.8	176.16	0	135	0.5	0.12	BDL	BDL
A41	7	520.26	934	2	360.00	325	40.80	76	23.9	124	390.4	98.4	45	60	0.5	0.52	BDL	BDL
A42	6.4	354.56	593	0	129.17	75	19.00	20	24.7	160.5	147.6	73.96	0	155	0.5	0.12	BDL	BDL
A43	6.3	411.23	665	0	123.33	50	18.80	18	14.5	183.5	156.8	78.31	10	160	0.5	0.07	BDL	BDL
A44	7	307.03	521	0	143.33	125	16.40	30	13	138.9	186.4	80.4	0	110	0.5	2.68	BDL	BDL
A45	7.4	305.71	548	3	114.58	175	11.90	26	8	201.1	237.6	96.16	0	155	0.5	1.24	BDL	BDL
A46	6.1	361.05	645	0	123.33	75	18.80	18	16.2	190.4	141.2	105.21	25	155	0.5	0.19	BDL	BDL
A47	6.9	300.78	530	0	274.17	275	33.40	54	6.66	108.6	294.4	62.75	0	85	0.5	1.8	BDL	BDL
A48	7.3	400.76	710	0	185.83	200	12.20	54	13.7	136.4	246	98.62	0	100	0.5	0.92	BDL	BDL
A49	6.9	250.54	380	0	74.17	25	11.20	11	14.8	68.2	55.6	55.1	0	70	0.5	0.07	BDL	BDL
A50	5.4	200.86	280	0	196.67	25	40.00	12	16	78.8	109.6	102.65	10	85	0.5	2.1	BDL	BDL
Max	**8.2**	**1402.89**	**1885**	**5**	**363.33**	**450**	**40.80**	**110**	**82.4**	**335.6**	**536.8**	**195.2**	**65**	**235**	**1.5**	**4.28**	-	-
Min	**5.4**	**160.31**	**280**	**0**	**60.00**	**25**	**2.00**	**9**	**3.6**	**19.15**	**55.6**	**27.88**	**0**	**25**	**0**	**0**	-	-
Mean	**6.95**	**560.96**	**863.18**	**0.4**	**165.56**	**133.5**	**19.03**	**34.5**	**19.84**	**139.48**	**199.65**	**86.46**	**13.3**	**106.6**	**0.43**	**0.44**	-	-
SD	**0.59**	**278.03**	**354.49**	**1.18**	**82.47**	**108.40**	**9.95**	**22.69**	**14.16**	**64.02**	**112.62**	**43.03**	**17.31**	**43.63**	**0.25**	**0.89**	-	-
CV	**8.42**	**49.56**	**41.07**	**294.51**	**49.81**	**81.20**	**52.26**	**65.76**	**71.39**	**45.90**	**56.41**	**49.77**	**130.14**	**40.93**	**57.59**	**202.36**	-	-

Max= Maximum, Min= Minimum, SD= Standard Deviation, CV= Coefficient of Variance, BDL= Below detection limit

Table 5.4: Analytical data of the groundwater samples of the study area (Pre-monsoon 2021)

SAMPLE NO.	pH	TDS (mg/L)	EC (µS/cm)	Turbidity (NTU)	TH (mg/L)	TA (mg/L)	Mg (mg/L)	Ca (mg/L)	K (mg/L)	Na (mg/L)	HCO3 (mg/L)	SO4 (mg/L)	NO3 (mg/L)	Cl (mg/L)	F (mg/L)	Fe (mg/L)	Cd (mg/L)	Cu (mg/L)
A1	6.5	203.01	351	0	120.56	50	16.80	20	11	80.3	97.95	85.41	9.9	63.19	0	0.04	0	0
A2	6.5	233.12	410	2	170.64	100	19.20	36	17.5	145.5	104.31	73.54	0.4	185.46	0	1.08	0	0
A3	8.3	153.87	262	0	110.48	50	14.40	20	6.5	123.8	81.13	46.17	5.9	170.92	0	0.48	0	0.16
A4	7.5	169.56	303	0	130.48	75	14.40	28	15.9	113.8	121.13	79.57	3.9	99.92	0	0	0	0.11
A5	7.1	575.34	968	1	521.84	350	30.20	74	23.3	134.6	417.24	84.02	1.4	176.65	0.5	0.25	0	0.08
A6	6.2	368.72	641	1	180.88	50	26.40	28	11.4	128	97.95	62.01	9.9	174.11	0.5	0.06	0.009	0.07
A7	7.3	396.03	677	0	160.64	225	19.20	32	12.5	157.1	301.34	54.98	2.4	153.19	0.5	0.5	0	0
A8	6.5	386.91	695	0	240.96	175	28.80	48	5.5	104.4	208.62	71.15	5.5	101.65	0	0	0	0
A9	7.2	271.19	466	0	170.64	125	19.20	36	6.2	119.4	173.85	18.95	1.5	178.92	0	0.08	0	0
A10	6.5	243.18	379	0	210.80	125	24.00	44	14.2	129.5	162.26	87.37	1.7	135.46	0.39	0.03	0	0
A11	6.9	187.73	335	1	140.56	75	16.80	28	3.6	120	118.13	86.75	0	111.92	0	0.08	0	0
A12	7.1	378.37	629	0	351.52	275	29.60	44	12.7	157.3	301.34	93.26	0	120.92	0.5	0.03	0	0
A13	7.4	729.56	991	0	411.52	125	35.60	68	24	205.1	324.52	122.12	17.8	178.65	0.5	0	0	0
A14	8	782.02	1112	0	280.88	325	26.40	48	23	286.6	394.06	111.76	20	194.11	0.5	0.3	0	0.06
A15	7.4	625.98	1080	1	422.00	300	40.00	37	27	250.3	452.01	118.52	3.1	148.65	0.62	0.06	0	0.08
A16	6.1	376.85	603	0	190.88	225	33.40	32	19.6	305.3	369.54	127.85	1.3	216.38	0.06	1.45	0	0
A17	7.1	422.17	720	5	341.68	225	40.40	52	7.9	244.1	359.75	129.48	0	188.65	0.33	1.64	0.056	0.45
A18	7.7	254.67	438	1	160.72	75	21.60	21	19	311	267.95	150.05	11.2	223.19	0	0.33	0	0
A19	7.1	788.46	1120	10	401.84	225	45.20	48	53.7	388.9	715.36	56.98	0.4	283.68	0.44	5.33	0.048	0.09
A20	7	271.83	470	0	200.96	50	21.80	22	22.1	191.9	159.54	95.46	19.2	168.65	0.06	0.06	0	0.11
A21	6.6	120.85	203	0	120.64	25	12.20	16	21	56.73	86.36	55.79	0	48.46	0	0	0	0.08
A22	7.1	145.95	224	0	70.24	75	7.20	16	3.15	36.96	57.95	48.51	0	27.73	0	0.03	0	
A23	7.2	203.67	350	0	130.56	50	16.80	18	5.9	126.5	99.54	72.87	5	123.19	0.5	0.14	0	0.15
A24	7.5	271.82	470	5	190.80	50	24.00	26	6.1	128.1	127.95	104.79	0	113.19	0.5	0.7	0	0.38
A25	8	134.16	239	0	80.32	50	9.60	16	3.88	34.35	79.54	6.31	0.4	45.46	0	0.03	0	0
A26	6.8	209.28	325	0	120.56	50	16.80	17	8.8	217.4	164.77	120.62	0	169.19	0	0.03	0	0
A27	7.5	326.68	580	0	180.72	75	15.60	20	11.7	205.8	148.13	88.57	8.6	180.92	0	0.03	0	0
A28	7.6	282.43	393	0	150.56	75	12.80	16	29.8	174.9	151.13	84.77	5.7	145.92	0.05	0.41	0	0.25
A29	6.4	282.72	398	0	140.64	50	19.20	16	18.9	146.6	115.95	89	0	139.92	0	0.05	0	0
A30	5.8	398.79	553	0	160.72	50	17.60	21	28.2	149.2	89.36	59.85	47.2	164.11	0	0.04	0	0
A31	6.5	326.64	573	1	220.96	125	18.80	33	3.9	170.3	178.67	79.83	3.6	146.92	0	1.53	0.015	0.19
A32	7.6	675.45	998	0	230.64	400	19.20	60	9.4	323.2	409.96	167.42	0	196.38	1.77	0.05	0	0.06
A33	7.7	451.83	779	1	220.88	175	16.40	31	27.1	209.5	208.62	85.69	10.5	184.11	0.15	0.31	0	0.09
A34	7.5	422.92	749	0	241.04	50	21.20	18	28.9	261.6	187.95	163.97	21.6	188.65	0.5	0.05	0	0
A35	7.2	575.38	960	1	331.28	150	24.40	32	15.7	242.2	232.26	109.33	24	199.57	0.5	0.38	0	0.17
A36	7.2	388.18	639	0	190.56	100	12.80	38	41.7	209.4	197.49	96.65	13.5	188.65	0	0.04	0	0.06
A37	7.3	271.03	472	0	211.04	75	21.20	19	40.4	219.6	162.72	125.02	4.1	198.65	0.15	0.39	0	0.05
A38	7.3	364.24	622	10	120.24	50	7.20	22	27.6	262.8	169.95	138.2	0	199.11	1.08	0.11	0	0.1
A39	7.1	521.33	891	0	351.20	350	26.00	50	3.7	291.5	359.29	139.74	0.4	196.38	0.5	0.13	0	0
A40	7.8	625.91	995	0	230.80	100	17.00	32	41.9	260	219.38	164.88	0	196.98	0.5	0.26	0	0
A41	6.8	526.95	944	0	452.00	300	30.00	40	7.2	280.9	361.24	194.17	0.4	188.65	0.5	0.44	0	0
A42	6.3	428.17	761	0	220.88	75	26.40	30	21.5	241.3	225.9	164.36	0	178.11	0.28	0.26	0	0.5
A43	6.9	451.34	813	0	261.04	150	21.20	32	11.7	292.7	277.03	170.91	11.6	186.38	0.1	0	0	0
A44	7.6	428.87	758	0	180.64	200	13.20	30	12.3	298.6	243.39	176.52	0	188.65	0.23	0.04	0	0
A45	7.7	526.42	897	1	210.72	275	21.60	41	14.5	299.1	347.7	157.08	0	183.19	0.13	0.57	0	0
A46	5.9	401.11	698	0	140.40	50	12.00	36	22.4	218.7	243.92	113.01	30	141.84	0.5	0.18	0	0
A47	6.7	344.95	561	1	300.64	200	19.20	58	8.52	110.54	263.52	74.88	0	103.19	0	0.2	0	0.11
A48	7	428.85	752	1	321.20	175	36.00	41	12.1	224.4	301.34	152.06	0	176.38	0.15	0.38	0	0.2
A49	6.8	216.78	384	0	140.48	100	14.40	32	11	212.3	174.31	114.31	0	175.46	0.5	0.03	0	0
A50	5.7	159.34	284	0	60.32	25	9.60	8	25.4	236.8	193.18	118.18	5.1	153.19	0.5	0.06	0	0.09
Max	**8.3**	**788.46**	**1120**	**10**	**521.84**	**400**	**45.20**	**74**	**53.7**	**388.9**	**715.36**	**194.17**	**47.2**	**283.68**	**1.77**	**5.33**	**0.06**	**0.5**
Min	**5.7**	**120.85**	**203**	**0**	**60.32**	**25**	**7.20**	**8**	**3.15**	**34.35**	**57.95**	**6.31**	**0**	**27.73**	**0**	**0**	**0**	**0**
Mean	**7.05**	**374.61**	**618.3**	**0.86**	**218.06**	**138**	**21.26**	**32.62**	**17.22**	**196.78**	**226.13**	**103.85**	**6.14**	**160.06**	**0.28**	**0.37**	**0.00**	**0.08**
SD	**0.59**	**170.83**	**259.64**	**2.16**	**103.86**	**100.03**	**8.63**	**14.45**	**11.34**	**80.53**	**125.45**	**42.15**	**9.49**	**48.14**	**0.33**	**0.81**	**0.01**	**0.12**
CV	**8.32**	**45.60**	**41.99**	**250.84**	**47.63**	**72.49**	**40.62**	**44.29**	**65.85**	**40.93**	**55.48**	**40.59**	**154.40**	**30.07**	**119.30**	**218.09**	**410.77**	**153.65**

Max= Maximum, Min= Minimum, SD= Standard Deviation, CV= Coefficient of Variance, BDL= Below detection limit

Table 5.5: Analytical data of the groundwater samples of the study area (Post-monsoon 2021)

SAMPLE NO.	pH	TDS (mg/L)	EC (µS/cm)	Turbidity (NTU)	TH (mg/L)	TA (mg/L)	Mg (mg/L)	Ca (mg/L)	K (mg/L)	Na (mg/L)	HCO3 (mg/L)	SO4 (mg/L)	NO3 (mg/L)	Cl (mg/L)	F (mg/L)	Fe (mg/L)	Cd (mg/L)	Cu (mg/L)
A1	6.8	423.12	589	0	121.67	50	10.00	32	25.2	123.2	91.3	73.5	10	112	0	0.06	0	0
A2	6.9	560.13	756	3	137.50	75	6.00	45	15.67	138.3	187.7	56.8	0	80	0	1.02	0	0
A3	7.9	313.14	499	0	87.92	50	7.90	22	11.08	85.34	76.8	45.6	10	60	0.4	0.33	0	0.06
A4	7.6	399.98	701	0	115.42	75	3.10	41	11.45	92.51	115.7	45.9	0	30	0.3	0.01	0	0.08
A5	7.5	875.34	1569	0	391.25	250	20.10	123	56.2	172.2	529.5	86.1	0	80	0.6	0.12	0	0.04
A6	6.4	675.86	1176	0	150.00	50	15.60	34	56.9	256.8	202.7	143.1	34	120	0.4	0.04	0.003	0.02
A7	6.9	526.14	937	1	137.08	150	13.10	33	35.56	156.8	191.8	100.7	12	65	0.6	0.3	0	0
A8	6.8	557.11	962	0	205.42	150	15.70	56	34.54	212.2	284.5	76.3	23	80	0.2	0	0	0
A9	7.4	451.23	785	0	241.25	150	35.70	37	25.34	165.8	161.7	121.6	11	95	0	0.05	0	0
A10	6.6	343.65	598	0	129.17	75	14.80	27	2.8	56.45	121.8	56.8	0	45	0	0.08	0	0
A11	7.3	435.12	654	0	139.58	75	25.70	13	22.7	165.3	74.1	121.3	12	100	0	0.05	0	0
A12	6.7	496.67	834	0	282.92	275	22.30	76	7.8	83.23	267.8	78.4	0	56	0	0	0	0
A13	7.8	799.84	1416	0	360.00	275	36.60	83	35.6	286.5	311.3	186.3	12	200	0.6	0	0	0
A14	8.1	812.02	1456	0	414.17	325	41.20	97	45.7	311.6	336.8	163.2	54	115	0.4	0.13	0	0.03
A15	7.6	695.16	1217	0	330.00	300	45.60	56	43.5	225.9	381.3	165.9	23	80	0.3	0.04	0	0.05
A16	6.5	496.77	886	1	212.50	250	34.80	27	8.9	131.2	141.7	36.2	12	85	0.2	0.61	0	0
A17	7.5	489.32	858	1	254.17	225	34.00	45	13.2	117.9	211.3	109.7	0	112	0.4	0.53	0.011	0.4
A18	8	454.87	785	0	206.67	175	29.80	33	23.1	130.1	193.2	134.1	13	85	0	0.23	0	0
A19	7.2	824.22	1456	0	311.83	225	25.04	83	98.4	340	421.8	176.8	34	214	0.2	1.5	0.027	0.01
A20	7.5	331.15	587	0	146.88	75	18.45	28	16.6	80.65	62.5	57.6	8	89	0.4	0.03	0	0.06
A21	6.8	360.82	503	0	94.17	50	17.80	8	4.6	75.67	68.2	56.8	9	76	0.3	0	0	0.01
A22	7.8	235.45	391	0	62.92	50	6.70	14	7.8	21.23	69.1	34.6	0	45	0.6	0.01	0	0
A23	7.7	453.61	723	0	123.75	75	14.70	25	16.7	73.35	81.5	43.8	11	60	0.3	0.11	0	0.11
A24	7.1	341.82	551	0	172.08	50	25.70	26	15.4	76.12	88.3	76.3	13	70	0.4	0.2	0	0.19
A25	7.9	374.14	546	0	159.17	75	19.60	31	16.7	123.7	173.1	32.9	8	81	0.6	0.05	0	0
A26	7.3	439.22	612	0	123.75	50	15.30	24	16.4	110	79.5	89.6	9	65	0	0	0	0
A27	7.8	526.56	915	0	185.83	75	22.40	37	26.7	186.8	134.6	121.3	14	95	0	0.12	0	0
A28	7.8	428.23	723	0	150.42	100	20.50	26	39.6	122	211.7	34.6	35	70	0	0.18	0	0.15
A29	6.6	432.14	711	0	100.42	75	8.50	26	11.3	113.6	98.2	78.7	7	65	0	0.03	0	0
A30	6.1	458.66	814	0	122.08	75	15.50	23	33.6	165.7	111.5	65.4	13	95	0	0.08	0	0
A31	6.9	476.17	857	0	165.42	150	23.50	27	18.6	131.2	145.6	76.6	17	95	0.5	0.78	0.01	0.06
A32	8	695.56	1138	0	242.08	375	25.70	54	11.8	167.8	498.1	45.2	6	145	1	0	0	0
A33	7.6	584.16	803	0	176.67	100	26.80	26	32.1	234.7	211.5	89.5	5	120	0.4	0.26	0	0
A34	7.8	422.56	671	0	130.42	50	16.30	25	15.7	122	95.6	66.7	22	85	0.4	0	0	0
A35	7.1	645.11	985	0	156.25	75	15.90	36	22.4	91.23	132.8	49.1	7	90	0.2	0.11	0	0.05
A36	7.8	658.13	954	0	227.08	175	16.70	63	4.7	154.7	246.7	47.2	9	95	0.2	0	0	0
A37	7.5	494.37	714	0	189.17	75	25.60	33	9.9	67.12	111.4	35.5	6	116	0.2	0.26	0	0
A38	7.8	484.76	761	0	117.50	50	12.60	26	22.3	153.5	109.8	68.5	5	115	0	0.11	0	0.01
A39	7.8	521.87	891	0	280.42	225	34.90	54	19.5	211.6	287.9	141.3	7	115	0.4	0	0	0
A40	7.5	665.11	1023	0	198.33	125	20.60	45	35	254.7	114.9	98.5	9	120	0.4	0.18	0	0
A41	7.3	656.23	983	1	332.50	300	39.60	67	20.8	135.7	367.2	77.5	32	65	0.5	0.39	0	0
A42	6.8	428.76	665	0	169.17	75	27.40	22	32.1	188.7	114.8	57.2	11	145	0.4	0.18	0	0.08
A43	6.8	451.13	813	0	164.17	75	25.60	23	22.3	191.2	141.5	66.5	9	154	0.4	0	0	0
A44	7.9	428.19	674	0	177.50	175	22.20	34	16.5	127.9	178.8	73.1	7	80	0.5	0.03	0	0
A45	7.2	526.52	773	4	149.17	200	16.60	32	7.8	194.5	223.7	89.6	0	87	0.4	0.74	0	0
A46	6.3	527.87	762	0	160.83	50	23.60	25	22.6	186.5	138.1	97.4	13	145	0.4	0.13	0	0
A47	6.8	394.23	651	0	303.75	225	35.10	63	9.5	98.45	291.1	56.3	0	95	0	0.15	0	0.06
A48	6.9	428.51	712	0	222.08	200	16.70	61	16.8	125.8	234.1	89.1	0	90	0.4	0.23	0	0.14
A49	7.3	296.15	435	0	103.33	75	16.40	14	17.8	61.23	49.8	65.1	0	67	0.4	0	0	0
A50	5.6	219.54	304	0	296.25	75	62.10	15	20	71.23	89.3	98.2	9	80	0.3	0.1	0	0.02
Max	**8.1**	**875.34**	**1569**	**4**	**414.17**	**375**	**62.10**	**123**	**98.4**	**340**	**529.5**	**186.3**	**54**	**214**	**1**	**1.5**	**0.03**	**0.4**
Min	**5.6**	**219.54**	**304**	**0**	**62.92**	**50**	**3.10**	**8**	**2.8**	**21.23**	**49.8**	**32.9**	**0**	**30**	**0**	**0**	**0**	**0**
Mean	**7.25**	**500.33**	**815.58**	**0.22**	**192.64**	**136**	**22.52**	**39.52**	**23.14**	**147.39**	**185.27**	**83.16**	**11.22**	**94.58**	**0.29**	**0.19**	**0.00**	**0.03**
SD	**0.56**	**147.88**	**272.37**	**0.74**	**82.76**	**89.52**	**11.17**	**23.17**	**16.59**	**68.27**	**113.39**	**38.96**	**11.03**	**35.42**	**0.23**	**0.29**	**0.00**	**0.07**
CV	**7.78**	**29.56**	**33.40**	**334.78**	**42.96**	**65.83**	**49.60**	**58.63**	**71.68**	**46.32**	**61.20**	**46.85**	**98.27**	**37.45**	**77.92**	**152.43**	**421.8**	**211.5**

Max= Maximum, Min= Minimum, SD= Standard Deviation, CV= Coefficient of Variance, BDL= Below detection limit

5.2.1 pH

pH (potential of hydrogen) is used to express the hydrogen ion activity in water on a logarithmic scale. The pH value shows the balance between acids and bases in groundwater. Water that is close to 7 in pH is referred to as neutral, pH less than 7 is acidic and greater than 7 is basic.

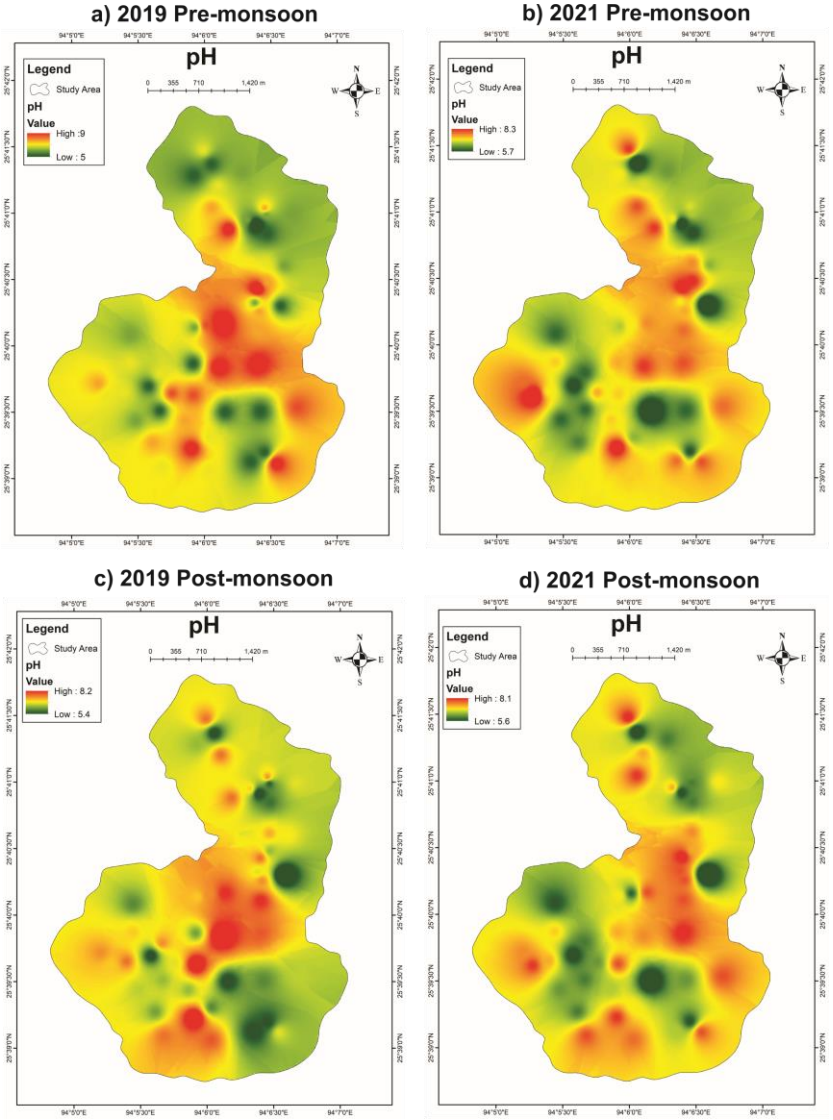

Fig. 5.1: Geospatial distribution maps of pH during (a) 2019 Pre-monsoon (b) 2021 Pre-monsoon (c) 2019 Post-monsoon (d) 2021 Post-monsoon

The pH ranged from 5 to 9 in the study area indicating the acidic to alkaline nature. The descriptive statistics of pH pre-monsoon and post-monsoon groundwater samples in 2019 and 2021 are shown in Tables 5.2 to 5.5 and the spatial distribution map is shown in Fig. 5.1. The hydrogen ion concentration of the groundwater in 2019 pre-monsoon varies from 5-9 with a mean of 7.04; in 2021 pre-monsoon, pH varies from 5.7- 8.3 with a mean of 7.1. Whereas, the hydrogen ion concentration of the groundwater in 2019 post-

monsoon varies from 5.4- 8.2 with a mean of 6.95 and in 2021 post-monsoon pH varies from 5.6- 8.1 with a mean of 7.25.

The areas with high pH (alkaline) are mostly distributed in the central and southern parts of the study area (Fig. 5.1a, b, c and d). This is because of the dominance of dissolved HCO_3^- ions, which have been known to change the pH of water (Laar et al., 2011).

5.2.2 Total Dissolved Solids (TDS)

All solid materials that are present in solution in an ionized state and do not include suspended colloids or dissolved gases are known as Total dissolved solids (TDS). The amount of TDS in groundwater determines whether it is suitable for irrigation, drinking, and other industrial uses. TDS is classified into four types of water: fresh water (TDS < 1000 mg/L), brackish water (TDS 1,000- 10,000 mg/L), saline water (TDS 10,000- 1,00,000 mg/L) and brine water (TDS >1,00,000 mg/L) (Freeze and Cherry, 1979).

The concentration of TDS in the study area ranged from 120.85 to 1402.89 mg/L. The descriptive statistics of TDS pre-monsoon and post-monsoon groundwater samples in 2019 and 2021 are shown in Tables 5.2 to 5.5 and the spatial distribution map is shown in Fig. 5.2. The TDS of the groundwater in 2019 pre-monsoon varies from 131.1- 1207 mg/L with a mean of 417.11 mg/L and in 2021 pre-monsoon, TDS varies from 120.85-788.46 mg/L with a mean of 374.61 mg/L. Whereas, TDS concentration of the groundwater in 2019 post-monsoon varies from 160.31- 1402.89 mg/L with a mean of 560.96 mg/L and in 2021 post-monsoon TDS varies from 219.54- 875.34 mg/L with a mean of 500.33 mg/L.

The areas with high TDS are mostly distributed in the central and northern parts of the study area (Fig. 5.2a, b, c and d). The high TDS values are mostly found in the Disang Group of rocks which are abundant in shale rocks. The geology of shale rocks affects the concentration of TDS because they weather more readily than others (Water Resources Mission Area, 2019). The TDS in the study area is within the permissible limit for drinking (Table 5.1).

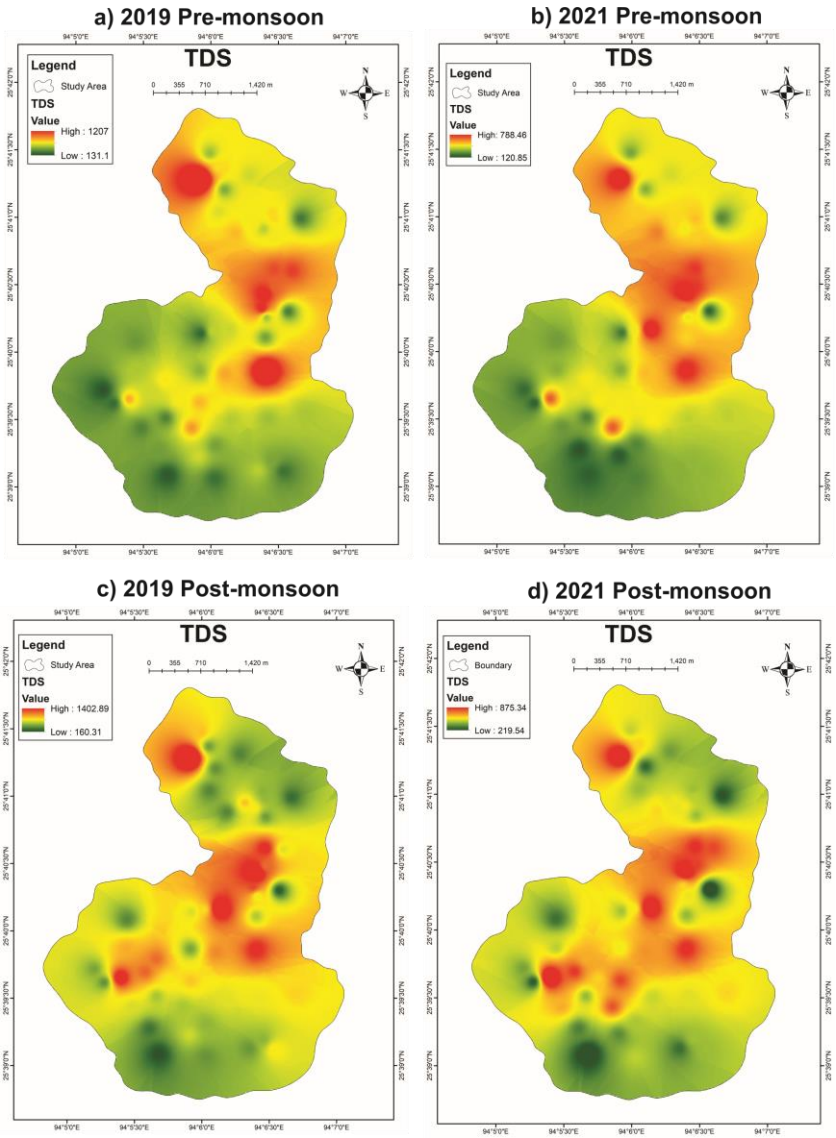

Fig. 5.2: Geospatial distribution maps of TDS during (a) 2019 Pre-monsoon (b) 2021 Pre-monsoon (c) 2019 Post-monsoon (d) 2021 Post-monsoon

5.2.3 Electrical Conductivity (EC)

The EC is the ability to conduct an electric current and measure of the salt content of water which is expressed as µS/cm (micro Siemens/cm) (Karanth, 1987). EC is found to directly affect the percentage of TDS (Shrinivasa Rao and Venkateswara, 2000).

The descriptive statistics of EC pre-monsoon and post-monsoon groundwater samples in 2019 and 2021 are shown in Tables 5.2 to 5.5 and the spatial distribution map is shown in Fig. 5.3. The concentration of EC in the study area ranged from 203 to 1885 µS/cm. The EC of the groundwater in 2019 pre-monsoon varies from 230- 1700 µS/cm with a mean of 634.7 µS/cm and in 2021 pre-monsoon, EC varies from 203- 1120 µS/cm with a mean of 618.3 µS/cm Whereas, EC concentration of the groundwater in 2019 post-

monsoon varies from 280-1885 µS/cm with a mean of 863.18 µS/cm and in 2021 post-monsoon EC varies from 304-1569 µS/cm with a mean of 815.58 µS/cm.

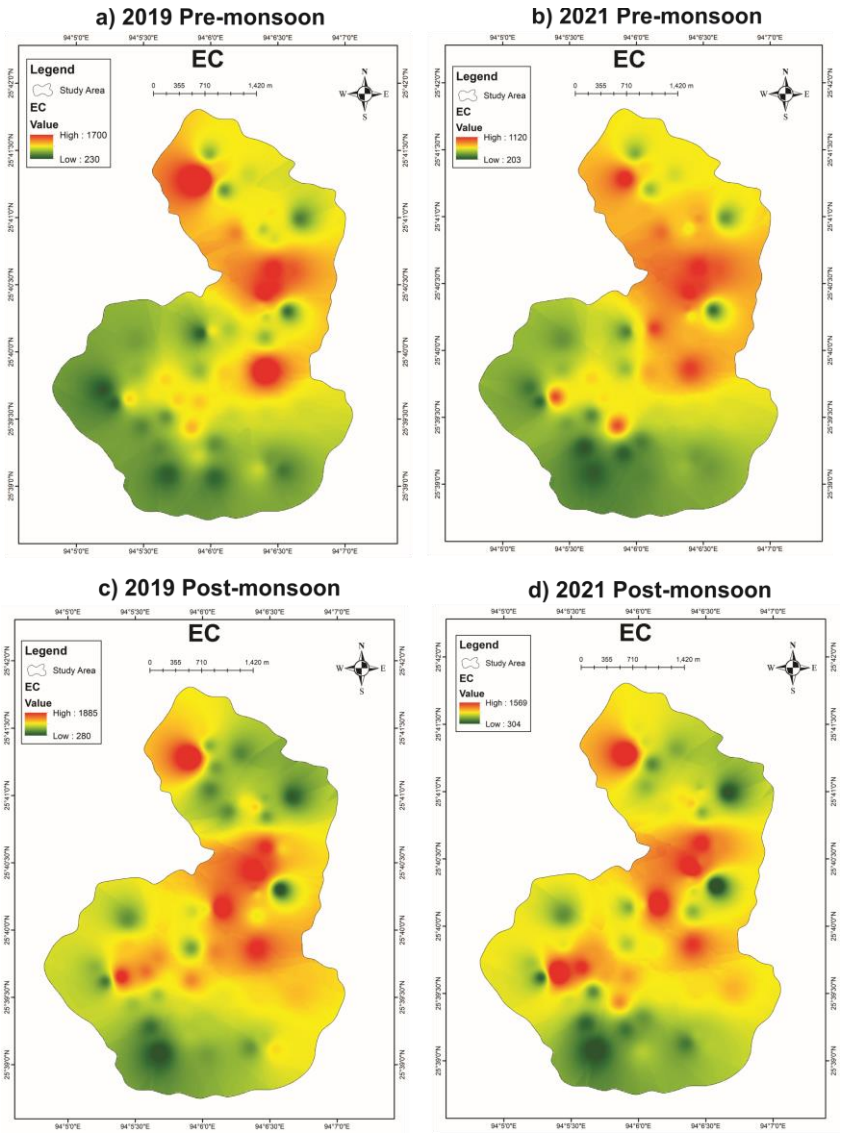

Fig. 5.3: Geospatial distribution maps of EC during (a) 2019 Pre-monsoon (b) 2021 Pre-monsoon (c) 2019 Post-monsoon (d) 2021 Post-monsoon

The EC in the pre-monsoon seasons of 2019 and 2021 are mostly distributed in the central, eastern and northern parts while in the post-monsoon seasons of 2019 and 2021, the EC has also increased towards the western part of the study area (Fig. 5.3a, b, c and d). The high EC values in the study area denote that there is a high concentration of soluble salts in groundwater and anthropogenic influences like seepage of domestic and municipal sewage are present (Hussain et al., 2002). The geospatial distribution of EC of all the samples showed almost similar trends to that of TDS.

5.2.4 Turbidity

Turbidity is a measurement of the cloudiness in water and is mostly caused by suspended particles like silt, clay, plankton and other organisms, as well as light scattering and absorption. It is expressed in NTU (Nephelometric Unit).

The turbidity in the study area ranged from 0-10 NTU. The descriptive statistics of turbidity pre-monsoon and post-monsoon groundwater samples in 2019 and 2021 are shown in Tables 5.2 to 5.5 and the spatial distribution map is shown in Fig. 5.4. The highest value of turbidity in the groundwater during 2019 pre-monsoon is 8 NTU and has a mean of 0.24 NTU while in 2021 pre-monsoon, the highest value of turbidity is 10 NTU with a mean of 0.86 NTU. Whereas the highest turbidity concentration of the groundwater in 2019 post-monsoon is 5 NTU with a mean of 0.4 NTU while in 2021 post-monsoon the highest value of turbidity is 4 NTU with a mean of 0.22 NTU.

The high turbidity in 2019 pre-monsoon is found in the northern area and a small pocket in the central area. In 2021 pre-monsoon, high concentrations of turbidity are observed in the northern area and in small pockets towards the south. In 2019 and 2021 post-monsoon, the higher concentration of turbidity is found towards the north-west and south-west.

There are several sources of turbidity in the groundwater of the study area. In pre-monsoon seasons of 2019 and 2021, the groundwater level had decreased and almost reached the bottom of the well which has mostly led to increased turbidity. Turbidity may also be from wastewater containing residual particles, decaying plant and animal matter, or soil erosion from building construction near the sampling sites.

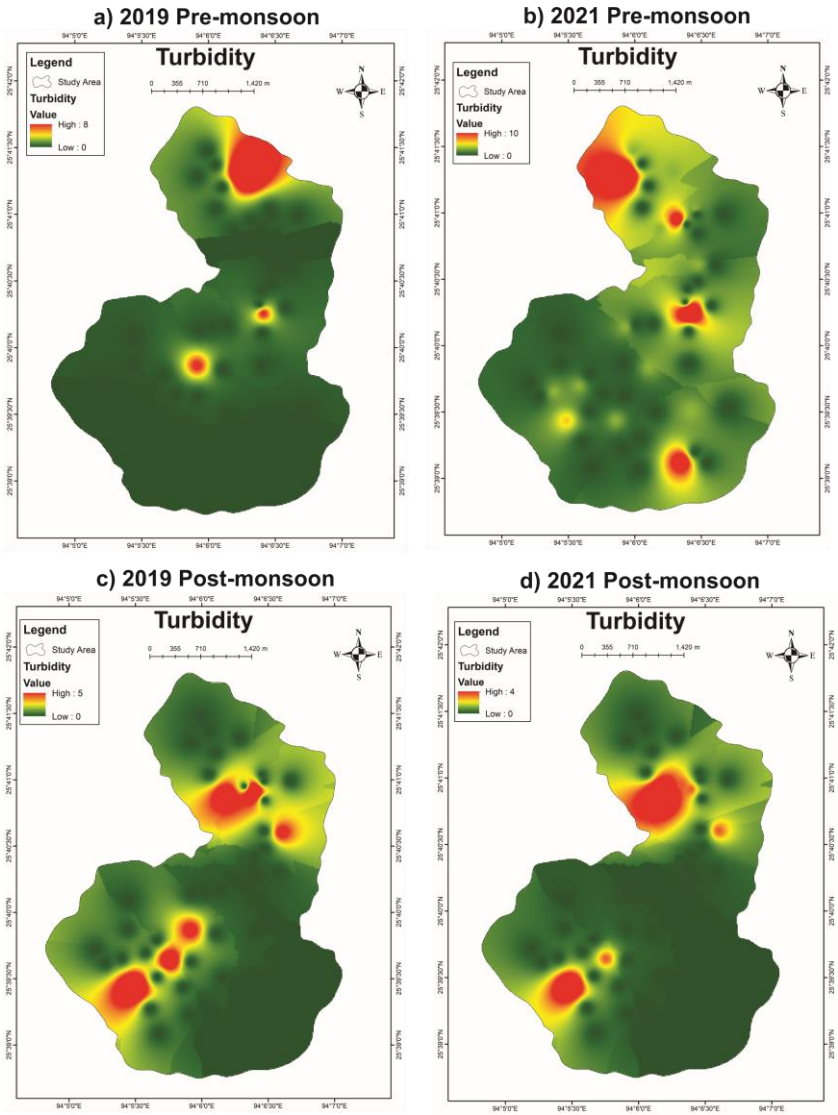

Fig. 5.4: Geospatial distribution maps of Turbidity during (a) 2019 Pre-monsoon (b) 2021 Pre-monsoon (c) 2019 Post-monsoon (d) 2021 Post-monsoon

5.2.5 Total Hardness (TH)

TH is an important measure for determining the usability of water for drinking and other domestic supplies, as it causes an unpleasant taste and reduces the ability of soap to produce lather. Hardness is defined by the sum of the concentrations of Ca and Mg ions which is expressed in mg/L of $CaCO_3$. TH values are subdivided into four degrees (Sawyer and Mc Carty, 1967) which are: soft (<75 mg/L), moderately hard (75–150 mg/L), hard (150–200 mg/L) and very hard (>300 mg/L).

The nature of the groundwater samples is presented in the integrated water quality diagram using TH and TDS (Fig. 5.5). The study area's groundwater quality is predominantly hard and fresh water type. The pre-monsoon 2019 groundwater is dominated by hard-fresh water with 58%, pre-monsoon 2021 groundwater is dominated

by hard-fresh water with 25%, post-monsoon 2019 groundwater is dominated by moderately hard-fresh water with 44% and post-monsoon 2021 groundwater is dominated by hard-fresh water with 42%.

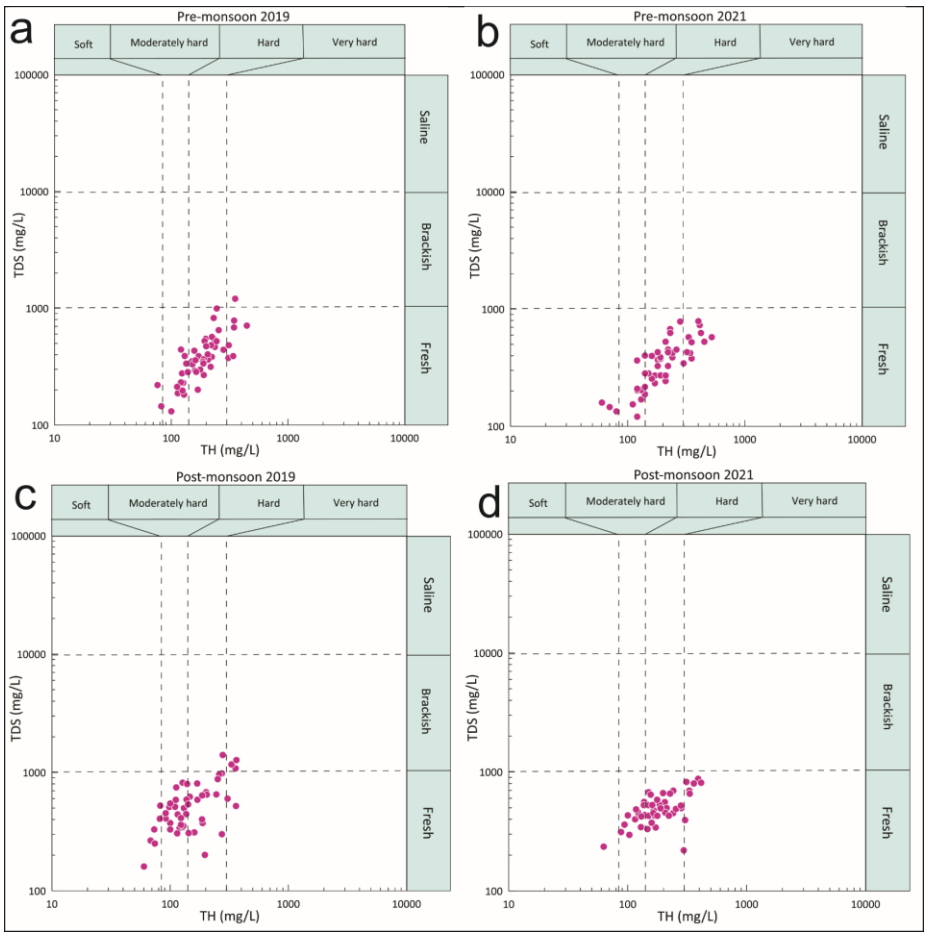

Fig. 5.5: Relationship between TH and TDS reflecting groundwater quality (a) 2019 Pre-monsoon (b) 2021 Pre-monsoon (c) 2019 Post-monsoon (d) 2021 Post-monsoon

The value of TH was observed to be between 60 mg/L- 521.84 mg/L. The descriptive statistics of TH pre-monsoon and post-monsoon groundwater samples in 2019 and 2021 are shown in Tables 5.2 to 5.5 and the spatial distribution map is shown in Fig. 5.6. The TH of the groundwater in 2019 pre-monsoon varies from 76.22-444.29 mg/L with a mean of 198.22 mg/L and in 2021 pre-monsoon, TH varies from 60.32- 521.84 mg/L with a mean of 218.06 mg/L. Whereas, TH concentration of the groundwater in 2019 post-monsoon varies from 60- 363.33 mg/L with a mean of 165.56 mg/L and in 2021 post-monsoon TH varies from 62.92- 414.17 mg/L with a mean of 192.64 mg/L.

High TH values are distributed around the northern and central parts in the study area. The TH of water is mainly due to the dispersion of chlorides, bicarbonates and sulphates in water (Dash, 1999). The domestic effluent also increases the TH of the

groundwater. The TH in the study area is found to be within the permissible limit for drinking (Table 5.1).

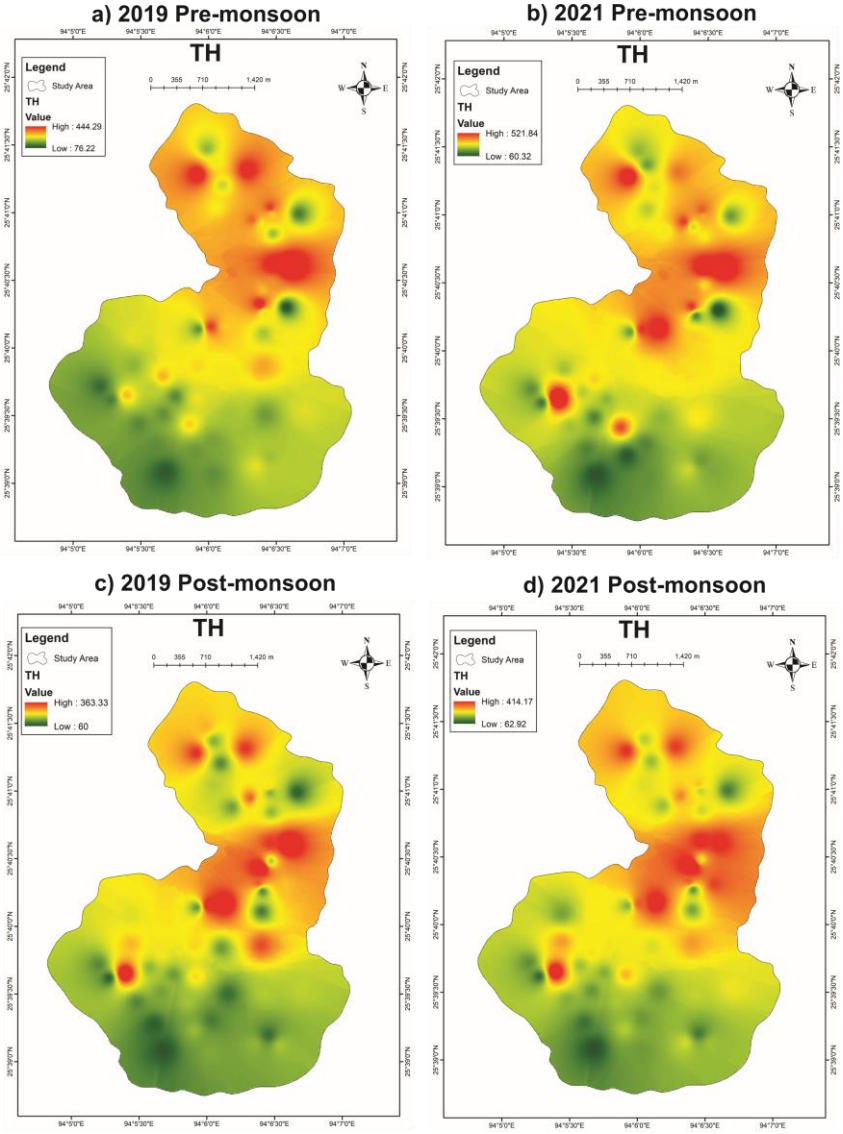

Fig. 5.6: Geospatial distribution maps of TH during (a) 2019 Pre-monsoon (b) 2021 Pre-monsoon (c) 2019 Post-monsoon (d) 2021 Post-monsoon

5.2.6 Total Alkalinity (TA)

The ability to neutralize acids is referred to as alkalinity. TA is not a chemical in water but it is a property of water that depends on the presence of carbonate and bicarbonate salts along with hydroxyl ions in the free salts.

The value of TA was observed to be between 25 mg/L- 575 mg/L. The descriptive statistics of TA pre-monsoon and post-monsoon groundwater samples in 2019 and 2021 are shown in Tables 5.2 to 5.5 and the spatial distribution map is shown in Fig. 5.7. The TA of the groundwater in 2019 pre-monsoon varies from 25-575 mg/L with a mean of 139 mg/L and in 2021 pre-monsoon, TA varies from 25-400 mg/L with a mean of 138

mg/L. Whereas, TA concentration of the groundwater in 2019 post-monsoon varies from 25-450 mg/L with a mean of 133.5 mg/L and in 2021 post-monsoon TA varies from 50-375 mg/L with a mean of 136 mg/L. The higher TA values are distributed around the north-western and eastern parts of the study area. The TA concentrations in the study area are found to be within the permissible limit for drinking (Table 5.1).

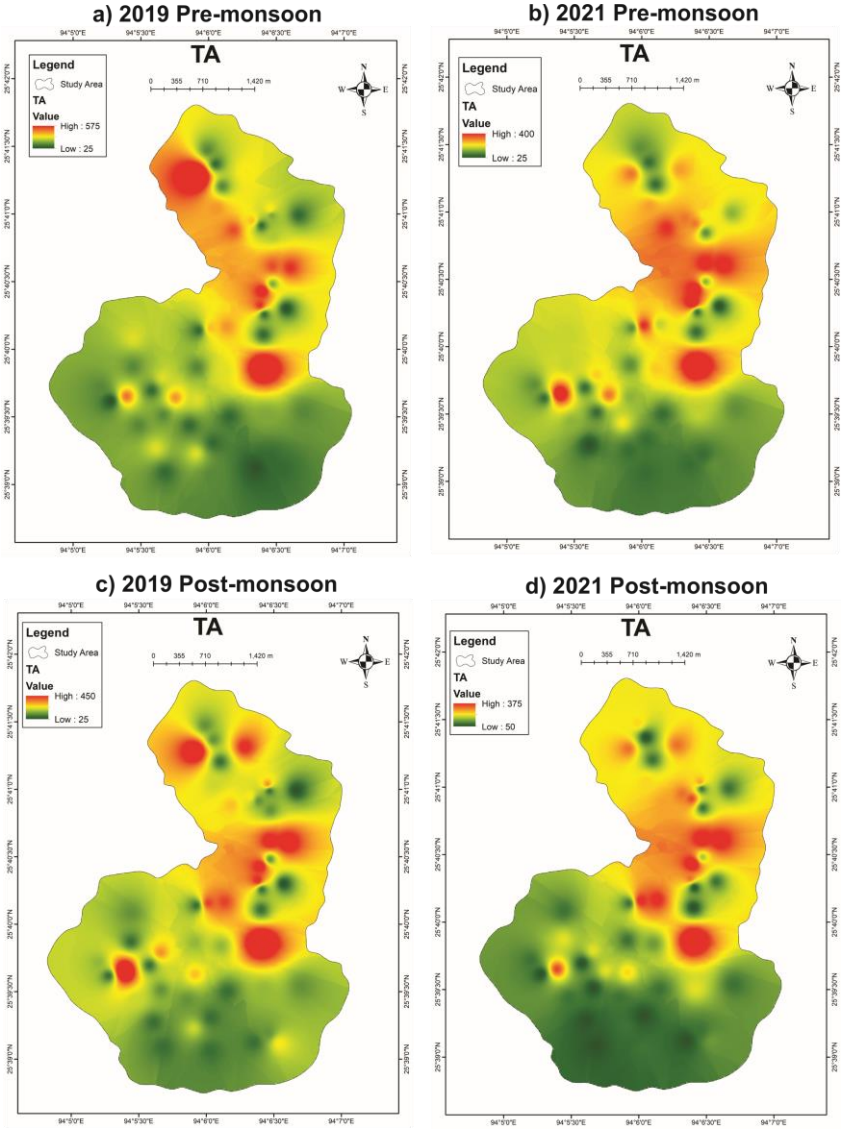

Fig. 5.7: Geospatial distribution maps of TA during (a) 2019 Pre-monsoon (b) 2021 Pre-monsoon (c) 2019 Post-monsoon (d) 2021 Post-monsoon

5.2.7 Magnesium (Mg^{2+})

Mg^{2+} is a common element in the earth's crust and is found in all natural waters. The value of Mg^{2+} was observed to be between 2- 62.93 mg/L. The descriptive statistics of Mg^{2+} pre-monsoon and post-monsoon groundwater samples in 2019 and 2021 are shown in Tables 5.2 to 5.5 and the spatial distribution map is shown in Fig. 5.8.

The Mg^{2+} of the groundwater in 2019 pre-monsoon varies from 2.2- 62.93 mg/L with a mean of 22.46 mg/L and in 2021 pre-monsoon, Mg^{2+} varies from 7.2- 45.2 mg/L with a mean of 21.26 mg/L. Whereas Mg^{2+} concentration of the groundwater in 2019 post-monsoon varies from 2- 40.8 mg/L with a mean of 19.03 mg/L and in 2021 post-monsoon Mg^{2+} varies from 3.1-62.1 mg/L with a mean of 22.52 mg/L.

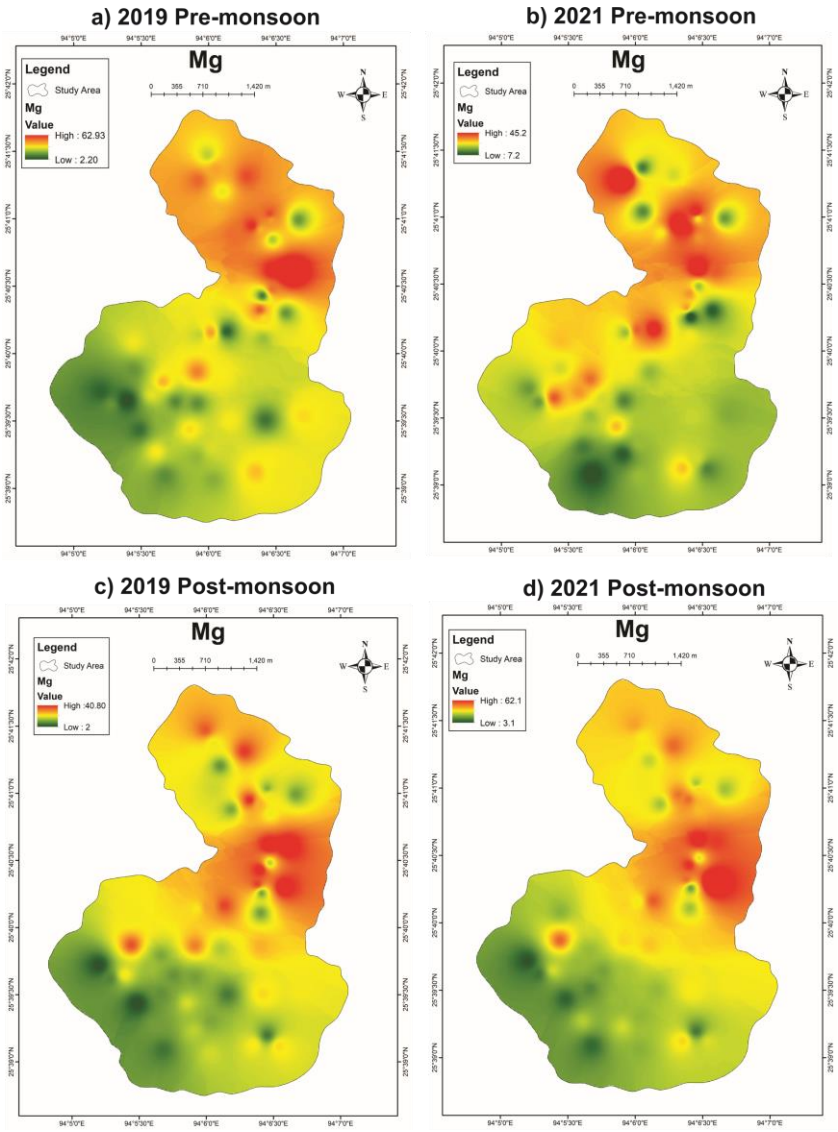

Fig. 5.8: Geospatial distribution maps of Mg^{2+} during (a) 2019 Pre-monsoon (b) 2021 Pre-monsoon (c) 2019 Post-monsoon (d) 2021 Post-monsoon

High Mg^{2+} values are distributed around the northern parts of the study area during pre-monsoon season and the high Mg^{2+} concentrations are more towards the central-east during post-monsoon seasons. Mafic minerals (pyroxene, amphibole, and olivine)

chlorite and clay minerals are the sources of Mg^{2+}. The Mg^{2+} concentrations in the study area are found to be within the permissible limit for drinking (Table 5.1).

5.2.8 Calcium (Ca^{2+})

Ca^{2+} is a widely distributed element of the alkaline earth metals found in natural waters. Additionally, aquifer water that has been present for a longer period of time may include more Ca^{2+}, which was likely released during feldspar alteration (Hem, 1970).

The value of Ca^{2+} was observed to be between 8-123 mg/L. The descriptive statistics of Ca^{2+} pre-monsoon and post-monsoon groundwater samples in 2019 and 2021 are shown in Tables 5.2 to 5.5 and the spatial distribution map is shown in Fig. 5.9. The Ca^{2+} of the groundwater in 2019 pre-monsoon varies from 10-90 mg/L with a mean of 41.56 mg/L and in 2021 pre-monsoon, Ca^{2+} varies from 8-74 mg/L with a mean of 32.62 mg/L. Whereas Ca^{2+} concentration of the groundwater in 2019 post-monsoon varies from 9-110 mg/L with a mean of 34.5 mg/L and in 2021 post-monsoon Ca^{2+} varies from 8-123 mg/L with a mean of 39.52 mg/L.

The geospatial distribution of Ca^{2+} in pre-monsoon and post-monsoon seasons are almost similar i.e., higher values are found towards the northern and central part of the study area. In soils and rocks, Ca^{2+} can be found as absorbed ions on negatively charged mineral surfaces. Most clastic deposits, including sandstone, shale, and others, use $CaCO_3$ as a cementing material. Ca^{2+} ions are released into groundwater during the weathering of silicate rocks in the presence of CO_2 (Mazor et al., 1980). The Ca^{2+} concentrations in the study area are found to be within the permissible limit for drinking (Table 5.1).

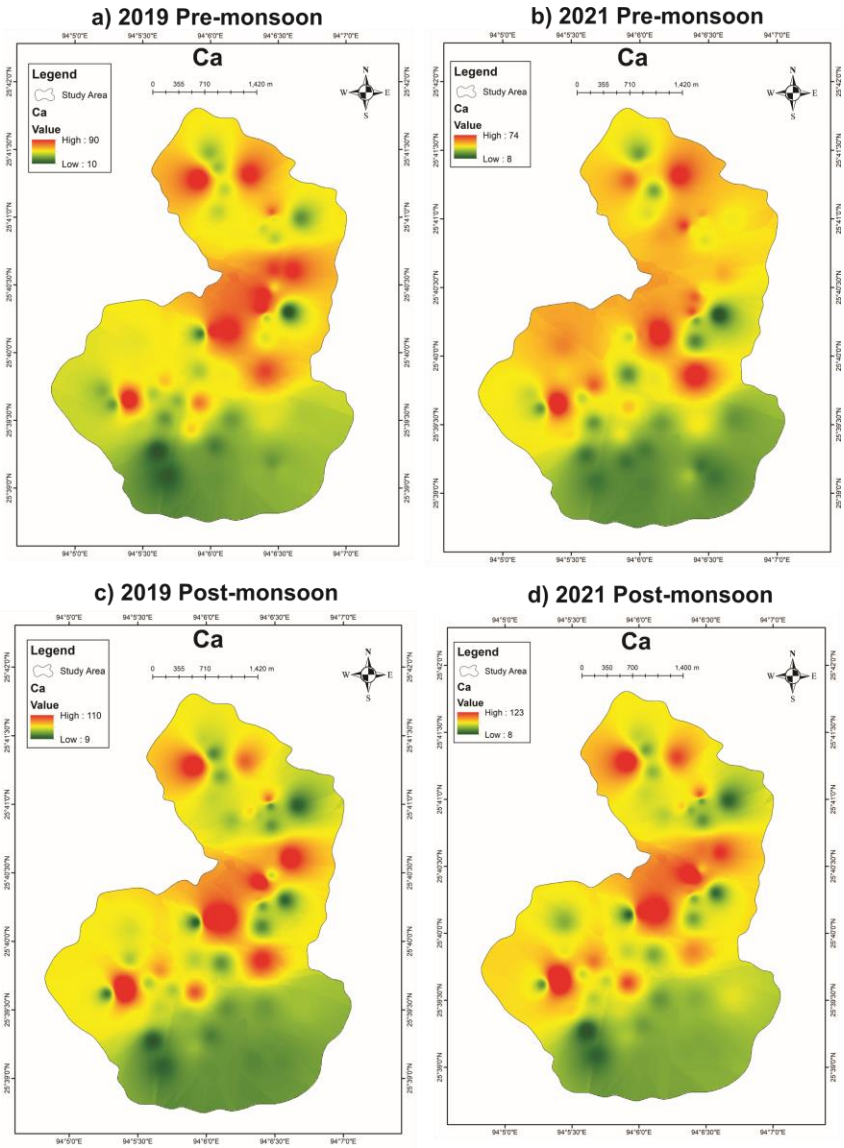

Fig. 5.9: Geospatial distribution maps of Ca^{2+} during (a) 2019 Pre-monsoon (b) 2021 Pre-monsoon (c) 2019 Post-monsoon (d) 2021 Post-monsoon

5.2.9 Potassium (K^+)

K^+ is substantially less abundant in groundwater than Na^+, Ca^{2+} and Mg^{2+} (Kumar et al., 2015). The resistance of K^+ minerals to break down due to weathering and the fixation of K^+ in clay minerals due to weathering are the two causes of the low concentration of K^+ in groundwater (Karanth, 1989). When rocks dissolve, potassium is slowly released; as a result, concentration rises with increasing population.

The value of K^+ was observed to be between 2.8- 98.4 mg/L. The descriptive statistics of K^+ pre-monsoon and post-monsoon groundwater samples in 2019 and 2021 are shown in Tables 5.2 to 5.5 and the spatial distribution map is shown in Fig. 5.10. The K^+ of the groundwater in 2019 pre-monsoon varies from 3.31-56.06 mg/L with a mean of

31.36 mg/L and in 2021 pre-monsoon, K^+ varies from 3.15- 53.7 mg/L with a mean of 17.22 mg/L. Whereas, K^+ concentration of the groundwater in 2019 post-monsoon varies from 3.6- 82.4 mg/L with a mean of 19.84 mg/L and in 2021 post-monsoon K^+ varies from 2.8- 98.4 mg/L with a mean of 23.14 mg/L.

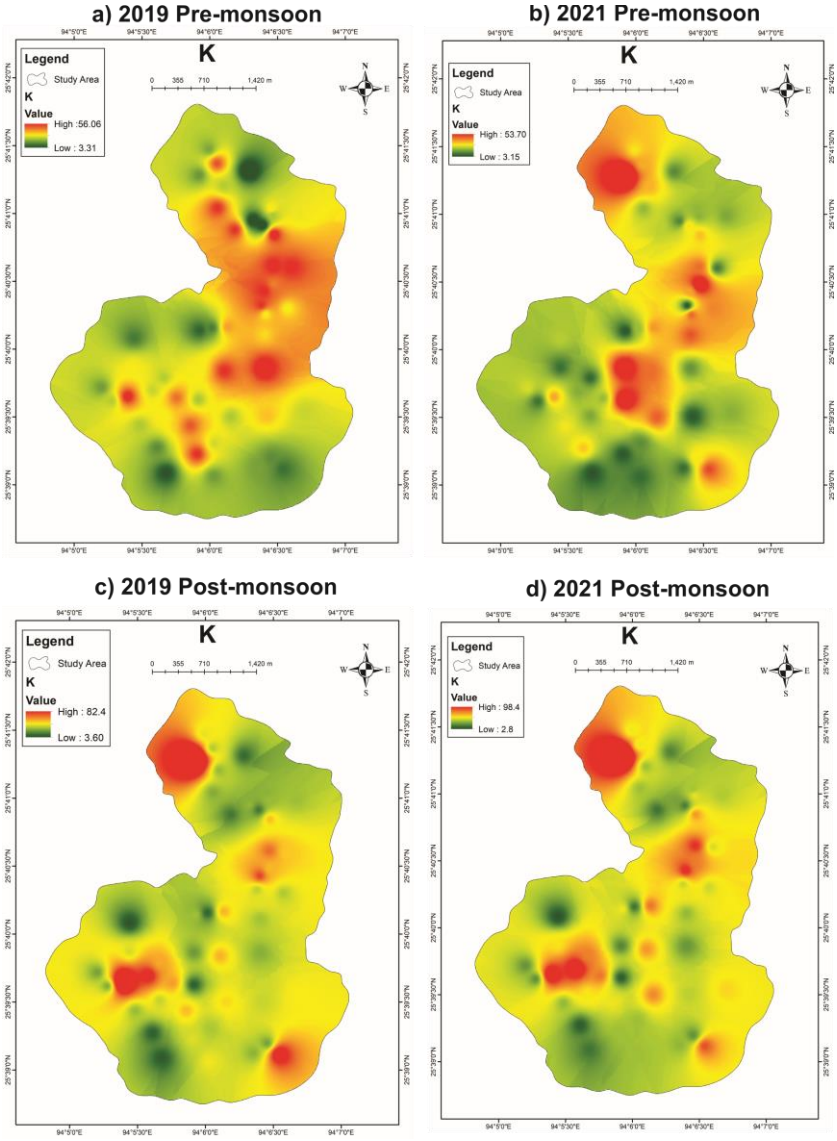

Fig. 5.10: Geospatial distribution maps of K^+ during (a) 2019 Pre-monsoon (b) 2021 Pre-monsoon (c) 2019 Post-monsoon (d) 2021 Post-monsoon

From the geospatial distribution of K^+ in 2019 pre-monsoon, the higher values of K^+ are mostly scattered towards the central, eastern and south-western parts while in pre-monsoon of 2021, higher values of K^+ are mostly scattered towards the north-western, eastern and central areas. The post-monsoon season of 2019 and 2021 has similar geospatial distribution of K^+ with higher values found in isolated pockets towards the north-western, western and south-eastern areas.

Feldspar, feldspathoids and micas are the principal sources of K^+ in groundwater. High K^+ concentrations in the study area are probably resultant from the chemical decomposition of sylvite (KCl), silicates and especially clay minerals which are derived from the dominant shale rocks in the study area. High K^+ concentrations have been found in shallow and deep aquifers at different depths, which suggests both geogenic and anthropogenic activities for increasing K^+ in groundwater (Vero et.al., 2023). Anthropogenic activities such as fertilizers and the breakdown of animal or waste products can also add K^+ to groundwater (Saha et al., 2019). "Despite the possibility of certain health effects, the amount of K^+ consumed through drinking water is substantially lower at which adverse health effects may occur" (WHO, 2011).

5.2.10 Sodium (Na^+)

The precipitation of sodium salts that saturated the soil in shallow water tracts, the infiltration of sea water in coastal locations, and connate water are the main sources of Na^+ in groundwater (Karanth, 1989). In humid and snow-fed areas, the sodium level of groundwater ranges from 1 mg/L to more than 100,000 mg/L in brines. Sodium is mostly found in natural waters due to the release of soluble byproducts from the weathering of aquifer material.

The major cation in the study area Na^+ was observed to be between 19.15- 388.9 mg/L. The descriptive statistics of Na^+ pre-monsoon and post-monsoon groundwater samples in 2019 and 2021 are shown in Tables 5.2 to 5.5 and the spatial distribution map is shown in Fig. 5.11. The Na^+ of the groundwater in 2019 pre-monsoon varies from 24.74- 201 mg/L with a mean of 72.10 mg/L and in 2021 pre-monsoon, Na^+ varies from 34.35- 388.9 mg/L with a mean of 196.78 mg/L. Whereas, Na^+ concentration of the groundwater in 2019 post-monsoon varies from 19.15- 335.6 mg/L with a mean of 139.48 mg/L and in 2021 post-monsoon Na^+ varies from 21.23- 340 mg/L with a mean of 147.39 mg/L.

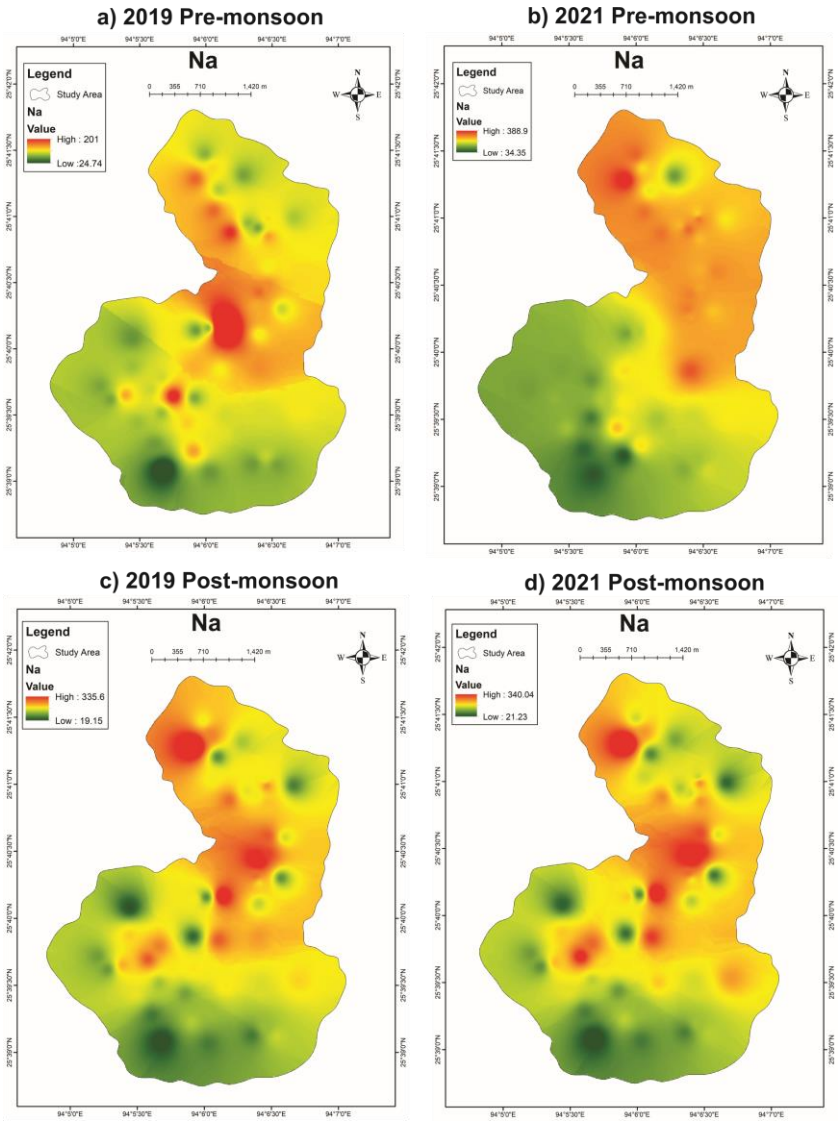

Fig. 5.11: Geospatial distribution maps of Na^+ during (a) 2019 Pre-monsoon (b) 2021 Pre-monsoon (c) 2019 Post-monsoon (d) 2021 Post-monsoon

From the geospatial distribution of Na^+ in 2019 pre-monsoon, the higher values of Na^+ are mostly scattered towards the central and north-western parts while in pre-monsoon of 2021, higher values of Na^+ are mostly scattered towards the northern part. The post-monsoon seasons of 2019 and 2021 geospatial distribution shows that the higher values of Na^+ are found towards the north-western and central areas.

Vizovol (2016) stated that the high concentrations of Na^+ in the study area may be due to the mixing of seawater controlled by tectonic activities. Feldspar and clay minerals are also the natural sources of Na^+ and the high shale content in the study area contributes to the Na^+ concentrations. According to WHO (2003), "the contribution of Na^+ from drinking water to daily intake is small and not much of health concern at levels found in

drinking water. No firm conclusions can be drawn concerning the possible association between Na^+ in drinking water and the occurrence of hypertension. However, concentrations in excess of 200 mg/L may give rise to unacceptable taste."

5.2.11 Bicarbonate (HCO_3^-)

According to Khan and Jhariya (2018), CO_2 reacts with basic minerals in the soil to form bicarbonate and carbonate, which are then concentrated in groundwater. The weathering of silicate minerals produces HCO_3^- ions (Gastmans et al., 2010).

HCO_3^- was found to be the dominating anion in the groundwater and its value ranges from 49.8- 715.36 mg/L. The descriptive statistics of HCO_3^- in pre-monsoon and post-monsoon groundwater samples of 2019 and 2021 are shown in Tables 5.2 to 5.5 and the spatial distribution map is shown in Fig. 5.12. The HCO_3^- of the groundwater in 2019 pre-monsoon varies from 70.15- 505.1 mg/L with a mean of 202.37 mg/L and in 2021 pre-monsoon, HCO_3^- varies from 57.95- 715.36 mg/L with a mean of 226.13 mg/L. Whereas, HCO_3^- concentration of the groundwater in 2019 post-monsoon varies from 55.6- 536.8 mg/L with a mean of 199.65 mg/L and in 2021 post-monsoon HCO_3^- varies from 49.8- 529.5 mg/L with a mean of 185.27 mg/L.

From the geospatial distribution of HCO_3^- in 2019 pre-monsoon, the higher values of HCO_3^- are mostly scattered towards the north-western and central parts while in pre-monsoon of 2021, higher values of HCO_3^- are mostly scattered towards the northern parts of the study area. The post-monsoon season of 2019 and 2021 has similar geospatial distribution of HCO_3^- with higher values found in isolated pockets towards the north-western, western and eastern areas. The increased HCO_3^- concentration in groundwater indicates an intense weathering of rocks, which facilitates active mineral dissolution (Stumm and Morgan, 1996).

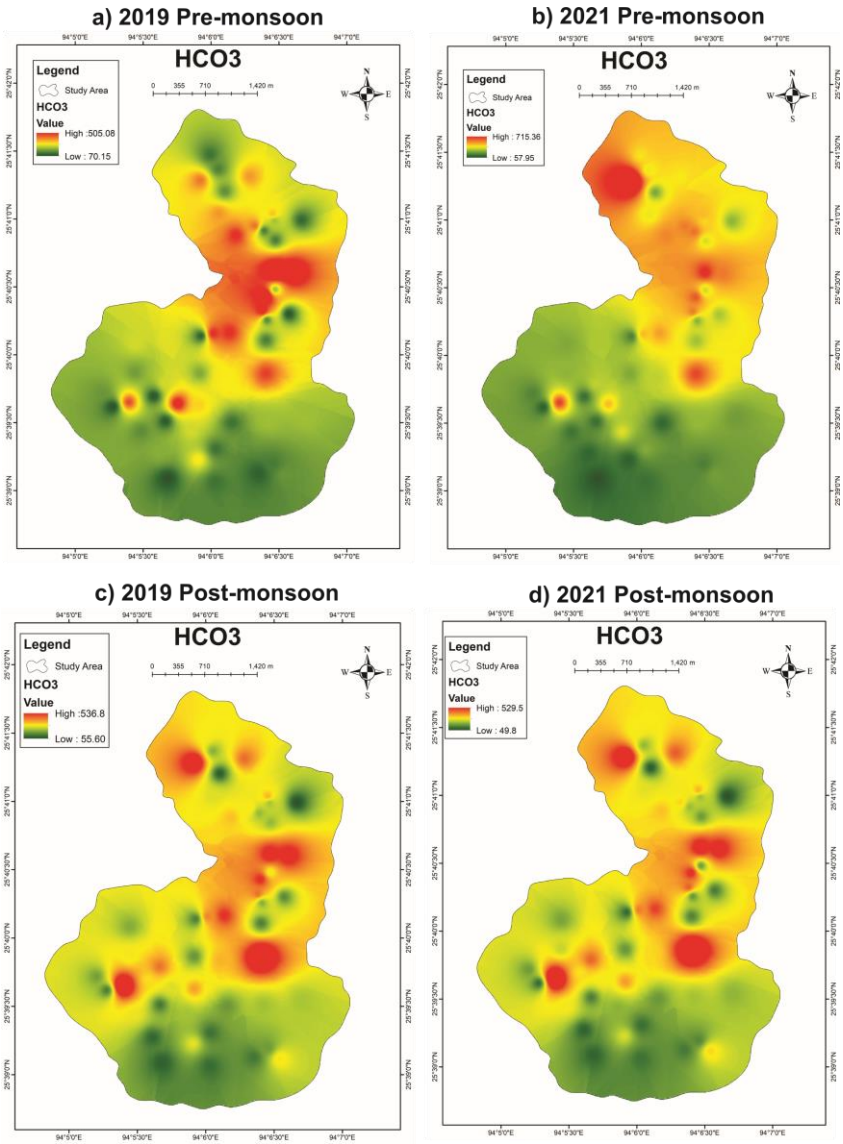

Fig. 5.12: Geospatial distribution maps of HCO_3^- during (a) 2019 Pre-monsoon (b) 2021 Pre-monsoon (c) 2019 Post-monsoon (d) 2021 Post-monsoon

5.2.12 Sulphate (SO_4^{2-})

SO_4^{2-} naturally arises in water as a result of rock leaching. Sulphur is oxidized to produce sulphate ions, which dissolve in the water during weathering of sulphide minerals in contact with aerated water.

The value of SO_4^{2-} was observed to be between 6.31- 195.2 mg/L. The descriptive statistics of SO_4^{2-} pre-monsoon and post-monsoon groundwater samples in 2019 and 2021 are shown in Tables 5.2 to 5.5 and the spatial distribution map is shown in Fig. 5.13. The SO_4^{2-} of the groundwater in 2019 pre-monsoon varies from 14.87- 167.4 mg/L with a mean of 58.07 mg/L and in 2021 pre-monsoon, SO_4^{2-} varies from 6.31- 144.17 mg/L with a mean of 103.85 mg/L. Whereas, SO_4^{2-} concentration of the groundwater in 2019 post-

monsoon varies from 27.88- 195.2 mg/L with a mean of 86.46 mg/L and in 2021 post-monsoon SO_4^{2-} varies from 32.9- 186.3 mg/L with a mean of 83.16 mg/L.

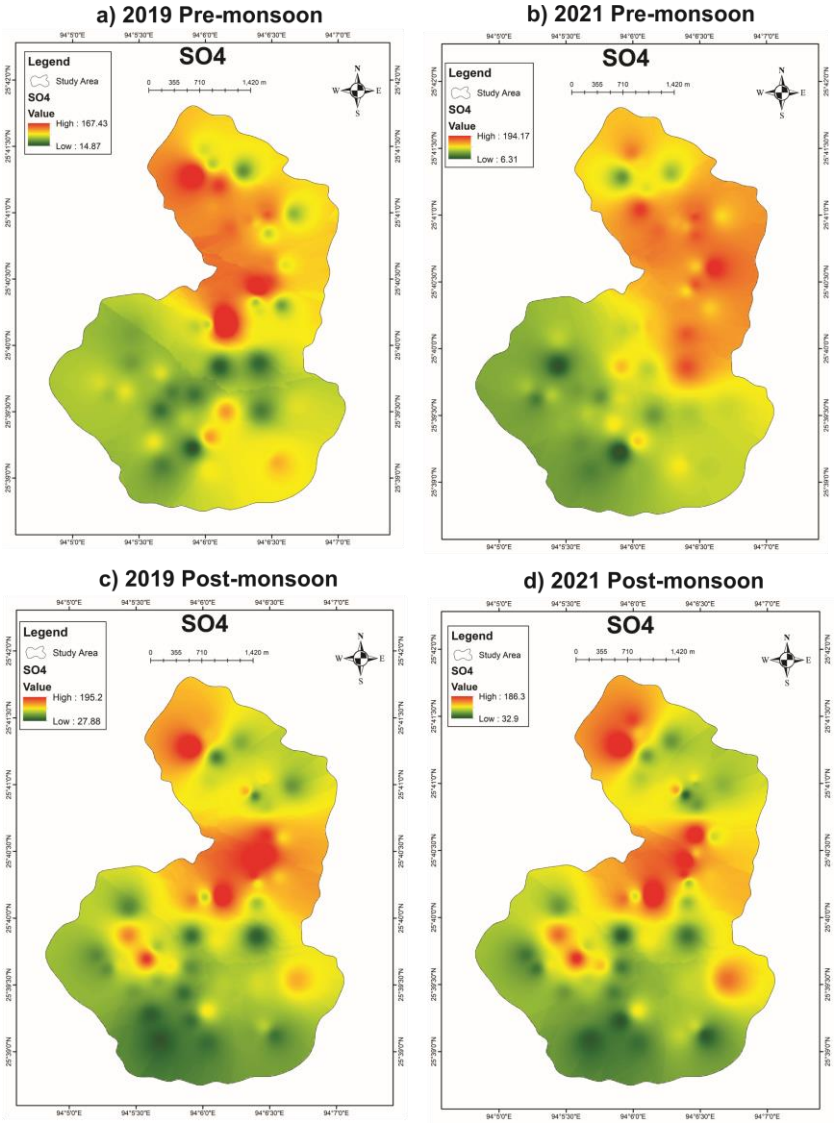

Fig. 5.13: Geospatial distribution maps of SO_4^{2-} during (a) 2019 Pre-monsoon (b) 2021 Pre-monsoon (c) 2019 Post-monsoon (d) 2021 Post-monsoon

From the geospatial distribution of SO_4^{2-} in 2019 pre-monsoon, the higher values of SO_4^{2-} are mostly scattered towards the north-western parts while in pre-monsoon of 2021, higher values of SO_4^{2-} are mostly scattered towards the northern areas. The post-monsoon season of 2019 and 2021 has similar geospatial distribution of SO_4^{2-} with higher values found in isolated pockets towards the central and northern areas. The concentrations of SO_4^{2-} are found to be within permissible limit in all the groundwater samples from the study area during pre- monsoon and post-monsoon seasons (Table 5.1). The lower concentrations of SO_4^{2-} suggest that bacterial SO_4^{2-} reduction has occurred

(Kirk et al. 2004). The low SO_4^{2-} content of groundwater also indicates that the study area lacks industries as high SO_4^{2-} content indicates anthropogenic activities and industrial processes (Mostafa et al. 2017).

5.2.13 Nitrate (NO_3^-)

NO_3^- in drinking water usually originates from fertilizers or animal and human wastes. NO_3^- concentrations in water tend to be highest in areas of intensive agriculture or with a high density of septic systems.

The value of NO_3^- was observed to be between 0-65 mg/L. The descriptive statistics of NO_3^- pre-monsoon and post-monsoon groundwater samples in 2019 and 2021 are shown in Tables 5.2 to 5.5 and the spatial distribution map is shown in Fig. 5.14. The NO_3^- of the groundwater in 2019 pre-monsoon varies from 0-45 mg/L with a mean of 11.5 mg/L and in 2021 pre-monsoon, NO_3^- varies from 0-47.2 mg/L with a mean of 6.14 mg/L. Whereas, NO_3^- concentration of the groundwater in 2019 post-monsoon varies from 0-65 mg/L with a mean of 13.3 mg/L and in 2021 post-monsoon NO_3^- varies from 0-54 mg/L with a mean of 11.22 mg/L.

From the geospatial distribution of NO_3^- in 2019 pre-monsoon, the higher values of NO_3^- are mostly scattered in isolated pockets in the central, south-eastern and south-western parts while in pre-monsoon of 2021, higher values of NO_3^- are mostly scattered in isolated pockets in the north and central parts. The post-monsoon season of 2019 and 2021 has similar geospatial distribution of NO_3^- with higher values found distributed unevenly throughout the study area. NO_3^- is a non-lithological source. In natural conditions, the concentration of NO_3^- does not exceed 10 mg/l in the water (Cushing et al., 1973) so the higher concentration of NO_3^- beyond 10 mg/l indicates anthropogenic activity.

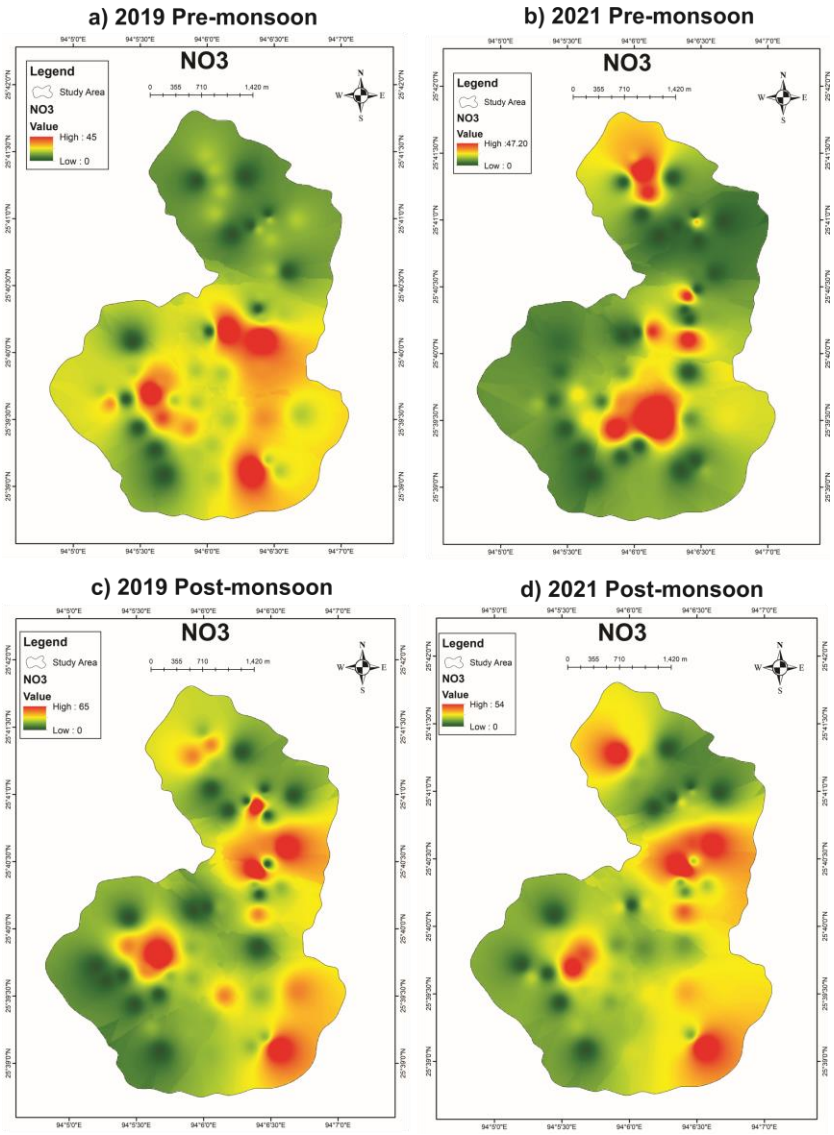

Fig. 5.14: Geospatial distribution maps of NO_3^- during (a) 2019 Pre-monsoon (b) 2021 Pre-monsoon (c) 2019 Post-monsoon (d) 2021 Post-monsoon

5.2.14 Chloride (Cl^-)

Although Cl^- is a minor constituent of the earth's crust, it is a major dissolved component of natural water. In sedimentary rocks and soils, the mineral halite (NaCl) is the principal source of its dissolution. Sewage, oil field brines, industrial waste, and seawater all contain Cl^-. Cl^- in combination with Na^+ can give drinking water a salty taste and make it more corrosive when it is present in concentrations more than 100 mg/L.

The value of Cl^- was observed to be between 25- 283.68 mg/L. The descriptive statistics of Cl^- pre-monsoon and post-monsoon groundwater samples in 2019 and 2021 are shown in Tables 5.2 to 5.5 and the spatial distribution map is shown in Fig. 5.15. The Cl^- of the groundwater in 2019 pre-monsoon varies from 25-150 mg/L with a mean of 81 mg/L and in 2021 pre-monsoon, Cl^- varies from 27.73-283.68 mg/L with a mean of

160.06 mg/L. Whereas, the Cl^- concentration of the groundwater in 2019 post-monsoon varies from 25-235 mg/L with a mean of 106.6 mg/L and in 2021 post-monsoon Cl^- varies from 30-214 mg/L with a mean of 94.58 mg/L.

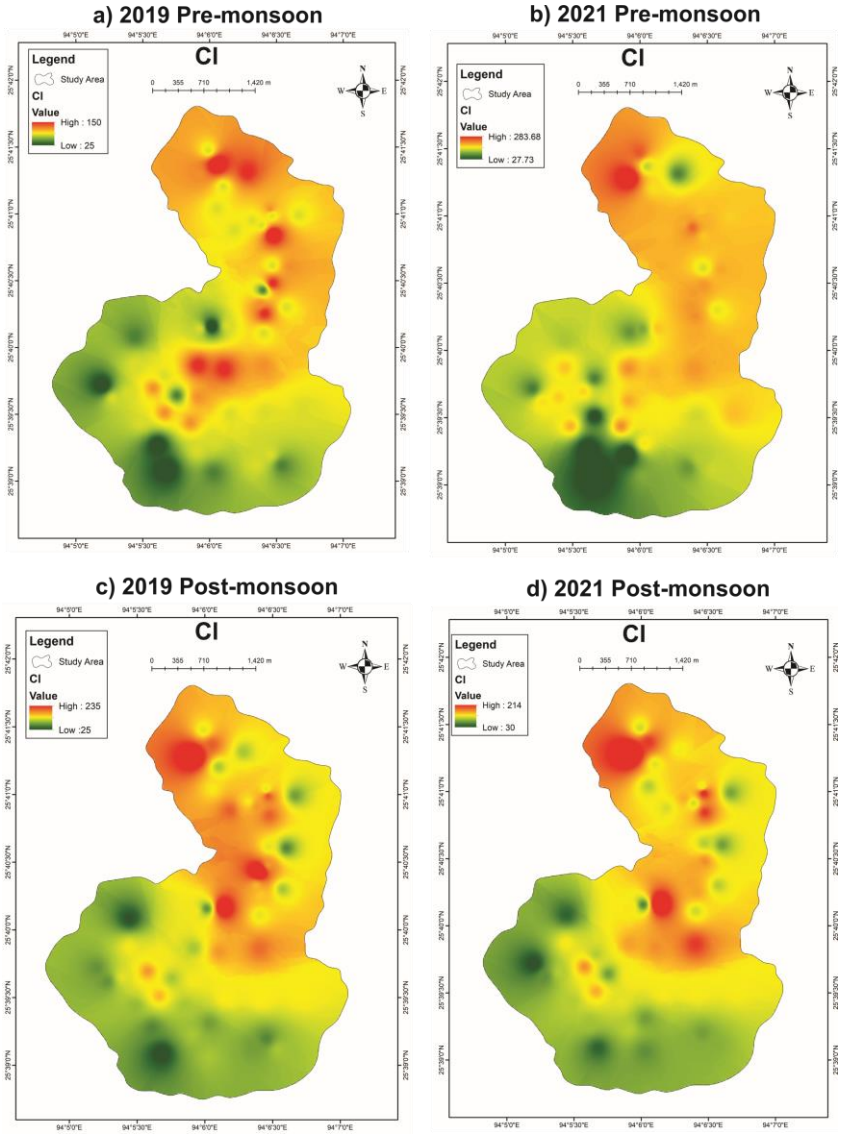

Fig. 5.15: Geospatial distribution maps of Cl^- during (a) 2019 Pre-monsoon (b) 2021 Pre-monsoon (c) 2019 Post-monsoon (d) 2021 Post-monsoon

From the geospatial distribution of Cl^- in 2019 pre-monsoon, the higher values of Cl^- are scattered throughout the study area towards the north, central and eastern parts while in pre-monsoon of 2021, higher values of Cl^- are mostly scattered throughout the north-western, central, eastern and some small pockets in the western part. The post-monsoon season of 2019 and 2021 has similar geospatial distribution of Cl^- with higher values found towards the north-western part and small pockets in the central and eastern part.

The concentrations of Cl^- are found to be within the permissible limit in all the groundwater samples from the study area during pre-monsoon and post-monsoon seasons (Table 5.1). According to Hem (1991), Cl^- is primarily obtained from non-lithological sources. However, the groundwater could get Cl^- from the local shale rocks (Subba Rao et.al., 2012). The poor sewage system in the study area is also an additional source of Cl^- in the groundwater.

5.2.15 Fluoride (F^-)

F^- is released into groundwater from minerals like fluorite, apatite, certain amphiboles and micas. Besides fluorine bearing minerals, F^- is released into the subsurface water by the manufacture and use of phosphate fertilizers. For the calcification of dental enamel, F^- is beneficial when present in drinking water in small amounts (0.8 to 1.0 mg/L). If levels are high, it can lead to dental and skeletal fluorosis.

The value of F^- was observed to be between 0-3 mg/L. The descriptive statistics of F^- pre-monsoon and post-monsoon groundwater samples in 2019 and 2021 are shown in Tables 5.2 to 5.5 and the spatial distribution map is shown in Fig. 5.16. The F^- of the groundwater in 2019 pre-monsoon varies from 0-3 mg/L with a mean of 0.33 mg/L and in 2021 pre-monsoon, F^- varies from 0-1.77 mg/L with a mean of 0.28 mg/L. Whereas F^- concentration of the groundwater in 2019 post-monsoon varies from 0-1.5 mg/L with a mean of 0.43 mg/L and in 2021 post-monsoon F^- varies from 0-1 mg/L with a mean of 0.29 mg/L.

From the geospatial distribution of F^- in 2019 pre-monsoon, the high values of F^- is clustered in the eastern part while in pre-monsoon of 2021, the high F^- values are scattered in the eastern part and also in small pockets in the northern and southern areas. The geospatial distribution of F^- in 2019 post-monsoon shows high values clustered in the eastern areas while in post-monsoon of 2021, the high F^- values are scattered in the eastern parts and also in small pockets in the south-western areas. The main causes of the concentration of F^- are a combination of geogenic (apatite, biotite, and clays) and anthropogenic (chemical fertilizers) sources and prolonged water interaction with the aquifer materials (Subba Rao, 2009).

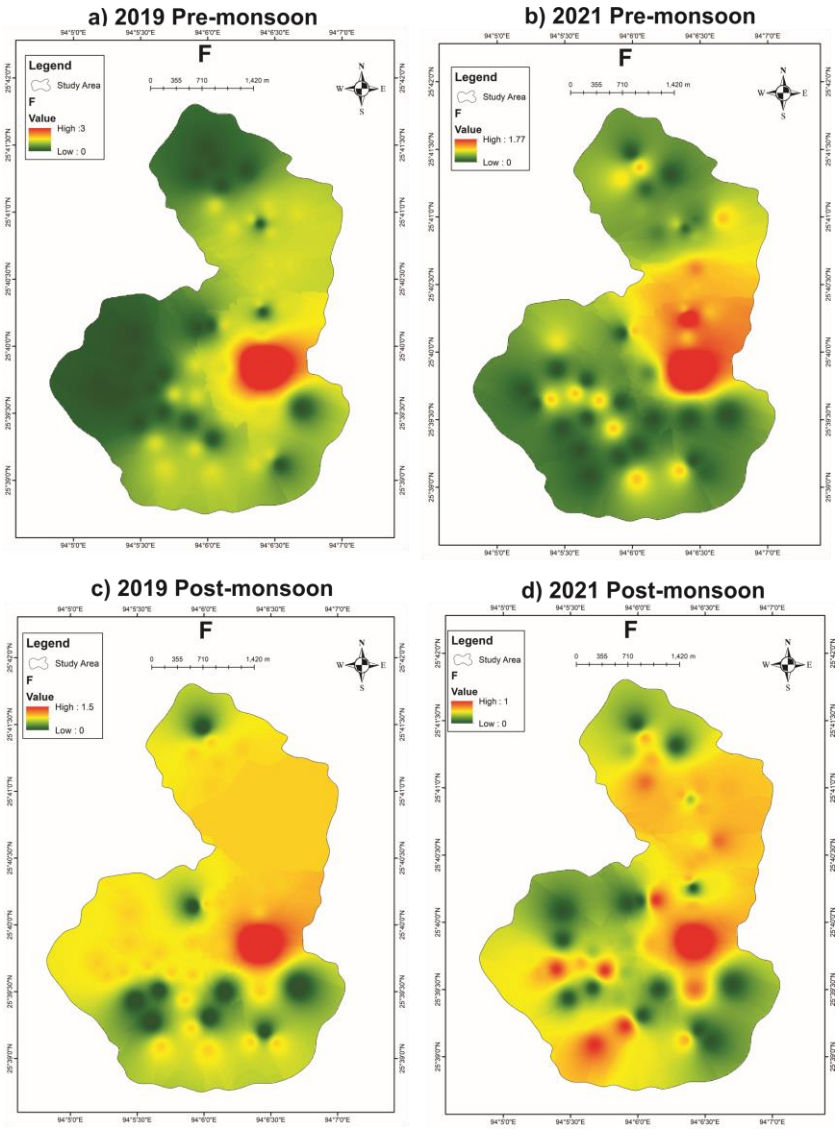

Fig. 5.16: Geospatial distribution maps of F^- during (a) 2019 Pre-monsoon (b) 2021 Pre-monsoon (c) 2019 Post-monsoon (d) 2021 Post-monsoon

5.2.16 Iron (Fe)

Iron concentration in groundwater is mainly caused by the dissolution of iron oxides (Singhal and Gupta, 1999). In the case of excess Fe, aeration and sedimentation are the two major processes used to remove iron from water.

The value of Fe was observed to be between 0-5.33 mg/L. The descriptive statistics of Fe pre-monsoon and post-monsoon groundwater samples in 2019 and 2021 are shown in Tables 5.2 to 5.5 and the spatial distribution map is shown in Fig. 5.17. The Fe of the groundwater in 2019 pre-monsoon varies from 0-3.53 mg/L with a mean of 0.44 mg/L and in 2021 pre-monsoon, Fe varies from 0-5.33 mg/L with a mean of 0.37 mg/L. Whereas Fe concentration of the groundwater in 2019 post-monsoon varies from 0-4.28

mg/L with a mean of 0.44 mg/L and in 2021 post-monsoon Fe varies from 0-1.5 mg/L with a mean of 0.19 mg/L.

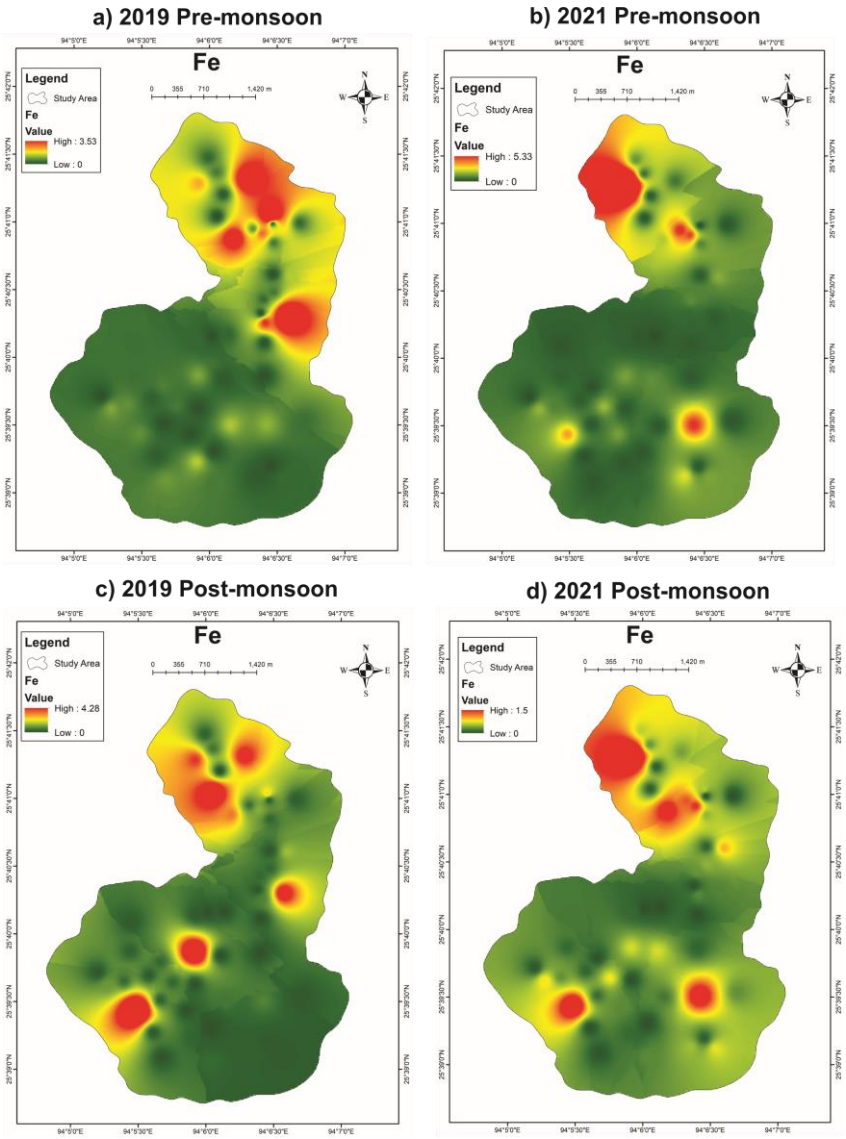

Fig. 5.17: Geospatial distribution maps of Fe during (a) 2019 Pre-monsoon (b) 2021 Pre-monsoon (c) 2019 Post-monsoon (d) 2021 Post-monsoon

From the geospatial distribution of Fe in 2019 pre-monsoon, the higher values of Fe are found in pockets mostly in the north and east direction while in pre-monsoon of 2021, higher values of Fe are found in isolated pockets in the north-west, south-east and south-west parts. The geospatial distribution of Fe in 2019 post-monsoon has higher values of Fe in pockets mostly in the north, east and south-west while in post-monsoon of 2021, the Fe geospatial distribution has higher values found in isolated pockets towards the north-west, south-east and south-west.

Fe is naturally present in the form of metal in rocks, soil, and minerals. Rainwater absorbs Fe and other elements from the geological formations as it percolates through the

soil and rocks, increasing the concentration of these elements in groundwater. Pumps, pipes, and well casings may also add iron to the water. The high Fe concentration in groundwater in the study area may result from a combination of the area's predominantly weathered shales and anthropogenic activities. In the groundwater sampling locations with high Fe concentrations, open drainage and sewage systems are present and one of the sites is located next to an automobile workshop contributing to groundwater contamination (Vero et.al., 2023).

5.2.17 Trace elements

According to Karanth (1989), specific metallic components were present in groundwater in extremely small amounts or traces, normally not exceeding 1 ppm. These substances are known as trace metals or trace elements. The most significant natural source of trace elements reaching water bodies is through rock-water interaction (Purushothan et al., 2017). According to Sujatha (2004), human activities including the discharge of municipal sewage and industrial effluent directly transfer trace elements into the groundwater. Due to a lack of data on heavy/ trace metal accumulation in the study environment, Cd, Cu and As concentrations were studied to create a data background for the study area.

5.2.17a Cadmium (Cd)

Cd concentrations in groundwater can be increased by both geogenic and anthropogenic factors. Cd is usually found in batteries, in plastic colours and other electronic wastes. When these get into the water system, it causes health issues. High Cd dosages can cause cancer in humans. Cd builds up in the body of a person, particularly in the kidneys, where it causes kidney disease which is a serious health consequence.

The value of Cd was observed to be between 0-0.06 mg/L. The descriptive statistics of Cd pre-monsoon and post-monsoon groundwater samples in 2019 and 2021 are shown in Tables 5.2 to 5.5. The spatial distribution map of Cd pre-monsoon and post-monsoon is shown in Fig. 5.18. The concentration of Cd in the groundwater of the study area during 2019 pre-monsoon and post-monsoon seasons was found to be below detection limit. Whereas the concentration of Cd in the groundwater in 2021 pre-monsoon samples are ranging from 0-0.06 mg/L with a mean of 0 mg/L and in the 2021 post-monsoon samples, it is ranging from 0-0.03 mg/L with a mean of 0 mg/L.

In the geospatial distribution of Cd in 2021 pre-monsoon and post-monsoon periods, the higher values of Cd are found in pockets in the north-west, south-east and

south-west parts. The concentration of Cd in rocks is generally 1 mg/L and Cd is not very much soluble, so the natural concentrations of Cd in groundwater is usually less than 0.0005 mg/L (MPCA, 1999). The Cd in the study area is found to be exceeding the permissible limit of 0.003 mg/L (Table 5.1) in four locations (A6, A17, A19 and A31). The measured metal concentrations might not be adequately explained by natural processes alone. The findings of this study show that Cd concentrations have risen in 2021. This will be due to pollution from anthropogenic activities such as sewage sludge, batteries and fuel combustion products.

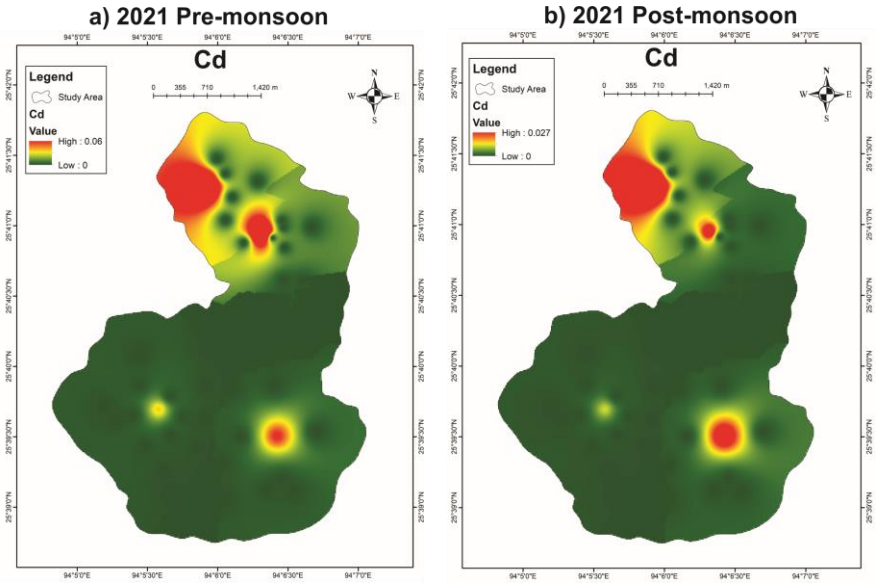

Fig. 5.18: Geospatial distribution maps of Cd during
(a) 2021 Pre-monsoon (b) 2021 Post-monsoon

5.2.17b Copper (Cu)

Cu is found in both the native form and its compounds. The water containing copper corrodes steel fittings and galvanized iron. Laundries are also stained by Cu (Park, 2015). With increased stagnation in the pipe, the concentration of Cu can increase. Cu is necessary for developing haemoglobin and human metabolism at low trace concentrations (Tiwari et.al., 2013). The typical daily consumption of Cu from food is 3 mg, but too much Cu might have negative health effects (Krishna and Govil, 2004).

The value of Cu was observed to be between 0-0.5 mg/L. The descriptive statistics of Cu pre-monsoon and post-monsoon groundwater samples in 2019 and 2021 are shown in Tables 5.2 to 5.5. The spatial distribution map of Cu 2021 pre-monsoon and post-monsoon is shown in Fig. 5.19. The concentration of Cu in the groundwater of the study area during 2019 pre-monsoon and post-monsoon was found to be below detection limit.

Whereas the concentration of Cu in the groundwater in 2021 pre-monsoon samples are ranging from 0-0.5 mg/L with a mean of 0.08 mg/L and in the 2021 post-monsoon samples, it is ranging from 0-0.4 mg/L with a mean of 0.03 mg/L.

In the geospatial distribution of Cu in 2021 pre-monsoon and post-monsoon periods, the higher values of Cu are found in pockets in the north-east, west and south-west parts. The concentrations of Cu are found to be within permissible limit in all the groundwater samples from the study area during pre- monsoon and post-monsoon seasons (Table 5.1).

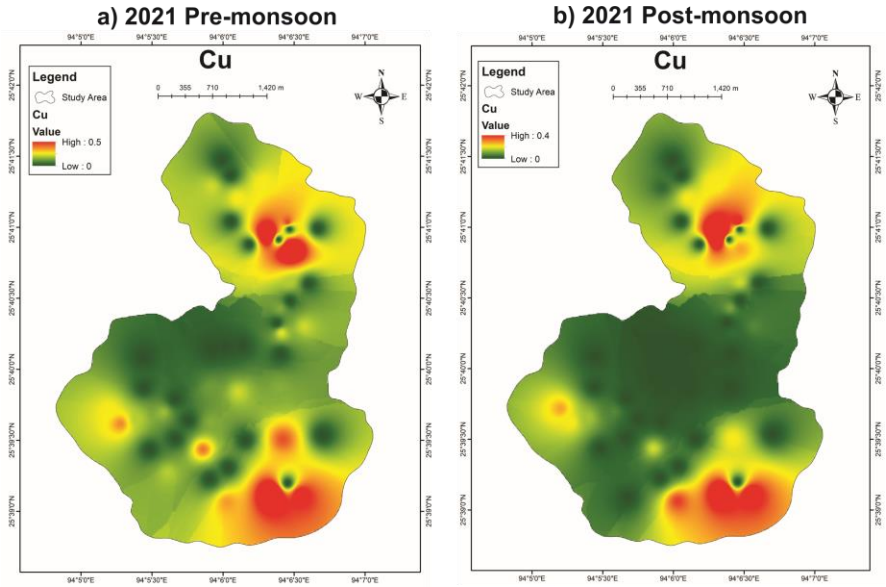

Fig. 5.19: Geospatial distribution maps of Cu during
(a) 2021 Pre-monsoon (b) 2021 Post-monsoon

5.2.17c Arsenic (As)

As occurs in many oxidation states in the environment but in water, it mostly occurs in inorganic forms such as As^{+3} and As^{+5}. As from weathered rocks and soils dissolves in groundwater (Puzari et al., 2015). Anthropogenic activities such as industrial effluents, pesticides, insecticides, and herbicides can all transmit As into groundwater. According to Polizzotto et al. (2008), groundwater can be contaminated by As, which may come from eroded sediments and enter the solution after being reductively released from solid phases under anaerobic conditions. An excessive level of As in drinking water poses serious health risks. As is toxic and carcinogenic and even trace amounts of As in water can cause serious health problems. The groundwater samples in the study area were confirmed to have zero As concentrations.

5.3 PIPER'S TRILINEAR DIAGRAM

Piper's trilinear diagram is one of the key methods for interpreting hydrogeochemical facies (Piper, 1944). The graphical representation highlights the similarities and differences between the water samples since they tend to cluster together according to their similar qualities (Todd, 1980; Ramesh et al., 2014). The two basal triangles show the principal cations (Ca^{2+}, Mg^{2+}, Na^{+}, and K^{+}) and anions (HCO_3^-, SO_4^{2-} and Cl^-), all of which are expressed in meq/L. The classification of water is described in the diamond-shaped field of the diagram.

The Piper's trilinear diagram for both pre-monsoon and post-monsoon (2019 and 2021) has been prepared and reveals that the groundwater samples of the study area fall in the following sub-divisions -1, 2, 3, 4, B, D, E, H and G (Fig. 5.20 and 5.21). The number of samples in each division is given in Table 5.6.

Table 5.6: Number of groundwater samples in sub-divisions of Piper's trilinear diagram

Sub-division	**Pre-monsoon 2019**	**Pre-monsoon 2021**	**Post-monsoon 2019**	**Post-monsoon 2021**
1 (Ca^{2+}- HCO_3^- type)	8 samples	-	4 samples	-
2 (Na^{+}-Cl^- type)	21 samples	45 samples	37 samples	46 samples
3 (Mixed Ca^{2+}-Na^{+}- HCO_3^- type)	11 samples	3 samples	6 samples	4 samples
4 (Mixed Ca^{2+}-Mg^{2+}-Cl^- type)	10 samples	2 samples	3 samples	-
B (No dominant type)	20 samples	2 samples	7 samples	-
D (Na^{+}+ K^{+} type)	30 samples	48 samples	43 samples	50 samples
E (HCO_3^- type)	20 samples	3 samples	10 samples	4 samples
H (No dominant type)	22 samples	35 samples	35 samples	39 samples
G (Cl^- type)	8 samples	12 samples	5 samples	7 samples

In 2019 pre-monsoon, the maximum number of groundwater samples with 42% fall under sodium-chloride type of water, 16% of groundwater samples fall under calcium-bicarbonate type, 22% of groundwater samples fall under mixed type of calcium-sodium-

bicarbonate type and 20% of groundwater samples fall under mixed type of calcium-magnesium-chloride type. From the cationic triangle, the maximum number of groundwater samples with 60% fall under sodium and potassium type and 40% of groundwater samples are under no dominant type. From the anionic triangle, the maximum number of groundwater samples with 44% fall under no dominant type, 40% of groundwater samples are under bicarbonate type and 16% of groundwater samples are under chloride type.

In 2021 pre-monsoon, the maximum number of groundwater samples with 90% fall under sodium-chloride type of water, 6% of groundwater samples fall calcium-sodium-bicarbonate type and 4% of groundwater samples fall under mixed type of calcium-magnesium-chloride type. From the cationic triangle, the maximum number of groundwater samples with 96% fall under sodium and potassium type and 4% of groundwater samples are under no dominant type. From the anionic triangle, the maximum number of groundwater samples with 70% fall under no dominant type, 6% of groundwater samples are under bicarbonate type and 24% of groundwater samples are under chloride type.

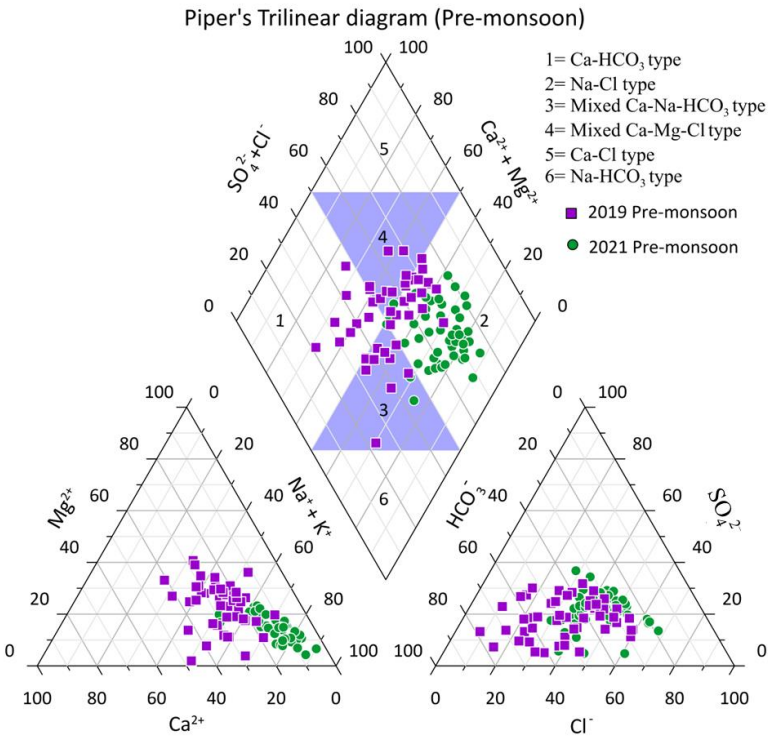

Fig. 5.20: Trilinear graphical representation of pre-monsoon groundwater samples

In 2019 post-monsoon, the maximum number of groundwater samples with 74% fall under sodium-chloride type of water, 8% of groundwater samples fall under calcium-

bicarbonate type, 12% of groundwater samples fall under mixed type of calcium-sodium-bicarbonate type and 6% of groundwater samples fall under mixed type of calcium-magnesium-chloride type. From the cationic triangle, the maximum number of groundwater samples with 86% fall under sodium and potassium type and 14% of groundwater samples are under no dominant type. From the anionic triangle, the maximum number of groundwater samples with 70% fall under no dominant type, 20% of groundwater samples are under bicarbonate type and 10% of groundwater samples are under chloride type.

In 2021 post-monsoon, the maximum number of groundwater samples with 92% fall under sodium-chloride type of water and 8% of groundwater samples fall calcium-sodium-bicarbonate type. From the cationic triangle, all the groundwater samples with 100% fall under sodium and potassium. From the anionic triangle, the maximum number of groundwater samples with 78% fall under no dominant type, 8% of groundwater samples are under bicarbonate type and 14% of groundwater samples are under chloride type.

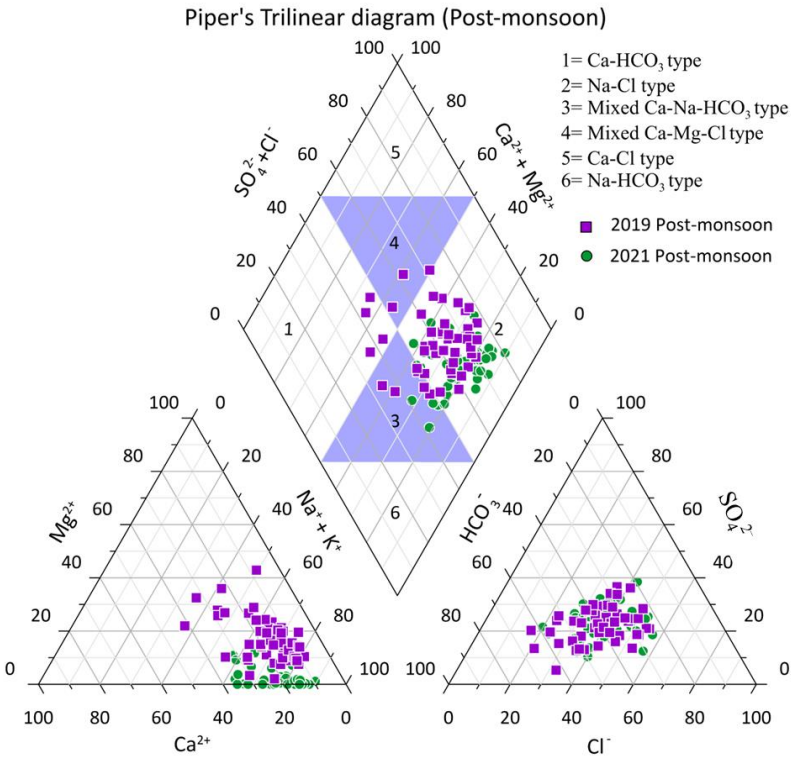

Fig. 5.21: Trilinear graphical representation of post-monsoon groundwater samples

Piper's trilinear diagram represented in both the pre-monsoon and post-monsoon seasons of 2019 and 2021 reveals that the aquifer in the study area is dominated by the

hydrochemical Na-Cl type. The alkalies exceed the alkaline earth while strong acids exceed weak acids in the studied groundwater samples.

5.4 FACTORS GOVERNING GROUNDWATER CHEMISTRY

To understand the factors influencing the hydrochemistry of groundwater, Gibbs diagram (Gibbs, 1970) was created for both the pre-monsoon and post-monsoon seasons of 2019 and 2021. The relationship between TDS versus $(Na^+ + K^+)/ (Na^+ + K^+ + Ca^{2+})$ and TDS versus $Cl^-/ (Cl^- + HCO_3^-)$ was used to generate the Gibbs diagrams. The diagram is separated into three categories that represent rock, evaporation, and precipitation dominance. The hydrogeochemical composition of groundwater is predominately controlled by water-rock interactions (weathering dominance), in both pre-monsoon and post-monsoon seasons as seen in Figs. 5.22 and 5.23, where all groundwater samples plot in the rock dominance area. As a result, it appears that the main source of the chemical elements dictating the groundwater quality in Kohima town is rock weathering.

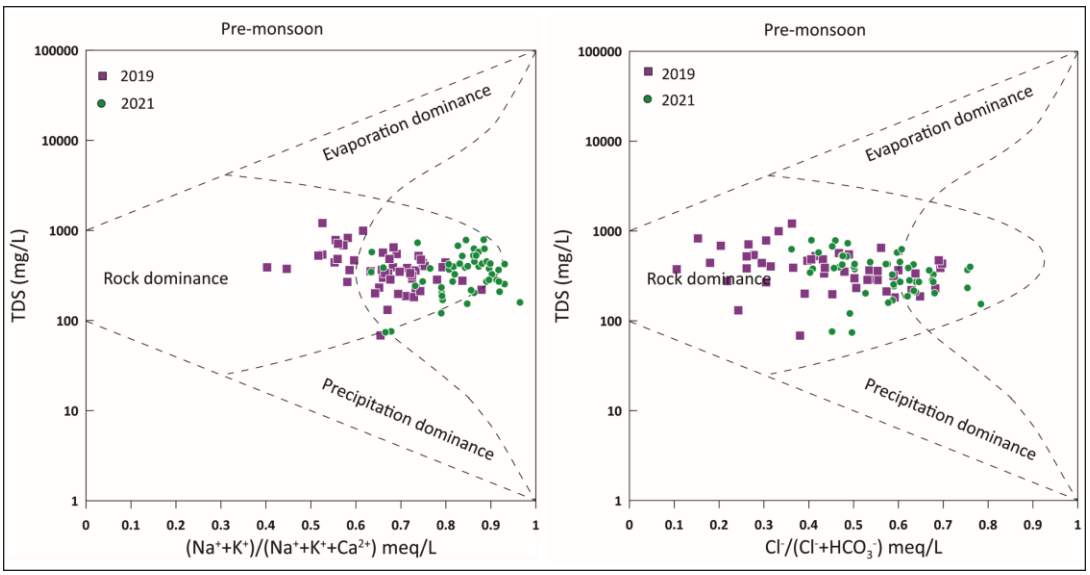

Fig. 5.22: Gibbs diagram showing the mechanism controlling groundwater chemistry in pre-monsoon

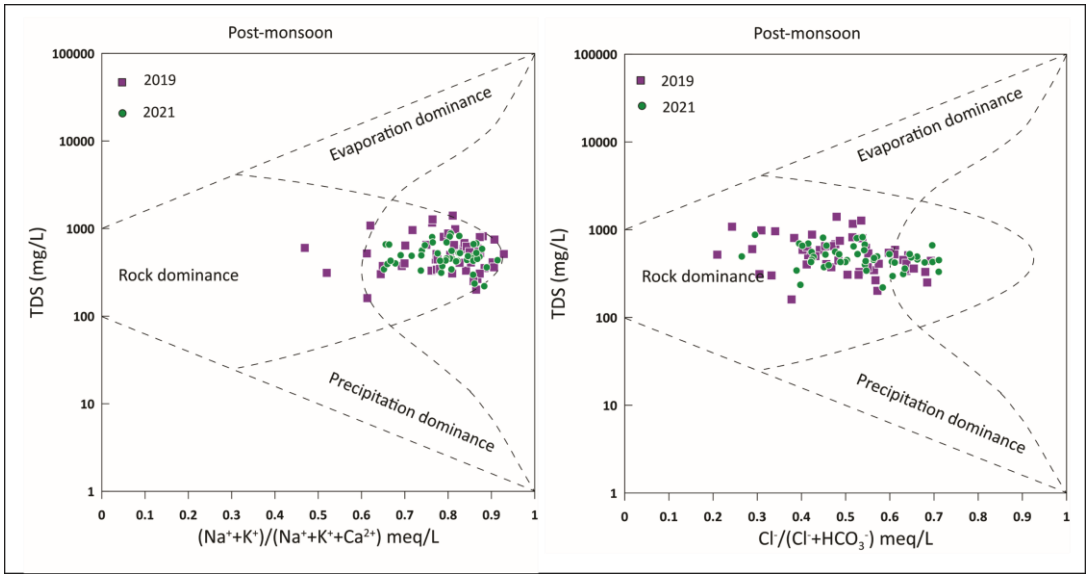

Fig. 5.23: Gibbs diagram showing the mechanism controlling groundwater chemistry in post-monsoon

"It is important to determine the minerals that were involved in the interaction between rocks and water using major ion correlation analysis" (Adimalla et al., 2020). In Cl^- versus Na^+ scatter plots, six groundwater samples plot above the 1:1 halite dissolution line in 2019 pre-monsoon (Fig. 5.24a). Groundwater samples which have greater Cl^-/Na^+ ratios are likely the result of cation exchange reactions that cause the adsorption of Ca^{2+} on clay minerals while simultaneously releasing Na^+ ions (Nganje et.al., 2017). While the majority of groundwater samples plot below the 1:1 halite dissolution line (Figs. 5.24a, e and 5.25a, e). This implies that the groundwater has Na^+ concentrations greater than Cl^-, which would be primarily due to rock weathering (silicate weathering) or ion exchange process. If this is the case, the dominating ion in groundwater is usually HCO_3^- (Rogers, 1989).

The total cation concentration has been plotted against HCO_3^- for the pre-monsoon and post-monsoon seasons of 2019 and 2021 (Figs. 5.24b, f and 5.25b, f). According to Kim (2003), "the ratio of HCO_3^-: TC would be 1 if the dissolution of silicate minerals is the major controlling process for ionic concentration in groundwater." All groundwater samples are seen above the 1:1 line. The deviation of the sampling points from the line indicates that it is due to anthropogenic sources acting as a secondary phase over the fundamental rock weathering and mineral dissolution process in the groundwater system.

In both the pre-monsoon and post-monsoon seasons of 2019 and 2021, the scatter plots of total cation (TC) versus Na^+ (Figs. 5.24c, g and 5.25c, g) were prepared. All of the groundwater samples plot above the 1:1 line. This suggests that the groundwater has

a significant contribution of cations which would mostly be from ion exchange processes or silicate weathering of shale rocks since shales play an essential part in the global silicate weathering process (Amiotte Suchet et al., 2003).

The plots of $Na^{+}+ K^{+}$ versus TC can be further used to assess the cation contribution in groundwater and are shown in Figs. 5.24d, h and 5.25d, h. All groundwater samples of pre-monsoon and post-monsoon seasons (2019 and 2021) were found to be below the 1:1 line and above the 1: 0.5 line. This shows that the cations in the groundwater samples are from rock weathering process or soil salts preserved due to evaporation (Stallard and Edmond, 1983; Subba Rao, 2012).

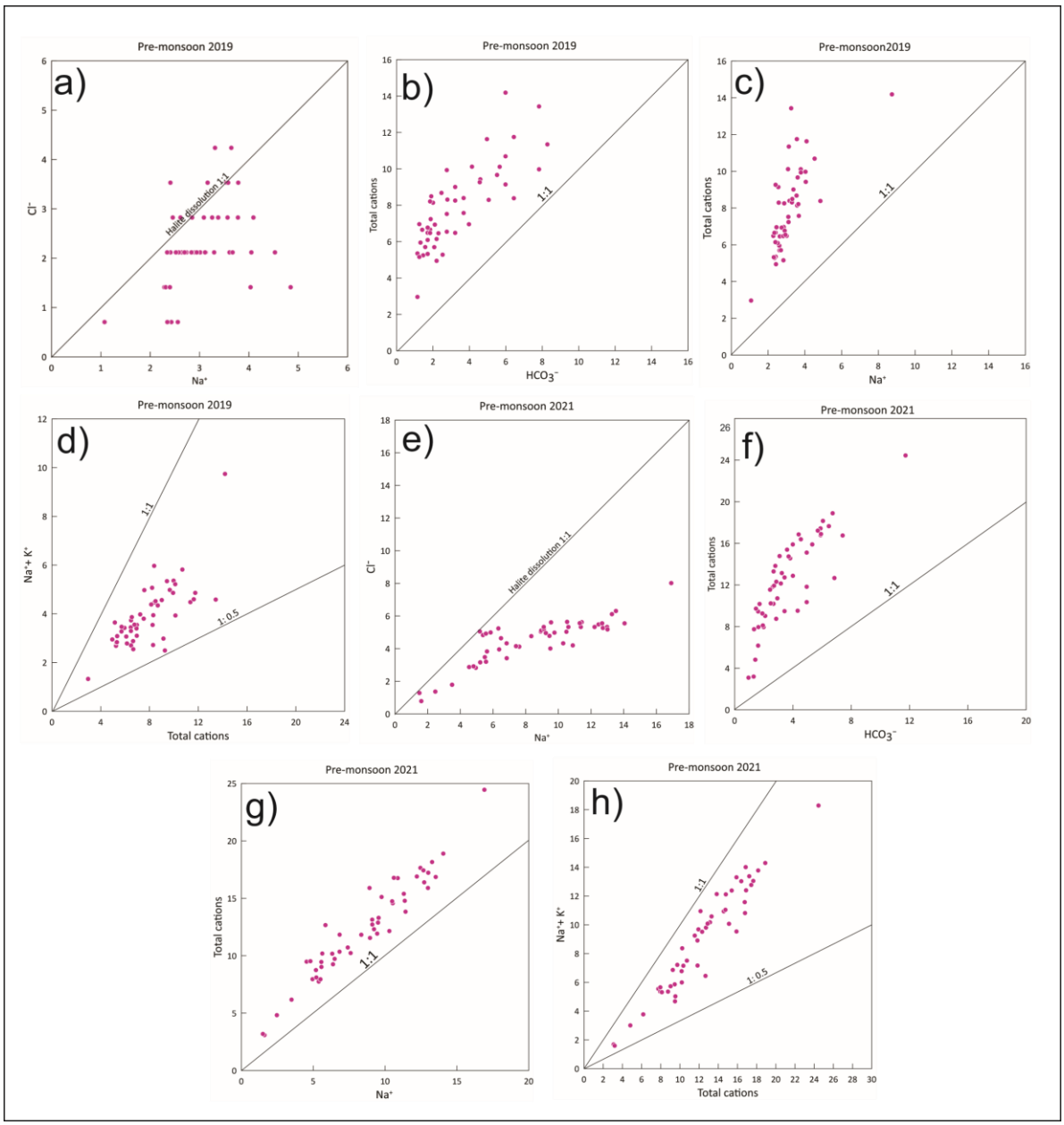

Fig. 5.24: Scatter plots of pre-monsoon (2019 and 2021) groundwater samples (a, e) Cl^- versus Na^+ (b, f) TC versus HCO_3^- (c, g) TC versus Na^+ and (d, h) $Na^+ + K^+$ versus TC

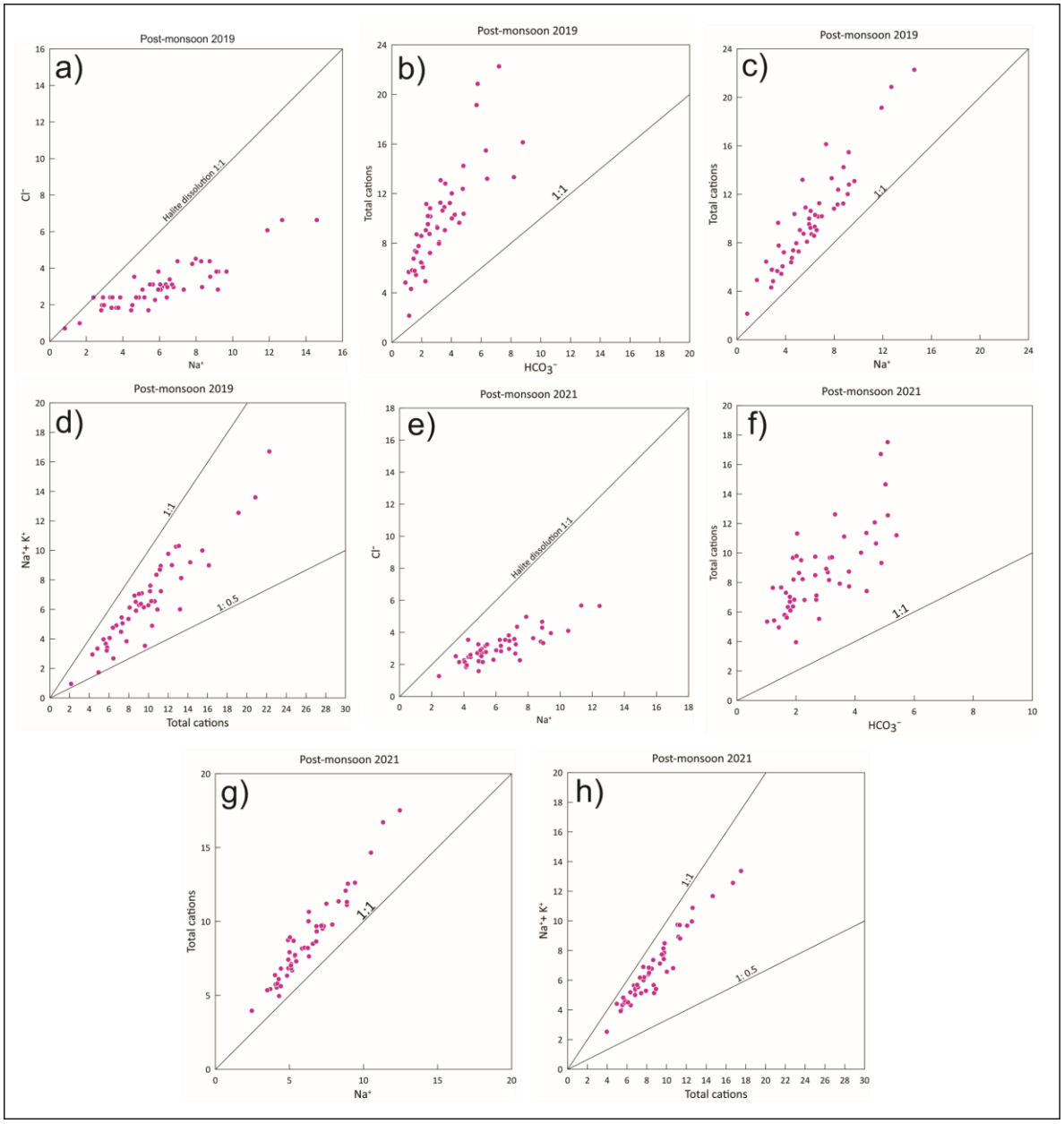

Fig. 5.25: Scatter plots of post-monsoon (2019 and 2021) groundwater samples (a, e) Cl^- versus Na^+ (b, f) TC versus HCO_3^- (c, g) TC versus Na^+ and (d, h) $Na^+ + K^+$ versus TC

Many anthropogenic activities such as agricultural, industrial, and municipal sewages have an impact on NO_3^- contaminations (Adimalla, 2021). The pre-monsoon and post-monsoon groundwater samples for 2019 and 2021 have been plotted between NO_3^- /Na^+ ratios and Cl^-/Na^+ ratios (Yunhui Zhang et al., 2021; Wang Yi et al., 2023), which is shown in Fig. 5.26. In pre-monsoon and post-monsoon groundwater samples of the year 2019, the majority of the samples have been plotted below and along the y = x line,

indicating the source of NO_3^- concentrations to be mostly from municipal sewage operations and some agricultural activities. In 2021 pre-monsoon and post-monsoon groundwater samples, the samples have been plotted below the y=x line and more toward the municipal sewage area indicating that the sources of NO_3^- concentrations are mostly from municipal sewage operations in the year 2021.

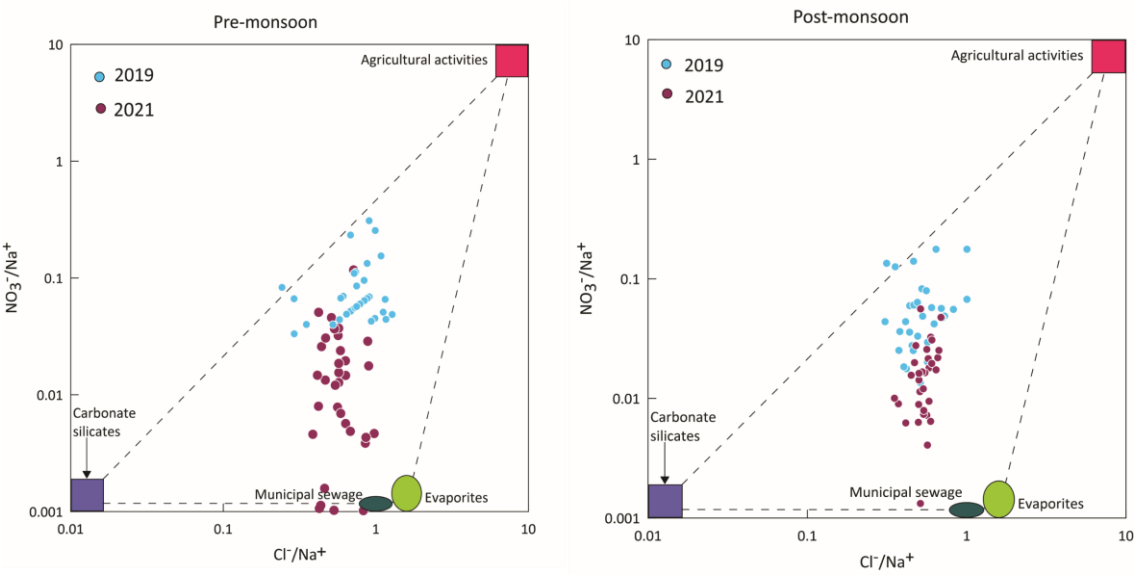

Fig. 5.26: Scatter plots of NO_3^-/ Na^+ versus Cl^-/ Na^+ for the pre-monsoon and post-monsoon groundwater samples (2019 and 2021)

5.5 STATISTICAL ANALYSIS USING CORRELATION COEFFICIENT

Pearson's correlation (Karl Pearson, 1896) coefficient measures the statistical relationship between two continuous variables and is known as the best method of measuring the association between variables of interest. If the correlation coefficient (r) is near ± 1, then it indicates a perfect correlation, i.e., as one variable increases, the other also increases if it is positive and decreases if it is negative. When the value is zero then it is said to have no correlation. If r > 0.7 or -0.7, it shows a strong correlation between the variables and if r ranges from 0.5 to 0.7 or -0.5 to -0.7, the correlation between the variables is moderate (Jabal et al., 2014; Pazand et al., 2012).

Pearson correlation analysis was conducted to assess and analyze the relationship between different parameters The parameters of groundwater correlation were calculated, and the results are shown in Table 5.7 to Table 5.10 for both pre-monsoon and post-monsoon for the years 2019 and 2021. The Pearson correlation coefficient analysis among the water quality parameters, namely pH, TDS, EC, Turbidity, TH, TA, major cations

(Ca^{2+}, Mg^{2+}, K^{+}, Na^{+}), anions (HCO_3^{-}, SO_4^{2-}, NO_3^{-}, Cl^{-}, F^{-}) and Fe were calculated for correlation analysis.

In 2019 pre-monsoon groundwater samples (Table 5.7), TDS with EC (r=0.96) show the highest correlation coefficient. The TDS strongly correlates with TH, TA, and Ca^{2+} while moderately correlating with HCO_3^{-}. EC and TA are strongly correlated with each other while EC is moderately correlated with TH, Ca^{2+} and HCO_3^{-}. TH is strongly correlated with Mg^{2+}, Ca^{2+} and HCO_3^{-} while moderately correlated with TA. TA is strongly correlated with Ca^{2+} and HCO_3^{-}. Ca^{2+} and HCO_3^{-} strongly correlate with each other while Na^{+} is moderately correlated with K^{+} and SO_4^{2-}.

Table 5.7: Correlation matrix of 2019 Pre-Monsoon groundwater samples

	pH	TDS	EC	Turbidity	TH	TA	Mg	Ca	K	Na	HCO3	SO4	NO3	Cl	F	Fe
pH	1															
TDS	0.17	1														
EC	0.20	0.96	1													
Turbidity	-0.10	-0.05	-0.04	1												
TH	0.04	0.72	0.70	0.25	1											
TA	0.30	0.85	0.83	0.00	0.65	1										
Mg	-0.20	0.42	0.43	0.21	0.79	0.30	1									
Ca	0.24	0.73	0.69	0.19	0.82	0.74	0.29	1								
K	0.36	0.49	0.49	-0.26	0.22	0.39	0.03	0.32	1							
Na	0.42	0.38	0.38	-0.07	0.25	0.43	-0.04	0.43	0.52	1						
HCO3	0.44	0.68	0.69	0.05	0.73	0.81	0.38	0.79	0.48	0.49	1					
SO4	0.21	0.30	0.33	-0.14	0.32	0.31	0.15	0.37	0.03	0.58	0.32	1				
NO3	0.03	-0.13	-0.09	-0.14	-0.24	-0.26	-0.27	-0.12	0.08	0.29	-0.26	0.11	1			
Cl	-0.25	0.36	0.33	0.31	0.32	0.05	0.34	0.19	0.38	0.21	-0.04	-0.10	0.09	1		
F	0.27	0.41	0.38	-0.11	0.11	0.44	0.04	0.13	0.39	0.21	0.29	-0.08	0.10	0.08	1	
Fe	-0.12	0.01	0.02	0.38	0.15	0.04	0.20	0.05	-0.10	0.01	0.02	0.02	-0.27	0.18	-0.03	1

In 2021 pre-monsoon groundwater samples (Table 5.8), TDS with EC (0.98) show the highest correlation coefficient. The TDS strongly correlates with TH and HCO_3^{-} while TDS moderately correlates with TA, Ca^{2+}, Mg^{2+}, Na^{+}, Cl^{-} and F^{-}. EC strongly correlates with TH, TA and HCO_3^{-} while EC is moderately correlated with Mg^{2+}, Ca^{2+}, Na^{+}, SO_4^{2-}, Cl^{-} and F^{-}.Turbidity is showing a moderate correlation with Fe. TH is strongly correlated with TA, Mg^{2+}, Ca^{2+} and HCO_3^{-}. TA is strongly correlated with Ca^{2+} and HCO_3^{-} while moderately correlating with Mg^{2+}. Mg^{2+} has a strong correlation with HCO_3^{-} and a moderate correlation with Ca^{2+} and Fe. Ca^{2+} is moderately correlating with HCO_3^{-}. Na^{+} is strongly correlated with HCO_3^{-}, SO_4^{2-} and Cl^{-} while HCO_3^{-} is moderately correlated with Cl^{-} and Fe.

Table 5.8: Correlation matrix of 2021 Pre-Monsoon groundwater samples

	pH	TDS	EC	Turbidity	TH	TA	Mg	Ca	K	Na	HCO3	SO4	NO3	Cl	F	Fe
pH	1															
TDS	0.22	1														
EC	0.21	0.98	1													
Turbidity	0.08	0.22	0.20	1												
TH	0.11	0.76	0.79	0.17	1											
TA	0.22	0.70	0.72	0.03	0.72	1										
Mg	-0.04	0.62	0.62	0.26	0.80	0.55	1									
Ca	0.07	0.68	0.67	0.12	0.77	0.76	0.60	1								
K	0.03	0.39	0.33	0.29	0.17	-0.07	0.14	-0.01	1							
Na	0.14	0.66	0.68	0.28	0.39	0.46	0.40	0.25	0.42	1						
HCO3	0.13	0.81	0.80	0.35	0.75	0.79	0.73	0.67	0.32	0.71	1					
SO4	0.06	0.43	0.50	-0.01	0.32	0.31	0.22	0.17	0.14	0.75	0.37	1				
NO3	-0.18	0.18	0.14	-0.20	-0.02	-0.23	-0.07	-0.10	0.27	0.06	-0.12	-0.04	1			
Cl	0.13	0.60	0.60	0.32	0.41	0.34	0.43	0.29	0.48	0.85	0.59	0.49	0.12	1		
F	0.13	0.52	0.51	0.28	0.30	0.45	0.17	0.37	0.10	0.43	0.43	0.40	-0.06	0.31	1	
Fe	-0.02	0.33	0.28	0.65	0.29	0.20	0.50	0.20	0.36	0.39	0.58	-0.10	-0.16	0.45	0.01	1

In 2019 post-monsoon groundwater samples (Table 5.9), TDS with EC (0.98) show the highest correlation coefficient. The TDS strongly correlates with Na^+ and HCO_3^- whereas it moderately correlates with TH, TA, Ca^{2+}, K^+, SO_4^{2-} and Cl^-. EC strongly correlates with Na^+ and HCO_3^- while EC is moderately correlating with TH, TA, Ca^{2+}, K^+, SO_4^{2-} and Cl^-. Turbidity is showing a moderate correlation with Fe. TH is showing a strong correlation with TA, Mg^{2+}, Ca^{2+} and HCO_3^-. TA is strongly correlated with Ca^{2+} and HCO_3^- while moderately correlating with Na^+. Ca^{2+} has a strong correlation with HCO_3^-. K^+ has a moderate correlation with Na^+, HCO_3^- and SO_4^{2-}. Na^+ is strongly correlated with SO_4^{2-} and Cl^- while it has a moderate correlation with HCO_3^-. SO_4^{2-} is moderately correlated with Cl^-.

Table 5.9: Correlation matrix of 2019 Post-Monsoon groundwater samples

	pH	TDS	EC	Turbidity	TH	TA	Mg	Ca	K	Na	HCO3	SO4	NO3	Cl	F	Fe
pH	1															
TDS	0.27	1.00														
EC	0.28	0.98	1.00													
Turbidity	-0.15	-0.08	-0.08	1.00												
TH	0.19	0.67	0.64	-0.04	1.00											
TA	0.34	0.69	0.67	0.01	0.83	1.00										
Mg	-0.08	0.36	0.34	-0.08	0.78	0.43	1.00									
Ca	0.34	0.70	0.68	0.00	0.89	0.90	0.40	1.00								
K	0.01	0.70	0.68	-0.13	0.38	0.47	0.13	0.46	1.00							
Na	0.14	0.83	0.83	-0.01	0.46	0.51	0.26	0.48	0.62	1.00						
HCO3	0.33	0.78	0.77	0.00	0.83	0.95	0.46	0.88	0.56	0.64	1.00					
SO4	-0.04	0.69	0.68	-0.14	0.48	0.31	0.44	0.37	0.50	0.80	0.43	1.00				
NO3	-0.11	0.38	0.40	0.20	0.26	0.15	0.28	0.17	0.30	0.35	0.21	0.19	1.00			
Cl	0.05	0.68	0.68	-0.02	0.39	0.36	0.26	0.37	0.48	0.89	0.46	0.65	0.29	1.00		
F	0.24	0.22	0.23	-0.08	0.34	0.44	0.25	0.31	0.06	0.16	0.45	-0.08	0.01	0.21	1.00	
Fe	-0.20	-0.16	-0.21	0.51	0.04	0.07	0.03	0.04	-0.04	-0.04	0.03	-0.06	-0.14	-0.01	-0.08	1.00

In 2021 post-monsoon groundwater samples (Table 5.10), TDS with EC (0.96) show the highest correlation coefficient. The TDS and EC both strongly correlates with Ca^{2+}, Na^+ and HCO_3^- whereas TDS and EC both moderately correlates with TH, TA, K^+, SO_4^{2-} and Cl^-. Turbidity is showing a moderate correlation with Fe. TH is showing a strong correlation with TA, Mg^{2+}, Ca^{2+} and HCO_3^- while TH moderately correlates with Na^+ and

SO_4^{2-}. TA is strongly correlated with Ca^{2+} and HCO_3^- while moderately correlating with Mg^{2+}. Ca^{2+} has a strong correlation with HCO_3^- while it has a moderate correlation with Na^+. K^+ has a strong correlation with Na^+ and a moderate correlation with SO_4^{2-}, NO_3^- and Cl^-. Na^+ strongly correlates with SO_4^{2-} and Cl^- while it correlates moderately with HCO_3^- and NO_3^-. SO_4^{2-} is moderately correlated with Cl^-.

Table 5.10: Correlation matrix of 2021 Post-Monsoon groundwater samples

	pH	TDS	EC	Turbidity	TH	TA	Mg	Ca	K	Na	HCO3	SO4	NO3	Cl	F	Fe
pH	1															
TDS	0.23	1														
EC	0.22	0.96	1													
Turbidity	-0.10	0.08	0.01	1												
TH	0.12	0.65	0.69	-0.06	1											
TA	0.24	0.62	0.66	0.14	0.81	1										
Mg	-0.09	0.19	0.23	-0.10	0.73	0.52	1									
Ca	0.23	0.77	0.80	0.00	0.84	0.75	0.25	1								
K	0.01	0.63	0.68	-0.16	0.41	0.20	0.17	0.45	1							
Na	0.12	0.77	0.77	0.05	0.51	0.42	0.28	0.50	0.74	1						
HCO3	0.23	0.77	0.79	0.08	0.79	0.85	0.35	0.85	0.47	0.54	1					
SO4	0.07	0.53	0.59	-0.04	0.57	0.40	0.48	0.43	0.62	0.73	0.40	1				
NO3	0.10	0.42	0.46	-0.17	0.33	0.21	0.30	0.23	0.60	0.54	0.27	0.43	1			
Cl	0.02	0.53	0.51	-0.10	0.37	0.25	0.32	0.28	0.54	0.72	0.34	0.50	0.26	1		
F	0.27	0.22	0.23	0.01	0.19	0.33	0.11	0.18	0.05	0.14	0.34	0.00	0.01	0.20	1	
Fe	-0.11	0.25	0.23	0.55	0.12	0.18	0.02	0.16	0.35	0.26	0.21	0.15	0.14	0.28	-0.04	1

From the statistical analysis using Pearson's correlation coefficient, we find that the groundwater in the study area has a strong correlation between TDS and EC. The TDS and EC are both strongly correlated with most of the physico-chemical parameters such as TH, TA, Ca^{2+}, Na^+ and HCO_3^-. The TH and HCO_3^- are also strongly correlated with each other and they both have a strong correlation with TDS, EC, TA, Ca^{2+} and Mg^{2+}. The Na^+ also shows a strong correlation with TDS, EC, Cl^-, SO_4^{2-} and HCO_3^-. Thus, the parameters EC, TDS, TH, HCO_3^- and Na^+ can be determined to be important physico-chemical parameters for drinking water quality parameters because they correlate with the majority of the groundwater parameters in the study area.

CHAPTER 6

ASSESSMENT OF GROUNDWATER QUALITY

6.1 INTRODUCTION

The quality of water directly affects the overall well-being of life. The pollution of water leads to health issues and causes degradation of habitat. Wastewater is a byproduct of various harmful substances released from domestic, agricultural or industrial practices. The degradation of water quality is caused by an increase in contaminants, including heavy metals, pesticides, and infectious and non-communicable diseases. Monitoring these risk factors at the right time can prevent habitat destruction and harm to public health.

The discharge of untreated sewage is the main polluting source for surface and groundwater in India. Given the fast changes in groundwater through the effects of natural and artificial sources, the investigation of groundwater quality in all parts of the country is required to improve health conditions. The study area, Kohima town has witnessed a growth in urban population. Therefore, it has become essential to check the quality of water for both drinking and irrigation uses for the future development of the town.

6.2 ASSESSMENT OF WATER QUALITY FOR DRINKING PURPOSES

The assessment of water for drinking purposes is critical and the groundwater in the study area was determined by using the Water Quality Index (WQI). The main objective of the WQI is to assign a single value to the water quality of a source by converting the parameters and their concentrations present in a sample into one value, which then gives an extensive evaluation of the water quality and its suitability for different uses like drinking, irrigation, etc. (Abbasi, 2002).

The "Weighted Arithmetic Water Quality Index" method (Brown et al., 1972 and Cude, 2001) has been utilized, which was compared with the acceptable limit standards of BIS (2012) and WHO (2004) for drinking purposes to know the general water quality of Kohima Town. Brown's WQI is one of the most used WQI techniques. A set 12 most commonly used water quality parameters (pH, TDS, major cations (Na^+, Ca^{2+}, K^+, Mg^{2+}), major anions (HCO_3^-, SO_4^{2-}, Cl^-, NO_3^-, F^-) and Fe) which reflect the overall water quality were chosen for calculating the WQI of all fifty groundwater samples in both pre-

monsoon and post-monsoon periods of 2019 and 2021. Based on WQI values, the samples have been classified into their respective water status in Table 6.1.

Table 6.1: WQI and status of water quality (Brown et al., 1972)

WQI Level	Water Quality Status
0-25	Excellent water
26-50	Good water
51-75	Poor water
76-100	Very Poor water
>100	Unsuitable for drinking

In order to calculate WQI using the "weighted arithmetic index" approach, the unit weight for each parameter that will be used in the computation must first be estimated. All parameters of various units and measurements are converted to a standard scale by assigning “unit weights.” The unit weights allocated to each parameter used to calculate the WQI, along with the drinking water quality standards are shown in Table 6.2. The maximum unit weight of 0.7211049 is given to Fe, indicating its importance in determining water quality and its significant influence on the index (Bora and Goswami, 2017).

Table 6.2: Relative weights of parameters (W_n) used for WQI determination (All parameters except pH are in mg/L)

Sl. no.	Parameters	Standard values (S_n) *BIS (2012) & **WHO (2004)	Unit weight (W_n)	Ideal value (V_o)
1.	pH	8.5*	0.02545076	7
2.	TDS	500*	0.00043266	0
3.	Magnesium	30*	0.00721105	0
4.	Calcium	75*	0.00288442	0
5.	Potassium	12**	0.01802762	0
6.	Sodium	200**	0.00108166	0
7.	Bicarbonate	300**	0.0007211	0
8.	Sulphate	200*	0.00108166	0
9.	Nitrate	45*	0.00480737	0
10.	Chloride	250*	0.00086533	0

11.	Fluoride	1*	0.21633147	0
12.	Iron	0.3*	0.7211049	0
			$\Sigma W_n = 1$	

6.2.1 WQI of pre-monsoon seasons (2019 and 2021)

The WQI values have been determined for pre-monsoon season for the years 2019 and 2021 which is presented in Table 6.3. The WQI geospatial distribution map has been prepared for the 2019 pre-monsoon and 2021 pre-monsoon and is shown in Fig. 6.1.

Table 6.3: WQI values for pre-monsoon season (2019 and 2021)

Sample no.	Pre-Monsoon 2019		Pre-Monsoon 2021	
	WQI	Description	WQI	Description
A1	7.29	Excellent	12.85	Excellent
A2	77.24	Very Poor	263.90	Unsuitable
A3	100.72	Unsuitable	119.06	Unsuitable
A4	4.36	Excellent	3.91	Excellent
A5	80.78	Very Poor	75.92	Poor
A6	26.25	Good	29.37	Good
A7	70.26	Poor	134.27	Unsuitable
A8	60.43	Poor	2.82	Excellent
A9	43.87	Good	21.31	Excellent
A10	42.57	Good	19.61	Excellent
A11	34.87	Good	20.63	Excellent
A12	5.35	Excellent	21.25	Excellent
A13	47.79	Good	16.77	Excellent
A14	54.18	Poor	89.54	Very Poor
A15	20.41	Excellent	34.10	Good
A16	298.50	Unsuitable	355.67	Unsuitable
A17	85.54	Very Poor	404.24	Unsuitable
A18	32.85	Good	84.48	Very Poor
A19	246.49	Unsuitable	1300.76	Unsuitable
A20	16.84	Excellent	20.13	Excellent
A21	29.56	Good	4.28	Excellent
A22	94.40	Very Poor	8.15	Excellent

A23	65.03	Poor	46.40	Good
A24	26.64	Good	181.73	Unsuitable
A25	156.35	Unsuitable	9.83	Excellent
A26	5.04	Excellent	9.63	Excellent
A27	45.22	Good	10.64	Excellent
A28	39.35	Good	105.81	Unsuitable
A29	16.15	Excellent	16.63	Excellent
A30	144.63	Unsuitable	17.12	Excellent
A31	126.78	Unsuitable	370.06	Unsuitable
A32	77.07	Very Poor	53.92	Poor
A33	31.61	Good	83.94	Very Poor
A34	17.89	Excellent	29.20	Good
A35	8.99	Excellent	106.18	Unsuitable
A36	17.06	Excellent	18.65	Excellent
A37	112.09	Unsuitable	104.51	Unsuitable
A38	364.72	Unsuitable	55.08	Poor
A39	20.67	Excellent	44.03	Good
A40	64.96	Poor	81.89	Very Poor
A41	156.13	Unsuitable	119.33	Unsuitable
A42	69.76	Poor	74.08	Poor
A43	35.83	Good	5.25	Excellent
A44	20.35	Excellent	18.27	Excellent
A45	514.89	Unsuitable	144.29	Unsuitable
A46	60.34	Poor	60.38	Poor
A47	572.37	Unsuitable	50.78	Good
A48	819.22	Unsuitable	97.80	Very Poor
A49	48.05	Good	20.78	Excellent
A50	866.31	Unsuitable	31.90	Good

WQI of 2019 pre-monsoon

WQI in the study area during 2019 pre-monsoon ranges from 4.36 to 866.31 with an average of 119.68. The results showed that most groundwater samples fall under the good and unsuitable water categories with 26% each. 24% of the total groundwater

samples have been classified under excellent water which is suitable for drinking, 14% of the total groundwater samples as being of poor water quality while 10% were under very poor water and unsuitable for drinking. The lowest WQI value 4.36 was found at sample number A4. The highest WQI value was found in sample number A50 recorded at 866.31. The high WQI could be attributed to the iron concentration in sample number A50 which was measured at 3.53 mg/L and is far beyond the permissible limit for drinking (0.3 mg/L).

The geospatial distribution of 2019 pre-monsoon WQI in Kohima Town is demonstrated in Fig. 6.1a. Excellent water is spatially limited and distributed in small isolated patches mostly in the southern parts of the study area. Good water is distributed in the western, south-eastern and small isolated patches in the northern areas. Groundwater of relatively poor quality is found distributed throughout the southern part of the study area and some pockets in the northern part. The very poor water is found distributed in a linear trend from the north-west to the south-eastern part and also in small pockets in the south-western and northern areas. The water which falls under the unsuitable category is found distributed mostly throughout the northern and eastern parts and some small isolated areas towards the south.

WQI of 2021 pre-monsoon

WQI in the study area during 2021 pre-monsoon ranges from 2.82 to 1300.76 with an average of 100.22. The results showed that majority of the groundwater samples fall under excellent water category with 40%. 26% of the total groundwater samples were classified as unsuitable for drinking, 14% of the total groundwater samples were of good water quality while 10% were under poor and very poor water each. The lowest WQI value with 2.82 was found at sample number A8. The highest WQI value recorded at 1300.76 was found in sample number A19. The high WQI at A19 is found to be due to the iron concentration which was measured at 5.33 mg/L and is far beyond the permissible limit for drinking (0.3 mg/L).

The WQI of 2021 pre-monsoon has been geospatially plotted and presented in Fig. 6.1b. Excellent water is spatially limited and distributed in small isolated patches mostly in the south-western parts of the study area, some in the western and south-eastern areas. Good water is distributed in the western, central, southern and small isolated patches in the south-eastern and north-eastern areas. Groundwater of relatively poor

quality is found distributed throughout the south-western and eastern parts of the study area and some pockets in the northern part. The very poor water is found distributed in the south-eastern, south-western part and north-eastern areas. The water which falls under unsuitable category is found distributed mostly throughout the northern parts and some small patches towards the south-eastern and south-western areas.

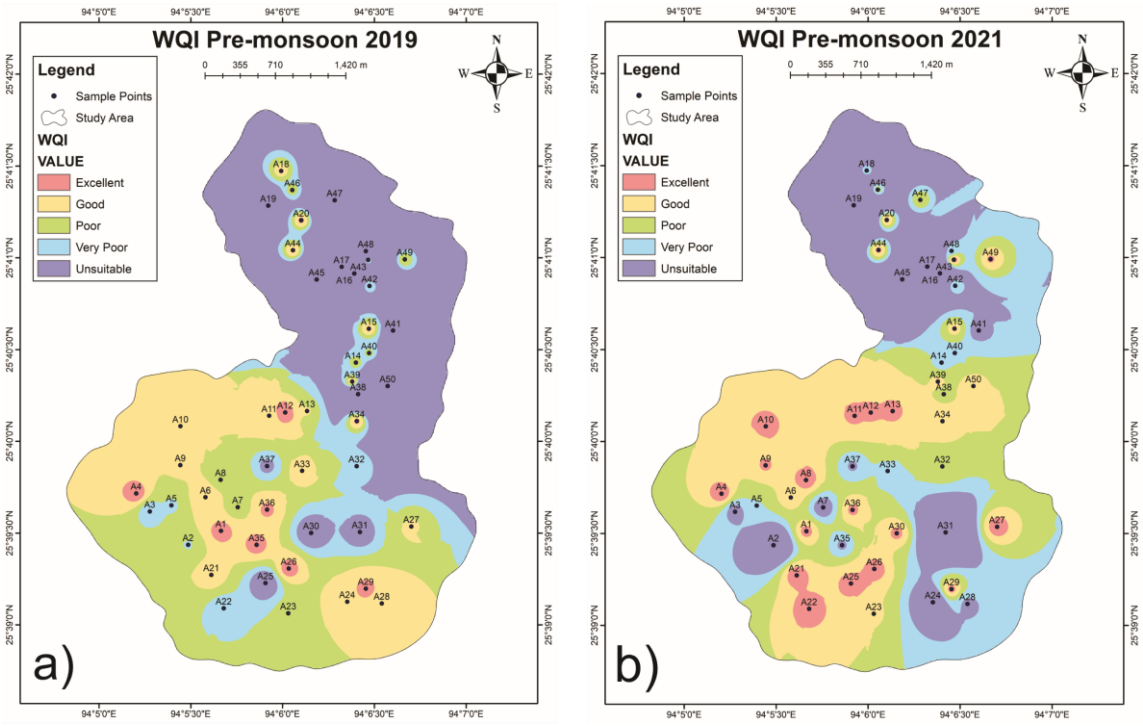

Fig. 6.1: WQI geospatial distribution map of (a) 2019 Pre-monsoon and (b) 2021 Pre-monsoon

6.2.2 WQI of post-monsoon seasons (2019 and 2021)

The WQI values have been determined for post-monsoon season for the years 2019 and 2021 which is presented in Table 6.4. The WQI geospatial distribution map has been prepared for 2019 post-monsoon and 2021 pre-monsoon and is shown in Fig. 6.2.

Table 6.4: WQI values for post-monsoon season (2019 and 2021)

Sample no.	Post-Monsoon 2019		Post-Monsoon 2021	
	WQI	Description	WQI	Description
A1	27.67	Good	19.21	Excellent
A2	1031.69	Unsuitable	248.23	Unsuitable
A3	97.47	Very Poor	91.51	Very Poor

A4	13.51	Excellent	9.61	Excellent
A5	56.20	Poor	52.43	Poor
A6	31.54	Good	29.07	Good
A7	47.03	Good	91.41	Very Poor
A8	48.02	Good	10.99	Excellent
A9	36.79	Good	17.87	Excellent
A10	24.92	Excellent	20.91	Excellent
A11	12.80	Excellent	16.98	Excellent
A12	13.37	Excellent	2.72	Excellent
A13	17.51	Excellent	21.47	Excellent
A14	50.39	Good	51.01	Poor
A15	24.84	Excellent	25.61	Excellent
A16	123.46	Unsuitable	154.39	Unsuitable
A17	52.80	Poor	140.12	Unsuitable
A18	26.42	Good	61.67	Poor
A19	390.71	Unsuitable	381.80	Unsuitable
A20	14.22	Excellent	19.98	Excellent
A21	11.59	Excellent	8.21	Excellent
A22	14.86	Excellent	18.20	Excellent
A23	51.43	Poor	37.32	Good
A24	36.84	Good	60.21	Poor
A25	40.49	Good	29.90	Good
A26	3.84	Excellent	3.72	Excellent
A27	14.26	Excellent	35.31	Good
A28	30.86	Good	51.73	Poor
A29	15.73	Excellent	10.14	Excellent
A30	53.83	Poor	26.63	Good
A31	77.67	Very Poor	202.32	Unsuitable
A32	36.48	Good	26.32	Good
A33	17.58	Excellent	78.11	Very Poor
A34	15.06	Excellent	13.27	Excellent
A35	15.86	Excellent	35.08	Good
A36	14.33	Excellent	7.38	Excellent

A37	742.52	Unsuitable	70.12	Poor
A38	72.51	Poor	31.82	Good
A39	22.13	Excellent	14.40	Excellent
A40	44.79	Good	59.10	Poor
A41	141.43	Unsuitable	110.03	Unsuitable
A42	45.17	Good	58.18	Poor
A43	31.89	Good	13.40	Excellent
A44	19.50	Excellent	22.99	Excellent
A45	311.42	Unsuitable	188.83	Unsuitable
A46	61.51	Poor	45.55	Good
A47	445.86	Unsuitable	39.12	Good
A48	235.28	Unsuitable	67.67	Poor
A49	30.46	Good	12.41	Excellent
A50	521.99	Unsuitable	37.73	Good

WQI of 2019 post-monsoon

WQI in the study area during 2019 post-monsoon ranges from 3.84 to 1031.69 with an average of 106.37. The results showed that majority of the groundwater samples with 36% fall under excellent water category. 30% of the total groundwater samples fall under good water and is suitable for drinking. 18% of the total groundwater samples were classified under unsuitable which is not fit for drinking. 12% of the total groundwater samples were under poor water and 4% were under very poor water. The lowest WQI value 3.84 was found at sample number A26. The highest WQI value recorded at 1031.69 was found in sample number A2. The high WQI at A2 is found to be due to the iron concentration which was measured at 4.28 mg/L and is far beyond the permissible limit for drinking (0.3 mg/L).

The WQI of 2019 post-monsoon has been geospatially plotted and presented in Fig. 6.2a. Excellent water is spatially limited and distributed in small isolated patches mostly in the south-eastern parts of the study area, some in the western and central areas. Good water is mostly distributed in the south-eastern area and small isolated patches all throughout the study area. Groundwater of relatively poor quality is found distributed in a continuous zone from central to south-east and then to the south-western areas, some poor water is also found towards the western and northern areas. The very poor water is

found distributed in the south-western, western, north-eastern and small isolated patches in the northern areas. The water which falls under unsuitable category is found distributed mostly throughout the northern parts and some towards the south-western areas.

WQI of 2021 post-monsoon

WQI in the study area during 2021 post-monsoon ranges from 2.72 to 381.80 with an average of 57.64. The results showed that the majority of the groundwater samples with 40% fall under the excellent water category. 22% of the total groundwater samples fall under good water and are suitable for drinking. 18% of the total groundwater samples were classified under poor water. 14% of the total groundwater samples were under unsuitable water and 6% were under very poor water. The lowest WQI value 2.72 was found at sample number A12. The highest WQI value recorded at 381.80 was found in sample number A19. The high WQI at A19 is found to be due to the high Fe (1.5 mg/L) and K^+ (98.4 mg/L) concentration which is far beyond the permissible limit for drinking (0.3 mg/L and 12 mg/L).

The WQI of 2021 post-monsoon has been geospatially plotted and presented in Fig. 6.2b. Excellent water is distributed in isolated patches mostly in the central and south-western parts of the study area and a few patches in the north-eastern area. Good water is mostly distributed in a continuous zone from east to west and extends to the southern area. Good water is also found in patches in the northern and north-eastern areas. Groundwater of relatively poor quality is found distributed in the north-eastern, south-western and south-eastern areas. The very poor water is mostly found distributed in the northern areas and isolated patches towards the south-west and south-east. The water which falls under unsuitable category is found distributed mostly in the north-western parts and some isolated patches towards the south-western and south-eastern areas.

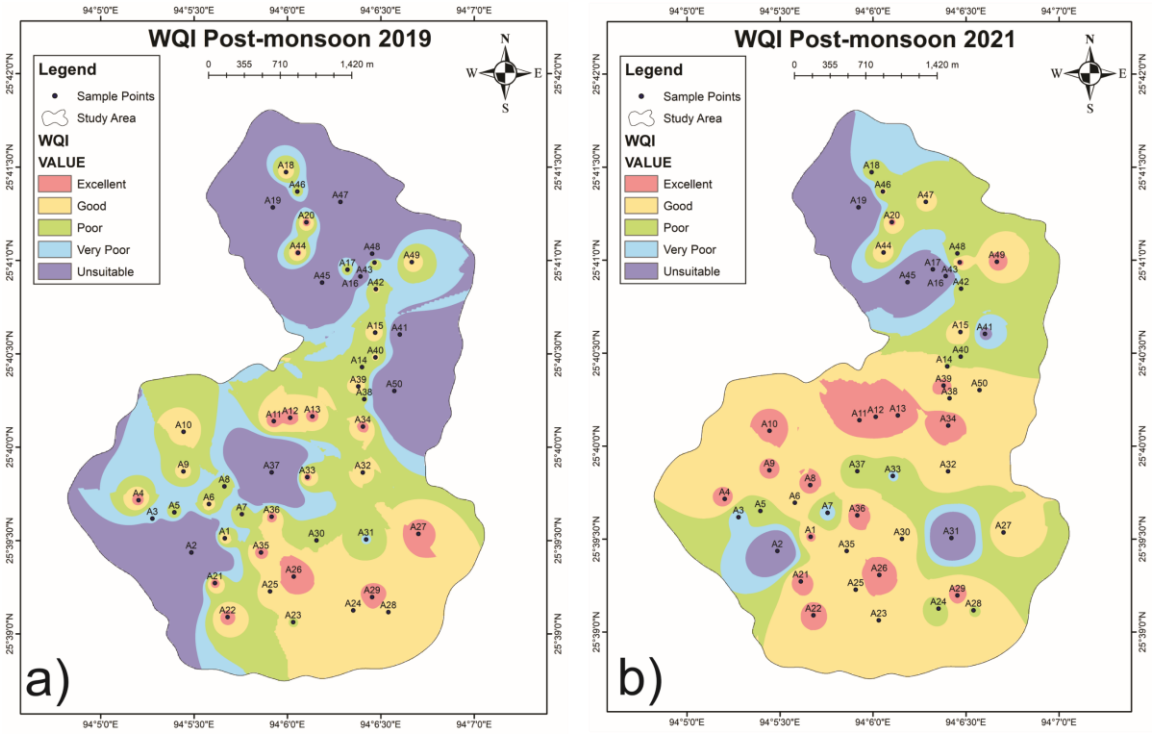

Fig. 6.2: WQI geospatial distribution map of (a) 2019 Post-monsoon and (b) 2021 Post-monsoon

6.2.3 WQI of 2019 and 2021

The WQI values of pre-monsoon and post-monsoon of the year 2019 have been calculated to find the mean WQI values of 2019. Similarly, this was also calculated for the year 2021. The WQI values for 2019 and 2021 are presented in Table 6.5.

Table 6.5: WQI values of 2019 and 2021

Sample no.	2019 WQI		2021 WQI	
A1	17.48	Excellent	16.03	Excellent
A2	554.46	Unsuitable	256.06	Unsuitable
A3	99.10	Very Poor	105.28	Unsuitable
A4	8.94	Excellent	6.76	Excellent
A5	68.49	Poor	64.18	Poor
A6	28.89	Good	29.22	Good
A7	58.65	Poor	112.84	Unsuitable

A8	54.23	Poor	6.90	Excellent
A9	40.33	Good	19.59	Excellent
A10	33.75	Good	20.26	Excellent
A11	23.84	Excellent	18.80	Excellent
A12	9.36	Excellent	11.99	Excellent
A13	32.65	Good	19.12	Excellent
A14	52.28	Poor	70.28	Poor
A15	22.63	Excellent	29.85	Good
A16	210.98	Unsuitable	255.03	Unsuitable
A17	69.17	Poor	272.18	Unsuitable
A18	29.64	Good	73.08	Poor
A19	318.60	Unsuitable	841.28	Unsuitable
A20	15.53	Excellent	20.06	Excellent
A21	20.58	Excellent	6.25	Excellent
A22	54.63	Poor	13.17	Excellent
A23	58.23	Poor	41.86	Good
A24	31.74	Good	120.97	Unsuitable
A25	98.42	Very Poor	19.87	Excellent
A26	4.44	Excellent	6.67	Excellent
A27	29.74	Good	22.98	Excellent
A28	35.11	Good	78.77	Very Poor
A29	15.94	Excellent	13.38	Excellent
A30	99.23	Very Poor	21.87	Excellent
A31	102.22	Unsuitable	286.19	Unsuitable
A32	56.77	Poor	40.12	Good
A33	24.59	Excellent	81.03	Very Poor
A34	16.48	Excellent	21.24	Excellent

A35	12.42	Excellent	70.63	Poor
A36	15.69	Excellent	13.01	Excellent
A37	427.31	Unsuitable	87.32	Very Poor
A38	218.61	Unsuitable	43.45	Good
A39	21.40	Excellent	29.21	Good
A40	54.88	Poor	70.50	Poor
A41	148.78	Unsuitable	114.68	Unsuitable
A42	57.46	Poor	66.13	Poor
A43	33.86	Good	9.33	Excellent
A44	19.93	Excellent	20.63	Excellent
A45	413.16	Unsuitable	166.56	Unsuitable
A46	60.93	Poor	52.96	Poor
A47	509.12	Unsuitable	44.95	Good
A48	527.25	Unsuitable	82.73	Very Poor
A49	39.25	Good	16.60	Excellent
A50	694.15	Unsuitable	34.81	Good

The WQI in the study area during the year 2019 ranges from 4.44 to 694.15 with an average of 113.03. The results showed that the majority of groundwater samples fall under the excellent water category with 30%. The groundwater samples with poor and unsuitable water were at 22% each. 20% of the total groundwater samples were classified under good water while 6% of the total groundwater samples were under very poor water. The lowest WQI value 4.44 was found at sample number A26 while the highest WQI value at 694.15 was found in sample number A50. Whereas the WQI in the study area during the year 2021 ranges from 6.25 to 841.28 and averages at 78.93. The results showed that most of the groundwater samples fall under the excellent water category with 42%. The groundwater samples with 20% were categorized under unsuitable water. 16% of the total groundwater samples were classified under good water. 14% of the total groundwater samples were under poor water while 8% of the total groundwater samples

were under very poor water. The lowest WQI value 6.25 was found at sample number A21 while the highest WQI value at 841.28 was found in sample number A19.

The WQI of 2019 and 2021 have been geospatially plotted and shown in Fig. 6.3. In 2019, excellent water is distributed in small isolated patches mostly in the southern parts of the study area. Good water is distributed in the south-eastern area and small isolated patches mostly in the western part and towards the northern areas. Groundwater of relatively poor quality is found distributed mostly in the western areas, in the south, south-east and isolated patches in the northern areas. Very poor water is found scattered in the south-western, central, eastern and small isolated patches in the northern areas. The water which falls under the unsuitable category is found distributed mostly throughout the northern parts and some in the south-western areas. Whereas, in 2021, excellent water is distributed in isolated patches mostly in the south-western areas and in a small patch towards the north-east. Good water is distributed mostly in a linear zone from west to east, the southern part and small isolated patches in the south-east and towards the northern areas. Groundwater of relatively poor quality is found scattered throughout the south in the south-eastern, south-western, eastern and isolated patches in the north-eastern areas. Very poor water is found distributed in the north-eastern areas and isolated patches in the south-east and south-west. The water which falls under the unsuitable category is found distributed mostly towards the north-western parts and some isolated patches in the south-western and south-eastern areas.

Comparing the WQI values of 2019 and 2021, we find that 46% of the groundwater samples had no change in the WQI category of water while there was 34% increase of the WQI category of water from bad to good and a 20% decrease in the WQI category of water from good to bad. Overall, there has been a decrease in the WQI values which has led to better groundwater quality in 2021. This has also been found in many other regions and this is attributed to the pandemic which has led to less pollution of the environment during the year 2020 (Smart water magazine, 2020; Chakraborty et al., 2021; Pacaol, 2021).

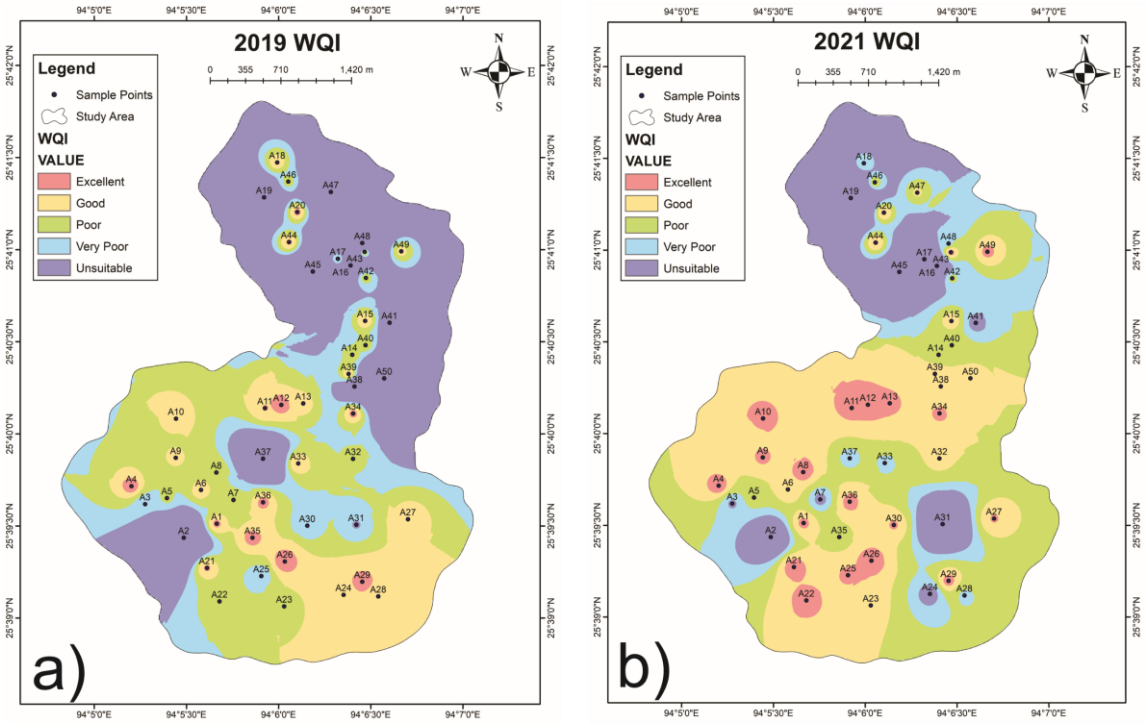

Fig. 6.3: WQI geospatial distribution maps of (a) 2019 and (b) 2021

6.3 ASSESSMENT OF WATER QUALITY FOR IRRIGATION PURPOSES

The suitability of water for irrigation is influenced by a number of chemical components in water. It is also affected by the nature and composition of the soil and subsoil, the depth of the water table, the terrain, the climate, the type of crop, etc. Salts in irrigation water if present in excess amounts can alter the qualities of the soil and be hazardous to plant growth. Salts are more likely to accumulate in plant root zones when the soil permeability is low, low water table, flat topography, and arid climate. Some crops can tolerate salt better than others. Different types of ions are present in groundwater such as CO_3^-, HCO_3^-, Ca^{2+}, Mg^{2+}, SO_4^{2-}, TH etc. The important cations that have an impact on the suitability of groundwater for irrigation purposes are Ca^{2+}, Mg^{2+} and Na^+. Some concentrations of these cations are beneficial for plant growth. EC is also an important parameter for the suitability of water for irrigation (Brindha et al., 2014).

In the present study, the water quality criteria for irrigation purposes have been ascertained using sodium percentage (%Na), Wilcox diagram, sodium adsorption ratio (SAR), US salinity diagram and permeability index (PI).

6.3.1 Sodium percentage (%Na)

When sodium concentrations are high in irrigation water, sodium produces an increase in soil hardness by being absorbed by clay particles and displacing Mg^{2+} and Ca^{2+} ions. This exchange mechanism lowers permeability and results in soil with inadequate internal drainage (Tijani, 1994). The %Na was calculated for pre-monsoon and post-monsoon seasons for the years 2019 and 2021 which is tabulated in Table 6.6. The water class suitable for irrigation according to the %Na proposed by Wilcox (1955) is given in Table 6.7.

Table 6.6: %Na values of groundwater samples in pre-monsoon and post-monsoon (2019 and 2021)

Sample no.	% Na of groundwater samples in meq/L			
	Pre-monsoon 2019	Pre-monsoon 2021	Post-monsoon 2019	Post-monsoon 2021
A1	57.57	61.12	68.59	78.33
A2	57.50	66.58	75.69	65.27
A3	57.63	71.61	73.05	73.64
A4	59.58	67.32	67.01	67.69
A5	51.54	50.92	55.70	79.73
A6	50.91	61.94	80.09	86.22
A7	71.20	69.08	76.06	79.85
A8	42.91	49.37	72.68	80.13
A9	53.30	61.14	64.20	80.53
A10	41.71	58.80	35.10	63.85
A11	51.21	65.47	74.75	90.32
A12	32.63	60.56	36.59	69.02
A13	68.64	59.96	65.53	76.31
A14	53.75	73.94	65.16	79.66
A15	39.49	69.07	64.57	79.37
A16	38.22	75.86	64.35	79.86
A17	32.78	64.45	54.94	66.79
A18	50.37	83.10	61.59	78.21
A19	39.51	74.78	75.00	75.16
A20	49.06	75.34	64.75	73.27
A21	53.39	62.32	68.33	88.91
A22	44.81	54.66	44.21	78.32
A23	53.25	71.07	58.76	78.08

A24	43.30	63.44	55.55	79.66
A25	65.66	49.89	67.17	78.05
A26	57.50	81.14	72.84	84.32
A27	50.51	80.08	71.14	81.39
A28	45.34	81.76	69.60	80.21
A29	50.89	74.08	74.46	79.08
A30	52.56	74.13	80.77	84.54
A31	59.02	70.00	67.61	78.97
A32	51.58	75.65	60.98	76.42
A33	53.17	77.07	81.27	87.59
A34	54.93	81.96	74.84	81.85
A35	50.66	75.06	62.14	73.44
A36	44.57	77.42	63.74	65.58
A37	50.06	79.57	41.58	73.79
A38	53.89	87.71	77.90	83.42
A39	41.38	73.23	64.54	77.55
A40	48.91	80.41	78.73	85.87
A41	34.15	73.37	45.47	63.95
A42	61.72	74.90	74.66	84.19
A43	47.43	79.46	77.20	86.73
A44	56.64	83.65	68.97	77.81
A45	54.40	77.65	79.61	76.43
A46	53.25	78.27	77.90	85.20
A47	26.93	52.75	47.15	58.81
A48	38.84	66.59	62.83	60.58
A49	60.79	77.26	69.28	85.77
A50	70.61	90.12	49.38	80.93

Table 6.7: Water classification for irrigation based on %Na

%Na	**Water class**	**Percentage (%) of groundwater samples**			
		Pre-monsoon (2019)	**Pre-monsoon (2021)**	**Post-monsoon (2019)**	**Post-monsoon (2021)**
<20	Excellent	-	-	-	-
20-40	Good	16	-	4	-

40-60	Permissible	72	14	18	2
60-80	Doubtful	12	68	72	62
>80	Unsuitable	-	18	6	36

The majority of the groundwater samples in the pre-monsoon of 2019 fall under the permissible water class with 72%, 16% of the groundwater samples are classed under good water and 12% under doubtful water. In the pre-monsoon of 2021, the majority of the groundwater samples fall under doubtful water with 68%, 18% of the groundwater samples are classed under unsuitable water and 14% under permissible water. In the post-monsoon of 2019, the majority of the groundwater samples fall under doubtful water with 72%, 18% of the groundwater samples are classed under permissible water, 6% under unsuitable water and 4% under good water. Whereas, the majority of the groundwater samples in post-monsoon of 2021 fall under the doubtful water class with 62%, 36% of the groundwater samples are classed under unsuitable water and 2% under permissible water.

6.3.2 Wilcox Diagram

The groundwater samples of pre-monsoon and post-monsoon seasons (2019 and 2021) in the study area are plotted in the Wilcox diagram (1955) shown in Figs. 6.4 and 6.5 by using sodium percentage against EC to find the water which is suitable for irrigation purposes. The Wilcox diagram is divided into five divisions- excellent to good, good to permissible, permissible to doubtful, doubtful to unsuitable and unsuitable. The percentage of groundwater samples which falls under the different water classes for irrigation based on the Wilcox diagram is presented in Table 6.8.

Table 6.8: Water classification for irrigation based on Wilcox diagram

Wilcox water class	**Percentage (%) of groundwater samples**			
	Pre-Monsoon (2019)	**Pre-Monsoon (2021)**	**Post-Monsoon (2019)**	**Post-Monsoon (2021)**
Excellent to Good	70	32	14	6
Good to Permissible	22	2	6	-

Permissible to Doubtful	8	66	80	94

The groundwater in the study area varies from excellent to doubtful. In the pre-monsoon season of 2019, most of the groundwater samples come under the excellent to good water category with 70%, 22% of the groundwater samples come under the good to permissible water class and 8% fall under permissible to doubtful water. In the pre-monsoon season of 2021, the majority of groundwater samples with 66% fall under the permissible to doubtful water category, 32% of the groundwater samples come under the excellent to good water class and 2% fall under the good to permissible water class. In the post-monsoon season of 2019, the majority of the groundwater samples come under the permissible to doubtful category with 80%, 14% of groundwater samples come under excellent to good water and 6% come under good to permissible. In the post-monsoon season of 2021, the majority of the groundwater samples come under the permissible to doubtful category with 94% and 6% of groundwater samples come under excellent to good water.

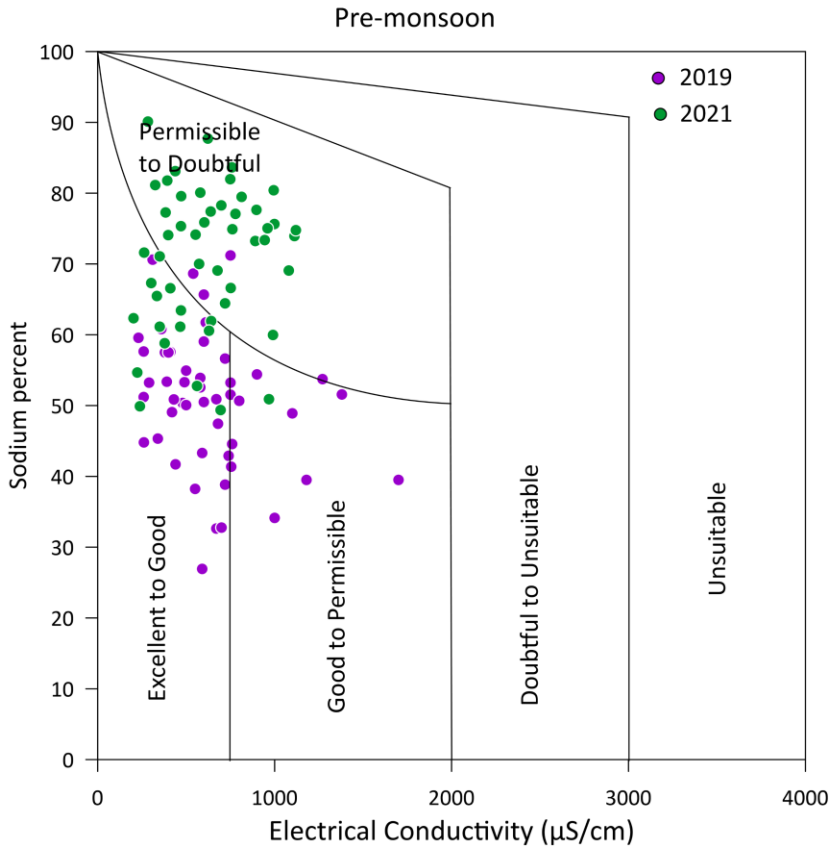

Fig. 6.4: Suitability of groundwater for irrigation based on EC and sodium percent for pre-monsoon groundwater samples

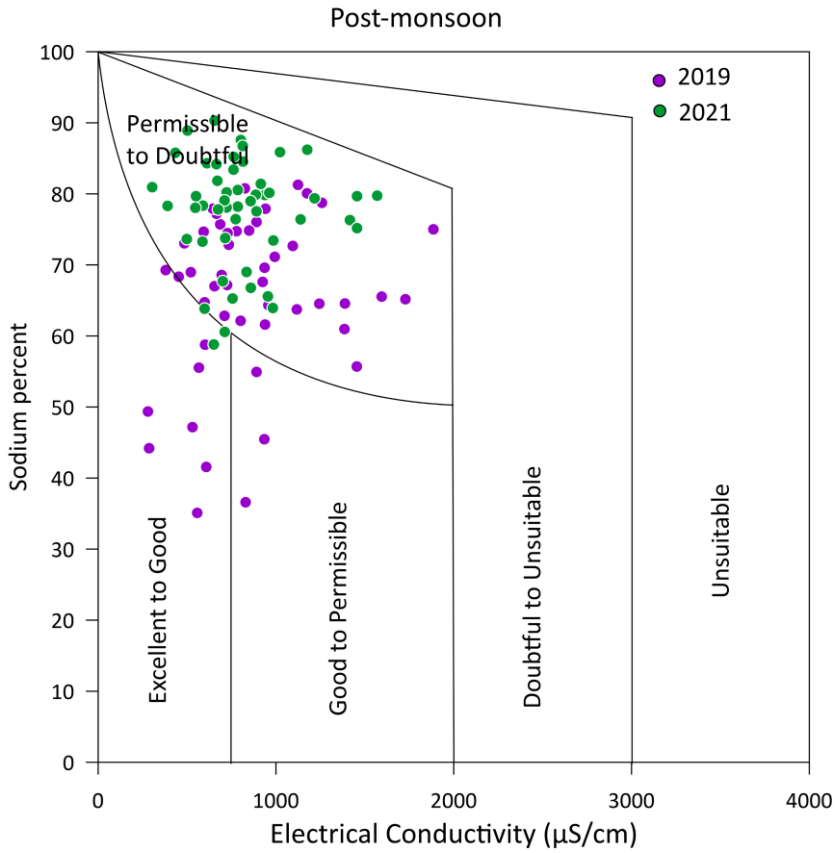

Fig. 6.5: Suitability of groundwater for irrigation based on EC and sodium percent for post-monsoon groundwater samples

6.3.3 Sodium Adsorption Ratio (SAR)

The sodium adsorption ratio (SAR) is a measure of the Na^+ content in a water sample in comparison to the concentrations of Ca^{2+} and Mg^{2+}. High quantities of Na^+ ions in water reduce soil permeability and can cause water infiltration problems. The SAR of water reflects its use for agricultural irrigation. The SAR was calculated for pre-monsoon and post-monsoon seasons for the years 2019 and 2021 which has been given by Richards (1954) and is tabulated in Table 6.9. The water class suitable for irrigation according to SAR values given by Todd (1980) is given in Table 6.10.

Table 6.9: SAR values of groundwater samples in pre-monsoon and post-monsoon (2019 and 2021)

Sample no.	SAR of groundwater samples in meq/L			
	Pre-monsoon 2019	Pre-monsoon 2021	Post-monsoon 2019	Post-monsoon 2021
A1	2.33	3.19	4.29	5.88
A2	2.38	4.85	5.80	4.29

A3	2.27	5.13	4.25	4.39
A4	2.43	4.34	3.75	3.96
A5	2.36	3.32	3.87	7.03
A6	2.18	4.15	8.16	10.10
A7	4.41	5.40	6.05	6.90
A8	1.87	2.93	6.40	8.03
A9	2.15	3.98	4.76	7.40
A10	1.66	3.89	1.30	2.90
A11	2.07	4.41	5.84	10.39
A12	1.46	4.48	1.93	4.59
A13	5.86	5.00	6.55	8.65
A14	2.65	8.22	6.66	8.60
A15	1.69	6.76	5.55	7.86
A16	1.68	8.97	4.55	7.12
A17	1.54	6.14	3.59	4.36
A18	2.05	11.33	4.24	6.20
A19	2.18	9.63	8.75	7.85
A20	2.06	6.91	3.30	4.14
A21	2.12	2.59	3.40	8.19
A22	1.19	1.92	1.07	5.34
A23	2.07	5.13	2.66	5.12
A24	1.71	4.34	2.52	5.45
A25	3.22	1.67	4.26	5.69
A26	2.57	8.91	4.71	7.15
A27	2.27	8.34	5.52	7.70
A28	1.85	7.87	4.41	6.15
A29	2.24	5.82	4.93	6.05
A30	2.29	5.78	6.98	7.26
A31	2.54	5.84	4.60	6.47
A32	2.41	9.27	4.83	6.52
A33	2.26	7.54	8.59	10.69
A34	2.44	9.85	5.29	6.38
A35	2.27	7.81	3.29	4.65
A36	1.77	7.48	4.70	4.78
A37	2.41	8.19	1.74	4.77
A38	2.61	12.39	6.56	7.57
A39	1.92	8.30	5.52	7.36
A40	2.38	9.20	8.19	9.92

A41	1.55	8.14	2.84	4.55
A42	2.91	7.71	6.14	8.37
A43	2.23	9.81	7.18	9.79
A44	2.83	11.39	5.04	5.75
A45	2.90	9.37	8.17	6.68
A46	2.35	8.04	7.45	8.50
A47	1.31	3.20	2.85	3.66
A48	1.76	6.14	4.35	3.79
A49	2.55	7.80	3.44	6.99
A50	3.26	13.29	2.44	6.23

Table 6.10: Classification of SAR values of groundwater samples in pre-monsoon and post-monsoon (2019 and 2021)

SAR	Water class	Percentage of groundwater samples			
		Pre-Monsoon (2019)	Pre-Monsoon (2021)	Post-Monsoon (2019)	Post-Monsoon (2021)
<10	Excellent	100	92	100	94
10-18	Good	-	8	-	6
18-26	Fair	-	-	-	-
>26	Poor	-	-	-	-

All groundwater samples in the pre-monsoon and post-monsoon seasons of 2019 fall under the excellent water class for irrigation. The excellent water type can be used for irrigation in almost all types of soil. The majority of the groundwater samples in pre-monsoon 2021 and post-monsoon 2021 fall under the excellent water class for irrigation. 8% and 6% of the total groundwater samples in the pre-monsoon and post-monsoon seasons of the year 2021 are classified under good water. This class of water can be used for irrigation in coarse-texture soils or in organic soils which have good permeability.

6.3.4 U.S. Salinity Diagram

The salinity hazard of groundwater has been classified according to United States Salinity Laboratory (USSL) diagram after Richards (1954). The USSL diagram was prepared for the pre-monsoon and post-monsoon seasons of 2019 and 2021 which is shown in Figs. 6.6 and 6.7. Electrical conductance and SAR were used in the USSL (1954) diagram where EC represents salinity along the x-axis and SAR represents sodium hazard

along the y-axis. Based on USSL Staff, 1954, the groundwater for irrigation can be divided into four salinity classes- C1, C2, C3 and C4 whereas the groundwater for irrigation can be divided into four sodicity classes with respect to SAR or sodium hazard- S1, S2, S3 and S4. The different classes in the salinity and sodicity division have been given in tabular form in Table 6.11. The USSL (1954) diagram was made for the groundwater in Kohima town and it has been classified into four categories which is given in Table 6.12.

Table 6.11: USSL classification for salinity and sodicity

Salinity classes	**Description/ Uses**
C1 (Low salinity)	This water is suitable for irrigating most crops in most soils.
C2 (Medium salinity)	This water can be used to irrigate crops that are moderately salt tolerant.
C3 (High salinity)	This water is not suitable for usage in soils with poor drainage.
C4 (Very high salinity)	This water is not suitable to use for irrigation under normal conditions.
Sodicity classes	**Description/ Uses**
S1 (Low sodium)	This water is suitable for irrigation on most soils.
S2 (Medium sodium)	This water is suitable for irrigation on coarse-textured soils.
S3 (High sodium)	This water causes harmful exchangeable sodium levels in most soil.
S4 (Very high sodium)	This water is generally unacceptable for irrigation.

Table 6.12: USSL classification of groundwater samples in pre-monsoon and post-monsoon (2019 and 2021)

USSL water class	Percentage (%) of groundwater samples			
	Pre-Monsoon (2019)	**Pre-Monsoon (2021)**	**Post-Monsoon (2019)**	**Post-Monsoon (2021)**
Very Good (C1S1)	2	6	-	-
Good (C2S1, C2S2)	74	60	46	44
Medium (C3S1)	24	4	30	12
Bad (C3S2)	-	30	24	44

The groundwater in pre-monsoon 2019 in the study area falls under C1S1, C2S1 and C3S1. Based on the classification of USSL diagram, the groundwater samples have 74% of good water, 24% of medium water and 2% of very good water fit for irrigation use. In the pre-monsoon 2021, the groundwater falls under C1S1, C2S1, C3S1, C2S2, and C3S2 where 60% of groundwater is good water, 30% of groundwater is bad water, 6% of groundwater is very good water and 4% of groundwater is medium water. The post-monsoon 2019 groundwater falls under C2S1, C3S1, C2S2, and C3S2 where 46% of groundwater is good water, 30% of groundwater is medium water and 24% of groundwater is bad water. The post-monsoon 2021 groundwater falls under C2S1, C3S1, C2S2, and C3S2 where 44% of groundwater is good water, 44% of groundwater is bad water and 12% of groundwater is medium water. From the USSL diagram, we find that the majority of the groundwater is good and can be used for irrigation on coarse grained soils and also in almost all soil types. It can be used to irrigate crops that are moderately salt tolerant.

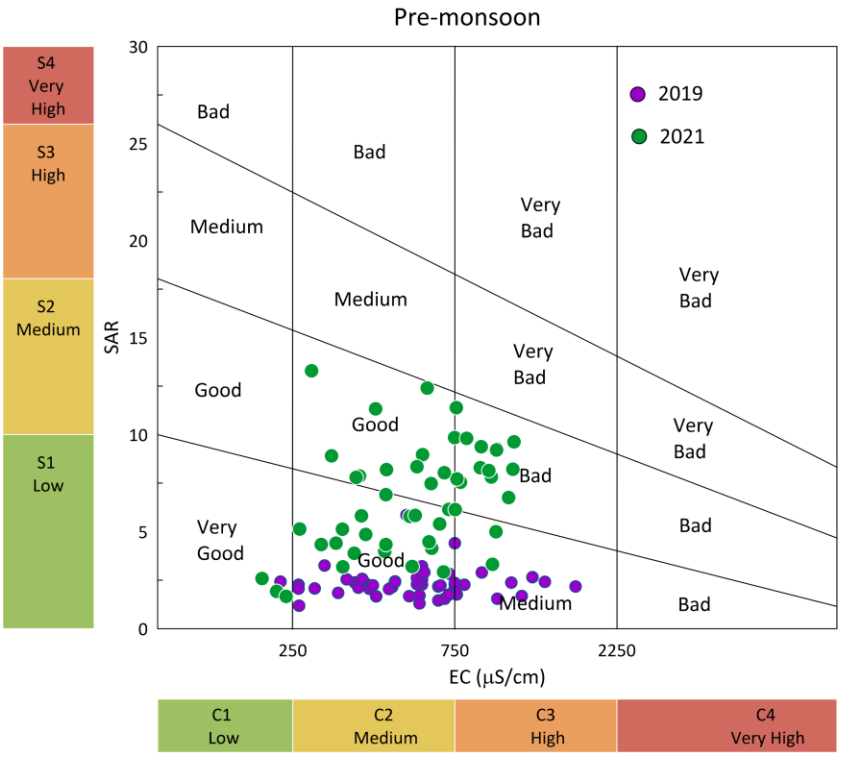

Fig. 6.6: USSL classification of groundwater for irrigation during pre-monsoon

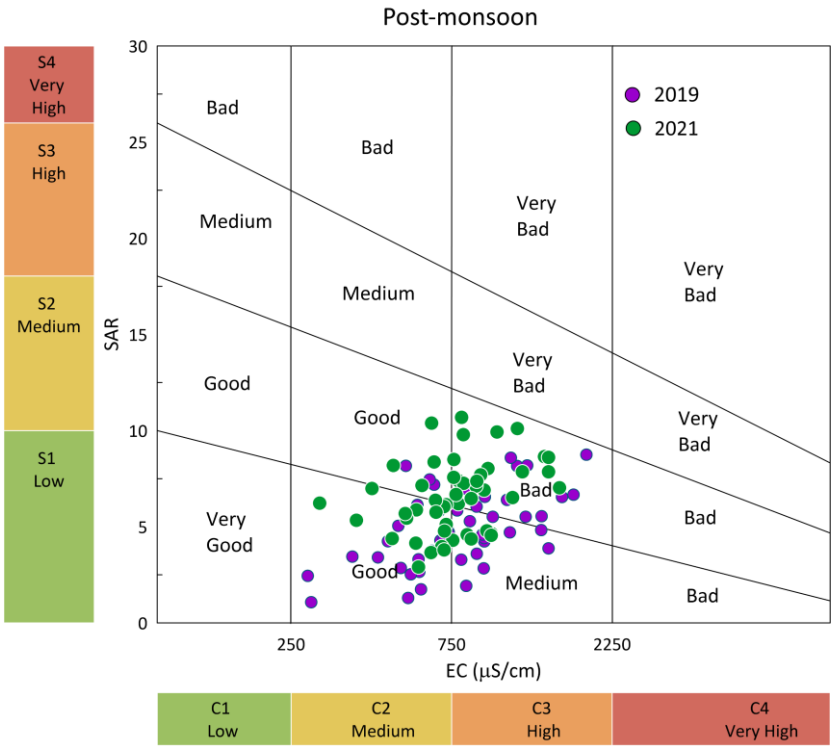

Fig. 6.7: USSL classification of groundwater for irrigation during post-monsoon

6.3.5 Permeability Index (PI)

The long-term use of irrigation water affects soil permeability, which is influenced by the Na^+, Ca^{2+}, Mg^{2+} and HCO_3^- concentrations of the soil. Doneen (1964) developed a criterion for determining the suitability of groundwater for irrigation based on the permeability index (PI), with concentrations measured in meq/L. The permeability index is classed as class I (>75%, suitable), class II (25-75%, good) and class III (<25%, unsuitable). Waters in classes I and II are considered good for irrigation. The PI values of the groundwater samples in the study area are given in Table 6.13 and the groundwater classification for irrigation as per the PI values are shown in Table 6.14.

Table 6.13: PI of groundwater samples in pre-monsoon and post-monsoon (2019 and 2021)

Sample no.	PI of groundwater samples in meq/L expressed as %			
	Pre-monsoon 2019	Pre-monsoon 2021	Post-monsoon 2019	Post-monsoon 2021
A1	73.18	80.77	84.63	102.03
A2	80.53	78.49	97.64	84.74
A3	74.51	86.20	96.20	94.01
A4	88.35	84.22	90.37	88.77
A5	71.85	70.16	71.09	88.98
A6	63.29	74.55	94.42	101.22
A7	101.70	90.26	94.31	97.76
A8	61.54	68.41	89.75	96.70
A9	73.48	80.08	79.35	96.70
A10	67.27	73.87	64.90	91.56
A11	72.43	82.43	89.03	97.80
A12	57.40	78.76	57.98	96.98
A13	84.81	73.44	77.21	88.17
A14	78.98	87.94	75.63	103.77
A15	60.09	84.68	79.76	105.86
A16	57.71	89.11	80.24	91.81
A17	59.22	78.66	71.20	87.14
A18	69.03	95.39	77.92	102.01
A19	56.79	88.12	85.70	88.65
A20	66.77	88.46	82.32	98.89
A21	81.90	85.37	94.49	115.10

A22	79.25	85.86	94.04	113.17
A23	75.40	86.89	76.79	108.97
A24	57.75	79.12	75.46	101.69
A25	89.12	85.19	88.81	123.99
A26	74.86	94.82	90.17	105.47
A27	69.79	93.41	86.21	101.80
A28	67.42	96.91	89.12	116.84
A29	69.63	88.36	96.51	106.78
A30	68.87	85.49	96.98	102.39
A31	81.86	85.83	85.03	92.05
A32	70.99	89.24	82.01	104.46
A33	71.63	91.12	97.84	105.56
A34	70.28	93.51	92.08	103.09
A35	66.13	88.12	82.80	96.75
A36	70.51	90.33	83.47	100.61
A37	64.93	91.17	61.59	101.87
A38	68.12	99.76	94.28	100.27
A39	58.39	87.08	79.30	96.11
A40	61.46	92.18	92.18	98.35
A41	50.01	87.64	62.91	95.54
A42	73.67	87.49	89.25	98.38
A43	64.80	92.32	91.73	97.19
A44	76.12	96.13	87.44	100.55
A45	74.16	91.32	97.12	92.80
A46	64.45	93.50	91.20	98.21
A47	49.54	73.98	67.80	79.52
A48	55.21	80.90	82.29	86.53
A49	80.11	90.78	88.12	98.93
A50	90.83	105.04	64.77	99.99

Table 6.14: PI classification of groundwater samples in pre-monsoon and post-monsoon (2019 and 2021)

PI water class	**Percentage (%) of groundwater samples**			
	Pre-Monsoon (2019)	**Pre-Monsoon (2021)**	**Post-Monsoon (2019)**	**Post-Monsoon (2021)**
Class I	26	88	84	100
Class II	74	12	16	-

The majority of groundwater samples in pre-monsoon 2019 fall into the Class II category with 74% while 26% of the groundwater samples fall into the Class I category of Doneen's chart (Table 6.14). In the pre-monsoon 2021, the majority of groundwater falls under Class I category with 88% while 12% of the groundwater samples fall under Class II category. In post-monsoon 2019, the majority of groundwater falls under the Class I category with 84% and 16% falling into Class II category while in the post-monsoon of 2021 all groundwater samples fall under the Class I category. According to Doneens, we find that the groundwater is suitable for irrigation as per the permeability index values.

CHAPTER 7

SUMMARY AND CONCLUSIONS

The study area Kohima town lies in between the Latitudes 25˚37′30″ N to 25˚42′32″ N and Longitudes 94˚04′40″ E to 94˚07′34″ E and falls in the survey of India Toposheet No. 83 K/2. It covers a total area of 915.43 hectares out of which 99.4% is covered by built-up areas based on the LULC map. Kohima town lies in the Kohima Synclinorium of the Inner Fold belt and is occupied by Tertiary sedimentary rocks ranging in age from Upper Cretaceous to Recent which trends along the linear NNW-SSE ridge.

The older Disang Group of rocks ranges in age from Upper Cretaceous to Middle Eocene and consists of well-bedded, dark grey, thick, monotonous sequences of shale intercalated with fine-grained, flaggy sandstone and siltstone. There is a transitional sequence between the older Disang and the younger Barail Group called the Disang-Barail Transitional sequence (DBTS) belonging to the Upper Eocene age. The rocks of the DBTS consist of mixed lithology of silt, shale, and very fine to fine-medium sand fractions. To the south of Kohima town lies the younger Barail Group of rocks of Oligocene age. These are an arenaceous suite of rocks that conformably overlies the DBTS and Disang Group and consists of thick sequences of sandstones intercalated with thin shales. The rocks in and around the township are affected by a series of faults, thrusts, fractures and multiple joint sets. The shales with intercalations of sandstone/siltstone are crushed and weathered, which makes it easy for the local streams to vigorously erode the base and toes of their channels and groundwater flow in these areas.

Geomorphologically, the terrain in the study area consists of moderate and highly dissected hills and valleys. The area has a relatively rugged landscape with sub-rounded hills, narrow valleys and deep gorges. The southern hill ranges, which are covered with evergreen forests, are quite rugged and cultivation is done on the lower slopes of the hills.

Hydrogeologically, the study area comes under semi-consolidated formations. The dominant Disang Group of rocks in the study area is highly fractured, splintery and sheared, and is found to be the most potential formation for groundwater development in the hilly area. The occurrences and movement of groundwater in any area are governed by several factors like topography, lithology, geological structures, porosity, slope, drainage pattern, land use/land cover, climate conditions, depth of weathering, extent of fractures, and interrelation between these factors.

Kohima town has witnessed an increase in urbanization in recent years and with the growing population in search of improved social and economic development, there is a high demand of fresh water for domestic and agricultural usage. The main sources of drinking water supply in Kohima town come from the reservoirs of Zarü River and the streams from the slopes of Pulie Badze but they do not meet the needs of the population and many end up buying water from private individuals at a high cost, especially during the dry seasons. Groundwater usage has increased over the years in Kohima. At present, there are no major industries in and around the study area, but human activities like garbage and domestic waste water are directly disposed of in and around the town without being treated. It has thus become important to check the groundwater quality, especially for drinking purposes.

No extensive published research work on groundwater has been done in Kohima, so the present research is one of the first in-depth studies on groundwater quality to be conducted in the study area. The main purpose of the research study is to investigate groundwater quality based on geological, geochemical and geophysical data and present it in the form of a Ph.D. thesis comprising seven chapters.

The **first** chapter presents the general information on the study area including location and accessibility, habitation, climate and rainfall, land use land cover, soil, geomorphology, drainage, vegetation, agriculture and irrigation, groundwater resources and groundwater importance, literature review, previous works on the study area and aim & scope of the work.

The **second** chapter includes the regional geology; major structures and stratigraphy of Nagaland; geology, tectonic setting, hydrogeology and hydrological data of the study area. Various lithological units of the study area were identified. The rock types in Kohima town consist of shales, sandstone, and siltstone with the Disang shales being the major rock type. The depth to water level measurements and water level fluctuations were investigated in Kohima town.

The **third** chapter describes the various field and laboratory studies that were done. Field studies include the hydrological and subsurface studies and collection of groundwater samples during pre-monsoon and post-monsoon periods. Laboratory work includes the estimation of various physical and chemical parameters by using various instruments as per the standard procedures and then processing the data by using different methods and software.

The **fourth** chapter deals with the study of subsurface geology in the study area using the geoelectrical VES resistivity method. Five VES stations were chosen and data were interpreted using IPI2Win software. A maximum of four subsurface layers with topsoil, fractured shale, weathered shale and sandstone layers were identified in the VES stations.

The **fifth** chapter includes the study of the hydro-geochemistry of groundwater in the study area. Fifty groundwater samples were analyzed to examine the physico-chemical characters, which include pH, TDS, EC, Turbidity, TH, TA, major cations (Ca^{2+}, Mg^{2+}, K^{+}, Na^{+}), anions (HCO_3^{-}, SO_4^{2-}, NO_3^{-}, Cl^{-}, F^{-}), Fe and trace elements like Cd, Cu and As. The physico-chemical parameters were also geospatially plotted. The data was then processed and studied using Piper's trilinear diagram to know the type of water. The major ion chemistry was studied to understand the factors affecting the hydrochemistry of groundwater and statistical analysis using Pearson's correlation coefficient was analyzed to find the relationship between different parameters.

The **sixth** chapter focuses on the quality of water for various uses. The assessment of the groundwater quality for drinking purposes was done using the Weighted Arithmetic Water Quality Index method and the assessment for irrigation purposes was done using the %Na, Wilcox diagram, sodium adsorption ratio, U.S. salinity diagram and permeability index methods.

The **seventh** chapter summarises the whole work done in the study area based on the studies conducted and so the conclusions have been generated.

The salient features of the research work are as follows:

- Hydrogeologically, Kohima town consists of semi-consolidated formations which are mostly argillaceous, highly fractured, weathered and sheared through which groundwater flows. The main rock types consist of shales, sandstone and siltstone.
- The DTWL maps show that the deepest groundwater level in the study area is found in the western part and the very shallow groundwater level is found towards the southwestern area.
- In the year 2019, there is a decrease in groundwater level in post-monsoon as compared to the pre-monsoon season in small pockets mostly around the

central part of the study area indicating that there has been an increase in groundwater extraction over groundwater recharge in these areas.

- In the year 2021, there is a rise in groundwater level in post-monsoon as compared to the pre-monsoon season.
- The depth to water level of groundwater decreased in major parts of the study area in the year 2021 compared to the year 2019 which is due to less annual rainfall.
- The water table and topographic elevation maps reveal that the groundwater level follows the topographic elevation of the study area.
- QH, KQ, KH, HK, and Q type curves have been derived from the VES data and the subsurface layers- topsoil, fractured shale, weathered shale and sandstone layers have been established from the curves. The best layer which acts as a good aquifer is the weathered shale layer.
- Kohima town is located at a high altitude but groundwater can be found in shallow aquifers at less than 50 m which may be due to the fractured and weathered rocks in the study area where groundwater flows.
- The sequence of the ionic dominance pattern in the study area is: $Na^+ > Ca^{2+} > K^+ > Mg^{2+}$ for cations and $HCO_3^- > Cl^- > SO_4^{2-} > NO_3^- > F^-$ for anions.
- The hydrochemistry based on pH value reveals that the groundwater in the study area is predominantly alkaline in nature.
- The high TDS values are mostly found in the Disang Group of rocks which are abundant in shale rocks. The geology of shale rocks affects the concentration of TDS because they weather more readily.
- The high EC values in the study area denote that there is a high concentration of soluble salts in groundwater and anthropogenic influences like seepage of domestic and municipal sewage are present.
- The quality of groundwater in Kohima town is predominantly hard and fresh water in character based on TDS and TH.
- High K^+, Na^+ and HCO_3^- were found in the groundwater samples exceeding the permissible limit which is found to be due to rock weathering (silicate weathering) or the ion exchange process.

- High Fe concentration of up to 5.33 mg/L was found in pre-monsoon (2021) which is due to the geological formation of the area composed mostly of weathered ferruginous shales.
- Cd was found to be exceeding the permissible limit in four locations during the year 2021 indicating that pollution of groundwater has taken place in these locations by anthropogenic activities.
- The Piper's diagram directly reflects the hydrogeochemical characteristics and water types showing that the groundwater aquifers are dominated by alkali elements ($Na^+ + K^+$), strong acids ($Cl^- + SO_4^{2-}$) and Na-Cl is the dominant water type in the study area.
- Gibb's diagram indicates that the hydrochemical composition is governed by water-rock interactions and rock weathering is the main source of chemical components in the groundwater of Kohima town.
- Cl^- versus Na^+ plot shows that Na^+ concentration is more than Cl^- concentration which is due to silicate weathering.
- The plots of TC versus HCO_3^- revealed that there was an anthropogenic influence on ionic concentrations in groundwater.
- The plots of TC versus Na^+ and ($Na^+ + K^+$) versus TC revealed that cation concentrations are from silicate weathering of rocks which were largely from the major shale rocks in the research area since these rocks play an important role in global silicate weathering processes.
- The scatter plots of NO_3^-/Na^+ ratios and Cl^-/Na^+ ratios indicate the presence of NO_3^- contamination and the groundwater in the study area was found to have a maximum of 65 mg/L NO_3^- concentration.
- High NO_3^- was found to be more in post-monsoon seasons which may be due to municipal sewage and some agricultural activities.
- Pearson's correlation analysis revealed that EC, TDS, TH, HCO_3^- and Na^+ are identified to be important physico-chemical parameters for drinking water quality because they correlate with the majority of the groundwater parameters.
- The WQI reveals that the groundwater in the southern part of Kohima town is primarily safe and suitable for drinking purposes. In contrast, the northern part of the town is mostly very poor and unsuitable for drinking.

- The groundwater quality for drinking purposes was found to be better in 2021 as compared with the WQI of 2019.
- The majority of the groundwater samples are suitable for irrigation purposes based on Wilcox diagram, SAR, USSD and PI.
- The groundwater quality in 2019 is found to be considerably better for irrigation purposes as compared to 2021.
- Human activities such as the disposal of municipal wastes in open sewage systems without being treated pose a serious concern for groundwater and the environment.
- The nature and composition of rocks is another major factor that governs the chemical composition and quality of groundwater in Kohima town.
- Overall study reveals that the groundwater is suitable for drinking purposes in the southern part of Kohima town and the northern part of the town is mostly very poor and unsuitable for drinking due to anthropogenic and geogenic components.

RECOMMENDATIONS

Based on the results and discussion of the various physicochemical characteristics examined for the groundwater samples in Kohima town, the following recommendations are made to minimise further degradation and conserve groundwater for the benefit of future generations.

- Proper monitoring system for assessing the groundwater quality for drinking at particular intervals is needed.
- Proper town planning should be done to preserve the catchment areas from urbanization for surface and groundwater recharge.
- The springs with high discharge should be maintained and protected. Springshed management will significantly help in mitigating the people's water requirements.
- Kohima town receives a good amount of annual rainfall, so surface basins and rainwater harvesting are suitable to conserve, recharge and meet the demands of water.
- Wells with high Fe content should be treated before being used for drinking purposes. An innovation from IIT Guwahati has made a traditional method for household use to remove iron below 0.3 ppm without increasing the pH above the acceptable limit by using the ash of banana pseudostem.
- Heavy metals such as Cd and Fe can also be removed by filtration through hydrogel-based devices and the use of ultra-filtration membranes (Fig. 7).

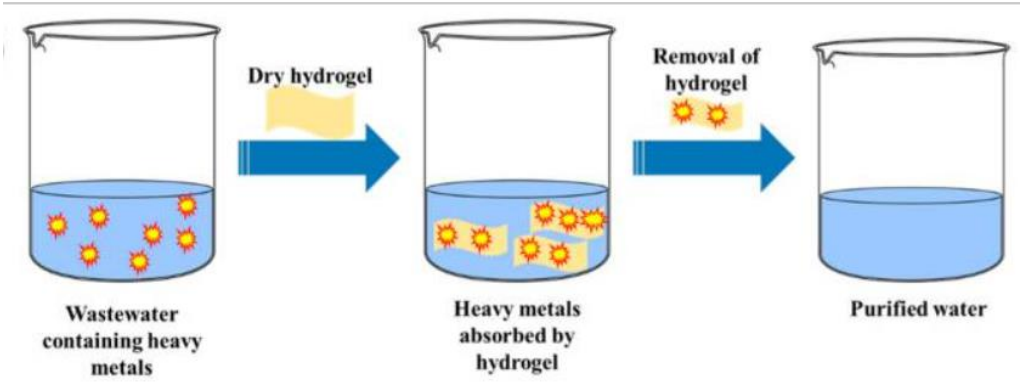

Fig. 7: Schematic diagram for removal of heavy metals from wastewater by using hydrogel-based adsorbent material (Source: Darban et al., 2022)

- The local government must empower the population with the means to purify the available water before using it to meet their daily needs.
- Further studies involving isotopic studies should be carried out to enhance and prove the origin of high sodium, potassium and iron in Kohima town.
- Maintaining a proper drainage and sewage system along with proper disposal of wastes is the need of the hour to protect the groundwater from being polluted.

****

BIBLIOGRAPHY

Abbasi, S.A. (2002). Water Quality Indices. State of the Art Report, National Institute of Hydrology, Scientific Contribution No. INCOH/SAR-25/2002, Roorkee. INCOH, 73 p.

Acharyya, S.K. (1986). Tectonostratigraphic history of Naga hills ophiolite. Memoir Geological Survey of India, v. 119, pp. 94-103.

Adimalla, N., Dhakate, R., Kasarla, A., and Taloor, A.K. (2020). Appraisal of groundwater quality for drinking and irrigation purposes in Central Telangana, India. Groundwater for Sustainable Development, v. 10, 100334 p.

Adimalla, N., Manne, R., Zhang, Y., Xu, P., and Qian, H. (2022). Evaluation of groundwater quality and its suitability for drinking purposes in semi-arid region of Southern India:An application of GIS.Geocarto International, v. 37, pp. 1-13. doi: 10.1080/10106049.2022.2040603.

Agarwal, O.P. and Ghose, N.C. (1986). Geology and stratigraphy of Naga Ophiolite between Meluri and Awankho, Phek District, Nagaland, India. In: Ophiolites and Indian Plate Margins, (Eds. N.C. Ghose and S. Vardharajan), pp. 163-195.

Aier, I., Thong, G.T., and Supongtemjen. (2011). Geological evaluation of surface instability along NH 39 (180 km), west of Raj Bhavan, Kohima, Nagaland. In: Singh T.N. and Sharma Y.C. (Eds), Slope stability - Natural and Man-Made Slope. Vayu Education of India, New Delhi, pp. 192–201.

Amiotte, S.P., Probst, J.L., and Ludwig, W. (2003). Worldwide distribution of continental rock lithology: Implications for the atmospheric/soil CO_2 uptake by continental weathering and alkalinity river transport to the oceans. Global Biogeochemical Cycles, v. 17(2), 1038 p. doi:10.1029/2002GB001891.

APHA (1998). Standard Methods for the Examination of Water and Wastewater. 20th Edition, American Public Health Association, American Water Works Association and Water Environmental Federation, Washington DC.

Balan, I.N., Shivakumar, M., and Kumar, P.D.M. (2012). An assessment of groundwater quality using water quality index in Chennai, Tamil Nadu, India. Chronicles of Young Scientists, v. 3(2), pp. 146-150.

Bambry, G.C and Sharda, Y.P, (1997). Progress report on preparation of geotechnical map of Kohima township, Nagaland. Geological Survey of India unpublished reports.

Barker, R. (1980). Application of Geophysics in Ground Water Investigations. Water Services, v. 84, pp. 489-492.

Barseem, M., Lateef, T., and Deen, H. (2015). Geoelectrical contribution for solving water logging in selected sites, kilometer 35, Cairo-Ismailia Desert Rode, Egypt. Egyptian Geophysical Society EGS Journal, v. 13(1), pp. 67-82.

Bhutiani, R., Faheem, A., Varun, T., & Khushi, R. (2018). Evaluation of water quality of River Malin using water quality index (WQI) at Najibabad, Bijnor (UP) India. Environment Conservation Journal, v. 19 (1&2), pp. 191-201.

BIS (2012). Guidelines for Drinking Water (10500). Bureau of India Standards, New Delhi.

Bora, M., and Goswami, D.C. (2017). Water quality assessment in terms of water quality index (WQI): Case study of the Kolong River, Assam, India. Applied Water Science, v. **7**, pp. 3125–3135. https://doi.org/10.1007/s13201-016-0451-y.

Brown, R.M., McClelland, N.I., Deininger, R.A., and O'Connor, M.F. (1972). A water quality index—crashing the physiological barrier. Indicators of Environmental Quality, v. 1, pp. 173-182.

Brindha, K., Neena Vaman, K.V., and Srinivasan, K. (2014). Identification of surface water-groundwater interaction by hydrogeochemical indicators and assessing its suitability for drinking and irrigational purposes in Chennai, Southern India. Applied Water Science, v. 4, pp. 159–174. https://doi.org/10.1007/s13201-013-0138-6.

Brunnschweiler, R.O. (1966). On the geology of Indo-Burman ranges. Journal of the Geological Society of Australia, v. 13, pp. 137-195.

Clark, J., and Page, R. (2011). Inexpensive Geophysical Instruments Supporting Groundwater Exploration in Developing Nations. Journal of Water Resource and Protection, v. 3(10), pp. 768-780. doi: 10.4236/jwarp.2011.310087.

CGWB (2013). Groundwater pollution by industrial clusters. Bhu-Jal News, v. 28(1-4), pp. 1-12.

CGWB, NER, Guwahati (2013). Groundwater information booklet Kohima district, Nagaland (Technical report: D).

CGWB (2020). National Compilation on Dynamic Ground Water Resources of India.

Chakraborty, B., Bera, B., and Adhikary, P.P. (2021). Positive effects of COVID-19 lockdown on river water quality: evidence from River Damodar, Indian Science Reports, v. 11, 20140 p. https://doi.org/10.1038/s41598-021-99689-9.

Chaurasia, A.K., Pandey, H.K., Tiwari, S.K., Prakash, R., Pandey, P. and Ram, A. (2018), Groundwater quality assessment using Water Quality Index (WQI) in parts of Varanasi district, Uttar Pradesh, India. Journal of the Geological Society of India, v. 92(1), pp. 76-82.

Cude, C. (2001). Oregon water quality index: A tool for evaluating water quality management effectiveness. Journal of the American Water Resources Association, v. 37, pp. 125-137.

Cushing, E.M., Kantrowitz, I.H., and Taylor, K.R. (1973). Water resources of the Delmarva Peninsular. U S Geological Survey Professional Paper 822, Washington DC.

Darban, Z., Shahabuddin, S., Gaur, R., Ahmad, I., and Sridewi, N. (2022). Hydrogel-Based Adsorbent Material for the Effective Removal of Heavy Metals from Wastewater: A Comprehensive Review. Gels, v. 8(5), 263 p. doi: 10.3390/gels8050263.

Darcy, H. (1856). Les fontaines publiques de la ville de Dijon: exposition et application des principes à suivre et des formules à employer dans les questions de distribution d'eau. Victor dalmont, v. 1.

Das, A. (2020). Hydrogeochemical assessment of shallow aquifer in Chakdah, West Bengal for safe water supply. Water Science, v. 34 (1), pp. 98-109.

Das, S., Gupta, A., and Ghosh, S. (2017). Exploring Groundwater potential zones using MIF technique in semiarid region: A case study of Hingoli district, Maharashtra. Spatial Information Research, v. 25(6), pp. 749-756.

Dash, S.K, and Sahoo, H.K. (1999). Quality assessment of groundwater in a part of Sundergarh district. Indian Journal of Environmental Protection, v. 19(4), pp. 273-278.

Datta, S., Kushwaha, A., and Gogoi, K.R.U. (2018). Weighted Arithmetic Water Quality Index Method for Ground Water Quality Determination in and around Guwahati, Assam, India: A Case Study.

Deshmukh, D.S., Prasad, K.N., Niyogi, B.N., Biswas, A.B., Guha, S.K., Seth, N.N., and Goswami, A.B. (1973). Geology and groundwater resources of alluvial areas of West Bengal. Bulletin of the Geological Survey of India, Series B, no. 34.

Devdas, V., and Gandhi, P. (1986). Systematic geological mapping in Maromi-Akaluto-Suruhuto areas Zunheboto district, Nagaland. Geological Survey of India, Unpublished Progress Report.

Directorate of Geology and Mining, Nagaland (1978). Himalayan Orogenesis.

Directorate of Geology and Mining, Nagaland (1978). Misc. Pub., no. 1.

Directorate of Geology and Mining, Nagaland (1996). Feasibility studies for groundwater development in the hilly terrain in and around Kohima town, Nagaland. Techincal Report.

Dobrin, M.B., and Savit, C.H. (1988). Introduction to geophysical prospecting, 4th ed.: McGraw-Hill, Inc., New York, 867 p.

Domenico, P.A. and Schwartz, F.W. (1990). Physical and Chemical Hydrogeology. John Wiley and Sons, New York, 824 p.

Doneen, L.D. (1954). Salinisation of soil by salts in the irrigate water. Transactions of the American Geophysical Union, v. 35(6), pp. 43-47.

Doneen, L.D. (1964). Water Quality for Agriculture. Department of Irrigation, University of California, Davis. 48 p.

Evans, P. (1932). Explanatory notes to accompany a table showing the Tertiary succession in Assam. Trans. Mining and Geological Inst. of India, v. 37, pp.155–260.

Evans, P. (1964). The tectonic framework of Assam, Journal of the Geological Society of India, v. 5, pp. 80-96.

Ezung, M., Walling, T. and Chelladurai. C. (2021). Vertical electrical sounding method to decipher the existing subsurface stratification and assess the cause leading to land instability: A case study. International Journal of Emerging Technologies and Innovative Research, v. 8(5), pp. f887-f893.

Ezung, M., Walling, T., and Chelladurai, C. (2022). Application of Vertical Electrical Sounding for Subsurface Characterization to Determine Slope Instability at Perizie, Nagaland. Current World Environment, v. 17(3). doi:http://dx.doi.org/10.12944/CWE.17.3.14.

Freeze, R. A., and J. A. Cherry. (1979). Groundwater. Englewood, New Jersey: Prentice-Hall Inc.

Frohlich, R.K. and Urish, D. (2002). The use of geoelectrics and test wells for the assessment of groundwater quality of a coastal industrial site. Journal of Applied Geophysics, v. 50, pp. 261-278.

Gaillardet, J., Dupre, B., Louvat, P., & Allegre, C.J. (1999). Global silicate weathering and CO2 consumption rates deduced from the chemistry of large rivers. Chemical Geology, v. 159, pp. 3-30.

Gastmans, D., Chang, H. K., and Hutcheon, I. (2010). Groundwater geochemical evolution in the northern portion of the Guarani aquifer system (Brazil) and its relationship to diagenetic features. Applied Geochemistry, v. 25(1), pp. 16-33.

Gaur, M.P., and Chakradhar, M. (1985). Systematic geological mapping around Jaluke, Kohima district, Nagaland. Geological Survey of India, Unpublished Progress report for Field Session, 1984-85.

Geological Society of India (2015). Seismic and landslide hazard assessment of Kohima city, Nagaland. Item no: SEI/NER/RHQ/2013/034

Gibbs, R.J. (1970). Mechanisms controlling world water chemistry. Science, v. 170, pp. 1088-1090.

Gish, O.H. and Rooney, W.J. (1925). Measurement of resistivity of large masses of undisturbed earth. Terrestrial Magnetism Atmospheric Electricity, v. xxx(4).

Gupta, A.B.D., and Biswas, A.K. (2000). Geology of Assam. Geological Society of India, Bangalore, 169 p.

Handa, B. K (1975). Geochemistry and genesis of fluoride containing groundwater in India. Ground Water, v. 13, pp. 275-281.

Hao, Q., Xiao, Y., Chen, K., Zhu, Y., & Li, J. (2020). Comprehensive Understanding of Groundwater Geochemistry and Suitability for Sustainable Drinking Purposes in Confined Aquifers of the Wuyi Region, Central North China Plain. Water, v. 12, 3052 p.

Harinarayana, T., and Naganjaneyulu, K. (2003). Regional Surface Electrical Conductance Map of India. Journal Geological Society of India, v. 61, pp. 724-728.

Hayden, H.H. (1910). Northeast Assam Coal Fields. Rec. Geological Survey of India, v. 30, pp 283-319.

Hem, J.D. (1970). Study and interpretation of the chemical characteristics of natural water (2nd Ed.) U.S. Geological Survey Water Supply Paper, 1473, U.S. Department of the Interior, Washington D.C., 363 p.

Hem, J. D. (1985). Study and interpretation of the chemical characteristics of natural water. Department of the Interior, US Geological Survey, v. 2254.

Hem, J.D. (1991). Study and Interpretation of Chemical Characteristics of Natural Water. Geological Survey Water Supply Paper, 1973, U.S. Government Printing Office, Washing DC, 363 p.

Hussain, I., Raschid, L., Hanjra, M.A., Marikar, F., and Hoek V.D.W. (2002). Wastewater use in agriculture: Review of impacts and methodological issues in valuing impacts. Colombo, Sri Lanka: International water management institute.

Jabal, M.S.A., Abustan, I., Rozaimy, M.R. and El Najar, H. (2014). Groundwater beneath the urban area of Khan Younis City, southern Gaza Strip (Palestine): Hydrochemistry and water quality. Arabian Journal of Geosciences, pp. 1-13.

Kalinski, R.J.W.E., Kelly, I., Bogardi and Pesti, G. (1993). Electrical resistivity measurements to estimate travel times through unsaturated ground water protective layers. Journal of Applied Geophysics, v. 30, pp. 161-173.

Karanth, K.R. (1987). Groundwater assessment development and management. Tata McGraw-Hill Publishing Company Limited, New Delhi.

Karanth, K.R. (1989). Quality of ground water assessment development and management. Tata McGraw-Hill, New Delhi, pp. 217-275.

Karuppannan, S. (2015). Delineation of Groundwater Potential Zone by Using Geo-Physical Electrical Resistivity Inverse Slope Method in the Kadayampatty Panchayat Union, Salem District, Tamil Nadu. International Journal of Recent Scientific Research, v. 6, pp. 5013-5017.

Katiwaba and Jami, M. (2009-2010). Appraisal of groundwater development and inventory of ground water structures in and around Kohima town. Directorate of Geology and Mining Report.

Keditsu, V., Rao, B.V., and Vero, A. (2022). Assessment of groundwater quality in and around Chiephobozou town, Kohima district, Nagaland. Journal of Applied Geochemistry, v. 24(3), pp. 165-173.

Keller, G.V., and Frischknecht, F.C., (1966). Electrical Methods in Geophysical Prospecting. Pergamon Press, 517 p.

Khan, R.A., Ferell, R.E. and Billings, G.K. (1972). Geochemical hydrology of the Baton Rouge aquifers, Louisiana. Water Resources Research Institute, Bull. B, pp.1-63.

Khan, R. and Jhariya, D.C. (2018). Hydrogeochemistry and Groundwater Quality Assessment for Drinking and Irrigation Purpose of Raipur City, Chhattisgarh. Journal of the Geological Society of India, v. 91(4), pp. 475-482. doi: 10.1007/s12594-018-0881-2.

Kikon, E. and Ao, K. (2006). Groundwater development in hilly terrain: Case studies in and around Kohima, Nagaland. Proceedings of the 12th National Symposium on

Hydrology "Groundwater Governance - Ownership of Groundwater and Its Pricing".

Kim, K. (2003). Long-term disturbance of groundwater chemistry following well installation. Ground Water, v. 41, pp. 780–789.

Kirk, M.F., Holm, T.R., Park. J., Jin, Q., Sanford, R.A., Fouke, B.W., and Bethke, C.M. (2004). Bacterial sulfate reduction limits natural arsenic contamination in groundwater. The Journal of Geology v. 32(11), pp. 953–956.

Kohima city population census (2011). Nagaland 2011 census of India.

Kshetrimayum, K. S., and Hegeu, H. (2016). The state of toxicity and cause of elevated Iron and Manganese concentrations in surface water and groundwater around Naga Thrust of Assam-Arakan basin, Northeastern India. Environmental Earth Sciences, v. 75, pp. 1-14.

Krishna, A.K. and Govil, P.K. (2004). Heavy metal contamination of soil around Pal Industrial area, Rajasthan, India. Journal of Environmental Geology, v. 47. pp. 38-44.

Krishnan, M.S. (1982). Geology of India and Burma, CBS Publishers, New Delhi, 635 p.

Kumar, R. and Naik, G.C. (2006). Late Eocene to early Oligocene depositional system in Assam Shelf, 6th International Conference & Exposition on Petroleum Geophysics, Kolkata, pp. 904-910.

Kumar, S.K., Logeshkumaran, A., Magesh, N.S., Godson, P.S, and Chandrasekar, N. (2015). Hydro-geochemistry and application of Water Quality Index (WQI) for groundwater Quality Assessment, Anna Nagar, part of Chennai City. Tamil Nadu, India. Applied Water Science, v. 5, pp. 335-343.

Kumar, P.J.S. (2022). GIS-based mapping of water-level fluctuations (WLF) and its impact on groundwater in an Agrarian District in Tamil Nadu, India. Environment, Development and Sustainability, vol. 24(1), pp. 994–1009. https://doi.org/10.1007/s10668-021-01479-w.

Laar, C., Akiti, T.T., Brimah, A.K., Fianko, J.R., Osae, S., and Osei, J. (2011). Hydrochemistry and isotopic composition of the Sakumo Ramsar site. Research Journal of Environmental and Earth Sciences, v. 3(2), pp. 146-152.

Li, P., Zhang, Y., Yang, N., Jing, L., and Yu, P. (2016). Major ion chemistry and quality assessment of groundwater in and around a mountainous tourist town of China. Expo Health, v. 8(2), pp. 239–252

Loke, M.H., and Barker, R.D. (1996). Practical techniques for 3D resistivity surveys and data inversion. Data inversion. Geophysical Prospecting, v. 44, pp. 499-523.

Mallet, F.R. (1876). On the coal fields of Naga Hills bordering Lakhimpur and Sibsagar district, Assam. Geological Survey of India, Memoir, v. 12(II).

Mathur, L.P. and Evans, P. (1964). Oil in India, 22nd session, International Geological Congress, New Delhi, India. 85 p.

Matias, M.J.S. (2002). Square array anisotropy measurements and resistivity sounding interpretation. Journal of Applied Geophysics, v. 49, pp. 186–194.

Matthess, G. (1982). The properties of groundwater. Wiley, New York. 397 p.

Mazor, E., Bielsky, M., Verhagen, B.Th., Sellschop, J.P.F., Hutton, L., and Jones, M.T. (1980). Chemical composition of groundwaters in the vast Kalahari flatland. Journal of Hydrology, v. 48(1-2), pp 147-165. https://doi.org/10.1016/0022-1694(80)90072-4.

Mekro, V. (2014). Rocks of Nagaland. Mittal Publications, 53 p.

Mekro, V. (2016). Brine and other Mineral Spring from Kohima (Nagaland) and Senapati (Manipur) districts. Recent trends in Earth Science Research with special reference to NE India, pp. 291-314.

Minnesota Pollution Control Agency (1999). Cadmium, Lead and Mercury in Minnesota's Ground Water. Environmental Outcomes Division. Ground Water Monitoring & Assessment Program.

Mondal, N.C., Singh, V.P., Singh, V.S., and Saxena, V.K. (2010). Determining the interaction between groundwater and saline water through groundwater major ions chemistry. Journal of Hydrology, v. 388(1-1), pp. 100-111. 10.1016/j.jhydrol.2010.04.032.

Mostafa, M.G., Uddin, S.M.H., and Haque, A.B.M.H. (2017). Assessment of Hydrogeochemistry and groundwater quality of Rajshahi City in Bangladesh. Applied Water Science, v. 7(8), pp. 4663-4671. https ://doi.org/10.1007/s1320 1-017-0629-y.

NABARD (2006). Annual Report, 2005-2006. Mumbai. www.nabard.org, 2006.

Nandy, D. R. (2017). Geodynamics of Northeastern India and the adjoining region. Revised Edition, 271 p.

Neuman, S.P. (1977). Theoretical derivation of Darcy's law. Acta Mechanica, v. 25, pp. 153–170. https://doi.org/10.1007/BF01376989.

Nganje, T.N., Hursthouse, A.S., Edet, A., Stirling, D., and Adamu, C.I. (2017). Hydrochemistry of surface water and groundwater in the shale bedrock, Cross River Basin and Niger Delta Region, Nigeria. Applied Water Science, v. **7**, pp. 961–985. https://doi.org/10.1007/s13201-015-0308-9.

Orellana, E., and Mooney, H.M. (1966). Water table and curves for vertical electrical sounding over layered structures. Interetencia: Madrid, Spain.

Pacaol, N.F. (2021). Improvement of water quality amidst COVID-19 pandemic: a paradoxical picture. Journal of Public Health, v. 43(2), pp. e383-e384. doi: 10.1093/pubmed/fdab094.

Palacky, G.J. (1987). Resistivity Characteristics of Geological Targets. In: M.N. Nabighian, (Ed.), Electromagnetic Methods in Applied Geophysics Theory: Tulsa, OK. Society of Exploration Geophysicists, v. 1, pp. 53-122.

Pandey, N. and Srivastava, S.K. (1998). A preliminary report on Disang-Barail Transition, NW of Kohima, Nagaland (Abst.). Workshop on Geodynamics and Natural Resources of NE India, Dibrugarh, 24 p.

Pandey, N (2005). Geology of Nagaland. Nagaland University Souvenir, pp. 17-22.

Pandey, N. (2005). Geology of Nagaland. In: Geology and Energy Resources of North-East India. Progress and Perspectives & AGM of the Geological Society of India, pp.17–21.

Park, K. (2015). Textbook of Preventive and Social Medicine. 23rd Edition. Bhanot Publishers, India, pp.705-731.

Pazand, K., Ardeshir, H., Yousef, G., and Nasrin, A. (2012), Groundwater geochemistry in the Meshkinshahr basin of Ardabil province in Iran. Environmental Earth Sciences, v. 65(3), pp. 871-879.

Pearson, K. (1896). Mathematical contributions to the theory of evolution. -III. Regression, heredity, and panmixia. Philosophical Transactions of the Royal Society of London. Series A, v. 187, pp. 253-318.

Peseyie, R., and Rao, B.V. (2017). Assessment of groundwater quality for drinking purpose in and around Dimapur town, Nagaland. Journal of Applied Geochemistry, v. 19(4), pp. 464-470.

Peseyie, R., & Rao, B.V. (2021). Hydro-geochemical Evaluation of Groundwater Quality in and around Dimapur Town, Nagaland. Recent Advances in Earth Science Research in North East India, pp. 77-90.

Piper, A.M. (1944). A graphic procedure in the geochemical interpretation of water analyses. Transactions, American Geophysical Union, v. 25, pp. 914-923.

Polizzotto, M.L., Kocar, B.D., Benner, S.G., Sampson, M. and Fendorf, S. (2008). Near-Surface Wetland Sediments as a source of arsenic release to Groundwater in Asia. Nature, v. 454, pp. 505-509.

Purushotham, D., Linga, D., Sagar, N., Mishra, S., Vinod, N.G., Venkatesham, K. and Saikrishna, K. (2017). Groundwater Contamination in parts of Nalgonda district, Telagana, India as Revealed by Trace Elemental Studies. Journal of Geological Society of India, v. 90, pp. 447- 458.

Puzari, A., Khan, P., Thakur, D., Kumar, M., Shanu, K., Chutia, P. and Ahmed, Z. (2015). Quality Assessment of Drinking Water from Dimapur district of Nagaland and Karbi-Anglong district of Assam for possible related health hazards. Current World Environment, v. 10(2), pp. 634- 640.

Rahman, M.M., Reza, A.H.M.S., Rahman, M.M., Islam, R., and Rahman, M.A. (2013). Geochemical characterization of groundwater in Bhangamor Union, Fulbari Upazila, Kurigram. International Journal of Chemistry and Material Sciences, v. 1(2), pp. 022–035.

Rajkumar, H.S., Soibam, I., Khaidem, K.S., Sanasam, S.S., Khuman, Ch. M. (2019). Ichnological Significance of Upper Disang Formation and Lower Barail Formation (Late Eocene to Early Oligocene) of Nagaland, Northeast India, in the Indo-Myanmar Ranges. Journal Geological Society of India, v. 93, pp. 471-481.

Ramesh, K., Nithya, K., and Vennila, S. (2014). Groundwater quality assessment of Kurunthancode block in Kanya Kumari District, India. International Journal of ChemTech Research, v. 6, pp. 4585-4594.

Ranjit, N., Rao, B.V., and Merangsoba (2013). Clinopyroxene compositions of the gabbro from the Naga Ophiolite belt: new evidence on supra-subduction zone type magma genesis. Journal of Applied Geochemistry, v. 15(1), pp. 61-69.

Rao, R. A. (1983). Geology and hydrocarbon potential of a part of Assam Arakan Basin and its adjoining region. Petroleum Asia Journal, v. 6(4), pp. 127–158.

Rao, B.V., Kavitha, Ch., Murty, N.N., and Polaki, L. (2016). Heavy Metal Contamination of Groundwater in Nacharam Industrial Area, Hyderabad, India. Journal of Indian Geophysical Union, v. 20, pp. 171-177.

Rao, B.V., Jamir, L., Ezung, R., Vero, A., & Keditsu, V. (2018). Hydrogeochemistry and groundwater quality in and around DC Court, Dimapur town, Nagaland. Rusie:

A journal of Contemporary Scientific, Academic and Social Issues v. 5, pp. 24-29.

Rao, B.V., Keditsu, V., Vero, A. and Vizo, R.R. (2021). Assessment of Groundwater Quality for Drinking Purpose in Kohima Village, Kohima District, Nagaland. Recent Advances in Earth Science Research in North East India, pp. 91-100.

Richards, L.A. (1954). Diagnosis and improvement of saline and Alkali soils. USDA handbook, v. 60, pp. 7-53.

Rogers, R.J. (1989). Geochemical comparison of groundwater in areas of New England, New York and Pennsylvania. Ground Water, v. 27, pp. 690–712.

Sadat-Noori, S.M., Ebrahimi, K., and Liaghat, A.M. (2013). Groundwater quality assessment using the water quality index and GIS in Saveh-Nobaran aquifer. Environmental Earth Sciences, v. 71(9), pp. 3827-3843.

Saha, S., Reza, A.H.M.S. and Roy, M.K. (2019). Hydrochemical evaluation of groundwater quality of the Tista floodplain, Rangpur, Bangladesh. Applied Water Science, v. 9, pp. 198. https://doi.org/10.1007/s13201-019-1085-7.

Sarma, H. (1985). Systematic geological mapping around Pukha-Lungwa-Chenwentyu-Champang areas of Mon district, Unpublished Progress report, GSI, FS 1984-1985.

Sawyer, C.N. and McCarty, P.L. (1967). Chemistry for Sanitary Engineers, McGraw-Hill Book Company, New York.

Sayyed, J.A., & Bhosle, A.B. (2011). Analysis of Chloride, Sodium and Potassium in Groundwater Samples of Nanded City in Mahabharata, India. European Journal of Experimental Biology, v. 1, pp. 74-82.

Schlumberger, M. (1939). The application of telluric currents to surface prospecting. Eos, Transactions American Geophysical Union, v. 20(3), pp. 271-277.

Selvam, S., Seshunarayan, T., Manimaran, G., Sivasubramanian, P., and Manimaran D. (2010). Groundwater investigation using geoelectrical survey: A case study from Kanukunta village, Andhra Pradesh. India Journal of Outreach, v. 4, pp. 59-61.

Selvam, S., and Sivasubramanian, P. (2012). Groundwater potential zone identification using geoelectrical survey: a case study from Medak district, Andhra Pradesh, India. International Journal of Geomatics and Geosciences, v. 3(1), pp. 55-62.

Sharma, M.K., Kumar, M., Malik, D.S., Singh, S., Patre, A.K., Prasad, B., Sharma, B., Saini, S., Shukla, A.K., & Das, P.C. (2022). Assessment of groundwater quality

and its controlling processes in Bemetara District of Chhattisgarh State, India. Applied Water Science v. 12, 102 p.

Shaughnessy, A. R., and Brantley, S.L. (2023). How do silicate weathering rates in shales respond to climate and erosion? Chemical Geology, v. 629, 121474 p. https://doi.org/10.1016/j.chemgeo.2023.121474.

Shenoy, N.K., and Lokesh, K.N. (2000). Electrical resistivity survey for groundwater exploration in Udupi municipal area. Journal of Applied Hydrology, v. 13(3-4), pp. 30-35. https://eurekamag.com/research/018/823/018823039.php.

Shimpi, S., Rokade, V.M., and Upasani, K. (2019). Application of Remote Sensing and GIS for Groundwater Potential Zonation: A Case Study of Bori-Chikli Watershed, Maharashtra, India. Bulletin of Pure and Applied Sciences, v. 38 F(1), pp. 114-127.

Shirazi, S.M., Imran H.M., and Akib, S. (2012). GIS-based DRASTIC method for groundwater vulnerability assessment: a review. Journal of Risk Research, v. 15(8), pp. 991-1011.

Shrinivasa Rao, B., and Venkateswara, P. (2000). Physicochemical Analysis of Selected Groundwater Samples. Indian Journal of Environ Protection, v. 20 (3), pp. 161.

Singhal, B.B.S. and Gupta, R.P. (1999). Applied hydrogeology of fractured rocks, Kluwer academic publishers, The Netherlands, 400 p.

Singh, S., Mondal, N.C., and Somvir, S. (2017). Groundwater quality in and around Tuticorin town, Southeast coast of India. Journal of Indian Geophysical Union, v. 21, pp. 34-43.

Sinha, N. K., Chatterjee, B. P., and Satsangi, P. P. (1982). Status of paleontological researches in North Eastern region. Geological Survey of India, Record No.112.

Sinha-oy, S. (2001). Neotectonic Significance of Longitudinal River Profiles: An Example from the Banas Drainage Basin, Rajasthan. Journal of Geological Society of India. v. 58 (2), pp.143-156.

Smart water magazine (2020). India's Rivers Benefit from Lockdown. Available online at: https://smartwatermagazine.com/news/smart-water-magazine/indias-rivers-benefit-lockdown.

Soil and Water Conservation Department, Govt. of Nagaland (2022). Rainfall data of Kohima

Srivastava, S.K. and Pandey, N. (2004). Tectono-sedimentary evolution of Disang-Barail Transition, North West of Kohima, Nagaland, India. Himalayan Geology, v.25(2), pp.121-128.

Stallard, R.E., and Edmond, J.M. (1983). Geochemistry of Amazon River: the influence of the geology and weathering environment on the dissolved load. Journal of Geophysical Research, v. 88, pp. 9671–9688.

Strahler, A. (1964). Quantitative Geomorphology of Drainage Basins and Channel Networks. In: Chow, V., Ed., Handbook of Applied Hydrology, McGraw Hill, New York, pp. 439-476.

Stumm, W., and Morgan, J. J. (1996). Aquatic Chemistry: Chemical equilibria and rates in natural waters, 3rd edition. Wiley, New York, USA, 462 p.

Subba Rao, N. (2002). Geochemistry of Groundwater in Parts of Guntur District, Andhra Pradesh, India. Environmental Geology, v. 41, pp. 552‑562.

Subba Rao, N. (2009). Fluoride in groundwater, Varaha River Basin, Visakhapatnam District, Andhra Pradesh, India. Environmental Monitoring and Assessment, v. 152, pp. 47‑60.

Subba Rao, S.N., Subrahmanyam, A., Kumar, S.R., Srinivasulu, N., Rao, G.B., Rao, S.P., and Reddy, G.V. (2012). Geochemistry and quality of groundwater of Gummanampadu sub-basin, Guntur District, Andhra Pradesh, India. Environmental Earth Science, v. 67, pp. 1451-1471.

Subba Rao, S.N. (2018). Groundwater quality from a part of Prakasam District, Andhra Pradesh, India. Applied Water Science, v. 8, pp. 30.

Sujatha, D. (2004). Heavy metal contamination of groundwater in Katedan Industrial Development Area, Hyderabad, India. Proceedings of International Conference on "Soil and Groundwater Contamination: Risk Assessment and Remedial Measures, ENVIROINDIA, NGRI, Hyderabad, pp. 15-25.

Sunitha, V., and Reddy, Y. S. (2019). Hydrogeochemical evaluation of groundwater in and around Lakkireddipalli and Ramapuram, Y.S.R District, Andhra Pradesh, India. Hydro Research, v. 2, pp. 85-96.

Thilagavathi, R., Chidambaram, S., Prasanna, M. V., Thivya, C., and Singaraja, C. (2012). A study on groundwater geochemistry and water quality in layered aquifers system of Pondicherry region, southeast India. Applied water science, v. 2, pp. 253-269.

Thiruneelakandan, B., Kumar, T.J.R., Dushiyanthan, C., and Suresh, R. (2014). Identification of coastal fresh water aquifer using geoelectric investigation in parts of Vanur block of Villupuram District, Tamil Nadu. Inventi Rapid: Water and Environment, v. 2014(1), pp. 1-6.

Thong, G.T., and Rao, B.V. (1999). Petrochemical studies of the Barail sediments of Botsa, Kohima District, Nagaland. Journal of the Indian Academy of Geoscience, v. 42, pp. 32-37.

Thong, G.T. (2001). Clay minerals in the Disang sediments of Botsa, Kohima District, Nagaland. Bulletin of Pure and Applied Sciences, v. 20F, pp. 67-70.

Tijani, M. N. (1994). Hydrochemical assessment of groundwater in Moro area, Kwara State, Nigeria. Environmental Geology, v. 24(3), pp. 194—202.

Tiwari, R.N., Mishra, S. and Pandey, P. (2013). Study of major and trace elements in groundwater of Birsighpur area, Satna district, Madhya Pradesh, India. International Journal of Water Resources and Environmental Engineering, v.5(7), pp. 380-386.

Todd, D. K. (1980). Groundwater hydrology, Second Edition. John Wiley & Sons New York: Wiley, 535 p.

Todd, D.K., and Mays, L.W. (2013). Groundwater Hydrology, Third Edition. John Willey and Sons, 636 p.

USGS (2019). Chloride, salinity and dissolved solids. https://www.usgs.gov/mission-areas/water-resources/science/chloride-salinity-and-dissolved-solids

US Salinity Laboratory Staff (1954). Diagnosis and improvement of saline and alkali soils. US Department of Agriculture Handbook 60, Washington, DC.

Vaidyanadhan, R. (1971). Evolution of the drainage Cauvery in south India. Journal of Geological Society of India, v. 12, pp. 14-23.

Valdiya, K.S., and Narayana, A.C. (2007). River response to neotectonic activity: Example from Kerala, India. Journal of the Geological Society of India, v. 70, pp. 427-443.

Van Overmeeren, R. (1989). Aquifer Boundaries Explored by Geoelectrical Measurements in the Coastal Plain of Yemen: A Case of Equivalence. Geophysics, v. 54, pp. 38-48. http://dx.doi.org/10.1190/1.1442575.

Vero, A., Rao, B.V., Haokip, P., Medo, T. and Keditsu, V. (2023). Assessment of groundwater quality using hydrochemistry and geospatial techniques in Kohima town, Nagaland. Journal of Applied Geochemistry, v. 25 (1), pp. 40-52.

Wang, Y., Li, R., Wu, X., Yan, Y., Wei, C., Luo, M., Xiao, Y., and Zhang, Y. (2023). Evaluation of Groundwater Quality for Drinking and Irrigation Purposes Using GIS-Based IWQI, EWQI and HHR Model. Water, v. 15(12), pp. 22-33. https://doi.org/10.3390/w15122233.

Ward, S.H., (1990). Resistivity and Induced Polarization methods: in Geotechnical and Environmental Geophysics. Ward, S.H., ed: Society of Exploration Geophysicists water Resources Management, v.1, pp. 06-14.

Water Resources Mission Area (2019). Chloride, salinity and Dissolved solids. USGS

Wenner, F. (1916). A method of measuring earth resistivity. Bulletin of the Bureau of Standards, v. 12, pp. 469-478. https://doi.org/10.6028/bulletin.282.

WHO (2004). Guidelines for drinking water quality. Geneva: World Health Organization, Geneva.

Wilcox, L.V. (1955). Classification and use of irrigation waters, USDA, circular 969, Washington DC, USA.

WHO (2003). Guidelines for Drinking Water Quality, World Health Organization, Geneva.

WHO (2004). Guidelines for drinking water quality. Geneva: World Health Organization, Geneva.

WHO (2011). Guidelines for Drinking Water Quality, World Health Organization, Geneva.

Yadav, A.S., & Sawant, P.T. (2016). Groundwater Pollution in Sheri Nala Basin, Sangli District, Maharashtra, India and its impact on Health- A case study. Journal of Applied Geochemistry, v. 18(1), pp. 76-89.

Zhang, Y., Dai, Y., Wang, Y., Huang, X., Xiao, Y., and Pei, Q. (2021). Hydrochemistry, quality and potential health risk appraisal of nitrate enriched groundwater in the Nanchong area, southwestern China. Science of the Total Environment, v. 784, pp. 147-186. https://doi.org/10.1016/j.scitotenv.2021.147186.

Zohdy, A.A.R., Eaton, G.P., and Mabey, D.R. (1974). Application of surface Geophysics to groundwater investigations, USGS, chapter 1. Map of India. Journal Geological Society of India, v. 61, 116 p.

Zohdy, A.A.R. (1989). A New Method for the Automatic Interpretation of Schlumberger and Wenner Sounding Curves. Geophysics, v. 54, pp. 245-253. http://dx.doi.org/10.1190/1.1442648

Bio Data of the Candidate

I. PAPER PUBLICATIONS

1) **Akhrulu Vero**, B. V. Rao, Paolenmang Haokip, Thsope Medo and Vilavonuo Keditsu (2023). Assessment of Groundwater Quality in Kohima town, Nagaland by Using Geospatial Technique and Hydrochemistry. Journal of Applied Geochemistry, Vol. 25, No.1&2, pp. 40-52. ISSN 0972-1967 (UGC Carelist Journal).
2) Vilavonuo Keditsu, B. V. Rao and **Akhrulu Vero** (2022). Assessment of Groundwater Quality in and around Chiephobozou town, Kohima District Nagaland. Journal of Applied Geochemistry, Vol.24, No.3, pp. 165-173. ISSN 2319-4316 (UGC Carelist Journal).
3) B. V. Rao, Vilavonuo Keditsu, **Akhrulu Vero** and R. Ruth Vizo (2021). Assessment of Groundwater Quality for Drinking Purpose in Kohima Village, Kohima District, Nagaland. Recent advances in Earth Science Research in North East India, pp. 91-100. ISBN:978-93-89262-08-7.
4) B.V.Rao, L.Jamir, R.Ezung, **Akhrulu Vero** and Vilavonuo Keditsu (2018). Hydrogeochemistry and Groundwater Quality in and around DC Court, Dimapur town, Nagaland, Rüsie: A Journal of Contemporary Scientific, Acadamic and Social Issues. Vol. 5, pp. 24-29, ISSN-2348-0637.

II. ORAL / POSTER PRESENTATIONS

1) "Water Quality Index in assessment of water quality for drinking purpose in Kohima town, Nagaland, India" poster presentation at the 6th National Geo-Research Scholars Meet held at University of Ladakh, Leh Campus, Ladakh in association with Wadia Institute of Himalayan Geology, Dehradun from 07-10 June 2022.
2) "Hydro-geochemistry and groundwater quality assessment for drinking purpose in Kohima town, Nagaland, India" oral presentation at the international conference on "Recent Advances in Water Science and Technology" Organized by Sri Shakthi Institute of Engineering and Technology during 02-03 December 2021.
3) "Assessment of groundwater quality in Kohima town, Nagaland" oral presentation at the online international conference on "Recent Developments

and Challenges in Earth & Environmental Sciences, Natural resource Management, & Climate change with special focus on Eastern Himalayas" organized by the Department of Geology, Sikkim University, Gangtok from 08-09 October 2020.

4) "Assessment of groundwater quality in parts of Kohima town, Nagaland" oral presentation at the Geoyouth, 10th All India Student's Symposium on Geology organized by the Department of Geology, Faculty of Earth Sciences, Mohanlal Sukhadia University, Udaipur, Rajasthan from 05-06 February 2020.

III. SEMINARS/ WEBINARS AND WORKSHOP ATTENDED

1) Online Tier III Training on "Local Groundwater Related issues and participatory groundwater management" held at Dept. of Geology, Nagaland University, Kohima by Central Groundwater Board, NER, Guwahati on 28 February 2022.
2) E-training on "Basic course on PGRS using ArcGIS for pre-field studies" by RTD, NER, GSITI, Shillong from 4th -10th June 2021.
3) Webinar on "A Novel Systems in Waste Water Treatment for Sustainable development" jointly organized by Department of Civil Engineering and Internal Quality Assurance Cell, Karpaga Vinayaga College of Engineering and Technology on 28th December 2020.
4) Virtual FDP on "Water Resources Engineering" jointly organized by Department of Civil Engineering and Internal Quality Assurance Cell, Karpaga Vinayaga College of Engineering and Technology from 17th to 23rd December 2020
5) Webinar on "Earthquake versus landslide with special reference to Mizoram" by Mizoram University on 13th August 2020
6) E-training on "Fundamentals of Structural Geology" by RTD, SR, GSITI, Hyderabad from 12th -14th August 2020.
7) Webinar on "Recent earthquakes in Indo-Burmese Ranges" by Dept of Geology, Pachhunga University College, Aizawl, Mizoram, India on 6th -7th August 2020.
8) Faculty development program on "Sustainable Water Resource Management" by Karpaga Vinayaga college of Engineering and Technology, Dept. of civil engineering, Tamil Nadu from 14th -16th July 2020

9) National workshop on “Sequence stratigraphy and basin analysis”, held at Department of Geology, Nagaland University and sponsored by Nagaland University and Oil India Ltd from 26th-30th November, 2018.